# Applied Geoinformatics for Society and Environment

13th International Summer School and Conference, Bogotá, Colombia, 8. – 12. September 2025

Paul Rawiel, William Benigno Barragan Zaque,
Ángela Blanco-Vogt, Franz-Josef Behr, Dietrich Schröder

## The Challenge of Climate Change & Geoinformation Solutions

Proceedings

Stuttgart Active Alumni Group

AGSE Publishing

# The Challenge of Climate Change & Geoinformation Solutions

Applied Geoinformatics for Society and Environment

AGSE 2025 Conference

8. – 12. September 2025, Universidad Distrital Francisco José de Caldas, Bogotá, Colombia

Paul Rawiel, William Benigno Barragan Zaque, Ángela Blanco-Vogt, Franz-Josef Behr, Dietrich Schröder (Editors)

AGSE Publishing

2026

ISBN 978-3-943321-23-4

Conference Web Site: http://applied-geoinformatics.org/

Publications of AGSE, Stuttgart, Germany, http://publishing.applied-geoinformatics.org/



The cover image was kindly provided by William Benigno Barragan Zaque.

# Table of Contents

# Preface

*Applied Geoinformatics for Society and Environment* (AGSE) series of conferences and summer workshops started in 2008 in Trivandrum, initiated by the initiatives of alumni and lecturers of the international Master's Degree Programme in Photogrammetry and Geoinformatics of the University of Applied Sciences, Stuttgart, Germany. After the successful follow-up conferences in Stuttgart (Germany, 2009), Arequipa (Peru, 2010), Nairobi (Kenya, 2011), Johor Bahru (Malaysia 2012), Ahmedabad (India, 2013), again Stuttgart (2014), on Kish Island (Iran, 2017), Windhoek (Namibia 2018), Stuttgart (2019), as hybrid conference in Kathmandu and Stuttgart (Nepal, Germany, 2021 and again Trivandrum (India, 2022). The conference is closely related to the Master's Programme in Photogrammetry and Geoinformatics which started with the first batch 26 years ago, meanwhile there is a global network of about 600 alumni graduated from the programme. Since its beginning, the course is supported by the German Academic Exchange Service (DAAD) in its program for Development-Related Postgraduate Courses (EPOS).

Also, AGSE 2025 is incorporated into the DAAD supported alumni work of the University of Applied Sciences Stuttgart. Therefore, participants from many countries worldwide contribute with experiences from their home countries.

As in previous years, the conference will address current topics in the field of geographic information (GI) science. With the broad theme of 'The Challenge of Climate Change and Geoinformation Solutions', the conference will focus on contributions from Earth Observation relating to environmental monitoring, natural hazards, and risk assessment in the context of climate change. Additionally, the conference will address new concepts and methods related to machine learning and deep learning for GeoAI applications. Finally, data sharing, which is one of the prerequisites for setting up these applications, will also be discussed.

The concept includes invited talks by invited international experts in combination with presentations and workshops by participants and lecturers on topics related to technological developments and recent data provision by Earth Observation Systems. Through a webinar also participants from counties worldwide who are not able to participate in person will be included in the networking activities.

The objective of the conference is to 'take the benefits of geographic information technologies to a wide canvas of applicable areas'. Since 2008 we – scientists, practitioners, students and alumni – continue this path to empower one another in a participative way.

We wish this event a successful exchange of knowledge crossing borders and disciplines.

Paul Rawiel  Angela Blanco-Vogt  William Barragan Zaque  Franz-Josef Behr  Dietrich Schröder

# Welcome

Dear participants and colleagues,

Greetings from Bogotá, Colombia.

On behalf of Universidad Distrital Francisco José de Caldas, it is an honor and a true pleasure to welcome you to the AGSE 2025 Conference, held from September 8 to 12, 2025, in our vibrant capital city. This international gathering, co-organized with the Hochschule für Technik Stuttgart (HFT), continues the rich legacy of the Applied Geoinformatics for Society and Environment (AGSE) initiative, bringing together professionals, researchers, and students from across the globe.

Under the timely theme **"The Challenge of Climate Change & Geoinformation Solutions,"** this year's conference aims to foster dialogue, innovation, and collaboration among the global geospatial community. Throughout five dynamic days, participants will engage in keynote lectures, technical sessions, hands-on workshops, and a field excursion — all addressing the critical role of geoinformation in confronting global challenges.

This compilation of abstracts reflects the diversity and richness of contributions to AGSE 2025. Each presentation and paper offer unique insights and perspectives, and we are proud to host such a breadth of expertise and experience in Bogotá.

We hope that, beyond the academic exchange, you will enjoy the spirit of our country, people, flavors, and rhythms. Colombia welcomes you with warmth and enthusiasm. At AGSE 2025, we will also have the opportunity to celebrate together with touches of traditional Colombian music and the joy that defines our culture.

We extend our deepest gratitude to all organizing institutions, contributors, volunteers, and participants who made this conference possible. May this event be not only a space for knowledge sharing, but also a seedbed for future collaboration and long-lasting friendships in the geoinformatics community.

**Welcome to AGSE 2025. Welcome to Bogotá.**

Let this be a memorable and inspiring experience for all.
Warm regards,

**William Benigno Barragan Zaque, PhD**
Full Professor
Topographic Engineering
Faculty of Environment and Natural Resources
Universidad Distrital Francisco José de Caldas

# Technical Session: Geoinformation Worldwide - Disaster and Environmental Monitoring

# Determination of Optimal Sites for Rainwater Harvesting (RWH) Structures in Kajiado Central, Kenya Using Long Short-Term Memory (LSTM) Networks.

Charles O. Gaya [a], Christopher O. Oningoa

[a] *Jomo Kenyatta University of Agriculture and Technology, cgaya@jkuat.ac.ke*

**Abstract:** Water scarcity in arid and semi-arid regions of Kenya continues to challenge sustainable development and local livelihoods. This study explores the use of Long Short-Term Memory (LSTM) neural networks to determine optimal sites for rainwater harvesting (RWH) structures in Kajiado Central sub-county, a semi-arid region in Kenya characterized by erratic rainfall and insufficient surface water infrastructure. Daily meteorological and discharge data from 2000 to 2021 were used to train and test an LSTM model, which achieved strong predictive accuracy ($R^2 = 0.82$) in simulating surface runoff. Unlike conventional GIS-based multi-criteria approaches, the LSTM model integrates temporal and spatial patterns to directly predict runoff volumes and identify high-yield zones for rainwater capture. The results revealed that approximately 55% of the study area is highly suitable for RWH implementation, primarily due to favorable slopes, clayey soils, and proximity to infrastructure. In contrast, 15% of the area was found to be unsuitable due to steep slopes and low runoff potential. This LSTM-driven methodology provides a robust, data-efficient framework for optimizing RWH site selection in data-scarce environments, supporting more resilient and sustainable water resource planning.

***Keywords***: Rainwater Harvesting, Long Short-Term Memory (LSTM)

## 1. Introduction

Water scarcity continues to be a significant challenge in arid and semi-arid regions (ASALs), particularly in sub-Saharan Africa, where erratic rainfall patterns, limited surface water sources, and inadequate infrastructure severely constrain access to clean and reliable water (Gaffoor et al., 2022). In Kenya, over 80% of the land area is classified as ASAL, with regions like Kajiado Central sub-county experiencing frequent droughts, high rainfall variability, and growing pressure from urban expansion and agricultural intensification. These conditions have led to widespread water insecurity and have heightened the urgency to adopt innovative and sustainable water management strategies (Vu et al., 2021).

Rainwater harvesting (RWH) offers a practical and cost-effective approach to supplement existing water sources, especially in areas where surface and groundwater resources are unreliable or contaminated (Mukonza & Chiang, 2022; Sadeghi Tabas & Samadi, 2022). However, the effectiveness of RWH systems depends critically on the identification of optimal locations that balance hydrological potential with practical constraints such as topography, soil type, and land use (Al-Ghobari et al., 2020).

In previous studies, the identification of RWH sites has relied on Geographic Information Systems (GIS) and Multi-Criteria Decision Analysis (MCDA) (Gupta et al., 2016; Karunanidhi et al., 2020). While these techniques are useful, they often require extensive ground-truthing and may not adequately model the temporal complexity of runoff behavior (Khairudin et al., 2020). This study proposes a novel approach that leverages Long Short-Term Memory (LSTM) neural networks, a form of deep learning particularly suited to sequence prediction and time-dependent modelling, to identify optimal RWH sites (Merizalde et al., 2023). LSTM is well-suited for modelling hydrologic processes due to its ability to retain long-term dependencies in sequential data. By training the LSTM model on long-term meteorological and catchment data, the framework captures both temporal rainfall-runoff dynamics and spatial variability across the landscape (Burrichter et al., 2024; Raza et al., 2025).

In contrast to conventional techniques, this method allows for the direct estimation of surface runoff potential and the assessment of site suitability for RWH buildings by using past trends and future forecasts (Afzaal et al., 2020). The Kajiado Central sub-county, with its semi-arid climate, sparse hydrological infrastructure, and increasing water demand, serves as a representative case study for this technique.

This research aims to demonstrate how deep learning models can be integrated into hydrological planning to improve the reliability, accuracy, and scalability of rainwater harvesting site selection—particularly in data-scarce and climate-sensitive regions.

## 2. Methodology

### 2.1 Study Area

Kajiado Central sub-county (Figure 1), located in southern Kenya, is classified as a semi-arid region characterized by highly variable rainfall, periodic droughts, and limited permanent water sources. The primary economic activity is pastoralism, and most water sources are seasonal or saline. The region was selected due to its vulnerability to water scarcity and its urgent need for sustainable water management interventions such as rainwater harvesting.

### 2.2 Data Collection and Pre-processing

Meteorological and catchment datasets were collected from 2000 to 2021. Key input variables included daily precipitation, temperature (min/max), potential evapotranspiration, radiation and vapour pressure. In addition, vegetation indices-Normalized Difference Vegetation Index (NDVI) and Normalized Difference Water Index (NDWI) were integrated. Static parameters such as elevation, slope, soil type, and land use/land cover (LULC) were also incorporated. Time-series data were processed using Google Earth Engine (GEE) and downloaded in CSV format for modelling.

All datasets were normalized to the range [0, 1] to ensure model stability and performance. The data were split into training (70%), validation (15%), and testing (15%) sets using a k-fold cross-validation strategy to enhance generalizability.

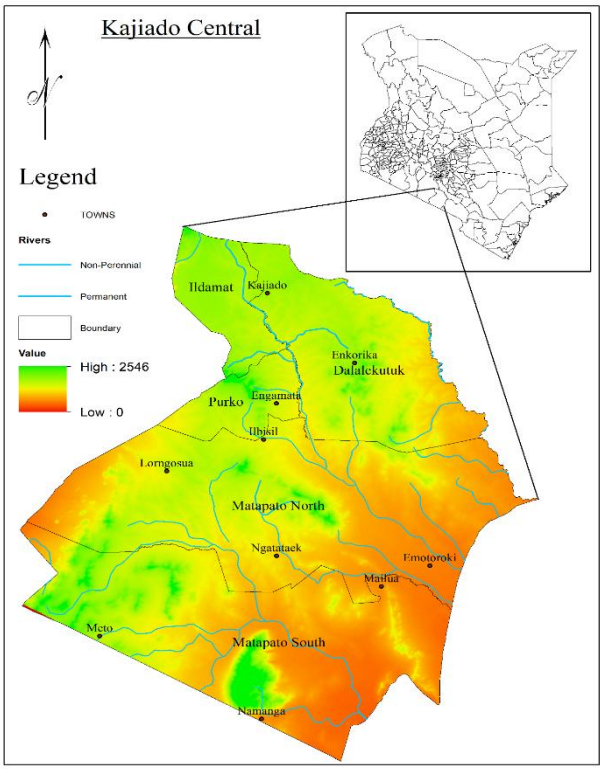


Figure 1. Study area map

### 2.3 LSTM Model Architecture and Training

The Long Short-Term Memory (LSTM) neural network was implemented using TensorFlow. The LSTM model was trained on meteorological and discharge data from 2000–2021. The model consisted of input, hidden (LSTM) layers, and a fully connected output layer to estimate daily surface runoff (Hu et al., 2018).

Training was conducted over 50 epochs with early stopping criteria to prevent overfitting. Hyper parameters such as learning rate, batch size, and number of hidden units were optimized through grid search (Moishin et al., 2021). The model was calibrated using the training set and validated with the unseen validation data to ensure robustness.

### 2.4 Model Evaluation Metrics

Model performance was assessed using standard hydrological evaluation metrics, namely Coefficient of Determination ($R^2$) to assess predictive strength, Root Mean Square Error (RMSE) to measure error magnitude and Nash–Sutcliffe Efficiency (NSE) to evaluate model skill.

### 2.5 Site Suitability Determination Using LSTM

The trained LSTM model was used to estimate runoff potential across the study area. Predicted runoff values were then combined with static spatial variables (soil type, slope, LULC, elevation, and proximity to roads and rivers) to classify site suitability for RWH structures (Mahakur et al., 2025).

A suitability index was generated using a weighted overlay approach, where LSTM-predicted runoff served as the primary input criterion (Lestari et al., 2019; Wu et al., 2020). Suitability classes included: highly suitable, moderately suitable, less suitable, and restricted. The output was mapped in GIS to visualize spatial patterns of optimal RWH zones.

## 3. Results

### 3.1 LSTM Model Performance

The final tuned LSTM model achieved an $R^2$ of 0.82 and demonstrated strong performance across both training and testing datasets in simulating daily surface runoff. The model achieved an $R^2$ of 0.82, RMSE of 5.96 $m^3/s$, and NSE of 0.78 on the testing dataset, indicating accurate and reliable hydrologic predictions (Table 1), indicating reliable simulation of runoff patterns.

| Metric | Value |
|---|---|
| $R^2$ | 0.82 |
| RMSE | 5.96 |
| NSE | 0.78 |

Table 1. Performance metrics of the LSTM model on test data

Figure 2 illustrates the close match between observed and predicted discharge, confirming the LSTM's capability to capture peak flows and seasonal variation.

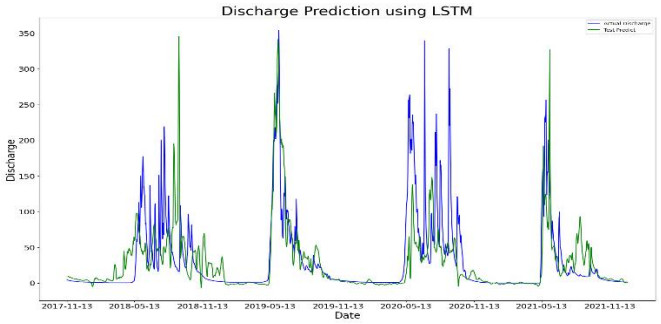


Figure 2. Observed vs. predicted discharge using LSTM model (2017–2021)

The loss curves during training (Figure 3) also show smooth convergence for the tuned model, indicating stable learning and effective parameter optimization.

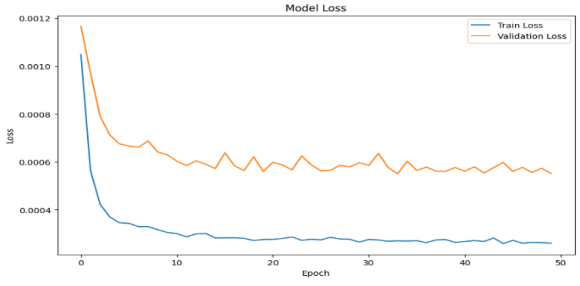


Figure 3. LSTM model training and validation loss curves

### 3.2 Spatial Runoff Distribution

Using the trained LSTM model, runoff predictions were spatially mapped across the study area. Figure 4 shows the simulated mean annual runoff, with higher runoff volumes in

low-lying regions characterized by fine-textured soils and low slopes.

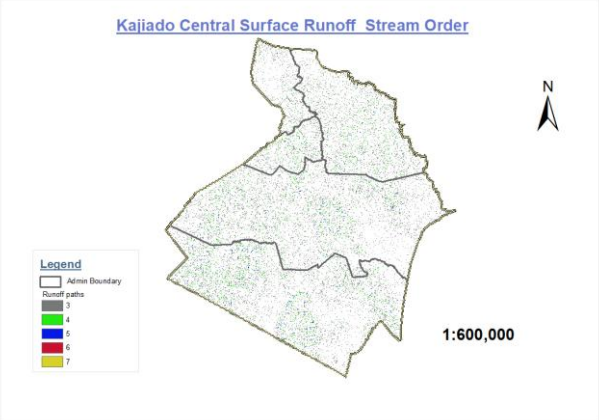


Figure 4. Spatial distribution of simulated runoff using LSTM predictions

These results highlight hydrologic hotspots for rainwater harvesting potential and serve as a quantitative foundation for suitability classification.

### 3.3 Site Suitability Classification for RWH

Runoff outputs from the LSTM model were combined with geospatial criteria - slope, soil, elevation, LULC, and infrastructure proximity - to generate a rainwater harvesting suitability map (Figure 5).

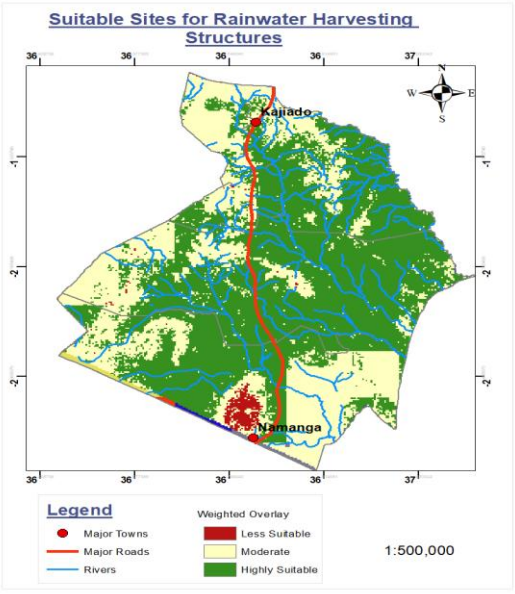


Figure 5. Rainwater harvesting suitability map

Suitability was classified into five categories as shown in Table 2.

| Suitability Class | Area Coverage (%) |
|---|---|
| Highly Suitable | 55% |
| Moderately Suitable | 30% |
| Less Suitable | 10% |
| Restricted | 5% |

Table 2. Suitability classes and coverage percentages

Highly suitable zones were mainly located in the south-east and south-west parts of the sub-county, characterized by favourable topography (gentle slopes), clay-rich soils (e.g., vertisols) and access to roads and river networks.

### 3.4 Summary of Key Findings

The LSTM model effectively captured rainfall-runoff dynamics, supporting its application in data-scarce regions.

The combined LSTM-GIS approach enables more targeted and evidence-based siting of RWH structures.

Over half of the study area is highly suitable for RWH development, offering practical opportunities to alleviate local water scarcity.

## 4. Discussion

The study's findings demonstrate how combining geospatial data and Long Short-Term Memory (LSTM) neural networks can enhance water resource management decision-making, especially in dry and semi-arid regions like Kajiado Central. The LSTM model provided a more reliable and data-driven substitute for conventional conceptual or empirical hydrological models by accurately simulating surface runoff dynamics over several seasons and years.

### 4.1 Effectiveness of LSTM in Hydrologic Modelling

The LSTM model achieved a high predictive accuracy ($R^2 = 0.82$), capturing both baseflow and peak runoff conditions. This demonstrates LSTM's ability to learn complex temporal relationships within hydrologic systems, especially in data-scarce contexts. the other hand, LSTM maintained long-term memory

across sequences, modeling seasonal impacts and delayed hydrologic responses without making any explicit assumptions about the behavior of watersheds.

Moreover, hyper parameter tuning significantly improved model performance, with training losses converging smoothly and minimal signs of overfitting. This confirms the adaptability of LSTM models to hydrological forecasting tasks when sufficient training data are available.

### 4.2 Integrating LSTM with GIS for Site Selection

By using LSTM-predicted runoff as the foundation for RWH site suitability analysis, this study offers a novel alternative to purely GIS-based or multi-criteria approaches. LSTM provided dynamic runoff estimates that reflect temporal rainfall patterns and catchment behavior, thereby enhancing the objectivity of site classification.

The integration with static spatial layers (slope, soil, LULC, elevation, and proximity to roads/rivers) allowed a holistic assessment of suitability. The outcome - a suitability map where 55% of the area was classified as highly suitable - offers actionable spatial intelligence for local planning and investment in RWH infrastructure. Notably, the unsuitable or restricted areas (~15%) coincided with steep slopes or sandy soils, validating the model's spatial logic.

### 4.3 Implications for Water Management in ASAL Regions

This LSTM-driven methodology is particularly valuable for ASAL regions, where field data are sparse and climate variability is high. Kajiado Central, like many ASAL counties, suffers from unreliable water supply and overreliance on seasonal sources. The identification of high-yield runoff zones enables more strategic siting of water harvesting infrastructure, reducing vulnerability to droughts and improving access for rural populations.

Additionally, the framework is transferable to other regions with similar climatic and hydrologic challenges. As long as minimal meteorological and terrain data are available, the LSTM-GIS model can be adapted to different geographic contexts.

### 4.4 Limitations and Recommendations for Future Work

While the results are promising, several limitations remain. First, the model may underperform during extreme events not captured in the historical training data. Future improvements could include integrating real-time rainfall forecasting or climate projections, including antecedent moisture indices as model inputs, and expanding the model's spatial resolution for localized applications.

Moreover, community engagement and socio-economic variables were not considered in the site selection process. Participatory mapping and stakeholder input can enhance the social acceptability and long-term sustainability of RWH projects.

## 5. Conclusion

This study successfully demonstrated the application of Long Short-Term Memory (LSTM) neural networks for determining optimal rainwater harvesting (RWH) sites in Kajiado Central, Kenya - a semi-arid region facing chronic water insecurity. By leveraging long-term meteorological and geospatial datasets, the LSTM model effectively simulated surface runoff with high accuracy ($R^2 = 0.82$), capturing both temporal dynamics and spatial variability in watershed responses.

Direct runoff estimation over the landscape was made possible by the LSTM-based methodology, in contrast to conventional GIS-only or multi-criteria decision-making (MCDM) methodologies. This served as the basis for an objective and data-driven suitability analysis. The model provided useful advice for the development of water infrastructure by identifying that roughly 55% of the sub-county is highly suited for RWH structures when combined with terrain, soil, land use, and infrastructure layers.

The results highlight the feasibility of using machine learning, especially recurrent neural networks like LSTM, for planning water resources in areas with little data and climate

change. The accuracy, scalability, and sustainability of RWH site selection are improved by this methodology's transferable framework, which also advances the more general objectives of water security and climate resilience in arid and semi-arid environments.

## 6. References


Afzaal, H., Farooque, A. A., Abbas, F., Acharya, B., & Esau, T. (2020). Computation of evapotranspiration with artificial intelligence for precision water resource management. Applied Sciences (Switzerland), 10(5). https://doi.org/10.3390/app10051621

Al-Ghobari, H., Dewidar, A., & Alataway, A. (2020). Estimation of surface water runoff for a semi-arid area using RS and GIS-Based SCS-CN method. Water (Switzerland), 12(7). https://doi.org/10.3390/w12071924

Burrichter, B., Koltermann Da Silva, J., Niemann, A., & Quirmbach, M. (2024). A Temporal Fusion Transformer Model to Forecast Overflow from Sewer Manholes during Pluvial Flash Flood Events. https://doi.org/10.3390/hydrology

Gaffoor, Z., Pietersen, K., Jovanovic, N., Bagula, A., Kanyerere, T., Ajayi, O., & Wanangwa, G. (2022). A Comparison of Ensemble and Deep Learning Algorithms to Model Groundwater Levels in a Data-Scarce Aquifer of Southern Africa. Hydrology, 9(7). https://doi.org/10.3390/hydrology9070125

Gupta, P. K., Chauhan, S., & Oza, M. P. (2016). Modelling surface run-off and trends analysis over India. Journal of Earth System Science, 125(6), 1089–1102. https://doi.org/10.1007/s12040-016-0720-z

Hu, C., Wu, Q., Li, H., Jian, S., Li, N., & Lou, Z. (2018). Deep learning with a long short-term memory networks approach for rainfall-runoff simulation. Water (Switzerland), 10(11). https://doi.org/10.3390/w10111543

Karunanidhi, D., Anand, B., Subramani, T., & Srinivasamoorthy, K. (2020). Rainfall-surface runoff estimation for the Lower Bhavani basin in south India using SCS-CN model and geospatial techniques. Environmental Earth Sciences, 79(13). https://doi.org/10.1007/s12665-020-09079-z

Khairudin, N. B. M., Mustapha, N. B., Aris, T. N. B. M., & Zolkepli, M. B. (2020, September 16). Comparison of machine learning models for rainfall forecasting. 2020 International Conference on Computer Science and Its Application in Agriculture, ICOSICA 2020. https://doi.org/10.1109/ICOSICA49951.2020.9243275

Lestari, E., Makarim, C. A., & Pranoto, W. A. (2019). Zero run-off concept application in reducing water surface volume. IOP Conference Series: Materials Science and Engineering, 508(1). https://doi.org/10.1088/1757-899X/508/1/012019

Mahakur, V., Mahakur, V. K., Samantaray, S., & Ghose, D. K. (2025). Prediction of runoff at ungauged areas employing interpolation techniques and deep learning algorithm. HydroResearch, 8, 265–275. https://doi.org/10.1016/j.hydres.2024.12.001

Merizalde, M. J., Muñoz, P., Corzo, G., Muñoz, D. F., Samaniego, E., & Célleri, R. (2023). Integrating geographic data and the SCS-CN method with LSTM networks for enhanced runoff forecasting in a complex mountain basin. Frontiers in Water, 5. https://doi.org/10.3389/frwa.2023.1233899

Moishin, M., Deo, R. C., Prasad, R., Raj, N., & Abdulla, S. (2021). Designing deep-based learning flood forecast model with ConvLSTM hybrid algorithm. IEEE Access, 9, 50982–50993. https://doi.org/10.1109/ACCESS.2021.3065939

Mukonza, S. S., & Chiang, J. L. (2022). Micro-Climate Computed Machine and Deep Learning Models for Prediction of Surface Water Temperature Using Satellite Data in Mundan Water Reservoir. Water

(Switzerland), 14(18). https://doi.org/10.3390/w14182935

Raza, M. A., Karim, A., Alqarni, M., Al-Khasawneh, M. A., Jumani, T. A., Aman, M., & Masud, M. I. (2025). An Intelligent Long Short-Term Memory-Based Machine Learning Model for the Potential Assessment of Global Hydropower Capacity in Sustainable Energy Transition and Security. Energies, 18(13). https://doi.org/10.3390/en18133324

Sadeghi Tabas, S., & Samadi, S. (2022). Variational Bayesian dropout with a Gaussian prior for recurrent neural networks application in rainfall-runoff modeling. Environmental Research Letters, 17(6). https://doi.org/10.1088/1748-9326/ac7247

Vu, M. T., Jardani, A., Massei, N., & Fournier, M. (2021). Reconstruction of missing groundwater level data by using Long Short-Term Memory (LSTM) deep neural network. Journal of Hydrology, 597. https://doi.org/10.1016/j.jhydrol.2020.125776

Wu, Y., Ding, Y., Zhu, Y., Feng, J., & Wang, S. (2020). Complexity to Forecast Flood: Problem Definition and Spatiotemporal Attention LSTM Solution. Complexity, 2020. https://doi.org/10.1155/2020/7670382

# Landslide Susceptibility Mapping of Sindhupalchok District, Nepal

Sanjeev Kumar Raut

*Land Management Training Center, Ministry of Land Management, Co-operatives and Poverty Alleviations, Nepal; sanjeevraut.4@gmail.com N*

The district of Sindhupalchok in Nepal is characterized by complex topography and a history of devastating landslides, making it crucial to understand and mitigate landslide risks. This study focuses on landslide susceptibility mapping in Sindhupalchok using advanced geospatial techniques to provide valuable insights for risk assessment and management. Remote sensing data, including high resolution satellite imagery and digital elevation models, are utilized to extract relevant terrain parameters such as slope, aspect, curvature, and land cover. Geographic Information System (GIS tools are employed to integrate these parameters with historical landslide data and other influencing factors, including geological and hydrological characteristics. Validation model is performed using independent landslide inventories and statistical measures such as area under curve (AUC). The resulting landslide susceptibility map provides a spatial representation of areas at high, moderate, and low risk, aiding in the identification of vulnerable zones and supporting informed decision-making for land-use planning and disaster preparedness. This research contributes to the understanding of landslide dynamics in Sindhupalchok and serves as a valuable tool for local authorities, land planners, and emergency responders. The findings are essential for developing proactive measures to reduce the impact of landslides on communities and infrastructure in the region, ultimately enhancing resilience and sustainable development.

***Keywords:*** Geographic Information System, Landslide Hazard, Susceptibility, Weights

# Cartographic Assessment of Hurricane Iota Damage in Providencia Using Photogrammetry and Spatial Analysis

Luisa Garzón Díaz [a], *William Barragan* [b], *Juan David Méndez* [c], Jhon López[d], Emily Nuñez[e]

*a Universidad Distrital Francisco José de Caldas, Luisa Garzón Díaz - lfgarzond@udistrital.edu.co*
*b Universidad Distrital Francisco José de Caldas, William Barragán Zaque - wbarraganz@udistrital.edu.co*
*c Universidad El Bosque, Juan David Méndez Niño - jmendezni@unbosque.edu.co*
*d Universidad Distrital Francisco José de Caldas, Jhon Fredy López - jflopezl@udistrital.edu.co*
*e Universidad Distrital Francisco José de Caldas, Emily Dayana Núñez - Emilyda9@gmail.com*

Hurricane Iota struck Providencia Island in November 2020 as a Category 5 event, causing the destruction of much of its infrastructure and ecosystems, becoming one of the most severe natural disasters in the recent history of the Colombian Caribbean. This study presents a cartographic assessment of the damage using drone photogrammetry, spatial analysis techniques, and products derived from geographic information systems (GIS). To this end, planned flights were carried out with a VTOL WINGTRAOne drone, complemented by high-precision GNSS stations and ground control points in the field, which made it possible to generate high-resolution orthophoto mosaics, digital surface models, and pre- and post-event comparisons. The analysis of buildings, conducted six months after the hurricane, showed that 12% were classified as having minor damage, 9% as moderate damage, and 32% as severe damage. The remaining 46% showed no visible impact, although part of this group corresponds to roofs rebuilt after the event. While most collapsed buildings were homes, the greatest territorial impacts were concentrated in large community and commercial infrastructures, disproportionately affecting the island's social and economic dynamics. The applied methodology confirms the usefulness of photogrammetry and spatial analysis as fast, accurate, and replicable tools for post-disaster monitoring, providing critical inputs for reconstruction, risk management, and sustainable territorial planning.

***Keywords***: Hurricane Iota, Providencia, UAV photogrammetry, damage assessment, GIS

## 1. Introduction

Hurricanes are large-scale meteorological phenomena that generate significant impacts on island territories, where environmental, social, and economic vulnerability is high. These extreme events are characterized by strong winds, torrential rainfall, and storm surges that cause human losses, structural damage, and prolonged disruptions to productive and service systems. In the Caribbean context, the recurrence of such disasters highlights the need to develop rapid and precise methodologies for damage assessment and recovery planning (de Beurs, 2019).

Hurricane Iota, which reached Category 5 in November 2020, represents one of the most devastating episodes in the recent history of the Colombian Caribbean. Its passage through Providencia Island caused the destruction of much of the urban and rural infrastructure, with losses exceeding 98% of the buildings, severe damage to coastal ecosystems, and a strong impact on local socioeconomic

dynamics (Hernández-Hamón et al., 2024). The San Andrés, Providencia, and Santa Catalina Archipelago, designated as a UNESCO biosphere reserve, experienced critical alterations in its ecological and urban fabric, evidencing the fragility of island systems in the face of extreme hydrometeorological phenomena.

Several studies have documented post-disaster assessment techniques based on satellite imagery, remote sensing, and hydrometeorological simulation models. However, in territorially complex contexts such as Providencia, these approaches often present limitations in spatial resolution, processing times, and field validation. In this sense, photogrammetry using unmanned aerial vehicles (UAVs) and their integration with geographic information systems (GIS) offers a robust and efficient alternative to generate high-resolution cartography and comparative analyses between pre- and post-event scenarios.

Within this framework, the purpose of this research was to evaluate the damage caused by Hurricane Iota on Providencia Island through the generation of cartographic products based on UAV photogrammetry and spatial analysis. The study seeks to answer the following research questions: What was the magnitude and spatial distribution of damage to island infrastructure and ecosystems? What types of damage can be identified from orthophoto mosaics and georeferenced databases? And how can the information derived from this analysis support reconstruction and risk management processes in vulnerable island territories?

## 2. Development of the Research

Providencia Island, located in the Caribbean Sea at 13° N and 81° W, belongs to the San Andrés, Providencia, and Santa Catalina Archipelago, designated as a UNESCO Biosphere Reserve. With an approximate area of 17 km², the island is of volcanic origin and features a mountainous relief with elevations reaching up to 350 m a.s.l. Its ecosystem combines forests, mangroves, and coral reefs (Dutta Roy et al., 2024; Velázquez-Salazar et al., 2025), which play a crucial role in coastal protection (Krauss et al., 2023) and in the local economy based on tourism and fishing. This insular condition, along with its dependence on critical infrastructure, makes it highly vulnerable to extreme meteorological phenomena such as Hurricane Iota.

The IGAC identifies the main land covers as basal dry forests, which occupy much of the island's interior, and mangroves, which account for 4.1% of the insular surface, associated with low-lying coastal areas and estuaries. These ecosystems, together with coral reefs and seagrass beds, are part of the Sea flower Biosphere Reserve, recognized by UNESCO. However, the Old Point Regional Mangrove Park and other mangrove sectors face anthropic pressures resulting from urbanization, inadequate solid waste disposal, and coastal pollution, which increases their vulnerability to extreme phenomena such as Hurricane Iota.

## 3. Materials and Methods

The research relied on multiple data sources:

**UAV imagery:** Flights were conducted with a VTOL WINGTRAOne drone, equipped with a high-resolution RGB camera (Sony RXRII), operated by Universidad Distrital Francisco José de Caldas. The flights were carried out at programmed altitudes of 120, 150, and 210 m, achieving spatial resolutions of 3–5 cm/pixel.

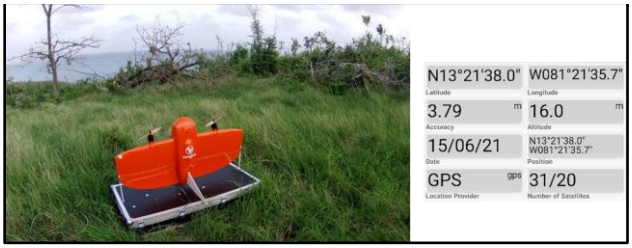


Figure 1. Dron VTOL WINGTRAOne.

**Geodetic control:** A dual-frequency GNSS base station (CHC) was installed with continuous tracking for more than 24 hours to ensure positional accuracy, along with ground control points (GCPs) and check points

measured in RTK and PPP mode, within the MAGNA-SIRGAS system.

Figure 2. Support network – GCP Providencia.

**Auxiliary information:** Digital elevation models (SRTM and IGAC), official cadastral cartography, satellite imagery (Google Hybrid and Esri World Imagery), and climatological data from IDEAM were integrated to plan flights and anticipate risks.

### 3.1 Methodology

The methodology applied in this study integrated photogrammetry tools using unmanned aerial vehicles (UAVs), high-precision geodetic positioning techniques, and spatial analysis in GIS environments to assess the damage caused by Hurricane Iota in Providencia. The process included the planning and execution of flights with a VTOL WINGTRAOne, equipped with a high-resolution RGB camera, the installation of GNSS stations, and the collection of ground control points to ensure positional accuracy. Subsequently, the captured images were processed in specialized software to generate orthophoto mosaics, digital surface and terrain models, and derived products used for change detection and damage classification. Finally, a comparative analysis between pre- and post-event scenarios was conducted, validated through positional accuracy and statistical indicators, which allowed quantifying the magnitude and spatial distribution of the impacts on the island.

#### 3.1.1 *Flight Planning and Execution*

The flight routes were designed in the WingtraPilot software, adjusting longitudinal overlaps (80%) and transversal overlaps (70%) to ensure full coverage. Before take-off, a verification protocol (checklist) was applied, which included battery status, communication with the base station, sensor calibration, and weather conditions.

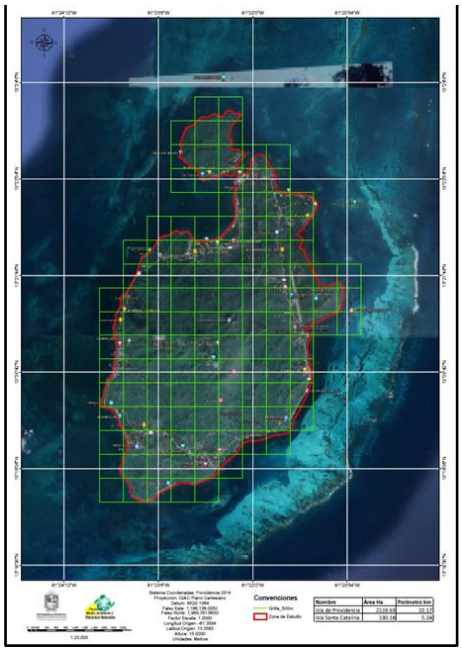

Figure 3. Flight grid design.

Auxiliary information such as recent Google Hybrid and Esri World Imagery was used to identify recent changes in land cover, as well as Digital Elevation Models (DEMs) from the Instituto Geográfico Agustín Codazzi and SRTM to anticipate risks associated with slopes and mountainous areas. Based on these inputs, flight grids were designed at altitudes of 120 m, 150 m, and 210 m, prioritizing the urban areas of Providencia most affected after the hurricane.

Strict operational safety measures were adopted during the missions, including delimiting take-off and landing zones, maintaining permanent communication between operators, and verifying meteorological conditions before and during each flight. Providencia's insular nature, combined with the influence of trade winds and strong gusts associated with the local

topography, represented an additional challenge for drone stability. To mitigate these risks, flights were carried out during favorable weather windows reported by IDEAM, with dynamic adjustments to operating altitude and sweep route direction.

Once the flight missions were completed, all photographic and GNSS records were downloaded and backed up on secure devices, following data traceability protocols. This process included organizing files into folders structured by date, flight block, and type of information, which facilitated subsequent integration into the photogrammetric processing software. Additionally, flight times, environmental conditions, and minor incidents during operations were documented, ensuring a detailed record that guaranteed the reproducibility and reliability of the survey.

#### 3.1.2 *Ground Control Point Survey*

GCPs and check points were established across the island, in some cases selecting natural terrain features to avoid additional interventions. These references were used to adjust the photogrammetric block and validate the absolute accuracy of the products.

The measurement of the GCPs was carried out using dual-frequency GNSS equipment in RTK (Real-Time Kinematic) mode, complemented with Precise Point Positioning (PPP) procedures to strengthen the quality of the recorded coordinates. These methods allowed horizontal accuracies in the range of 2 to 5 cm, and vertical accuracies of up to 10 cm, consistent with international standards (ASPRS, 2014) required for high-resolution cartographic applications. The operation was supported by a GNSS base station previously installed on the island, which was kept running for more than 24 hours, recording continuous data at a 1-second frequency. These records were subsequently used in differential correction processes, reinforcing the reliability of the final positioning.

Additionally, independent check points were collected that were not incorporated into the photogrammetric adjustment but were used exclusively to validate the absolute accuracy of the generated products. This practice made it possible to calculate the root mean square error (RMSE) in the X, Y, and Z directions, providing an objective indicator of the achieved quality. All records were referenced to Colombia's official geodetic system (MAGNA-SIRGAS), ensuring compatibility with the national geodetic network and facilitating the integration of results into geographic information systems. The procedure was documented using digital field forms (ODK Collect), which included location data, time, environmental conditions, and reported accuracies, strengthening process traceability and the reproducibility of results.

#### 3.1.3 *Photogrammetric Processing*

Image processing was carried out in the specialized software Pix4Dmapper, integrating both GNSS records obtained during flight and the precise coordinates of the ground control points (GCPs). This integration ensured the correct georeferencing of each photograph and reduced systematic errors in the photogrammetric block. Given the size of the area covered and computational capacity limitations, Providencia Island was segmented into nine independent processing blocks: east1, north1, north2, west1, west2, west3, west4, south1, and south2. This strategy facilitated a more efficient workflow, avoiding software overloads and ensuring effective data management.

Each block underwent an aerotriangulation process, which consisted of simultaneously adjusting all images based on their internal calibration parameters and external coordinates obtained in the field. This procedure linked the photographs into a single reference system, correcting distortions and ensuring the geometric consistency of the final mosaic. The results of this adjustment were evaluated by calculating the root mean square error (RMSE) in the X, Y, and Z directions, using the independent check points previously collected. The values obtained remained within the international standards recommended by the American Society for Photogrammetry and Remote Sensing

(ASPRS, 2014), certifying the accuracy achieved in the generated products.

From this process, various high-resolution cartographic products were developed. Among them, RGB orthophoto mosaics stand out, providing detailed and updated representations of the island's surface, with resolutions in the order of 3 to 5 cm/pixel. Likewise, Digital Surface Models (DSM), reflecting topography along with buildings and vegetation, and Digital Terrain Models (DTM), representing only the morphology of the bare terrain, were obtained. These products were complemented with the generation of derived thematic maps, aimed at land cover classification, damage zoning, and change detection between pre- and post-hurricane Iota scenarios. Taken together, the results constitute the cartographic basis on which quantitative and spatial damage analyses were structured.

#### 3.1.4 *Spatial Analysis*

Once the orthophoto mosaics and digital models were generated, the photogrammetric products were integrated into a GIS (Geographic Information System) environment to facilitate spatial analysis. The first step consisted of a pre- and post-event comparison, using reference satellite images and the UAV-acquired orthophotos. This analysis made it possible to identify significant transformations in vegetation cover, urban infrastructure, and land use. Among the most notable changes were biomass loss in forested and mangrove areas, alterations in coastal ecosystems, and modifications in urban patterns as a result of the collapse of buildings and road networks.

Figure 4. Road infrastructure loss

Secondly, a damage classification was developed using high-resolution orthophoto mosaics together with official cadastral databases from IGAC. Three main categories were established: minor damage, moderate damage, and severe damage/collapse. This classification was based on visual criteria (degree of structural alteration observable in the images) and metric criteria (relationship to the building footprint recorded in the cadastral database). This procedure made it possible to differentiate the magnitude of damage at the building level, providing a comprehensive view of both the frequency and the severity of the impacts.

Additionally, the estimation of affected areas was carried out, expressed in hectares (ha) and square meters ($m^2$), through the vector delineation of buildings and impacted areas. This quantification made it possible not only to determine the number of affected buildings but also the territorial extent of the impact, differentiating between construction typologies. This differentiation was crucial to understanding the disproportionate effects that the hurricane had on large-scale infrastructures, in contrast to smaller dwellings.

Finally, positional validation of the cartographic products was performed by calculating the Root Mean Square Error (RMSE) in the X, Y, and Z directions, using the independent check points collected in the field. The values obtained were compared with the standards established by the American Society for Photogrammetry and Remote Sensing (ASPRS, 2014), confirming that the achieved accuracy was within the accepted ranges for high-resolution cartographic applications. This process ensured the reliability of the results and their suitability for use in territorial planning, risk management, and post-disaster reconstruction processes.

## 4. Results

The database analysis made it possible to characterize the structural impact caused by Hurricane Iota on the island. A total of 5,032 affected constructions were recorded,

excluding water tanks, which constitutes a representative sample to assess the magnitude of the damage.

### 4.1 Generated Cartographic Products

The photogrammetric survey and spatial analysis process enabled the construction of a set of high-resolution cartographic products, which constitute the basis for assessing the damage caused by Hurricane Iota in Providencia. These products, obtained through UAV flights and processed in specialized software, were integrated into a GIS environment that allowed both the visualization and quantification of impacts.

First, very high-resolution RGB orthophoto mosaics (3–5 cm/pixel) were generated, providing an updated and detailed representation of the island's surface. These orthophoto mosaics clearly reveal collapsed buildings, partial roof damage, debris accumulation, and changes in vegetation cover, offering a key input for multi-scale damage analysis.

Complementarily, Digital Surface Models (DSM) and Digital Terrain Models (DTM) were obtained, useful for evaluating changes in urban and natural morphology. The DSM made it possible to characterize the height of buildings, vegetation, and structural elements, while the DTM facilitated slope analysis and the delimitation of areas susceptible to mass movements and debris accumulation. The comparison between both products provided an accurate approximation of the topographic and structural changes generated by the event.

Additionally, from the integration of orthophoto mosaics and cadastral databases, thematic maps of building damage classification were developed, categorized as minor, moderate, and severe. These maps spatially represent the distribution of impacts on the island and constitute an essential input for decision-making in reconstruction processes. Likewise, maps of the distribution of construction and vegetation debris were generated, whose quantification showed differentiated patterns: small-scale dispersed debris in urban areas and large vegetation accumulations in coastal and mangrove sectors.

Finally, impact zoning maps were developed, integrating information on damaged buildings, debris, and degraded ecosystems, providing a comprehensive view of critical areas. These products not only reveal the magnitude of the hurricane's impact but also serve as planning tools to guide differentiated interventions in housing, community infrastructure, and strategic ecosystems.

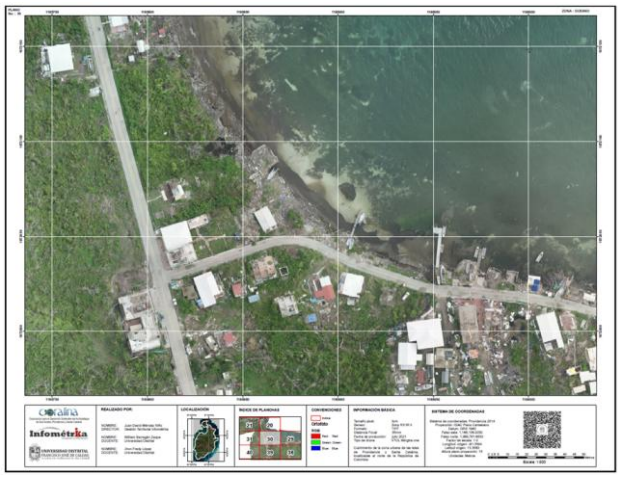

Figure 5. Generation of detailed plans at 1:5000 scale

One of the products obtained corresponds to the development of 295 orthophotograph maps at a 1:1500 scale, accurately covering the entire area of interest.

### 4.2 Distribution by Level of Damage

The analysis results, after excluding tents (installed as an emergency response measure) and water tanks, show that out of a total of 3,079 evaluated constructions, 12% (377 cases) presented minor damage, mainly to roofs and minor structural elements. Nine percent (279 cases) showed moderate damage, associated with partial absence of roofs and slight impacts on structural components. Thirteen percent (415 cases) corresponded to severe damage, characterized by the total loss of roofing elements and significant damage to supporting structures. Additionally, 574 buildings (19%) were collapsed or reduced to their footprint and foundation, evidencing the magnitude of the hurricane's impact on the island's infrastructure. Finally, 46% (1,434

constructions) showed no apparent damage, although part of this group is likely to correspond to roofs reconstructed after the event.

Figure 6. Damage characterization

### 4.3 Affected Area

The total affected area amounts to 725 ha, of which 315 ha correspond to buildings with minor damage, 240 ha to moderate damage, and 170 ha to severe damage. Although minor damage predominates in terms of frequency, the average surface values show that larger constructions were also the most vulnerable: 123.5 m² in the minor damage group, 215.4 m² in the moderate group, and 268.9 m² in the severe group. The maximum recorded value was 2,786.8 m² per building, while the standard deviation was highest in the severe damage group ($\sigma$ = 410 m²), reflecting high heterogeneity in the most compromised constructions.

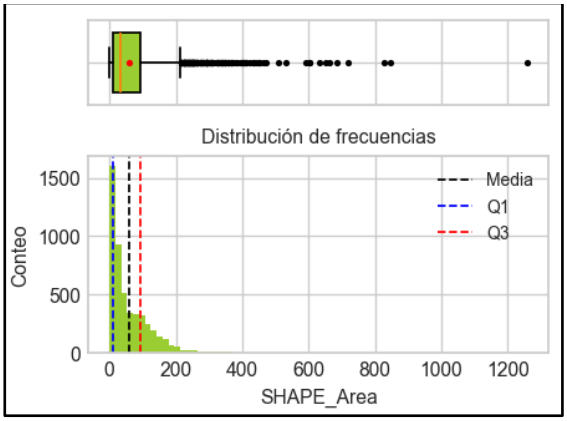


Figure 7. Size distribution of affected constructions

### 4.4 Environmental Damage and Debris

In addition to build infrastructure, significant impacts were recorded in mangrove ecosystems, whose degradation reduces natural protection against storms and undermines ecosystem services (Dutta Roy et al., 2024; Velázquez-Salazar et al., 2025). Added to this were the debris fields generated after the event, which remained on the island for months and whose removal has only recently begun through a clearance project. The accumulation of debris negatively affected environmental quality and tourism activity, generating critical points of visual pollution and sanitary risk.

Figure 8. Evidence of debris on Providencia Island

Figure 9. Evidence of environmental degradation and landscape alteration after Hurricane Iota

The spatial analysis of post-Iota debris reveals two complementary patterns. On the one hand, construction debris totaled 6.88 ha, distributed across 3,126 small-scale elements, reflecting the fragmentation of damage in the urban fabric. On the other hand, vegetative debris reached 121.95 ha with 2,505 polygons and large patches (up to 8.31 ha), suggesting extensive losses of tree cover and pressure on coastal ecosystems (Hernández-Hamón et al., 2024). Taken together, vegetative debris accounted for 94.66% of the total accumulated area, while construction debris, although more numerous, contributed 5.34% of the area. These results indicate that vegetation degradation, potentially including mangroves, reduced natural protection against storms (Dutta Roy et al., 2024; Velázquez-Salazar et al., 2025) and, combined with the persistence of debris fields, generated environmental and landscape impacts that affected tourism activity and posed health risks.

### 4.5 Territorial Implications

The results show that moderate and severe damage in large-scale buildings generates functional voids in both the urban and rural fabric, affecting social cohesion as well as the local economy. The loss of community and commercial infrastructures represents a disproportionate impact for the user population, making these spaces intervention priorities. In contrast, the high proportion of minor damage in housing opens the possibility for preventive structural reinforcement actions, with relatively smaller investments that could reduce the risk of collapse in future events.

Figure 10. Critical areas for urban and rural recovery after Hurricane Iota

## 5. Conclusions and Discussion

Hurricane Iota caused large-scale damage on Providencia Island, affecting a total of 3,079 buildings. When regrouping the results into three main categories, it is observed that 12% of the buildings showed minor damage, 9% moderate damage, and 32% severe damage, while the remaining 46% showed no visible impacts, although some correspond to reconstructed roofs.

The relationship between built surface and level of damage showed that larger buildings were more vulnerable to severe damage, which had disproportionate consequences on the island's social and economic dynamics.

From an environmental standpoint, the loss of vegetation cover, especially mangroves, and the accumulation of 121.95 ha of vegetative debris compared to 6.88 ha of construction debris reveal the magnitude of the impact on ecosystems and its implications for reducing natural storm protection.

The cartographic products generated (orthophoto mosaics, DSM, DTM, damage maps, and zoning maps) proved to be effective and replicable tools for post-disaster monitoring. Their resolution not only allowed for the quantification of damage but also for the prioritization of critical areas for reconstruction and the evaluation of the spatial distribution of impacts.

The prolonged persistence of debris on the island highlighted the need for more agile post-disaster waste management protocols, considering their environmental, landscape, and health impacts, as well as their effect on tourism activity.

The findings reinforce the importance of designing differentiated intervention strategies: reinforcing small-scale housing with low-cost solutions that reduce the risk of collapse, and ensuring the resilience of critical infrastructures through stricter building codes and maintenance plans adapted to climate risk scenarios.

Overall, the study not only provides a detailed diagnosis of the impact of Hurricane Iota but

also constitutes a key technical input for territorial planning and risk management in island contexts, integrating structural, environmental, and social components toward sustainable and resilient reconstruction.

The results obtained allow for a more detailed understanding of the dynamics of Hurricane Iota's impact on Providencia and its territorial implications. In quantitative terms, the classification of the damage shows that, although minor damages predominate in number, moderate and severe damages—particularly in large-scale buildings—generated the most significant impacts on the island's community and economic life. This finding is consistent with experiences in other island contexts, where collective infrastructures concentrate critical functions, whose loss disproportionately affects community resilience.

The relationship between building size and level of damage also provides relevant elements for interpretation. While single-family houses mostly presented minor or partial damage, large-scale buildings recorded a higher proportion of severe damage, confirming that exposure is measured not only by the number of structures but also by their surface area and territorial function. This duality highlights the need for differentiated strategies: reinforcing housing to reduce the risk of collapse, and at the same time establishing stricter design and construction protocols for community and service facilities.

From an environmental perspective, the loss of vegetation cover, and particularly the deterioration of mangroves, reinforces the scientific evidence that highlights their protective role against storms and hurricanes (Dutta Roy et al., 2024; Velázquez-Salazar et al., 2025). The degradation of these ecosystems not only increases the physical vulnerability of the territory but also compromises essential ecosystem services such as water regulation, coastal protection, and habitat provision (Krauss et al., 2023). The debris analysis complements this view by showing two distinct patterns: dispersed construction debris, reflecting building collapses, and extensive vegetative debris, indicative of the magnitude of environmental loss. The persistence of these debris fields for several months after the event generated secondary impacts on environmental quality, tourism, and public health—factors that were seldom considered in immediate post-disaster assessments.

In terms of land-use planning, Providencia is subject to regulatory determinants associated with the conservation of mangrove zones, riparian buffers, and environmental protection areas, which limit urban expansion and guide conservation-oriented land use. Official cartographic evidence therefore shows that the impacts of Iota must be analyzed not only in terms of material losses but also in relation to the compromise of areas with high environmental value and legal protection. This context highlights the need to link reconstruction with existing territorial planning instruments and environmental regulations in order to ensure the sustainability of recovery processes.

In summary, the discussion of results highlights that Hurricane Iota not only caused material damage but also exposed structural gaps in territorial planning, environmental management, and community preparedness for extreme events. This integrated perspective opens the possibility of proposing a reconstruction approach that combines physical recovery with the strengthening of social and ecological resilience.

## 6. References

Álvarez-Echeverry, A., Toro-Restrepo, L. J., Suárez-Gómez, J. A., & Osorio-Cano, J. D., 2025. Multitemporal analysis of land cover changes caused by Hurricanes Iota and Eta in the islands of San Andrés, Providencia, and Santa Catalina. DYNA-COLOMBIA.

ASPRS, 2014. ASPRS Positional Accuracy Standards for Digital Geospatial Data. American Society for Photogrammetry and Remote Sensing.

de Beurs, K. M., 2019. Hurricane damage detection on four major Caribbean islands.

International Journal of Applied Earth Observation and Geoinformation

Dutta Roy, A., Karpowicz, D. A., Hendy, I., Rog, S. M., Watt, M. S., Reef, R., Broadbent, E. N., Asbridge, E. F., Gebrie, A., Ali, T., & Mohan, M., 2024. Current status of remote sensing for studying the impacts of hurricanes on mangrove forests in the coastal United States. Remote Sensing, 16(19), 3596.

Esri, 2020. World Imagery Basemap. Website: www.arcgis.com (accessed July 20, 2023).

Google, 2020. Google Hybrid Imagery. Website: www.google.com/earth (accessed July 20, 2023).

Hernández-Hamón, H., Zapata-Ramírez, P. A., Vásquez, R. E., Zuluaga, C. A., Santana Mejía, J. D., & Cano, M., 2024. Rapid Remote Sensing Assessment of Impacts from Hurricane Iota on the Coral Reef Geomorphic Zonation in Providencia. Technical Report.

IDEAM, 2020. Instituto de Hidrología, Meteorología y Estudios Ambientales de Colombia. Website: www.ideam.gov.co (accessed July 20, 2023).

IGAC, 2020. Instituto Geográfico Agustín Codazzi, Official Cartography of Colombia. Website: www.igac.gov.co (accessed July 20, 2023).

Krauss, K. W., Whelan, K. R. T., Kennedy, J. P., Friess, D. A., Rogers, C. S., Stewart, H. A., Wilson Grimes, K., Trench, C. A., Ogurcak, D. E., Toline, C. A., Ball, L. C., & From, A. S., 2023. Framework for facilitating mangrove recovery after hurricanes on Caribbean islands. Review.

Pix4D, 2020. Pix4Dmapper Photogrammetry Software. Pix4D S.A., Lausanne, Switzerland.

Seaflower Foundation, 2023. Seaflower Biosphere Reserve. Website: seaflowerfoundation.org/reserva-de-la-biosfera.html (accessed July 20, 2023).

UNESCO, 2000. Seaflower Biosphere Reserve. Website: en.unesco.org/biosphere/lac/seaflower (accessed July 20, 2023).

Velázquez-Salazar, S., Valderrama-Landeros, L., Villeda-Chávez, E., Cervantes-Rodríguez, C. G., Troche-Souza, C., Alcántara-Maya, J. A., Vázquez-Balderas, B., Rodríguez-Zúñiga, M. T., Cruz-López, M. I., & Flores-de-Santiago, F., 2025. Mangrove damage and early-stage canopy recovery following Hurricane Roslyn in Marismas Nacionales, Mexico. Forests, 16(8), 1207.

Wingtra, 2020. WingtraOne Gen II VTOL Mapping Drone. Wingtra AG, Zurich, Switzerland.

# Urban Sprawl Detection and Land-Use Conflict Assessment in Santa Tecla Using Spectral Indices and Hybrid Machine Learning Classification of Sentinel-2A data.

Aguilar, Metzi

*Universidad Centroamericana José Simeón Cañas – maguilar@uca.edu.sv*

Abstract: This study evaluates the effectiveness of combining spectral indices to accurately delineate urban sprawl and identify land use conflicts in the municipality of Santa Tecla in El Salvador using remote sensing and machine learning techniques. Sentinel-2A satellite imagery was used to calculate the Normalized Difference Vegetation Index (NDVI) and the Normalized Difference Built-up Index (NDBI), which were then integrated into a hybrid classification approach combining unsupervised and supervised classification methods. This methodology enables precise mapping of urban expansion and facilitates the detection of inconsistencies between observed land use and existing regulatory planning instruments. The results indicate that the combined use of these indices significantly improves the identification of urban areas and associated land use conflicts, while reducing the need for extensive manual inspection. Moreover, the study identified land use conflicts, which are consistent with previous research highlighting a lack of planning largely due to the flexibility of regulatory planning instruments, thereby increasing socio-spatial vulnerabilities. Since the study was conducted using open source and free (*libre*) tools, it can be readily replicated, providing the basis for developing a generic methodology to monitor the spatio-temporal process of urbanization in the municipalities of the metropolitan area of San Salvador using open satellite images and current regulatory planning instruments as reference.

***Keywords***: remote sensing, machine learning, urbanization, unsupervised classification, supervised classification

## 1. Introduction

Currently, techniques such as remote sensing and machine learning make it possible to obtain and classify satellite images, quantify them, and measure urban growth for a given period, which facilitates the evaluation of the contrast between actual land use and the guidelines set out in planning instruments. In addition, there are global providers of free satellite images, such as the European Space Agency (ESA) and the United States Geological Survey (USGS), which allow these techniques to be applied to their products. Recent studies by Cavur (2019) and Makandar (2021) have successfully identified urban sprawl in other regions using remote sensing techniques, such as the use of vegetation/buildability indices and geoprocessing with Geographic Information Systems (GIS). In recent years, Nolè (2014) has demonstrated excellent results of this kind of research with the use of free (*libre*) tools.

A study conducted by Vargas et al. in 2020 at the National University of Costa Rica using Landsat satellite images concluded that the Central America region's capitals experienced

significant growth between 1975 and 2014, with a notable increase in the 1990s that consolidated and increased in 2014. As a result, the region has the highest urbanization rate in the world, according to the World Bank (2016) cited in Vargas (2020). The study also concluded that the total area of urban sprawl has tripled in the last forty years due to a process of peri-urbanization.

In the case of El Salvador, the urban sprawl of the San Salvador metropolitan area (AMSS, by its acronym in Spanish) has evolved spatially without planning and, as a result, in a disorderly manner, causing pressure, damage, and environmental deterioration in recent decades. The metropolitan region has undergone rapid urbanization, which has had negative effects on multiple socioeconomic and natural aspects (Fuentes, 2001). In the country, some methodologies are already available to identify the urban sprawl of the San Salvador metropolitan area. The planning office of the AMSS, OPAMSS (by its acronym in Spanish) has detected the urban sprawl from Sentinel-2A satellite images with unsupervised classifications and an expert validation process. A computer engineering thesis from the Universidad Centroamericana José Simeón Cañas (UCA) by Rosales et al. in 2022 also conducted the study "Analysis of urban expansion in the AMSS using remote sensing techniques and machine learning," which detected the urban sprawl from Landsat images for each year of a 30-year period (1991-2021) using Random Forest supervised classification, which was trained with a stratified sample of urban, non-urban, and water points. Studies of this nature at the international level have been developed by Kuc (2019) and Macarof (2017) and this one suggests improving the refinement methodology with the use of the normalized difference building index (NDBI), since these are indices that relate the electromagnetic spectrum and the percentage of reflectance associated with different materials (Kshetri, 2018).

## 2. Materials and Methods

### 2.1 Case study: city of Santa Tecla

#### 2.1.1 *Study area*

The analysis of the urban sprawl detection in this study focused on the city of Santa Tecla, which is the capital of the municipality of Santa Tecla in El Salvador. The municipality of Santa Tecla belongs to the metropolitan area of San Salvador, which is made up of 14 municipalities (Figure 1).


Figure 1. Case study location: city of Santa Tecla.

The city of Santa Tecla, which is the urban area of the municipality, is located at an altitude of approximately 920 meters above sea level. It is located in a valley and is surrounded by significant elevations, the most important of which are the San Salvador volcano, which belongs to the young volcanic chain north of the city, and the Cordillera del Bálsamo, which belongs to the coastal chain to the south. For this reason, according to Ministry of Environment, MARN (2004) the urbanizable area is limited to this space in the valley (Figure 1). The rural area of the municipality occupies a topographically very rugged territory and therefore according to

VMVDU (2011) that is not suitable for urbanization. In relation to the natural environment of the metropolitan area, this is an area that has historically been affected by multiple threats of geological origin (mass movements due to earthquakes in the Cordillera del Bálsamo), volcanic origin (volcanic eruptions or lahars), and hydrometeorological origin due to its geographical location. In 2001, as a result of a high-magnitude earthquake, there was a landslide in the northern part of the Cordillera del Bálsamo towards a residential area in the south of the city, "Las Colinas," which became a disaster due to the impact on 200 homes that were buried, the number of deaths, which was around 585, and the number of missing persons. The high social and economic vulnerability of the population, combined with a historical lack of territorial planning, has been the main cause of the disasters caused by these socio-natural events. The impacts of these disasters have also influenced changes in the urban structure, as they have forced the displacement of the population in the affected areas.

#### 2.1.2 *Land planning regulations*

Urban planning in the AMSS has a history of just over 50 years, and OPAMSS has developed a series of planning instruments aimed at organizing and planning the metropolitan area to provide technical criteria for planning. However, most of these instruments were not made official or implemented and have only served as technical references for the municipalities in this area. In 2004, at the request of the government, the National Plan for Territorial Planning and Development (PNODT) was elaborated, which included a proposal for regionalization and a system of cities for the country. However, this was never made official and remained only as a technical reference document. The National Law on Territorial Planning and Development (LNODT), approved in 2011, also had no impact. Although it took up the PNODT proposal, it was based on a departmental division rather than the recommended regionalization.

Currently, the Master Plan (*Esquema Director* in Spanish) is the official territorial planning instrument. It was developed by OPAMSS and approved in 2016, entering into force in 2017. The Master Plan complies with the legal framework of the metropolitan area and aims to address the current and future growth of the city through land use regulations. To make the application viable, regulations were included in 2018 to bring the proposal to life. The regulation involved amendments to the Regulations of the Law on Land Use Planning and Development for the metropolitan area and surrounding municipalities. One aspect worth highlighting is that these regulations enable the urbanization of non-urbanizable areas through a land use change appeal.

Based on an intermediate scenario for population, urban settlements, and infrastructure, the Master Plan was proposed for land use, urban treatments, and building regulations, including a strategic project bank and an environmental dimension. The 2030 intermediate scenario was the most realistic as it seeks territorial balance, considering financial and land limitations, combining low- and high-density areas.

Since the 1990s, limited developable land in Santa Tecla has forced the occupation of slopes and risk-prone areas, increasing geological hazards and flooding according to VMVDU (2011). The PNODT diagnosis by MARN (2004) stated that the 2001 earthquakes highlighted deficiencies in consideration of the geological environment for construction, development, and planning in the country. The current plan (Figure 2) shows that available land for development is already very limited.

Figure 2. Land uses proposed in the current Master Plan.

This has led to urban expansion in municipalities outside the metropolitan area to the west of the

city, and to a return to the compact city approach proposed in the Master Plan. It is important to mention that the current developable land proposed in the west of the city is very rugged. This developable land is located on slopes with a high susceptibility to landslides that have already been identified as high-risk areas in previous instruments and in the Master Plan itself, which classifies this area as having a higher tectonic density.

### 2.2 Datasets and software

For this study, vector data from the OPAMSS Master Plan geoportal were used, including the 2014 land use classification vector layer and the municipal boundary. In addition, bands B4, B8, and B11 of the harmonized high-resolution Sentinel-2A multitemporal satellite images corresponding to the 2018-2021 period were used to calculate raster images of the medians of the Normalized Difference Vegetation Index (NDVI) and the NDBI indices for the municipality of Santa Tecla. The Sentinel-2A sensor was selected because it provides free images with high spatial resolution suitable for the scale of the analysis. The resolution of the images is 10 meters for all bands, and in the case of band 11, it was resampled. The dataset is part of the Google Earth Engine (GEE) collection under the name S2_SR_harmonized. All layers were standardized using the WGS84 universal coordinate reference system, code EPSG: 4326. The images used correspond to the month of December of each year, as this is a dry month in El Salvador with low cloud cover. In addition, they were atmospherically corrected to filter out any clouds or to have a cloud cover percentage of less than 20%. For pre-processing, including image correction, index calculation, and data download, the GEE platform was used, which offers a free service for academic research. This platform was selected due to its faster cloud-based processing compared to local execution. In addition, GEE allows quick access to image datasets and, with a few lines of code, enables atmospheric corrections, cloud filtering, resolution resampling, and the calculation of vegetation and buildability indices. For image classification, free and open-source technologies were used: the R language (R Core Team, 2025) with its R Studio graphical interface and QGIS software (QGIS Development Team, 2025) for geoprocessing and visualization.

### 2.3 Methodology

To detect urban sprawl, this study used a hybrid classification technique (unsupervised and supervised). Sentinel-2A satellite images were used as input to calculate the normalized difference vegetation index (NDVI) and the normalized difference built-up index (NDBI). Once the urban sprawl was validated, land use conflicts were identified in a post-processing phase using raster analysis. Figure 3 shows the hybrid classification technique.

#### 2.3.1 *Preprocessing*

As a first step preprocessing was first carried out, which included the correction of satellite images, calculation of NDVI and NDBI indices, and downloading of raster images with the indices. Next, an image classification model was created that allows the urban area to be extracted for each year of the study period based on vegetation and buildability indices. This was done in a first phase using a hybrid method that combined the results of unsupervised classification with supervised classification. The accuracy of the urban area classification was then evaluated to validate the model. In a second phase, vector geoprocessing and map algebra techniques were used to identify land use conflicts, and finally, in a third phase, urbanization rates were calculated. The methodology was applied to a case study of the city of Santa Tecla. The first part of the preprocessing consisted of correcting satellite images, calculating vegetation and buildability indices, and downloading them. This stage was carried out using the GEE platform with a JavaScript script. The script obtains two raster images with the medians of the NDVI and NDBI indices for the indicated period and saves them in cloud storage for download. The vector layer of the land use classification of the Master Plan was preprocessed with QGIS software. First, a geometry correction was applied to ensure that subsequent geoprocesses would not have errors. Second, the layer was cropped with the municipality boundary to delimit the area of interest. As a final step, the land use

classification was dissolved by their geometries in order to simplify them.

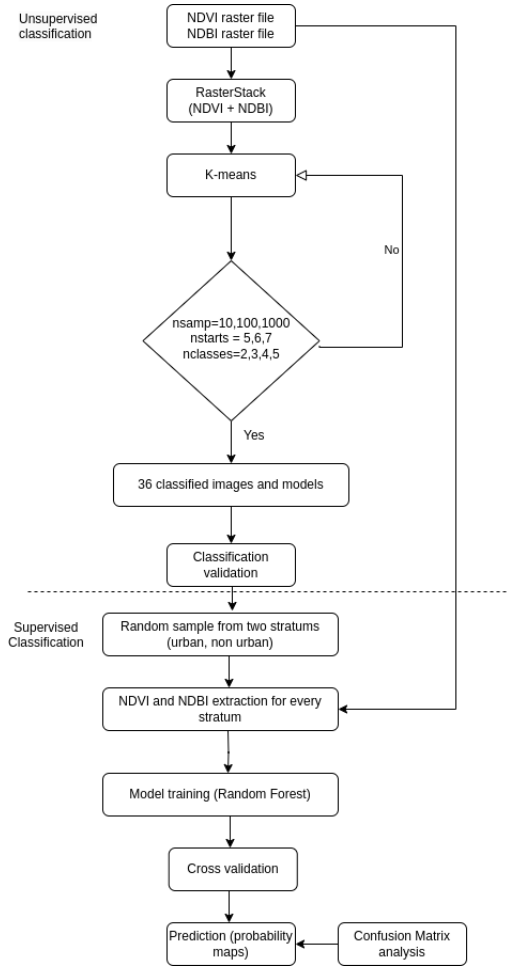


Figure 3. Hybrid classification methodology workflow.

2.3.2 *Unsupervised classification (K-means)*

The hybrid method for classifying satellite images from a four-year period consisted of dividing the period into two and creating a prediction model based on unsupervised classification (K-means) for 2018 and 2020, respectively. K-means algorithm is applied using different combinations of parameters (number of pixels in samples, number of random starting points and number of classes. Using this technique applied to vegetation and buildability indices, clustering patterns are found for several categories. At this stage, the expectation is that patterns describing urban areas and vegetation will be identified using algorithms. According to Berzal (2018) the clusters created by this type of classification must be validated by specialists in each phenomenon, as the results of this technique will always be subjective and there are no absolute answers. To perform this pattern validation procedure, QGIS software was used and, through visual inspection with the support of base satellite images, the image that best describes the clusters was selected.

2.3.1 *Supervised classification and validation*

To confirm that the patterns found with unsupervised classification can be modeled using machine learning, supervised classification was performed. This requires a stratified sample, i.e., proportional to each stratum (urban and non-urban). The sample was trained, and from this, a model was generated for 2018 and another for 2020. The parameters used in the R software for the Random Forest model were created using the CARET library (Kuhn, 2024), which allows for easy parameterization of the cross-validation stage and Random Forest algorithm. The cross-validation method used was Leave-One-Out Cross-Validation (LOOCV), which is an iterative method that uses all available data for both training and validation.

2.3.2 *Post-processing: raster analysis*

For post-processing, a raster analysis approach was chosen due to its computational advantages. To do this, it was necessary to rasterize the land use layer of the Master Plan. Of the possible land uses, only developable and non-developable land was considered. Urban land was not considered as it was not going to undergo any changes. In addition, rural land was not considered in the analysis either, as it is a category that is not being analyzed in this study. Next, raster calculations were performed using the R language and map algebra. The first case analyzed was the developable land in the Master Plan, which over time may remain undeveloped or become developed. The other case is that of non-developable land, which may remain undeveloped or have been developed. The latter case is the one that allows conflicts to be identified. By using masks applied to the input layer and the subtraction operation, new binary raster layers were obtained that allowed for automated comparison with the Master Plan and identification of land use conflicts.

## 3. Results

### 3.1 Phase 1: Application of the 2018-2021 model

Figure 4 shows the result of the urban sprawl delimitation for the period between 2018 and 2021 using the hybrid prediction model with Sentinel-2A satellite images. A higher resolution is observed than with Landsat images, and urban sprawl was classified quite accurately by refining the classification with the NDBI index. The best classification was obtained with 3 classes, a random sample of 1000 units, and 6 random starting points for the centroids. The model was able to classify accurately with an approximation of 99% for 2018 and a Kappa coefficient of 0.95, and for 2020, an approximation of 93% was obtained with a Kappa coefficient greater than 0.72. In general, the urban area appears stable for this four-year period, with no significant changes observed.

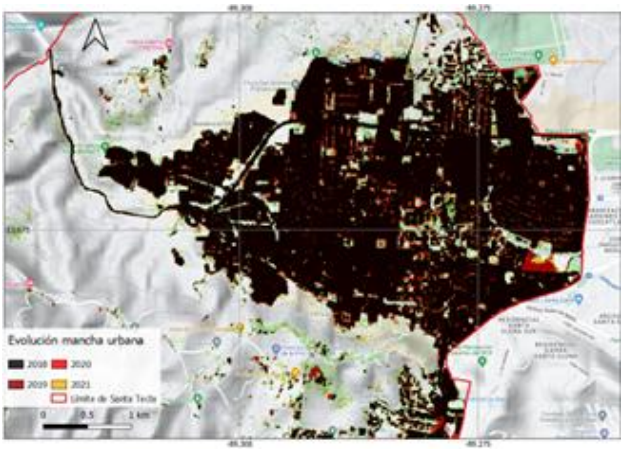


Figure 4. Estimation of urban sprawl for the period 2018–2021 using Sentinel-2A images.

### 3.2 Phase 2: Land use conflicts

In the maps in Figures 5 and 6, when comparing the areas of the Master Plan with the estimated image for 2018, the following can be observed: the evolution of urbanization on developable land (blue), developable areas (orange), and conflicts when urbanization has occurred in non-developable areas (red). The land use conflict was already present before. Previous studies show that the greatest conflict occurred between 2016 and 2018, exceeding limits and developing on non-developable land. As mentioned above, various planning instruments have indicated the high risk in Santa Tecla or San Salvador of urbanizing the slopes of the San Salvador volcano or the Bálsamo mountain range, as these are areas requiring maximum protection. This identified conflict must be validated by specialists. In addition, a few red pixels are observed in the rural area of the municipality because there are rural areas not covered by vegetation.

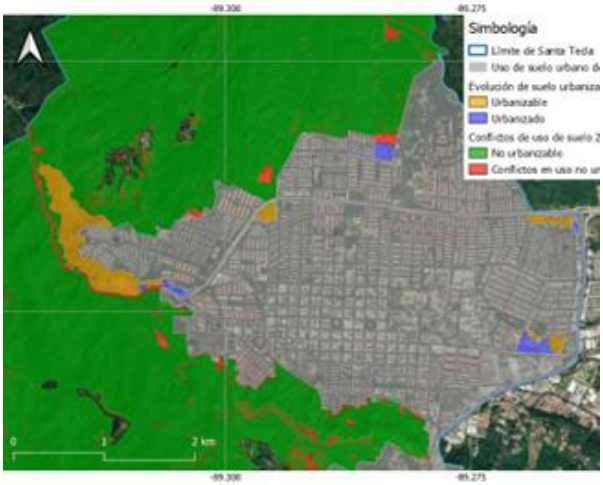


Figure 5. Land use conflicts in Santa Tecla based on data from the Master Plan by OPAMSS (2016).

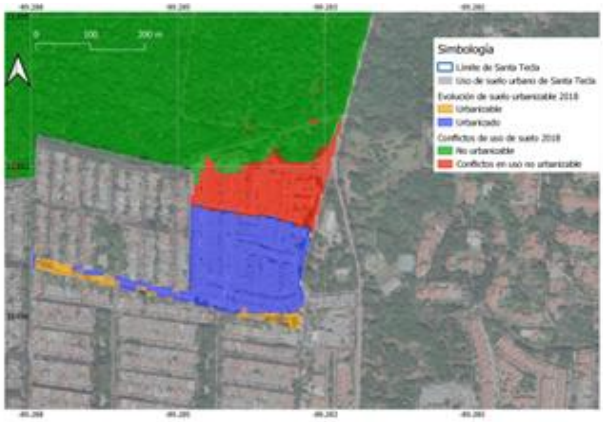


Figure 6. Close up of one land use conflict in Santa Tecla based on data from the Master Plan by OPAMSS (2016).

As can be seen on the maps, the city's horizontal expansion has slowed compared to previous years. In the results, it is also important to compare the urban area extracted with Landsat (see Figure 7) and contrast it with that extracted with Sentinel for the same period (see Figure 8). It can be observed that although Landsat offers the possibility of performing evolutionary analyses for long periods, it has the disadvantage of low resolution compared to Sentinel, which can lead to some errors in the calculations. On the other hand, combining NDBI and NDVI indices to extract the urban area proved to be more accurate, as shown in Figure 8.


Figure 7. Evolution 2018–2021 with Landsat. Based on data from Rosales et al. (2022)

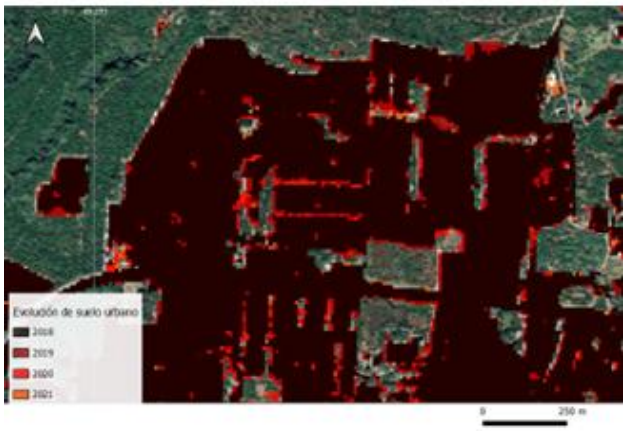


Figure 8. Evolution 2018-2021 with Sentinel. Created using QGIS and Google Hybrid base image.

## 4. Conclusions

The combination of the NDBI with the NDVI, as suggested in previous research, as inputs for a hybrid image classification method, made it possible to analyze the horizontal expansion of the Santa Tecla area over a given period of time, with an acceptable margin of error.

The study also identified land use conflicts, which are consistent with previous research highlighting that over the last 30 years, the application of the legal framework for land use and planning has been flexible: most instruments have not been formalized, and the regulation allows for the urbanization of non-urbanizable areas through land use changes, resulting in a disorderly process that has contributed to the construction of disaster risk in a climate change environment. A long-term land use and planning policy is needed that is in harmony with the natural environment and serves as a basis for planning instruments at the national, metropolitan, and local levels, so that there is coordination and risk areas are not proposed for urbanization. Since the study was conducted using open source and free (*libre*) tools, it can be readily replicated, providing the basis for developing a generic methodology to monitor the spatio-temporal process of urbanization in the municipalities of the metropolitan area of San Salvador using open satellite images and current regulatory planning instruments as reference.

## 5. Acknowledgements

The author would like to thank the director of the project, Dr. Ángel Miramontes Carballada, professor and researcher in the Department of Geography at the University of Santiago de Compostela, Galicia, and director of the CEER Foundation; to Felipe Carranza, independent researcher, for his contributions to the source code and to the free and open-source software development communities of R and QGIS for making their software available for GIS analysis and cartography and for their contribution to open science.

## 6. References

Berzal, F. (2018). Redes Neuronales and Deep Learning: Edición en Color. Independently Published.

Cavur, M. et al. (2019). Land use and land cover classification of Sentinel-2A: St Petersburg case study. The International Archives of the Photogrammetry, Remote Sensing and Spatial Information Sciences, XLII-1/W2.

COAMSS, OPAMSS, FundaUngo, UCA. (2016). Sistematización del esquema director Plan de desarrollo territorial del área metropolitana de San Salvador PDT-RMSS.

Fuentes, P. (2001). Síntesis del plan estratégico PLAMADUR AMSS. La Casa de todos. Universidad Centroamericana José Simeón Cañas.

Kshetri, T. (2018). NDVI, NDBI & NDWI Calculation Using Landsat 7, 8. https://www.linkedin.com/pulse/ndvi-ndbi-ndwi-calculation-using-landsat-7-8-tek-bahadur-kshetri/

Kuc, G., & Chormanski, J. (2019). Sentinel-2 Imagery for mapping and monitoring impreviousness in urban areas. The International Archives of the Photogrammetry, Remote Sensing and Spatial Information Sciences, XLII-1/W2.

Kuhn, M. (2024). caret: Classification and Regression Training (versión 6.0-94) [Paquete de R]. https://CRAN.R-project.org/package=caret

Macarof, P., & Statescu, F. (2017). Comparison of NDBI and NDVI as indicators of surface urban heat island effect in Landsat 8 imagery: A case study of IASI. PESD, 11(2).

Makandar, A., & Kama, S. (2021). Land use land cover study of Sentinel-2A and Landsat-5 images using NDVI and supervised classification techniques. https://doi.org/10.21917/ijivp.2021.0365

Ministerio de Medio Ambiente y Recursos Naturales, (MARN), Viceministerio de Vivienda y desarrollo territorial, y Ministerio de Obras Públicas (MOP). (2004). Plan nacional de ordenamiento y desarrollo territorial. Diagnóstico.

Nolè et al., G. (2014). Evaluation of urban sprawl from space using open-source technologies, Ecological Informatics. http://dx.doi.org/10.1016/j.ecoinf.2014.05.005

OPAMSS. (2016). Esquema director. Resumen ejecutivo. Área Metropolitana de San Salvador. https://opamss.org.sv/wp-content/uploads/2022/04/ResumenED.pdf

QGIS Development Team. (2025). QGIS Geographic Information System. Open-Source Geospatial Foundation Project. https://qgis.org

R Core Team. (2025). R: A language and environment for statistical computing. R Foundation for Statistical Computing. https://www.R-project.org/

Rosales, C., Merino, J., Renderos, D., & Trigueros, C. (2022). Análisis de la expansión urbana en el Área Metropolitana de San Salvador (AMSS) y el municipio de Colón de El Salvador.

Vargas, C., Orozco, R., Vargas, A., Aguilar, J. (2020). Metodología para la determinación del crecimiento de la mancha urbana en las capitales de la región centroamericana (1975-1995-2014)- Revista Geográfica de América Central, vol. 1, núm. 64, pp. 59-91

Viceministerio de vivienda y desarrollo urbano. (2011). Plan de desarrollo territorial para la subregión metropolitana de San Salvador. Santa Tecla. Síntesis Municipal.

# Drought monitoring in Coastal agricultural zones of Tola, Nicaragua using open-source satellite data

Emerson Javier Martínez García

*Independent Researcher, Stuttgart Technical University of Applied Science Alumni - ejmartinezg14@gmail.com*

**Abstract:** Drought is one of the most critical climatic hazards in Central America, with impact mainly on smallholder agriculture and water security. This study develops an open-source, satellite-based framework to monitor drought in the municipality of Tola, Rivas, Nicaragua, for the period 2019-2025. Sentinel-2 images were processed using Google Earth Engine, to generate three vegetation indices, each month; Normalized Difference Vegetation Index (NDVI), and two more indices derived from NDVI, Vegetation Condition Index (VCI), and Standardized Vegetation Index (SVI). CHIRPS precipitation data were also used, this to calculate six-month Standardized Precipitation Index (SPI-6) and see precipitation anomalies on time. Hotspots of recurrent vegetation stress were identified when VCI < 30% or SVI < −0.8 occurred in at least 33% of the months. Results show that vegetation anomalies closely follow rainfall variability, with SPI-6 highlighting drought episodes in 2019, 2022, and 2023. Hotspot analysis revealed that approximately 4.2% of Tola was consistently affected by drought, with overlapping areas between VCI and SVI marking the most reliable zones of vulnerability, the west part of the west side of the Area of Interest (AoI) was the most affected. The integration of precipitation anomalies and vegetation indices provides a scalable methodology for agricultural drought monitoring, giving local decision-makers critical information for risk management and adaptation planning.

***Keywords*:** Vegetation Indices, SPI, CHIRPS, Sentinel-2.

## 1. Introduction

Drought represents one of the most important environmental challenges in Central America, especially affecting agricultural productivity and rural livelihoods. In regions such as Tola[1], Rivas (Nicaragua), where rainfall variability is high (INETER, 2025), understanding that, the analysis of drought is critical for effective adaptation. Remote sensing offers a powerful solution: vegetation indices derived from satellite imagery provide spatially comprehensive and timely indicators of vegetation stress, while precipitation-based indices capture meteorological drivers and pattern of drought (Wenzhe, et al., 2016).

[1] Tola is characterized by a tropical climate, strong seasonal rainfall variability, and an economy largely dependent on agriculture and tourism.

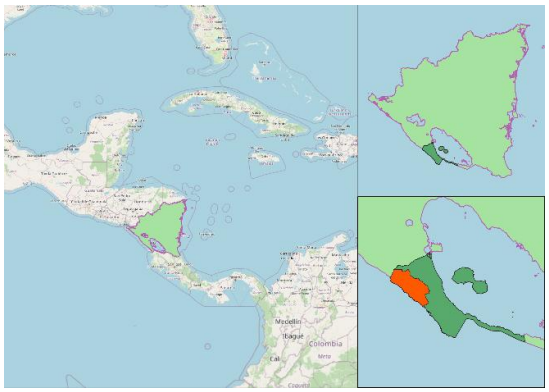

Figure 1 Research location

Among vegetation-based metrics, the **Vegetation Condition Index (VCI)**, which normalizes NDVI values by their historical minimum and maximum has been widely used to monitor drought intensity and severity (Binod, Qiuhong, Ximeng, Grebemedhin Gebremeskel, & Gyan, 2019). The **Standardized Vegetation Index (SVI)**, which expresses NDVI anomalies in terms of z-scores, enables the detection of significant departures from normal conditions (Peters, et al., 2002). On the meteorological side, the **Standardized Precipitation Index (SPI)**, particularly at multi-month scales, remains a standard tool to detect rainfall deficits and classify drought severity (Prajapati, et al., 2021).

Building on these methodologies, this study integrates vegetation and precipitation indices to characterize drought patterns in Tola between 2019 and 2025. The goal is to leverage high-resolution Sentinel-2 data for direct vegetation monitoring and CHIRPS precipitation data for rainfall anomalies, combining both into a hotspot analysis that highlights areas of recurrent drought stress. This integrated, open-source approach provides a scalable framework for agricultural drought risk monitoring in data-scarce settings (Lee, Kim, & Lee, 2021).

## 2. Methodology

This study was conducted in the municipality of Tola, Rivas, Nicaragua (476,5 km$^2$), a coastal agricultural area that is highly sensitive to rainfall variability and recurrent drought conditions. The analysis combined open-source satellite data and statistical methods to characterize vegetation stress and drought dynamics from 2019 to 2025. The approach relied on two complementary datasets: Sentinel-2 satellite imagery for vegetation monitoring (NDVI), specifically bands 4 for and band 8 for Near Infra-red for NDVI computation; and CHIRPS precipitation data for rainfall anomalies.

$$NDVI = \frac{NIR - Red}{NIR + Red} \quad (1)$$

Building on NDVI, the Vegetation Condition Index (VCI)[2] was calculated to place vegetation status in a relative context, comparing each observation with its historical minimum and maximum values within the study period.

$$VCI = \frac{NDVI - NDVI\_min}{NDVI\_max + NDVI\_min} \times 100 \quad (2)$$

This allowed us to identify whether a given month corresponded to unusually poor or favorable vegetation conditions. To further standardize the analysis, the Standardized Vegetation Index (SVI)[3] was applied, which expresses NDVI departures from the mean as a z-score. The SVI provides an anomaly-based perspective, facilitating the detection of abnormal vegetation stress relative to long-term patterns.

$$SVI = \frac{NDVI - \mu_{NDVI}}{\sigma_{NDVI}} \quad (3)$$

[2] The Vegetation Condition Index (VCI) normalizes NDVI values against their historical minimum and maximum, highlighting relative vegetation stress conditions.

[3] The Standardized Vegetation Index (SVI) expresses NDVI anomalies as z-scores, identifying significant departures from long-term vegetation conditions

Precipitation dynamics were analyzed using CHIRPS monthly rainfall data. From this dataset, standardized precipitation anomalies were computed. The SPI-6 was selected as the main reference because it best represents agricultural drought conditions and aligns with the temporal scale at which vegetation responds to rainfall deficits. The SPI categories (*Normal (≥ −0.99), Moderate (-1.0 to -1.49), Severe (-1.5 to -1.99), and Extreme (≤ −2.0)*) were used to classify drought severity consistently with widely adopted standards (McKee, Doesken, & Kleist, 1993).

$$SPI\text{-}6=\frac{P_6(t)\text{-}\mu_6}{\sigma_6} \quad (4)$$

All data processing was carried out in two main environments. Google Earth Engine (GEE) was used for pre-processing of Sentinel-2 imagery and CHIRPS rainfall, including cloud masking, filtering by date, monthly compositing (one image per month for NDVI, VCI and SVI), and clipping to the study AOI. The processed image collections were then exported as GeoTIFFs and CSVs for further analysis in Python, where statistical calculations, anomaly detection, and visualization were performed.

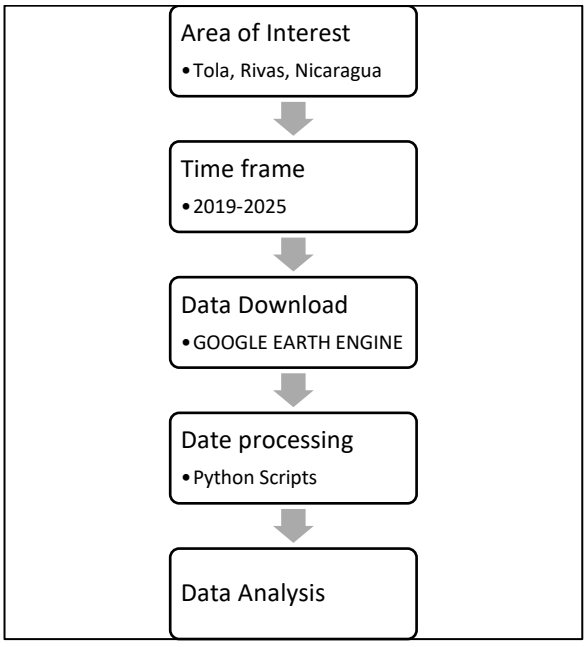


Figure 2 Methodology

A central part of the analysis was the hotspot detection. Vegetation hotspots were defined as pixels that repeatedly showed stress over time. For VCI, stress events were identified when values dropped below 30% (Bogale, Degefa, & Abebe, 2025), which indicates poor vegetation conditions relative to historical extremes. For SVI, stress was defined when values were lower than -0.75 (Fuentes, Padarian, & Vervoot, 2022), corresponding to one standard deviation below the mean and representing significantly abnormal vegetation conditions. A pixel was labeled as a hotspot when such events occurred in at least one third of the months in the period analyzed (Omar, Alasow, Farah, & Shahid, 2024). This frequency-based criterion allowed us to distinguish occasional stress from persistent drought-prone areas. By combining both indices, SVI-hotspots and VCI-hotspots where both indices consistently agreed, the latter being the most robust signal of recurrent drought vulnerability.

Rainfall anomalies and SPI categories were analyzed to evaluate the temporal evolution of droughts and their correspondence with vegetation stress. The SPI-6 series provided a standardized timeline for drought events. This integration of meteorological and vegetation-based indicators ensured that both the drivers and impacts of drought were accounted for.

## 3. Results

The analysis revealed clear spatial and temporal patterns of drought risk in Tola. Spatially, the vegetation indices hotspots map (Figure 3) shows that recurrent drought-prone areas are concentrated mainly in the northern-west part of the municipality. Red areas indicate VCI hotspots, orange areas show SVI hotspots, and black areas highlight the overlap where both indices detect consistent stress (main hotspots).

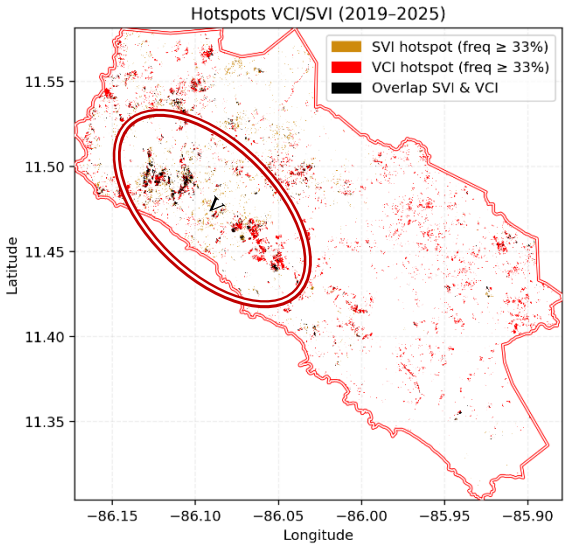


Figure 3 Vegetation Indices Hotspots Map

The overlap hotspots represent the most reliable zones of recurrent vulnerability (red and white circle), since they combine anomaly-based and condition-based evidence of stress. These areas, though smaller in extent (only black area is 0.4% of the AOI, approx.), provide key insights for local agricultural planning as they mark places where vegetation consistently fails to recover under rainfall deficits.

Average precipitation patterns derived from CHIRPS (Figure 4) complement this picture by showing spatial gradients of rainfall across the AOI. Northern-west parts receive less rainfall on average, while the southern and coastal zones are relatively with more rain. These rainfall gradients help explain why certain parts of Tola are more prone to recurrent vegetation stress.

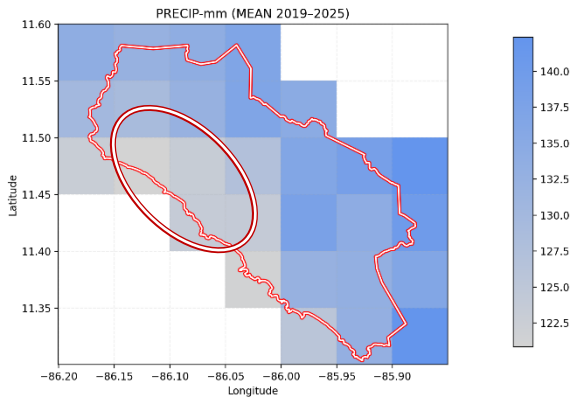


Figure 4. Average Precipitation Patterns

The CHIRPS analysis and vegetation index hotspot analysis demonstrate that the same zone within the AOI consistently experiences stress, which directly corresponds to the area most affected by agricultural difficulties linked to vegetation stress and limited water availability.

The SPI-6 timeline (Figure 5) offers a consolidated view of drought episodes. Moderate to severe droughts were detected in 2019, 2022, and 2023, aligning with observed drops in vegetation indices.

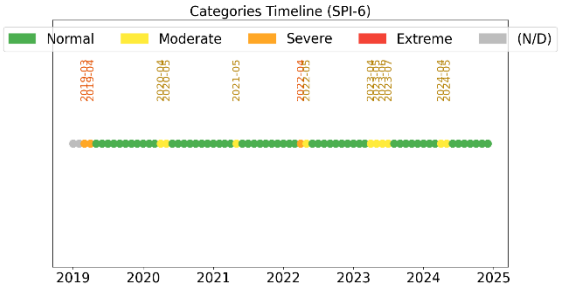


Figure 5 SPI-6 Precipitation Timeline

The timeline reveals how drought categories shift through time, with several months falling into moderate drought (yellow) and fewer into severe drought (orange). Importantly, the SPI-6 timeline corroborates vegetation stress observed in the indices, strengthening the case that rainfall anomalies are the main driver of drought impacts in the AOI.

Quantitative area statistics further confirm these findings. Hotspot area calculations indicate that about 3.5% of the AOI was affected by VCI-only hotspots, around 0.3% by SVI-only hotspots, and 0.4% by overlap hotspots. Altogether, approximately 4.2% of the municipal territory was under recurrent hotspot conditions between 2019 and 2025. While this may appear to be a relatively small fraction, it represents critical agricultural land that consistently experiences stress and thus carries disproportionate importance for food production and livelihoods. These results align with the interpretation of SPI-6, highlighting that drought events are uniformly distributed and affect specific locations and time periods.

## 4. Conclusions

This study demonstrates the value of integrating open-source satellite data for drought monitoring in data-scarce agricultural regions. By combining Sentinel-2 vegetation indices with CHIRPS precipitation anomalies and SPI analysis, we were able to capture both the drivers and impacts of drought in Tola, Nicaragua, during 2019–2025. The results show that vegetation stress strongly tracks rainfall variability, with SPI-6 successfully identifying key drought episodes. The hotspot analysis revealed that although only about 4% of the municipality was consistently classified as recurrently stressed, these areas represent critical zones of agricultural vulnerability, located in the north-west side of the AOI. The combined use of NDVI, VCI, SVI, and SPI thus provides a robust framework for local drought risk management, with potential for scaling to other regions of Central America.

## 5. Acknowledgements

Acknowledgements for the support and guidance of the professors at HFT Stuttgart for their academic encouragement and invitation to participate in this work. Special thanks are extended to the AGSE Team for providing the opportunity to present this research and for their financial support, which made participation possible.

## 6. References

*Assessment of Drought Indexes on Different Time Scales: A Case in Semiarid Mediterranean Grassland.* (2022). Basel: MDPI.

Binod, B., Qiuhong, T., Ximeng, X., Grebemedhin Gebremeskel, H., & Gyan, C.-S. (2019). *Spatial and Temporal Variation of Drought Based on Satellite Derived Vegetation Condition Index in Nepal from 1982–2015.* Basel: MDPI.

Bogale, T., Degefa, S., & Abebe, G. (2025). *Spatio-temporal variations of drought in the Welmel watershed, southeast of Ethiopia using the vegetation condition index and standardized precipitation index.* Addis Ababa: Springer Nature.

Fuentes, I., Padarian, J., & Vervoot, R. W. (2022). *Spatial and Temporal Global Patterns of Drought Propagation.* Sydney: Frontiers in Environmental Science.

Holyman, Z. D., Bocinsky, R. K., & Jencso, K. G. (2022). *Drought assessment has been outpaced by climate change: empirical arguments for a paradigm shift.* Montana: Nature Communications.

INETER. (20. 08 2025). *ineter.gob.ni*. Von mapserveride.ineter.gob.ni: https://mapserveride.ineter.gob.ni/IDE-LLUVIAS/ abgerufen

Lee, S.-J., Kim, N., & Lee, Y. (2021). *Development of Integrated Crop Drought Index by Combining Rainfall, Land Surface Temperature, Evapotranspiration, Soil Moisture, and Vegetation Index for Agricultural Drought Monitoring.* Basel: MDPI.

McKee, T. B., Doesken, N. J., & Kleist, J. (1993). *The relationship of drought frequency and duration to time scales.* Eighth Conference on Applied Climatology.

Omar, A. O., Alasow, A. A., Farah, A. A., & Shahid, S. (2024). *Spatiotemporal Analysis of Agricultural Drought Severity and Hotspots in Somaliland* . International Journal of Sustainable Development and Planning.

Peters, A. J., Walter-Shea, E., Lei, j., Viña, A., Hayes, M. J., & Svoboda, M. D. (2002). *Drought monitoring with NDVI-based Standardized Vegetation Index.* Nebraska: American Society for Photogrammetry and Remote Sensing.

Prajapati, V., Kaur, K., Khanna, M., Narayan Sahoo, R., Singh, M., & Singh, D. K. (2021). *Drought monitoring using multi-time-scale Standardized Precipitation Index.* The Indian Journal of Agricultural Sciences: The Indian Journal of Agricultural Sciences.

Wenzhe, J., Lifu, Z., Qing, C., Dongjie, F., Yi, C., & Qingxi, T. (2016). *Evaluating an Enhanced Vegetation Condition Index (VCI) Based on VIUPD for Drought Monitoring in the Continental United States.* Basel: MDPI.

# GNSS Space Geodesy and its Contribution to Society and the Understanding of Earth Dynamics in Colombia, South America: Achievements and Challenges

Héctor Mora-Páez [a, b] , Carlos Franco-Pineda [b], José-Fernando Mejía-Correa [a]

[a] *Universidad de Manizales – hmora@umanizales.edu.co ; jfmejia@umanizales.edu.co*
[b] *Agustín Codazzi" Geographical Institute hector.mora@igac.gov.co; carlos.franco@igac.gov.co*

**Abstract**: The northwestern corner of South America, where Colombia is located, southeastern Central America and the Caribbean region, is a zone characterized by high tectonic and volcanic complexity as a result of the interaction of the Cocos, Nazca, Caribbean and South American tectonic plates, and several geological blocks wedged between them, resulting in representative interplate deformation, a high density of geological faults, widely distributed seismicity and a representative number of active volcanoes. Under this premise, geodesy emerges as the discipline that allows for the detection of changes associated with the occurrence of geodynamic phenomena, supporting the challenges of understanding global change and contributing to improving the knowledge required for disaster risk management. Therefore, geodetic infrastructure is of vital importance for understanding Earth's dynamics and is also the cornerstone for generating geodetic data, a fundamental input in the geospatial information value chain. This information is required by society for its application in various areas of knowledge and in the management of land use planning, cartographic production and infrastructure and cadastre projects, among others, to facilitate intelligent decision-making aimed at meeting the needs of society. The actions taken in Colombia to implement a geodetic infrastructure that meets the country's needs are presented, as well as the challenges that arise with this type of instrumentation.

***Keywords:*** GNSS, geodetic networks, reference frame, velocity field, ionosphere

## 1. Introduction

The Earth is a dynamic planet, constantly changing, where internal and external processes interact, generating changes on diverse timescales. Understanding these processes is essential for addressing the current challenges facing society in scientific, social, political, and economic aspects. This requires international cooperation under the concept of scientific diplomacy for a common purpose, as well as the commitment and active participation of governments globally. This means that it is necessary to have the technological resources that allow for permanent monitoring of the Earth. In this sense, geodesy plays a crucial role in this endeavor as a fundamental science. Modern geodesy contributes to our understanding of the Earth system through three fundamental pillars: geometry and kinematics; rotation and orientation; and the gravity field, which are intrinsically connected and change as a consequence of the dynamic processes occurring in the Earth system (Angermann et al., 2022). This paper presents the progress made in Colombia in the implementation of

geodetic technology, primarily by government institutions, the achievements obtained, and highlights how the currently installed geodetic infrastructure is essential for the development of national-scale projects.

## 2. Geodynamics of Colombia and neighbouring region

The northwestern corner of South America, where Colombia is located, the southeastern of Central America and the Caribbean plate correspond to a wide plate convergence boundary, The tectonic and volcanic activity in this zone is a result of the interaction of the oceanic Cocos, Nazca and Caribbean plates, and the continental South American plate as well as the North Andean, Maracaibo, Chocó and Panamá blocks wedged in between as is proposed by several authors, Figure 1, mentioned by Mora-Páez et al., (2018). This highly complex tectono-dynamic situation of intense intraplate deformation is observed in a high density of geological faults, most of which are considered active or potentially active over northwestern South America and southeastern Central America. Also, the seismicity is spread over a broad area across the wide plate boundary in northwestern South America, Central America, and southwestern Caribbean, whose complexity was referred as a “Wide Plate Margin”, (Trenkamp et al., 2002). This, coupled with a potential of large magnitude megathrust and tsunami events related to the Pacific subduction zone, means that a high percentage of Colombia’s population lives under a constant threat of unannounced large magnitude earthquakes and tsunamis, with a potential of inflicting great damage in terms of loss of lives and destruction of infrastructure (Hermelin, 2005). Additionally, another threat is posed by the many active volcanoes located on the North Andean region that have a potential for devastating eruptions as shown in the Armero disaster of November 13, 1985, the second worst volcanic disaster in the last century, caused by the eruption of the Nevado del Ruiz volcano, Colombia (Banks et al, 1990).

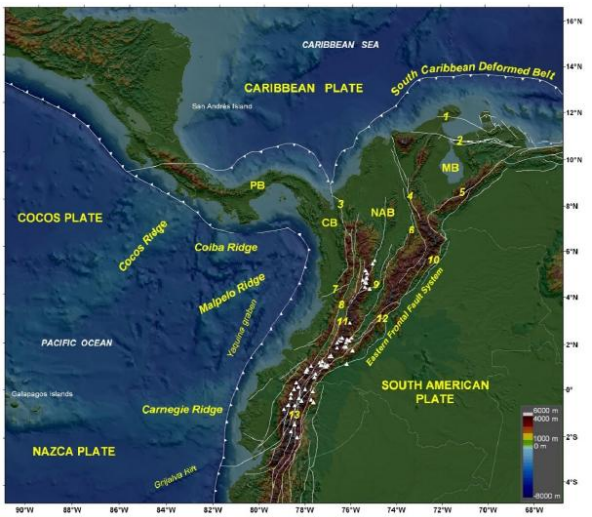


Figure 1. Geodynamics in the region. Geological blocks: MB (Maracaibo B.), NAB (North Andean B.), PB (Panama B.), CB (Choco B.). Faults: 1 (Cuisa F., 2 (Oca F.), 3 (Uramita F.), 4 (Bucaramanga-Santa Marta F.), 5 (Boconó F.), 6 (Suarez F.), 7 (Garrapatas F.), 8 (

Given the tectonic complexity in the mentioned region and the high possibility of occurrence of large earthquakes and tsunamis as well as volcanic eruptions among other hazards of geological origin, systematic studies to establish a monitoring system for the current situation of crustal deformation using space geodesy techniques is of great importance (Mora-Páez, 2020).

## 3. Implementation of Colombia's national geodetic network: stages and current status

Following the tragic eruption of the Nevado del Ruiz Volcano on November 13, 1985, with more than 25,000 deaths, a volcanic monitoring program was initiated, employing different types of disciplines and methods, including geodetic techniques based initially on terrestrial methods, which have supported the analysis of volcanic deformation. Thus, volcanological observatories were established over time in the cities of Manizales, Popayán, and Pasto to monitor active volcanoes located in the northern, central, and southern volcanic zones (Banks et al., 1990; Vargas et al., 2018; Ordóñez et al., 2024).

Colombia began exploring the use of GPS technology through the CASA (Central and South America) GPS Project, which established a network of stations in Colombia,

Costa Rica, Panama, Ecuador, and Venezuela. This project, funded by the National Science Foundation (NSF) of the United States, enabled data collection at geodetic monuments through episodic field campaigns between 1988 and 1998. This project was coordinated in the country by the former INGEOMINAS (Colombian Institute of Geology and Mining), now the Geological Survey of Colombia (SGC), and included the participation of the "Agustín Codazzi" Geographic Institute (IGAC), (Mora-Páez et al., 2020).

In 1993, the SIRGAS (South American Geocentric Reference System) Project was established during an international meeting in Paraguay by representatives of most South American countries, the International Association of Geodesy (IAG), the Pan American Institute of Geography and History (PAIGH), and the former National Imagery and Mapping Agency (NIMA), now the National Geospatial Intelligence Agency (NGA). Under the framework of this project, field campaigns named SIRGAS95 and SIRGAS2000 were carried out with the purpose of establishing a unique reference frame for the American continent (Fortes et al., 2006).

In Colombia, the IGAC began the process of installing permanent operating stations in 1995, which form part of the network known as MAGNA-ECO. Based on the SIRGAS stations, the IGAC began to determine the National Geocentric Reference Frame named MAGNA-SIRGAS. This geodetic reference is made up of approximately 70 stations with national coverage, of which six are continuously operating GPS stations, 8 are SIRGAS field stations, and 16 are from the aforementioned CASA project (IGAC, 2004).

In 1994, under a cooperation agreement signed between NASA and the former Geological Survey of Colombia (INGEOMINAS), the first permanent GPS station known as BOGT was installed in Colombia as part of the global FLINN (Fiducial Laboratories for an International Natural Science Network), now integrated into the IGS (International GNSS Service. Its operation and maintenance have since been the responsibility of the SGC (Mora-Páez et al., 2020).

Upon completion of the CASA project, the former Ingeominas considered as important to begin a systematic process of expanding the geodetic network, as the appropriate way to improve the knowledge of crustal deformation in Colombia. Thus, under the framework of the institutional project "Survey of Geodynamic Information of the Colombian Territory", the coverage of the network was expanded, including the volcanic zones of Nevado del Ruiz volcano and the Galeras volcano, given their activity conditions (Mora-Páez et al., 2020). In 2007, Ingeominas began implementing the National Network of Satellite Geodetic Stations for geodynamic purposes, according to a proposal conceived by Mora-Páez (2006). This project, known as GeoRED, corresponds to the Spanish acronym for "Geodesia: Red de Estudios de Deformación" and is based on the use of space geodetic technology to study geodynamics in the northwestern corner of South America and to establish the current state of the earth´s crustal strain, both interplate and intraplate, and of the current seismic cycle, among other research purposes. Thus, a process of installing permanent, continuously operating geodetic stations (cGNSS) was initiated, as well as field stations for data collection under the modality of episodic field campaigns (eGNSS), located in the continental and insular zones, (Mora-Páez et al., 2018; Mora-Páez et al., 2020).

The Colombian government institutions "Agustín Codazzi" Geographic Institute and the Geological Survey of Colombia, to fulfill their respective institutional missions, had implemented their respective geodetic networks (MAGNA-ECO and GeoRED, respectively) with clearly defined purposes. However, starting in 2018, based on an inter-institutional cooperation agreement, the two entities began working together to expand the national geodetic infrastructure based on continuously operating GNSS geodetic stations (cGNSS). These stations have been distributed throughout Colombia, considering

the guidelines established in the National Geodetic Infrastructure Strengthening Plan, developed with support from the World Bank (IGAC-SGC, 2019). These stations are identified as GNSS Colombia, which, together with the previously installed stations, allow for the introduction of various types of geodetic applications, both general and scientific. The two institutions have also strengthened and updated their respective high-level computing systems.

One of the key elements that has that has driven the strengthening of the national geodetic infrastructure, partly with international cooperation, is the National Multipurpose Cadastre policy, led by the IGAC, that is based on the La Havana Agreement signed in 2016 by the national government with one of the guerrilla groups to end the armed conflict in the pursuit of peace.

Geodetic infrastructure enables the generation of geodetic products and the effective provision of geodetic services, facilitating the execution of operations aimed at producing geospatial information, such as cartography at different scales, as well as supporting cadastral surveys, infrastructure projects, hydrographic, and geophysical studies, among others. It also allows for the execution of research projects on Earth's dynamics regarding the Earth´s crustal deformation and its potential association with earthquakes occurrence and volcanic eruptions, mass movements, subsidence, supporting actions related to disaster risk management, studying sea level variations, and performing ionosphere and troposphere studies, among others. Furthermore, this infrastructure is a source of data for academic exercises that support the training of future professionals in study fields related to geospatial information and its application in other disciplines. In this way, it is possible to provide information inherent to the territory for its environmental planning, providing valuable input to the digital transformation by guaranteeing timely access to geodetic data for various purposes, as well as promoting scientific and technological development, with the integration of other disciplines, and supporting actions related to the Sustainable Development Goals.

Figure 2 shows the current state of the existing geodetic infrastructure in Colombia owned by government institutions and private companies. Many these stations constitute the National Geodetic Network, whose data is processed and distributed through the National Geodetic Control Center, a platform for managing geodetic products and services in Colombia (IGAC, 2024).

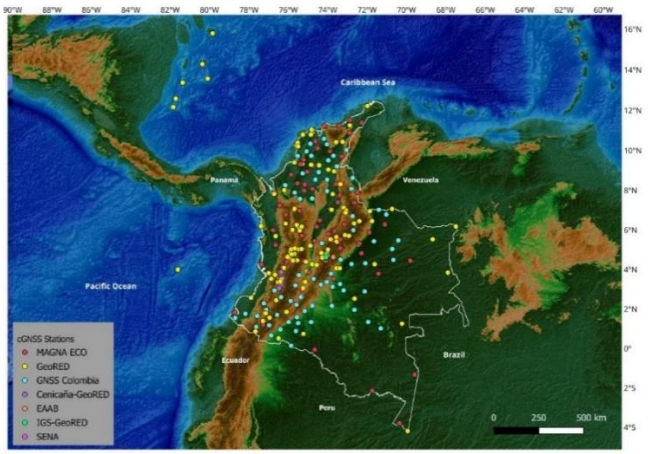


Figure 2. Current geodetic infrastructure installed in Colombia

## 4. Achievements and challenges

In addition to the aforementioned implementation and densification of geodetic networks in Colombia, several achievements have been obtained using geodetic data, including the following.

Adoption by the IGAC of the National Geocentric Reference Frame named MAGNA-SIRGAS as the only official datum, taking into account considerations regarding the International Terrestrial Reference Frame (ITRF) and its adoption by the International Association of Geodesy (IAG) and the International Union of Geodesy and Geophysics (IUGG), and SIRGAS as a densification of the ITRF and the recommendation of its adoption at the 7th. Cartographic Conference for the Americas of the United Nations in 2001 (IGAC, 2005).

The GeoRED project that belongs to the SGC, has contributed to the generation of GNSS geodesy-based models aimed at understanding

the deformation of the Earth's crust in the area of interest, such as the estimation of motion rates of the tectonic plates, Figure 3, as well as the North Andean Block (Kobayashi et al., 2014; Mora-Páez et al., 2016; Pérez et al., 2018; Mora-Páez et al., 2019; Mora-Páez and Audemard, 2021; Snay et al., 2021, Jarrin et al., 2023a, 2023b).

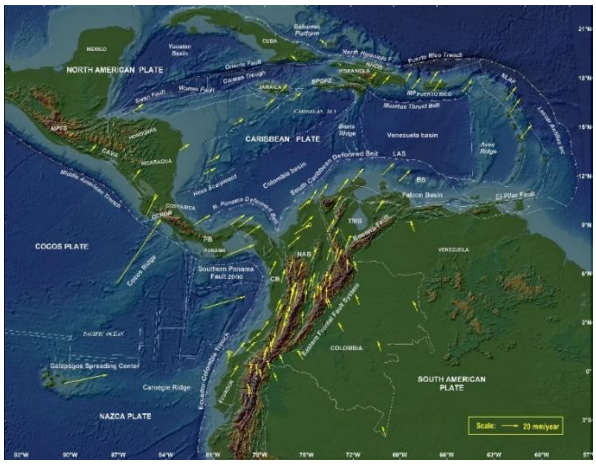


Figure 3. GPS velocities relative to ITRF2014 in the study region. Mora-Páez and Audemard, (2021).

In addition, intraplate coupling models have been generated along the Nazca subduction zone on the Pacific coast (Sagiya & Mora-Páez, 2020) and along the Caribbean cost of Colombia (Lizarazo et al., 2021), and their potential generation of earthquakes and tsunamis; calculation of the Euler pole for the motion model of the South American plate and the North Andean Block (Mora-Páez et al., 2019); estimation of the continuum model of the geodetic velocity field in the northwestern corner of South America and southeastern Central America (Terán-Enríquez et al., 2024). Additionally, by combining GNSS positioning geodesy and InSAR geodesy, progress was made in the study of the subsidence of the cities of Bogotá (Mora-Páez et al., 2020) and Cartagena (Restrepo-Angel et al., 2021).

The use of data from geodetic stations located in Colombia for atmospheric studies allows for the establishment of some analyses, although in fact, this field deserves further exploration. Regarding ionospheric studies, the analyses carried out by Nava et al., (2016), Rodríguez-Zuluaga et al., (2016) and Zewdie et al., (2021) are highlighted, while in the troposphere, those carried out by Hernández-Decker et al. (2018), Casallas et al., (2021) and Mackern et al. (2020) can be mentioned.

Of great importance and significance for Colombia is the recent initiative of the "Agustín Codazzi" Geographic Institute, through its Geographic Information Management Directorate, to develop, for the first time, a Strategic Geodesy Plan with a 10-year vision.

The plan is based on six strategic objectives, establishing actions aimed at developing and implementing activities to maintain and improve existing geodetic infrastructure, as well as those related to gravimetry and geomagnetism, providing data, services, and products that facilitate their use in various geodetic applications, as well as promoting research and fostering the creation of national and international cooperation mechanisms. The strategic objectives are:

- Strengthen, expand, and maintain the geodetic, gravimetric, and geomagnetic infrastructure of Colombia as sources of continuous data and information to effectively meet the needs of the country and its users.
- Guarantee the quality and availability of geodetic, gravimetric, and geomagnetic data in a timely manner.
- Promote scientific and technological development in geodesy, gravimetry, and geomagnetism.
- Promote the strengthening of capacities and competencies in geodesy, gravimetry, and geomagnetism to ensure the availability of suitable, qualified, and motivated personnel to face the challenges posed by the Earth's dynamics and those demanded by society.
- Promote the inclusion and integration of geodesy, gravimetry, and geomagnetism into public policies and strategies.

- Build appropriate mechanisms for the dissemination, socialization, and social appropriation of knowledge about geodesy, gravimetry, and geomagnetism, as well as geospatial information, as essential elements for the country´s development.

However, and without a doubt, the main challenge is associated with the sustainability of the installed geodetic infrastructure, which guarantees the operation, as well as the maintenance and replacement of the respective instrumentation due to damage or compliance with the life cycle, which implies having the support of the central government as well as establishing plans and programs by the institutions responsible for the operation of geodetic networks, under consideration of the importance and significance of this type of infrastructure for the generation of geospatial products of different kinds and with different purposes.

Furthermore, in order to start studying the ionosphere using GNSS geodetic data, the University of Manizales, located at the Manizales city, through its Faculty of Science and Engineering, established a cooperation agreement with the Radio Space Physics Laboratory of the University of New Brunswick, Canada, and the Abdus Salam International Centre for Theoretical Physics in Trieste, Italy. Under this cooperation frame, a GNSS geodetic station was installed and became part of the Eclipse NB network, a Network of Low-Cost GNSS Receivers for Studying the Ionosphere (Kashcheyev et al., 2025). Thus, the University of Manizales has initiated a process of institutional strengthening to explore this topic of study, starting now with the study of the ionosphere under the cooperation agreement established with the aforementioned international institutions. Under this initiative, the fundamental purpose and challenge of this university is to employ artificial intelligence techniques to optimize and automate data processing tasks, as well as perform noise analysis and corrections in the analysis of geodetic time series, interpret results, among many options enabled by this technological development.

## 5. References


Angermann, D., Pail, R., Seitz, F. and Hugentobler, U. (2022). Mission Earth. Geodynamics and Climate Change Observed Through Satellite Geodesy. Springer-Verlag GmbH, Germany, 254 p.

Banks, N.G., Carvajal, C., Mora, H. and Tryggvason, E., (1990). Deformation monitoring at Nevado del Ruiz, Colombia - October 1985-March 1988. In: N. Williams (Editor), Nevado del Ruiz Volcano, Colombia, I. J. Volcanol. Geotherm. Res., 41: 269-295.

Casallas-García A., D. Hernández-Decker, H. Mora-Páez, (2023), Understanding convective storms in a tropical, high-altitude location within-situ meteorological observations and GPS-derived water vapor, Atmósfera 36(2), 225-238, https://doi.org/10.20937/ATM.53051

Fortes, L. P., Lauría, L., Brunini, C., Amaya, W., Sánchez, L., Drewes, H. and Seemüller, W., (2006), Current Status and Future Developments of the SIRGAS Project, In: Univ.-Prof. Dr.-Ing. Prof. h.c. Günter Seeber anlässlich seines 65. Geburtstages und der Verabschiedung in den Ruhestand. Wissenschaftliche Arbeiten der Fachrichtung Geodäsie und Geoinformatik der Universität Hannover Nr. 258: 59-70, 2006

Hermelin, M. (2005). Desastres de Origen Natural en Colombia 1979–2004. Medellín, Colombia. Ed. Fondo Editorial Universidad EAFIT, 247. ISBN: 958-8173-89-2 (in spanish)

Hernández D, D, H. Mora Páez, L. Cardona, (2018), Aplicaciones atmosféricas de GNSS en Colombia, Geología Colombiana 41: 55-60, Bogotá, Colombia (in spanish)

IGAC (2004), Aspectos prácticos de la adopción del Marco Geocéntrico Nacional de Referencia MAGNA-SIRGAS como datum oficial de Colombia, Instituto Geográfico Agustín Codazzi, 97 p. (in spanish).

IGAC, (2005), Resolución 068, por la cual se adopta como único datum oficial de Colombia el Marco Geocéntrico Nacional de Referencia: MAGNA-SIRGAS (in spanish)

IGAC, (2024), Resolución 1771 por medio de la cual se oficializa el portal web (htps://redgeodesica.igac.gov.co/)

IGAC-SGC (2019), Plan de Fortalecimiento Infraestructura Geodésica Nacional, Instituto Geográfico Agustín Codazzi y Servicio Geológico Colombiano, (in spanish).

Jarrin P., J.-M- Nocquet, F. Rolandone, H. Mora-Páez, P. Mothes and D. Cisneros, (2023), Current motion and deformation of the Nazca Plate: new constraints from GPS Measurements, Geophys. J. Int 232, 842-863, https://doi.org/10.1093/gji/ggac353

Jarrin P., J.-M. Nocquet, F. Rolandone, L. Audin, H. Mora-Páez, A. Alvarado, P. Mothes., F. Audemard, J.C. Villegas-Lanza and D. Cisneros, (2023), Continental block motion in the northern Andes from GPS Measurements, Geophys. J. Int 00, 1-31, https://doi.org/10.1093/gji/ggad294

Kashcheyev, A., Nava, B., Watson, C., Jayachandran, P. T., & Langley, R. B. (2025). EclipseNB: A network of low-cost GNSS receivers to study the ionosphere. Space Weather, 23, e2024SW004194. https://doi.org/10.1029/2024SW004194

Kobayashi D., P. LaFemina, H. Geirsson, E. Chichaco, A. Abrego, H. Mora and E. Camacho, (2014), Kinematics of the Western Caribbean: Collision of the Cocos Ridge and Upper Plate Deformation, Geochem. Geophys. Geosyst. 15, 1671-1683, doi:10.1002/2014GC005234.

Lizarazo S.C., T. Sagiya, H. Mora-Páez, (2021), Interplate coupling along the Caribbean coast of Colombia and its implications for seismic/tsunami hazards, J. South Am. Earth Sci. 110, https://doi.org/10.1016/j.jsames.2021.103332.

Mackern, M. V., Mateo, M. L., Camisay, M. F., & Morichetti, P. V., (Tropospheric Products from High-Level GNSS Processing in Latin America, In: J. T. Freymueller, L. Sanchez (eds.), Beyond 100: The Next Century in Geodesy, IAG Symposia 152, https://doi.org/10.1007/1345_2020_12

Mora-Páez H. and F. Audemard (2021), GNSS Networks for Geodynamics in the Caribbean, Northwestern South America, and Central America. In: Geodetic Sciences - Theory, Applications and Recent Developments, B. Erol & S. Erol (eds), Intechopen Book Series, 22 p., doi: 10.5772/intechopen.97215

Mora-Páez H., Kellogg, J. N., Freymueller, J., Mencin, D., Fernandes, R., Diederix, H., LaFemina, P., Cardona-Piedrahita, L., Lizarazo, S., Peláez-Gaviria, J. R., Díaz-Mila, F., Bohórquez-Orozco, O., Giraldo-Londoño, L., Corchuelo-Cuervo, Y. (2019), Crustal Deformation in the Northern Andes – Space Geodesy Velocity Field, J. South American Earth Sciences 89 (76-91), doi: 10.1016/j.jsames.2018.11.002

Mora-Páez H., Peláez-Gaviria, J.R., Diederix, H., Bohórquez-Orozco, O., Cardona-Piedrahita, L., Corchuelo-Cuervo, Y., Ramírez-Cadena, J., and Díaz-Mila, F. (2018), Space Geodesy Infrastructure in Colombia for Geodynamics Research, Seismological Research Letter 89 (2A), 446-451, doi: 10.1785/0220170185

Mora-Páez, H. (2006). Red Nacional de Estaciones Geodésicas Satelitales GPS con propósitos geodinámicos, Propuesta de proyecto presentada al Ministerio de Minas y Planeación Nacional, Documento BPIN (in spanish)

Mora-Páez, H., (2020), Crustal Movements in Colombia based on GPS Space Geodesy with the GeoRED Network, PhD Dissertation, Department of Earth and Environmental Sciences, Graduate School of Environmental Studies, Nagoya University, Japan, https://nagoya.repo.nii.ac.jp/records/29808

Mora-Páez, H., D. J. Mencin, P. Molnar, H. Diederix, L. Cardona-Piedrahita, J.-R.

Peláez-Gaviria, and Y. Corchuelo-Cuervo (2016), GPS velocities and the construction of the Eastern Cordillera of the Colombian Andes, Geophys. Res. Lett., 43, 8407–8416, doi:10.1002/2016GL069795.

Mora-Páez, H., Kellogg, J. N. and Freymueller J. T., (2020). Contributions of Space Geodesy for Geodynamic Studies in Colombia: 1988 to 2017, The Geology Book, Colombian Geological Survey, Vol 4, Ch. 14, https://doi.org/10.32685/pub.esp.38.2019.14

Nava, B., Rodríguez-Zuluaga, J., Alazo-Cuartas, K., Kashcheyev, A., Migoya-Orué, Y., Radicella, S.M., Amory-Mazaudier, C., and Fleury, R. (2016), Middle- and low-latitude ionosphere response to 2015 St. Patrick's Day geomagnetic storm, J. Geophys. Res. Space Physics, 121, 3421–3438, doi:10.1002/2015JA022299.

Ordoñez, M., Idárraga, J., Adamo, R. and Battaglia, M., (2024). Geodetic monitoring of the recent activity and the dome forming eruption at Nevado del Ruiz (Colombia), 2010–2023. Sci Rep 14, 21441 https://doi.org/10.1038/s41598-024-72058-y

Pérez O. J., S. G. Wesnousky, R. De La Rosa, J. Márquez, R. Uzcátegui, C. Quintero, L. Liberal, H. Mora-Páez and W. Szeliga, (2018), On the interaction of the North Andes plate with the Caribbean and South American plates in northwestern South America from GPS geodesy and seismic data, Geophys. J. Int 214, 1986-2001, doi: 10.1093/gji/ggy230

Restrepo-Ángel, J.D., H. Mora-Páez., F. Díaz, M. Gorvocin, S. Wdowinski et al. (2021), Coastal subsidence increases vulnerability to sea level rise over twenty first century in Cartagena, Caribbean Colombia. Sci Rep 11, 18873 https://doi.org/10.1038/s41598-021-98428-4

Rodríguez-Zuluaga, J., S. M. Radicella, B. Nava, C. Amory-Mazaudier, H. Mora-Páez, and K. Alazo-Cuartas (2016), Distinct responses of the low-latitude ionosphere to CME and HSSWS: The role of the IMF Bz oscillation frequency, J. Geophys. Res. Space Physics, 121:11528 doi:10.1002/2016JA022539.

Sagiya, T. and Mora-Páez, H. (2020). Interplate coupling along the Nazca subduction zone on the Pacific coast of Colombia deduced from GeoRED GPS observation data. In: Gómez, J. & Pinilla–Pachon, A.O. (editors), The Geology of Colombia, Volume 4 Quaternary. Servicio Geológico Colombiano, Publicaciones Geológicas Especiales 38, p. 499–513. Bogotá. https:// doi.org/10.32685/pub.esp.38.2019.15

Snay R., Saleh, J., Dennis, M., DeMets, C. and Mora-Páez, H., (2021), Expanding TRANS4D´s Scope to Include 3D Crustal Velocity Estimates for a Neighborhood of the Caribbean Plate, J. Surveying Engineering, doi:10.1061/(ASCE)SU.1943-5428.0000377

Terán-Enríquez, I. K., Mora-Paéz, H., Gutiérrez, N., Atapuma, P., Martínez, G. (2024). Velocidades geodésicas GNSS en la esquina norocidental de Suramérica y sureste de Centroamérica: modelo continuo. Bogotá D.C.: Servicio Geológico Colombiano, 19 p.

Trenkamp, R., Kellogg, J.N., Freymuller, J.T., Mora, H., 2002. Wide plate margin deformation, South Central America and Northwestern South America, CASA GPS observations. J. S. Am. Earth Sci. 15, 157–171.

Vargas C., Caneva, A., Monsalve, H., Salcedo, E., and Mora, H. (2018), Geophysical Networks in Colombia, Seismological Research Letter 89 (2A), 440-445, doi: 10.1785/0220170168

Zewdie, G. K., Valladares, C., Cohen, M. B., Lary, D. J., Ramani, D., & Tsidu, G. M. (2021). Data-driven forecasting of low-latitude ionospheric total electron content using the random forest and LSTM machine learning methods. Space Weather, 19, e2020SW002639. https://doi.org/10.1029/2020SW002639

# Multitemporal Monitoring of Subsidence in Bogotá D.C. Using PS-InSAR Techniques: Geoinformatics Integration for Sustainable Urban Management

Paola Andrea Suarez Jaimes*, Edilberto Suárez Torres and José Luis Herrera Escorcia

*Universidad Distrital Francisco José de Caldas, Facultad de Ingeniería; * pasuarezj@udistrital.edu.co*

Land subsidence poses a significant challenge to urban sustainability, particularly in Bogotá D.C., which suffers from the overexploitation of groundwater and the rapid, inadequately planned growth of the city. This research applies PS-InSAR methodologies to study surface uplift and subsidence in Bogotá during the 2022–2023 period. Using Sentinel-1 imagery, approximately 2.6 million persistent scatterer points were obtained, allowing the identification of subsidence rates (LOS) of up to 7.5 cm/year in key industrial and residential areas. These results were corroborated with geotechnical and land-use data to define deformation patterns potentially caused by subsurface structures and human interaction in the area. Deformation and its temporal behavior were studied through interferometric processing, which, when combined with spatial-geopositional analysis, formed the foundation of the research. The development of this technique enabled systematic and continuous monitoring—an essential input for adjusting and updating urban planning and risk management models—reaffirming the utility of PS-InSAR. This geoinformatics approach is valuable for developing early warning systems, mitigation strategies, and resilient cities, thereby modernizing urban management. Integrating the PS-InSAR technique in urban monitoring alongside cadastral information, urban regulations, and geotechnical models will significantly enhance spatial planning decision-making. This research contributes to the design of open-data early warning systems using Earth observation techniques tailored for Latin American cities.

***Keywords:*** Subsidence, PS-InSAR, geoinformatics, ground deformation

# Dealing Dengue Fever with Drone Technology

Md Zahid Hasan Siddiquee

*GIS & RS Specialist, ICT Division, Institute of Water Modelling (IWM) – zhs@iwmbd.org*

**Abstract**: Dengue fever has escalated into a severe public health crisis in Dhaka, Bangladesh, with record-breaking outbreaks in recent years. In 2023 alone, Bangladesh reported 321,179 confirmed cases and 1,705 deaths—a dramatic surge from 62,382 cases and 281 deaths in 2022 (DGHS, Bangladesh). As Dhaka accounted for over 60% of national cases, the urgency for innovative vector control strategies is clear. This study explores the application of unmanned aerial vehicles (UAVs) to rapidly identify Aedes aegypti breeding grounds in selected urban areas of Dhaka during 2019. UAVs offer distinct advantages over traditional ground surveys, including efficient coverage of large or inaccessible areas, very high-resolution spatial data acquisition, and reduced human resource demands. Aerial imagery was processed using advanced analytical techniques to detect potential breeding habitats, such as waterlogged flowerpots, rooftop tires, and stagnant water pockets in building crevices. The analysis provided spatially explicit insights into the distribution of breeding sites, with high-resolution imagery enabling the identification of even small, overlooked water-holding containers critical for targeted interventions. The results demonstrate UAVs' potential to deliver timely, comprehensive data to Dhaka City Corporation, empowering data-driven vector control efforts. By optimizing resource allocation and precision, this approach could significantly reduce dengue transmission and mitigate future outbreaks, ultimately saving lives in a city repeatedly crippled by the disease.

***Keywords:*** Dengue Fever, Unmanned Aerial Vehicle, Public Health, Geographic Information System, Photogrammetry, Saving Lives

## 6. Introduction

The rapid and unprecedented rise of dengue fever cases in Bangladesh, particularly in the urban megacity of Dhaka, highlights a critical public health challenge. The traditional methods of vector surveillance and control, often relying on manual ground surveys, have proven insufficient to keep pace with the swift proliferation of the Aedes mosquito, the primary vector for the dengue virus.

This study introduces an innovative and integrated approach to vector control by leveraging Unmanned Aerial Vehicles (UAVs) and geospatial technologies. The aim is to move beyond conventional methods and provide a scalable, precise, and data-driven solution for identifying and managing dengue breeding grounds.

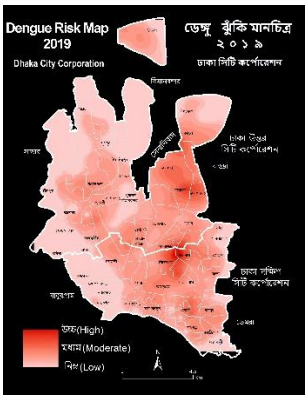


Figure 1. Heat-Map of Dengue in Dhaka City.

This initiative is involved with the use of drone-based photogrammetry and mapping of dengue vector breeding habitats.

## 7. Methodology

The study was carried out in selected dengue-prone areas of Dhaka in 2019. UAV platforms equipped with high-resolution cameras were deployed to capture orthophotos of urban landscapes. The workflow included image acquisition, preprocessing, and object detection for identifying water-holding containers. Geospatial analysis techniques were applied to detect potential mosquito breeding sites. The methodological framework involved four main stages such as follows

### 7.1 Project locations

The research was conducted in selected urban areas of Dhaka identified as dengue "hot spots," including Mirpur, Narinda, and Komlapur. The methodology involved three key phases: flight planning, image acquisition and processing, and habitat identification.

### 7.2 Flight Planning and Image Acquisition

For each target area, flight missions were planned using the Drone Deploy application to ensure comprehensive and systematic coverage. The UAVs were flown at an average altitude of 250 feet, which resulted in high-resolution aerial images with a Ground Sample Distance (GSD) of less than 5 cm. This high level of detail was crucial for identifying small and discrete breeding habitats.

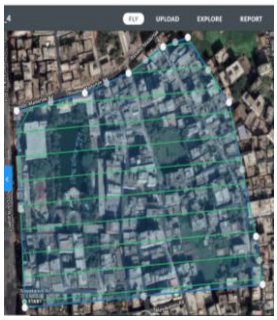

Figure 2. Flight planning for data acquisition.

### 7.3 Image Processing

The raw aerial images were processed using Pix4DMapper photogrammetry software. The processing workflow included three main stages: pre-processing, Point Cloud Generation, and DSM-Orthophoto Generations. The orthophoto served as the primary source for visual analysis and habitat identification.

### 7.4 Identification of Habitats

The generated ortho-mosaics were meticulously analysed to identify potential Aedes breeding sites. The analysis focused on finding water-holding containers, which included but were not limited to: discarded tires on rooftops and open grounds, waterlogged flower pots and buckets, open water tanks, polythene bags and plastic containers, and stagnant water in crevices and gutters on building rooftops. The analysis provided spatially explicit insights into the distribution of these breeding sites across the study areas.

## 8. Results and Discussion

The UAV survey successfully identified numerous micro-habitats of Aedes aegypti that are typically missed by conventional field surveys. High-resolution orthophotos enabled detection of rooftop water tanks, discarded tires, and small water-logged containers. GIS-based spatial mapping revealed clustering of breeding hotspots in high-density residential zones.

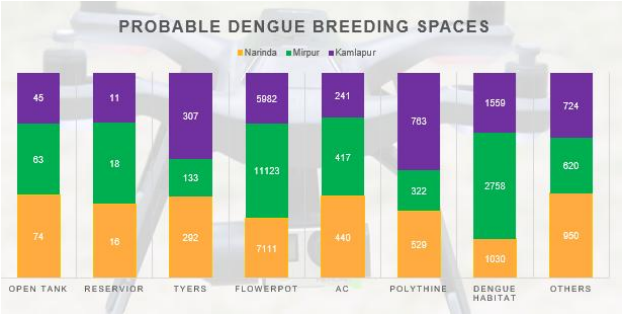


Figure 3. Dengue breeding sites in different locations.

The study demonstrates how UAV-enabled approaches provide timely, accurate, and actionable information for vector control authorities.

## 9. Conclusion

This study highlights the transformative role of UAVs in dengue prevention efforts. Drone technology enhances surveillance by covering large areas quickly, detecting hidden breeding sites, and supporting targeted interventions. Integration of drone imagery with GIS-based analysis provides a scalable solution for urban vector management.

With continued advancements in UAV sensors, machine learning, and real-time data integration, future dengue control programs can become more proactive and effective.

The findings of this study form the basis of a proposed integrated decision support system (DSS) for dengue control. This system goes beyond simple mapping and aims to connect various activities in a cohesive workflow. The proposed integrated system, which includes crowdsourcing and near-real-time mapping capabilities, offers a scalable model for urban public health management. By leveraging these modern technologies, authorities can implement more efficient and precise vector control measures, significantly reducing dengue transmission and, most importantly, saving lives. This research serves as a blueprint for how geoinformatics can be applied to mitigate future outbreaks and build a more resilient urban environment in the face of escalating climate and health crises.

This integrated approach enables city corporations to move from reactive to proactive, data-driven vector control strategies, optimizing the use of resources and maximizing the impact of interventions.

## 10. References

Directorate General of Health Services (DGHS), Bangladesh (2023). Dengue Situation Report.

WHO (2022). Dengue and Severe Dengue Factsheet.

Ritchie, S. A. (2018). Dengue Vector Control: New Tools & Strategies. Trends in Parasitology.

Vasconcelos, P. F. (2020). Global Dengue Epidemiology Trends.

# Multi-criteria proposal model for forest fire prediction based on the use of information processed in IA and the role of quantum sensors in Colombia.

Maria Paula Campos Diaz [a], William Benigno Barragan Zaque[a,b]

[a] *Forest Engineering Student - mpcamposd@udistrital.edu.co, 2nd Author- wbarraganz@udistrital.edu.co,*
[b] *Specialist in Geographic Information Systems and MSc in Photogrammetry and Geoinformatics, Universidad Distrital Francisco José de Caldas and University of Applied Sciences Stuttgart,*

**Abstract**: This article proposes a multicriteria model for predicting forest fires in the Cerros Orientales of Bogotá, integrating climatic and topographic variables through the Analytic Hierarchy Process (AHP). Meteorological data from IDEAM stations and a high-resolution raster model (1 m/pixel) were used to calculate ignition risk per spatial unit. The pairwise comparison matrix showed high consistency (CR ≈ 0.0074), highlighting precipitation and temperature as predominant factors, followed by slope and elevation. The model identified critical zones with south-western orientation and flammable vegetation, consistent with patterns of solar exposure and biomass accumulation. Furthermore, the future incorporation of quantum sensors is proposed to enhance environmental monitoring accuracy, along with the use of quantum computing to simulate fire propagation scenarios and optimize firebreak placement. These technological advances, combined with multicriteria approaches and machine learning algorithms, strengthen predictive capacity and preventive risk management. The study area, near Aguas Claras and the El Delirio reserve, was selected for its ecological significance and vulnerability to fire.

***Keywords:*** Wildfires, multi-criteria models, AHP, Quantum technology, Quantum sensors

## 1. Introduction

Wildfires are a recurrent global issue with multiple climatic and social origins, generating profound economic, ecological, and social impacts. Their effects are reflected in soil degradation, alteration of water resources, loss of biodiversity, deterioration of flora and fauna, as well as damage to material assets and the quality of life of human communities. The increasing frequency of these events, closely linked to climate change, has intensified the need to develop predictive models that enable anticipation and mitigation. In this context, scientific research has explored various approaches, including multitemporal series analysis, logistic regression, multinomial logistic regression, and more recently, the use of artificial intelligence (Umaña Ramírez, 2017).

In Colombia, the Cerros Orientales of Bogotá represent a priority setting for environmental management due to their high biological richness and the pressures derived from urbanization and climate change. The area near Aguas Claras, Cerro Guanosco, and the El Delirio reserve constitutes a representative zone for studying these dynamics (Rojas Botero, 2017). Previous research has documented the region's floristic diversity: 7,604 individuals belonging to 106 species and 46 families have been recorded, with a marked predominance of

native species. The greatest diversity is concentrated in dense shrublands, where species such as Fuchsia boliviana, Varronia cylindrostachya, and the invasive Ulex europaeus exhibit high ecological importance values. These findings reflect early successional processes and underscore the significance of these ecosystems as spaces for natural regeneration.

Technological advances have opened new possibilities for addressing this challenge. Currently, remote sensors, imagery, and satellite data play a fundamental role in environmental monitoring. However, the large volume of generated information demands robust systems for processing. Here, artificial intelligence becomes an indispensable tool, enabling agile and efficient analysis of large datasets. In parallel, quantum technologies are emerging as a disruptive alternative with the potential to revolutionize the field: their processing capabilities allow for the simulation of multiple fire scenarios in reduced timeframes, thereby improving the precision and effectiveness of monitoring and prediction.

This article offers a theoretical review of current methods for wildfire prevention and risk mapping, with particular emphasis on multicriteria models. These models allow for the integration of diverse approaches and variables that influence fire occurrences such as climatic, topographic, and environmental factors—in order to build more precise and adaptable predictive systems.

In this context, the use of quantum science and technology is proposed, developed from derivative technologies for advanced data processing, enabling the simulation of multiple fire occurrence scenarios. This innovation aims to expand analytical capacity and enhance the fidelity of predictive models by simultaneously evaluating various combinations of critical variables.

As part of the research, an initial model was developed and applied to a 2 km² area in the Cerros Orientales of Bogotá, Colombia, near Aguas Claras in the locality of San Cristóbal. This model focused on the influence of precipitation and temperature as determining factors, serving as an example of how climatic variables can be integrated into predictive systems. It is expected that future models will incorporate topographic elements—such as slope and elevation—with greater prominence to enrich the analysis from additional perspectives.

Finally, the future implementation of quantum sensors for field data collection is proposed. These sensors will enable more precise and real-time information acquisition, strengthening the capacity of specialized algorithms to generate highly reliable predictive models that are closely aligned with real-world conditions.

## 2. Background

### 2.1 Wildfires: Definition and Impact

Wildfires are uncontrolled disturbances that affect vegetation and ecosystem services, generating significant social and economic impacts (Umaña, 2017; Caride, 2022). In Colombia, their recurrence is primarily associated with the use of fire in agricultural practices and the expansion of the urban frontier, which increases the exposure of strategic ecosystems to ignition and propagation processes.

### 2.2 Wildfires in the Cerros Orientales

The Eastern Hills of Bogotá, covering approximately 14,170 hectares and ranging in elevation from 2,600 to 3,500 meters above sea level, exhibit high susceptibility to wildfires due to both natural and anthropogenic factors. The presence of highly flammable exotic species, such as gorse (Ulex europaeus), pine, and eucalyptus, has significantly contributed to the accumulation of combustible biomass, thereby increasing the risk of fire spread (Universidad del Rosario, 2024). Recent studies have employed tools such as map algebra and the FARSITE simulation software to model ignition and propagation scenarios, integrating variables including slope, vegetation, temperature, precipitation, and wind direction, to generate spatially explicit wildfire risk maps (Morales Salguero, 2017; Verano Velásquez, 2013).

### 2.3 Current Prediction Techniques and Wildfire Risk Mapping

Internationally, adaptive wildfire prediction systems have been developed that combine

statistical and evolutionary approaches. One example is the S2F2M model, along with evolutionary algorithms applied in Argentina, which allow for multiple simulations under different parameter sets to align predictions with actual fire behavior. Although these methods outperform traditional models in terms of accuracy, they face notable limitations: S2F2M requires extended computation times to yield reliable results, while evolutionary algorithms struggle to adapt to abrupt environmental changes during fire propagation (Rodríguez Aseretto et al., 2007).

#### 2.3.1 *Multicriteria Models*

In parallel, multicriteria methods have become key tools in wildfire risk assessment, as they enable the integration of environmental, topographic, and socioeconomic variables within a spatial framework (De Vicente & Crespo, 2012). Among these, the Analytic Hierarchy Process (AHP) has been widely applied to weight factors such as slope, temperature, humidity, and vegetation cover, with successful applications in Turkey, Greece, and Spain for susceptibility mapping (Saaty, 2008; Demir & Akay, 2024). Other approaches, such as the Analytic Network Process (ANP), have proven useful in scenarios where interdependencies between factors—such as the interaction between climate and topography—play a decisive role in fire propagation. Additionally, methods like TOPSIS and VIKOR have been used to establish threat levels by calculating the proximity of each spatial unit to ideal solutions, facilitating the prioritization of areas for prevention and restoration (Chen, 2000; Opricovic & Tzeng, 2004).

### 2.4 Machine Learning and Hybrid Approaches

In recent years, machine learning (ML) models such as Random Forest, Support Vector Machines (SVM), and deep neural networks have demonstrated remarkable predictive capabilities by processing large volumes of multitemporal data and complex wildfire-related variables (Fan et al., 2024; Zhou et al., 2025). An emerging research line seeks to integrate these algorithms with multicriteria models, combining the explanatory and hierarchical strengths of AHP with the predictive power of ML—opening new possibilities for improving risk management and prevention (Jain et al., 2020).

### 2.5 Quantum Science

Quantum science emerged in the early 20th century as a response to the limitations of classical physics in explaining phenomena at the subatomic scale. Its starting point was Max Planck's work in 1900, in which he introduced the concept of energy quanta to resolve the blackbody radiation problem (Garritz, 2014). Later, Niels Bohr proposed an atomic model incorporating discrete energy levels, which helped explain atomic stability and emission spectra. These advances laid the foundation for the development of quantum mechanics—a theory that redefined the understanding of matter and energy by introducing principles such as wave-particle duality and Heisenberg's uncertainty principle.

Throughout the 20th century, quantum mechanics became a fundamental theoretical framework across various scientific disciplines, including chemistry, computer science, and molecular biology. In quantum chemistry, for instance, models such as valence bond theory (Slater and Pauling) and molecular orbital theory (Hund and Mulliken) enabled precise descriptions of molecular electronic structures (Garritz, 2014). More recently, methodologies like density functional theory have expanded the possibilities for simulation and prediction in complex systems. These developments have positioned quantum science as a cornerstone of technological innovation and a deep understanding of natural processes—justifying its inclusion as a conceptual reference in advanced environmental models.

### 2.6 Quantum Technology

Quantum technology represents a revolution in information processing, grounded in the fundamental principles of quantum mechanics such as superposition, entanglement, and interference. Unlike classical systems, quantum devices—such as quantum computers—use qubits that can represent multiple states simultaneously, enabling the resolution of complex problems with exponential efficiency (Ramírez Puertas, 2021). This capability has

opened new possibilities in fields such as cryptography, molecular system simulation, logistics optimization, and machine learning. Moreover, platforms like IBM Qiskit have democratized access to quantum programming, allowing researchers and students to experiment with algorithms such as Grover and Deutsch-Jozsa in virtual environments (Ramírez Puertas, 2021). Collectively, quantum technology not only x computational boundaries but also raises ethical and technical challenges for its safe integration into society.

Complementarily, quantum computing has been applied in recent studies to optimize the placement of firebreaks—critical areas for containing fire spread—using quantum optimization algorithms, which have outperformed traditional methods in operational simulations (Dent et al., 2025). Additionally, research led by NASA explores the use of quantum machine learning to enhance wildfire segmentation and detection from satellite imagery, enabling faster and more accurate processing of large geospatial datasets in global monitoring systems (NASA, 2023). These advances position quantum technology as a critical component in the evolution of digital wildfire management systems, strengthening resilience and response capacity in increasingly adverse environmental contexts.

#### 2.6.1 *Quantum Sensors*

Quantum temperature sensors represent an emerging technology with significant potential for environmental monitoring and wildfire management. These tools enable highly precise and stable measurements, surpassing conventional sensors in accuracy and providing reliable real-time data. The study on quantum temperature sensors conducted by Oukaira, Ettahri, and Lakhssassi (2024) demonstrates that these sensors can deliver “ultra-precise measurements with lower average error and reduced standard deviation compared to conventional sensors, indicating improved measurement stability.” Their integration with intelligent systems facilitates early detection of temperature changes, optimizing response to critical events and strengthening environmental management. The performance of quantum sensors is largely determined by the sensor material, with nitrogen-vacancy (NV) centers in diamonds, quantum semiconductors, and superconductors standing out to date.

Among the sensors applicable to wildfire monitoring and prediction, the quantum sensor prototype UIC-01 is notable for its ability to measure photosynthetically active radiation (PAR) in the vegetation canopy—key information for assessing plant productivity and stress (Barradas et al., 2023). PAR measurement enables the detection of variations in photosynthetic activity, which may indicate changes in biomass and the availability of vegetative fuel, thereby contributing to the identification of areas at higher wildfire risk.

## 3. Methodology and Materials

**3.1 Study Area** The study area is in the northeastern sector of the city, near the Aguas Claras neighborhood, Cerro Aguanoso, and the El Delirio reserve. Elevation ranges from 2,600 to 3,500 meters above sea level, within a temperate cold climate characterized by temperatures between 8–14 °C and annual precipitation ranging from 1,000 to 2,500 mm. The landscape consists of high Andean forests and sub-páramo ecosystems, with representative native species such as Weinmannia tomentosa (encenillo) and Myrcianthes leucoxyla (arrayán), which provide habitat for wildlife including the cusumbo and endemic bird species. The ecological significance of this mountainous strip lies in its role as a biological corridor and its function in hydrological regulation for the city of Bogotá.

The spatial extent of the study area is delineated by the following geographic coordinates.

Table 1. Coordinate reference of the study area

| Coordinate reference system: WGS 84 / Pseudo-Mercator (EPSG:3857), units in metres. | | |
|---|---|---|
| NW | 4,881,747.68 E | 2,062,489.62 N |
| NE | 4,883,140.90 E | 2,062,489.62 N |
| SE | 4,883,140.90 E | 2,061,096.40 N |
| SW | 4,881,747.68 E | 2,061,096.40 N |

The selection of the study area is based on its proximity to the El Delirio Ecological Reserve

and Cerro Aguanoso—sites of high ecological significance for Bogotá and the Cerros Orientales. The El Delirio Reserve, covering approximately 1,200–1,500 hectares, protects the headwaters of the Fucha River and serves as a major forest conservation area. It hosts valuable sub-páramo and high Andean Forest ecosystems, where a rich diversity of flora (such as Weinmannia tomentosa, Espeletia spp., ferns, and lichens) and fauna (including various bird species) coexist, contributing to water regulation, oxygen production, and $CO_2$ capture.

Cerro Aguanoso, part of the wetland complex of the Cerros Orientales, was the site of a forest fire in 2016 that directly affected native forest cover. Its study has enabled the assessment of fire severity and post-fire vegetation recovery using indices such as NDVI and NBR, highlighting the area's ecological resilience and dynamic processes (Pinilla Castañeda & Rodríguez Carlos, 2021). These attributes make both zones key areas for analyzing environmental variables related to wildfires and establish an important precedent for studying the region due to its ecological relevance.

### 3.2 Data Collection

To construct the model and map ignition risk, four critical variables were considered: temperature, precipitation, slope, and elevation, the latter derived from the Digital Elevation Model (DEM). The data used for wildfire risk mapping—specifically the required isotherms and isohyets—were selected for the month of March (from March 1 to March 31) and obtained from the corresponding IDEAM meteorological stations for each variable. The information from the stations is recorded in Table 2

### 3.3 AHP Model

Once the data from the relevant stations have been obtained, the pairwise comparison matrix of the AHP method is constructed, in which each criterion is compared against the others based on its relative importance. This comparison is carried out using the Saaty scale, which assigns values from 1 to 9, where 1 indicates equal importance between two criteria and 9 represents an extreme importance of one over the other (Saaty, 1980). The resulting matrix allows for the calculation of normalized weights for each variable using the column sum normalization method. Expert judgment consistency is verified through the Consistency Index (CI) and the Consistency Ratio (CR), which must be less than 0.1 to ensure the model's validity (Palacios & García, 2018).

For the calculation of normalized weights:

$$w_i = \frac{1}{n} \sum_{j=1}^{n} n_{ij} \quad , \qquad i = 1, 2, \ldots, n \tag{1}$$

Where $w_i$ is the normalized weight of criterion i. The sum of all criteria must equal 1.

| Station name | Location (department / municipality) | Altitude | Coordinates | Station type | Parameter |
|---|---|---|---|---|---|
| COLEGIO SAN CAYETANO [21206650] | Bogotá, D.C | 3100 msnm | 4.516752778 Lat<br>-74.0882222220 Lon | Ordinary Climatic | Monthly maximum temperature<br>Monthly mean precipitation |
| VENADO ORO VIVERO [21205580] | Bogotá, D.C | 2725 msnm | 4.598361111 Lat<br>-74.06155556 Lon | Ordinary Climatic | Monthly maximum temperature<br>Monthly mean precipitation |
| LA BOLSA [35025060] | Cundinamarca, Choachí | 3195 msnm | 4.587059 Lat<br>-73.995885 Lon | Principal Climatic | Monthly maximum temperature<br>Monthly mean precipitation |

Table 3. Stations information

For the Consistency Index:

$$IC = \frac{\lambda max - n}{n-1} \tag{2}$$

Where λmax is the maximum eigenvalue of the comparison matrix, and n is the number of criteria.

For the Consistency Ratio:

$$RC = \frac{IC}{IA} \tag{3}$$

Where RI is Saaty's Random Index, which depends on the number of criteria n.

This process ensures that the assigned weights adequately reflect the influence of each variable on the phenomenon under analysis. For the matrix considered in the case of the Cerros Orientales, the calculations yielded a Consistency Ratio (CR) of approximately

0.0074441, which classifies the matrix as highly consistent. Figure 1 below presents the relative weights of each variable as derived from the pairwise comparison matrix used.

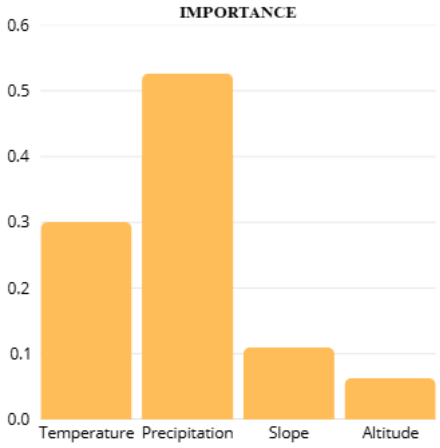


Figure 1. Variable relative weights

This figure highlights precipitation as the primary determining factor for wildfire risk. The precipitation regime has been shown to significantly increase the likelihood of wildfires in Bogotá. Garzón Franco (2023) conducted a correlational analysis between precipitation data and fire records in the city, concluding that there is a direct relationship between El Niño events and the rise in wildfires in the Cerros Orientales. During these episodes, dry conditions intensify, reducing relative humidity and promoting the combustion of vegetation cover.

Furthermore, according to the Bogotá Fire Department, the dry season associated with the El Niño phenomenon in 2024 and 2025 triggered multiple fires in protected areas such as the Cerros Orientales, wetlands, and urban parks. In response to the climate alert, local authorities deployed specialized forest brigades, acknowledging that the lack of rainfall was the main driver of these events.

Following precipitation, temperature emerges as the second most influential factor, playing a decisive role in wildfire dynamics—not only as an ignition trigger but also as an energetic modulator of the ecosystem. In the Cerros Orientales of Bogotá, sustained temperature increases can alter the phenological cycles of vegetation, leading to premature senescence, accumulation of dry biomass, and the release of flammable compounds, thereby increasing fire susceptibility (Ocampo-Zuleta & Beltrán-Vargas, 2018). This condition worsens during El Niño episodes, which raise average temperatures in the region and generate thermal anomalies that intensify the risk (IDIGER, 2021).

Lastly, slope and elevation are considered “less important” variables in the present model. However, it is recognized that terrain slope directly influences wildfire susceptibility, especially in peri-urban areas such as the Cerros Orientales of Bogotá. Areas with moderate slopes (between 10% and 30%) tend to be more accessible for human activities such as hiking, agricultural burning, or recreation, increasing the risk of ignition from anthropogenic causes. Additionally, these slopes promote the accumulation of combustible material in critical points due to surface runoff and the deposition of dry leaf litter. According to the District Institute for Risk Management and Climate Change – IDIGER (2021), slope is a relevant physical factor in risk zoning, as it conditions both exposure and ecosystem vulnerability to ignition events.

Elevation, in turn, acts as an ecological and climatic modulator that affects the probability of wildfire occurrence. In Bogotá, altitudinal ranges between 2,600 and 3,000 meters above sea level concentrate vegetation types such as shrubs and dry grasslands, which are highly flammable during low-humidity seasons. Moreover, higher elevations experience increased solar exposure and lower relative humidity, which favor the desiccation of vegetative fuel and heighten fire susceptibility (Capador Aguilar et al., 2021). Therefore, elevation should be considered a predictive criterion in multicriteria models, as it reflects spatial ignition patterns associated with vegetation and local microclimate.

## 4. Results and Discussion

### 4.1.1 *Wildfire risk model*

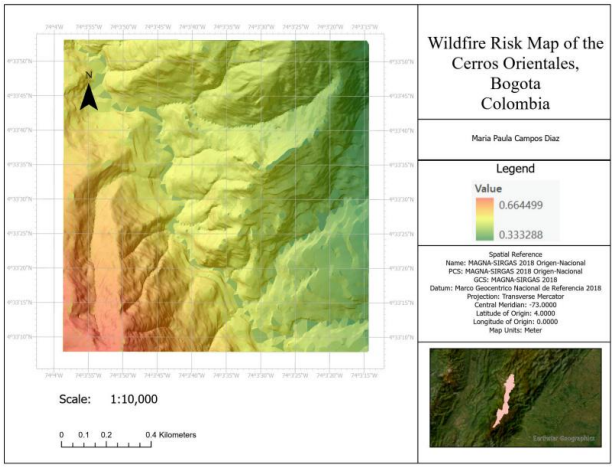


Figure 2. Wildfire Risk Map of the Cerros Orientales by AHP method

The wildfire risk model was implemented in raster format with a spatial resolution of 1 meter per pixel, allowing for a detailed representation of the territory. Each raster cell corresponds to a spatial analysis unit in which the wildfire occurrence risk factor is calculated by integrating the criteria defined in the AHP model, their normalized weights, and the value assigned to the pixel in question. Each cell is assigned a weighted value resulting from the combination of physical and climatic variables, previously normalized and ranked. This approach enables high-precision identification of areas most susceptible to ignition, thereby facilitating preventive planning and evidence-based territorial management.

$$\bar{R(c)} = \sum_{i=1}^{n} w_i * x_{i(c)} \qquad (4)$$

Where $w_i$ is the relative weight of variable i.
The maximum value of the wildfire risk map for the study area is approximately 0.66, which suggests a moderate relative ignition risk. Therefore, for March 2022, vegetation susceptibility did not indicate a high fire hazard. The most critical areas appear to be concentrated in zones with steep slopes and southwestern orientation, which aligns with the influence of factors such as solar exposure, biomass accumulation, and limited accessibility. These zones coincide with altitudinal ranges where vegetation tends to be more flammable due to prevailing climatic and environmental conditions.

### 4.1.2 *Analysis of Contributing Factors in Wildfires*

Based on the findings presented throughout this article, wildfires are recognized as complex phenomena resulting from the interaction of biophysical, climatic, and anthropogenic factors. Ecologically, fire requires three essential elements: oxygen, fuel, and an ignition source. However, its spread depends on conditions such as soil moisture, vegetation cover, and topography (Pausas, 2012). Variables such as slope, terrain orientation, and the availability of dry biomass directly influence the speed and direction of fire propagation (Villers, 2006). Additionally, wind acts as a natural accelerator, while temperature and precipitation determine ecosystem flammability—especially during prolonged drought periods (Reyes & Balcázar, 2021).

On the other hand, human activities such as land-use change, agricultural burning, and urban expansion significantly increase the probability of ignition, becoming key triggering factors in urban–rural interface zones (Myers, 2006). A comprehensive understanding of these elements is essential for designing predictive models and effective risk management strategies. For this reason, a schematic was developed presenting the key variables to be considered and the step-by-step multicriteria process for the wildfire-related research (Annex 1).

## 5. Conclusions

Quantum technology represents a transformative opportunity in wildfire risk management, offering data processing capabilities that far exceed the limitations of classical systems. Its application in the analysis of critical environmental variables—such as temperature, humidity, and photosynthetically active radiation—enables the development of predictive models that are more accurate, dynamic, and adaptable to changing conditions. Quantum sensors, in turn, allow for ultra-precise real-time measurements, significantly enhancing input data quality and strengthening early warning systems.

In complex ecosystems such as the Cerros Orientales of Bogotá, where the interaction among climatic, topographic, and anthropogenic factors is highly variable, quantum computing enables the simulation of multiple fire propagation scenarios with exponential efficiency. This capability is essential for anticipating critical events, optimizing the placement of firebreaks, and designing prevention strategies grounded in spatial evidence. The integration of these emerging technologies with multicriteria models such as AHP and machine learning algorithms opens new possibilities for more resilient, precise, and proactive environmental management in the face of climate change challenges.

## 6. References


Barradas, V., Gómez, L., & Ríos, M. (2023). Quantum PAR sensor UIC-01: Monitoring photosynthetic activity in forest canopies. Environmental Sensor Technology, 11(3), 88–97.

Capador Aguilar, Y. E., González Angarita, G. P., & Suárez Daza, P. A. (2021). Análisis de la cobertura vegetal en incendios forestales mediante índices espectrales: caso de estudio Cerros Orientales (Bogotá, Colombia).

Caride, V. (2022). Modelando el riesgo de incendios en Argentina: Una contribución a las políticas de manejo del fuego [PDF].

Chen, C. H. (2000). Extensions of the TOPSIS method for group decision-making under fuzzy environment. Fuzzy Sets and Systems, 114(1), 1–9. https://doi.org/10.1016/S0165-0114(97)00377-1

De Vicente, J., & Crespo, R. (2012). Evaluación multicriterio en la gestión ambiental. Revista de Evaluación Ambiental, 8(2), 55–70.

Demir, M., & Akay, A. E. (2024). AHP-based wildfire susceptibility mapping in Mediterranean forests. Forest Ecology and Management, 545, 121–134. https://doi.org/10.1016/j.foreco.2023.121134

Dent, J., Huang, Y., & Lee, S. (2025). Quantum optimization for firebreak placement in wildfire-prone regions. Nature Computational Science, 5(1), 22–31. https://doi.org/10.1038/s43588-024-00321-7

Fan, D., Biswas, A., & Ahrens, J. P. (2024). Explainable AI integrated feature engineering for wildfire prediction. arXiv. https://doi.org/10.48550/arXiv.2404.01487

Garritz, A. (2014). Historia de la química cuántica. Educación Química, 25(1), 14–22. https://www.revistas.unam.mx/index.php/req/article/view/46149

Instituto Distrital de Gestión de Riesgos y Cambio Climático (IDIGER). (2021). Precipitación y temperatura en Bogotá D.C.: variabilidad climática y fenómenos El Niño–La Niña.

Jain, P., Coogan, S. C. P., Subramanian, S. G., Crowley, M., Taylor, S., & Flannigan, M. D. (2020). A review of machine learning applications in wildfire science and management. Environmental Reviews, 28(4), 478–505. https://doi.org/10.1139/er-2020-0019

Morales Salguero, J. R. (2017). Determinación del riesgo de ignición y propagación de incendios forestales en los Cerros Orientales de Bogotá a través del álgebra de mapas y simulación [Trabajo de grado, Universidad Distrital Francisco José de Caldas]. Repositorio UDFJC.

Myers, N. (2006). Environmental services and urban expansion. Environmental Management Journal, 18(3), 211–225.

NASA. (2023). Quantum machine learning for wildfire segmentation. NASA Earth Science Division Technical Report. https://earthdata.nasa.gov/publications/qml-wildfire-2023

Ocampo-Zuleta, K., & Beltrán-Vargas, J. (2018). Modelación dinámica de incendios forestales en los Cerros Orientales de Bogotá, Colombia. Madera y Bosques, 24(3), e2431662. https://doi.org/10.21829/myb.2018.2431662

Opricovic, S., & Tzeng, G. H. (2004). Compromise solution by MCDM methods: A comparative analysis of VIKOR and TOPSIS. European Journal of Operational Research, 156(2), 445–455. https://doi.org/10.1016/j.ejor.2003.10.029

Oukaira, A., Ettahri, W., & Lakhssassi, A. (2024). Quantum temperature sensors for environmental monitoring. Journal of Quantum Devices, 9(2), 101–115.

Pausas, J. G. (2012). Incendios forestales. Editorial Catarata / CSIC.

Pinilla, C. A., & Rodríguez, P. A. (2022). Relación entre la severidad de quemado y la recuperación de la vegetación post-incendio en un bosque altoandino en el cerro Aguanoso, Cerros Orientales, Bogotá. http://hdl.handle.net/11349/31700

Pinilla Castañeda, C. A., & Rodríguez Carlos, P. A. (2021). Relación entre la severidad de quemado y la recuperación de la vegetación post-incendio en un bosque altoandino en el cerro Aguanoso, Cerros Orientales, Bogotá [Trabajo de grado, Universidad Distrital Francisco José de Caldas].

Ramírez Puertas, J. (2021). Introducción a la computación cuántica y sus aplicaciones ambientales. Revista de Tecnología y Sociedad, 15(1), 77–92.

Reyes, J., & Balcázar, J. (2021). Impacto climático en la propagación de incendios forestales. Revista de Ciencias Ambientales, 39(2), 45–62.

Rodríguez Aseretto, D., Universitat Autònoma de Barcelona. Departament d'Arquitectura de Computadors i Sistemes Operatius, & Universitat Autònoma de Barcelona. Escola d'Enginyeria. (2007). Sistema adaptativo para la predicción de incendios forestales basado en estrategias estadístico-evolutivas [PDF].

Rojas Botero, S. (2017). Diversidad de especies de plantas en áreas en restauración ecológica en los cerros orientales de Bogotá [Tesis de maestría, Pontificia Universidad Javeriana]. Repositorio Institucional Javeriana. https://repository.javeriana.edu.co/handle/10554/35168

Saaty, T. L. (1980). The analytic hierarchy process: Planning, priority setting, resource allocation. McGraw-Hill.

Saaty, T. L. (2008). Decision making with the analytic hierarchy process. International Journal of Services Sciences, 1(1), 83–98. https://doi.org/10.1504/IJSSCI.2008.017590

Umaña Ramírez, E. D. (2017). Zonificación de amenaza a incendios forestales en el municipio de Riohacha, La Guajira [PDF].

Universidad del Rosario. (2024). Restauración de los Cerros Orientales de Bogotá: un desafío crucial para la biodiversidad y el manejo sostenible. Periódico Nova et Vetera.

Verano Velásquez, D. F. (2013). Modelamiento y simulación de propagación de incendios forestales en los Cerros Orientales de la ciudad de Bogotá D.C. usando FARSITE [Trabajo de grado, Universidad de los Andes]. Repositorio Séneca.

Villers, R. (2006). Ecología del fuego: Fundamentos y aplicaciones. Universidad Nacional Autónoma de México.

Zhou, Z., He, Y., Im, E.-S., & Kwon, H.-H. (2025). Wildfire risk in a changing climate: Evaluating fire weather indices and their global patterns with CMIP6 multi-model projections. Weather and Climate Extremes. [Preprint PDF].

## Appendix

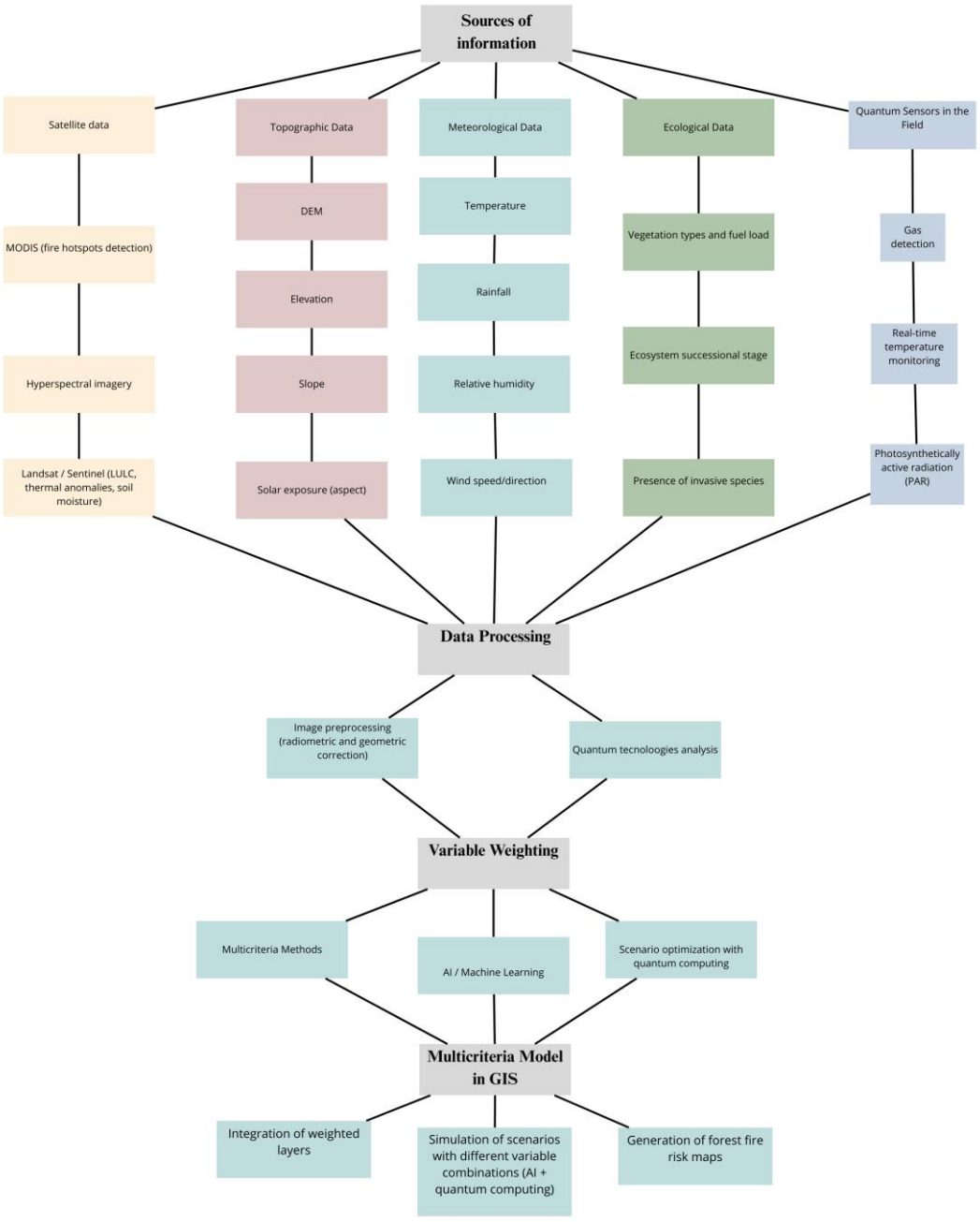


**Appendix A. Multicriteria diagram for wildfire study**

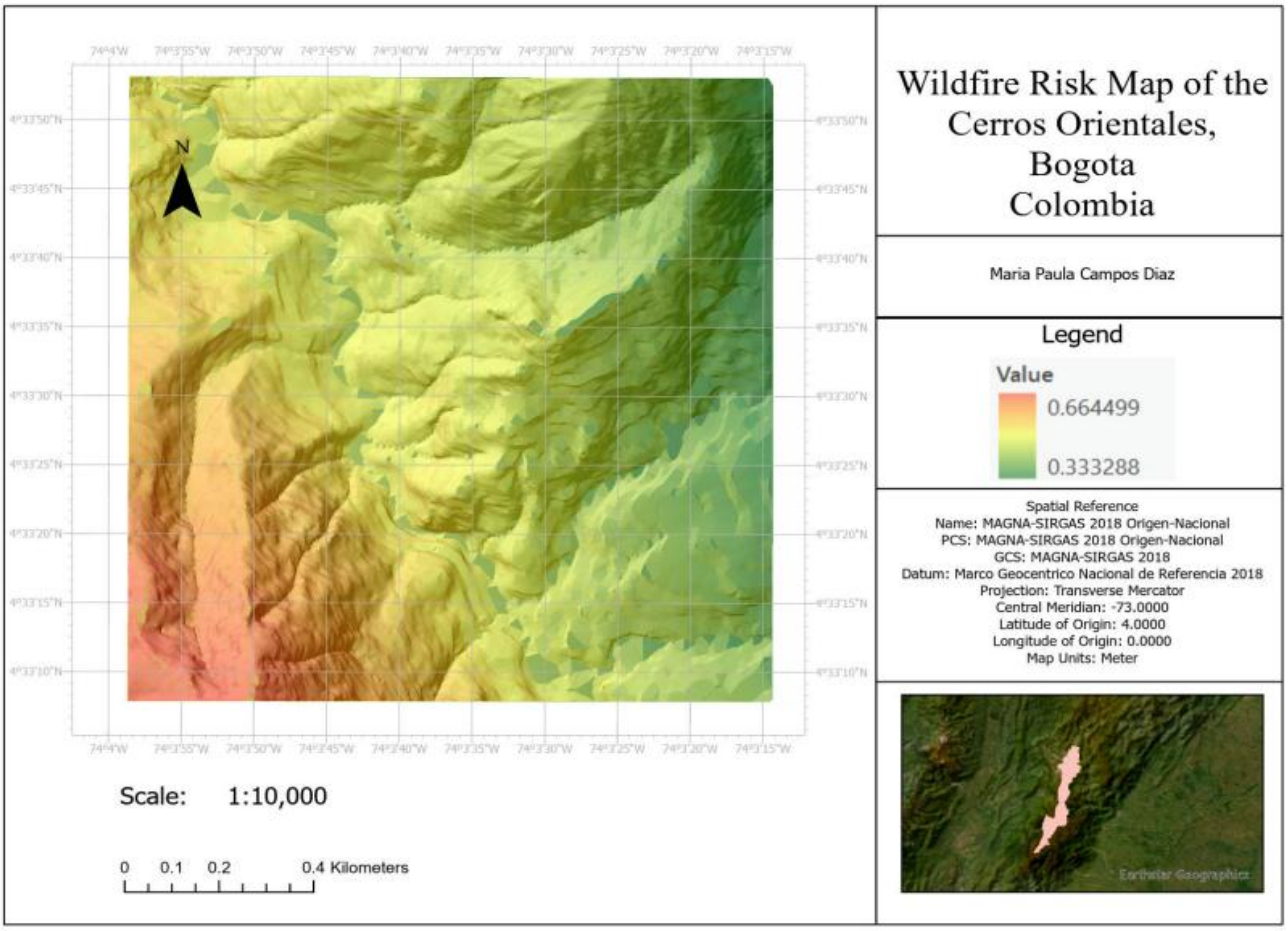


**Appendix B. Wildfire Risk Map**

# Climate Change Monitoring through Remote Sensing Imagery and Processing

Miguel Vallejo

*Instituto Pirenaico de Ecología - Spanish National Research Council (CSIC); miguel.vallejoo@gmail.com*

Accurate and timely data are essential for developing strategies to mitigate and adapt to global climate change. Geospatial data, along with key satellite missions and platforms such as the European Space Agency's (ESA) Sentinel, NASA's Landsat, and commercial providers (i.e., Planet and Maxar), are indispensable for monitoring climate-related variables across large spatial and temporal scales. Advanced processing techniques, such as time-series analysis, change detection, and machine learning, enable remote sensing applications to monitor various climate change indicators and proxies, including vegetation health, land surface temperature, sea level, and glacier coverage. However, the field still faces significant challenges, including technological asymmetries, the balance between data resolution and coverage, the limited availability of ground truth datasets, and high computational requirements. Future developments highlight the importance of scientific diplomacy, data standardization, citizen science, and cloud-based analytics. Overcoming these limitations and innovating AI and Earth observation platforms could enable geospatial technologies to enhance climate resilience, promoting global and local responses to climate risks.

# Technical Session: Climate Change Monitoring through Remote Sensing Imagery and Processing

# Thermal Dynamics in Agriculture: An In-depth Analysis of Land Surface Temperature and Its Impact on Crop Yield

Karthik Karunakarana[a], Karuppasamy Sudalaimuthu[b]

[a] *Research Scholar, Department of Civil Engineering, College of Engineering and Technology, SRM Institute of Science and Technology, Kattankulathur Campus, Chengalpattu, Tamil Nadu, India. E-Mail: kk4739s@srmist.edu.in*
[b] *Associate Professor, Department of Civil Engineering, College of Engineering and Technology, SRM Institute of Science and Technology, Kattankulathur Campus, Chengalpattu, Tamil Nadu, India.E-Mail: karuppas@srmist.edu.in*

**Abstract**: Climate change has emerged as a significant challenge to global agriculture, food security and sustainability. The rising Temperature, shifting precipitation patterns, and increasing frequency of extreme weather events have disrupted traditional farming practices, particularly in climate-sensitive regions like Thanjavur, Tamil Nadu. This study investigates the relationship between historical Landsat satellite-derived Land Surface Temperature (2001-2023), combined with field-based crop yield records using multiple machine learning techniques including Random Forest (RF), Artificial Neural Networks (ANN), and Support Vector Regression (SVR), to determine the most accurate model for yield estimation. By comparing these models, the research identifies key environmental factors influencing rice production and assesses the impact of temperature anomalies on crop health. The thermal response of paddy fields is analysed to understand seasonal variability and long-term trends in rice yield under different climatic conditions. The research findings align with global efforts to enhance agricultural resilience and contribute to Sustainable Development Goals (SDG) 2 (Zero Hunger) and SDG 13 (Climate Action). The findings of this study provide valuable insights for policymakers, agronomists, and farmers to develop data-driven strategies for improving agricultural sustainability. By integrating remote sensing and machine learning, policymakers can formulate climate adaptation strategies, optimize water resource management, and promote precision agriculture to mitigate climate risks. Additionally, the research underscores the importance of early warning systems and climate-resilient crop varieties, which can be promoted through government interventions and agricultural policies to ensure food security and sustainable farming practices.

***Keywords:*** Agriculture, Climate Change, Land Surface Temperature, Machine Learning, Sustainable Development Goals.

## 1. Introduction

Agricultural productivity is deeply related with climatic and environmental factors, among which Land Surface Temperature (LST) stands out as a critical parameter (Sabaghy et al., 2018). LST, defined as the radiative skin temperature of the land derived from satellite thermal infrared sensors, reflects the thermal energy emitted from the Earth's surface. It significantly influences crop growth and development by affecting physiological processes such as photosynthesis, evapotranspiration, and soil microbial activity (Abdullah-Al-Faisal et al., 2021). The measurement and analysis of LST provide vital insights into the thermal dynamics of agricultural land, helping identify areas under heat stress (Puppala & Singh, 2021), water deficit, and even pest vulnerability. Due to elevated global temperature, analysing LST has become increasingly important for ensuring food security

and sustainable agricultural practices. In agricultural ecosystems, temperature is one of the most limiting factors influencing the length of the growing season, crop phenology, and yield potential (Song et al., 2022). Both excessive heat and unseasonal cold can disrupt crop cycles and reduce productivity. LST is a more direct and localized measure of thermal conditions experienced by crops compared to ambient air temperature (Do Nascimento et al., 2022), especially in heterogeneous landscapes. This makes LST a valuable parameter in agro-climatological assessments, particularly for precision agriculture applications. Remote sensing technologies have revolutionized the way we monitor LST over large areas and time periods.

The sensors like MODIS, Landsat, and Sentinel, are used to retrieve high-resolution thermal data on a near-real-time basis (Sattari & Hashim, 2014). These datasets, when integrated with vegetation indices (Badugu et al., 2024) such as BSI, NDMI, NDVI, provide a comprehensive understanding of vegetation stress due to thermal extremes. Furthermore, coupling LST with meteorological data (Mohammadinia et al., 2019), soil characteristics, and crop models enhances the capacity to simulate, monitor, and predict yield fluctuations under varying temperature regimes. One of the critical impacts of LST on agriculture is its role in determining evapotranspiration (ET), which controls plant water use and soil moisture levels (Senay et al., 2016). Elevated LST generally leads to higher ET rates, which, if not balanced by sufficient irrigation or rainfall, results in water stress. This stress is particularly detrimental during sensitive crop stages like flowering or grain filling, where heatwaves and dry spells can severely reduce yields (Song et al., 2022). Another important aspect of LST analysis is its ability to detect urban heat islands (UHIs) and land use changes that indirectly affect adjacent agricultural areas (Kikon et al., 2016). As rural landscapes undergo urbanization or deforestation, thermal properties of the land surface alter, modifying local microclimates. Additionally, long-term LST trends can serve as indicators of climate change impacts (Ilavarasan, 2022) on agricultural zones, aiding in risk assessment and adaptation planning. It contributes to decision support systems in precision agriculture by enabling robust LST-based stress monitoring and dynamic yield forecasting using explainable ML approaches.

The machine learning models are trained (Mansourmoghaddam et al., 2024) on historical LST data and field-level crop yield statistics to identify patterns, anomalies, and thresholds beyond which yields decline significantly. For instance, in rice or wheat cultivation (Song et al., 2022), sustained LST values above critical thresholds during reproductive stages have been linked with poor grain setting and reduced harvest index. Such empirical evidence emphasizes the need to integrate LST in yield forecasting and early warning systems. Furthermore, understanding the thermal dynamics of soil and canopy can improve irrigation scheduling, fertilizer application, and pest management (Zhang et al., 2015). Real-time LST monitoring enables farmers and agronomists to respond to thermal stress proactively, applying water or shade nets as needed.

Previous research that focuses on single models or uses generalized climatic parameters, this study offers a comparative machine learning framework to assess the predictive performance of Artificial Neural Networks (ANN), Random Forest (RF), and Support Vector Machine (SVM) in modelling the impact of Land Surface Temperature (LST) on crop yield. It introduces a model comparison approach that evaluates the sensitivity and accuracy of each algorithm in detecting thermal stress impacts across different years. The main Objective of the study is 1) To analyze spatial and temporal variations in Land Surface Temperature (LST) across different agricultural zones using thermal remote sensing data. 2) To investigate the influence of LST on crop yield during peak vegetative stages by integrating LST with vegetation indices. 3) To develop and compare the performance of ANN, RF, and SVM models in paddy crop yield stress based on LST and other influencing parameters and validate through performance metrics

## 2. Materials & Methods

### 2.1 Data Preparation

The Landsat 5, 7, and 8 data with 30 m spatial resolution imageries are obtained from the U.S. Geological Survey (https://earthexplorer.usgs.gov/). The study area of 2627.66 Sq.km is clipped from the tile that falls under path 142 for all Level-1 imageries with cloud cover less than 10%. According to the data availability of paddy crop for kuruvai august or September and samba season December or January month data are considered for the study. Totally 18 imageries were processed, each season having 8 imageries were used for the study as shown in the Table 1. The LULC dynamics is concentrated only on the agriculture classes in each year. The district boundary information was obtained from the Geological Survey of India (GSI) (https://bhukosh.gsi.gov.in) and rainfall data are collected from the Indian Meteorological Department (IMD) (https://mausam.imd.gov.in/). Eventually, rainfall maps and crop yield are created using the Inverse Distance Weight method (IDW) in GIS platform. Paddy crop yield data were collected from the Department of Economics and statistics, Chennai and 153 fishnet generated field data points were collected using Trimble Handheld Global Positioning System (GPS) on the field in August end or September start, 2022 and December end or January start, 2023 for LULC validation.

| S.No. | Products | Kuruvai Period | Samba Period |
|---|---|---|---|
| | Landsat 7 ETM+ | 03-09-2001 | 03-01-2002 |
| | Landsat 5 TM | 28-08-2004<br>21-08-2007<br>18-08-2010 | 03-01-2005<br>29-12-2007<br>20-01-2011 |
| | Landsat 8 OLI/TIR | 21-08-2013<br>29-08-2016<br>07-09-2019<br>22-08-2022 | 27-12-2014<br>04-01-2017<br>13-01-2020<br>05-01-2023 |

Table 1. Landsat Data Acquisition

### 2.2 Study Area

Thanjavur district, located in the southern Indian state of Tamil Nadu, forms an integral part of the fertile Cauvery delta region and is often referred to as the "Rice Bowl of Tamil Nadu." Geographically positioned between 9°50′ and 11°25′ N latitude and 78°45′ to 79°25′ E longitude, the district occupies a strategically important location in the central part of the state. Its landscape is shaped significantly by the riverine systems, predominantly the Cauvery River and its numerous tributaries, which support extensive agricultural activities as shown in Figure 1. The average elevation of Thanjavur is around 57 meters above mean sea level. The district exhibits a dominant agricultural land use, supported by fertile alluvial soils and a well-established irrigation network fed by the Cauvery River making it favourable for multi-cropping practices.

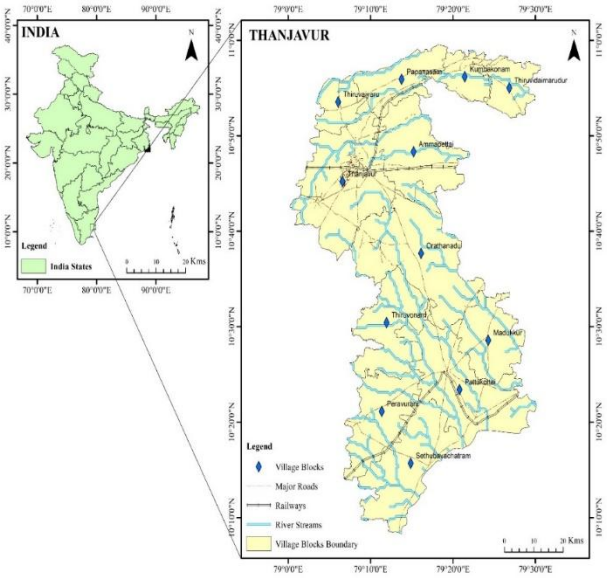


Figure 1. Spatial context of study area for climate-resilient agricultural analysis Methods

The methodology of this study involves a multi-stage approach (Figure 2) integrating remote sensing, GIS, and machine learning to investigate the impact of Land Surface Temperature (LST) on crop yield. Initially, satellite-based thermal infrared data from Landsat were used to derive LST at high temporal and spatial resolutions (Sánchez-Aparicio et al., 2020). These LST datasets were

processed for kuruvai and samba seasons. Concurrently, crop yield data was obtained from official agricultural statistics for corresponding regions and timeframes. To enhance model inputs, additional variables such as vegetation indices (BSI, NDMI, NDVI), rainfall were extracted and spatially aligned using GIS platform.

### 2.2.1 *LST calculation from Landsat*

LST can be calculated from Landsat thermal bands (band6 for Landsat5,7 and band 10 for Landsat 8), (Sarif et al., 2023) using the Single Window Algorithm. The spectral radiance is converted to brightness temperature (Kelvin) using Eq. (1).

$$T = \frac{K_2}{ln\left(\frac{K_1}{L_\lambda} + 1\right)} \qquad (1)$$

Where, Sensor-specific thermal constants $K_1$ and $K_2$ (Landsat 5 TM: 607.76 and 1260.56; Landsat 7 ETM+: 666.09 and 1282.71). Further, brightness temperature is converted to Celsius using Eq. (2).

$$LST\ (^oC) = T - 273.15 \qquad (2)$$

Landsat 8 utilised for LST begins with DN were converted to Top of Atmosphere (TOA) spectral radiance. Next, NDVI was computed using Eq. (3).

$$NDVI = \frac{NIR - RED}{NIR + RED} \qquad (3)$$

where NIR=Near Infrared. Followed by Proportion of Vegetation ($P_v$) and Emissivity (ε) were used to estimate the LST (ºC) using Eq. (4).

$$LST = \frac{T}{1+\left(\frac{\lambda T}{\rho}\right)ln(\varepsilon)} \qquad (4)$$

Where, λ-10.9 µm for Band 10, and $\rho = \frac{h.c}{\sigma} = 1.438 \times 10^{-2}$ m.K with h-Planck's constant ($6.626\times10^{-34}$ Js), c-speed of light ($2.998\times10^{8}$ m/s), σ=Boltzmann constant ($1.38\times10^{-23}$ J/K)

Additionally, BSI, NDMI (Gowri & Manjula, 2019) is given by Eq. (5) and (6).

$$BSI = \frac{((Red+SWIR) - (NIR+ Blue))}{((Red+SWIR) + (NIR+ Blue))} \qquad (5)$$

$$NDMI = \frac{(NIR - SWIR)}{(NIR + SWIR)} \qquad (6)$$

Where, SWIR = short-wave infra-red

The processed dataset was then subjected to normalization and feature selection to ensure consistent scaling and remove redundant inputs. The dataset was split into training and testing sets using k-fold cross-validation to avoid overfitting and ensure model robustness. Three machine learning algorithms including ANN, RF, and SVM were implemented to model the non-linear relationships between LST and crop yield.

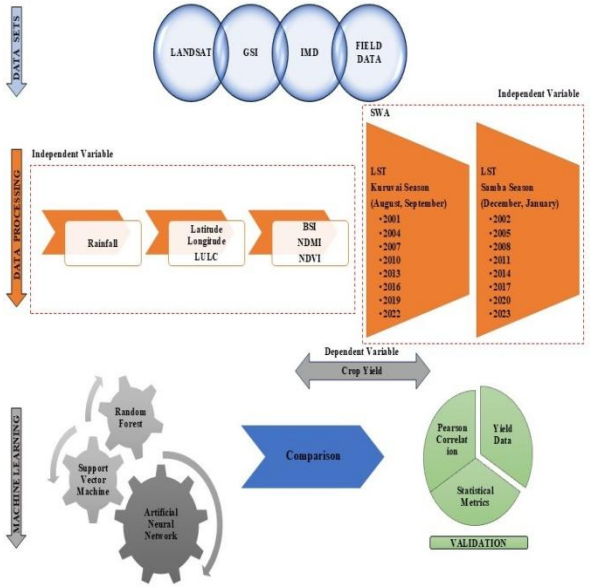


Figure 2. Methodological framework for thermal dynamics in agricultural analysis

### 2.2.2 *Machine Learning Approach*

An Artificial Neural Network (ANN) model was developed to capture the non-linear relationship between Land Surface Temperature (LST), vegetation indices, rainfall and crop yield. The model consists of a 5 input layers with multiple environmental variables, one hidden layer, and an output layer representing predicted yield. A backpropagation algorithm was used for training, and model performance was assessed. The ANN model used in this study is a feed-forward neural network trained using the backpropagation algorithm (Abdullah-Al-Faisal et al., 2021). It models the relationship between

input variables ($X=x_1, x_2, x_3 \ldots \ldots x_n$) and predicted crop yield (y) using non-linear activation functions.

Random Forest (RF), an ensemble learning method based on decision trees, was used to model the non-linear relationships between Land Surface Temperature (LST), vegetation indices, rainfall, and crop yield. The model constructs multiple decision trees using bootstrap samples and aggregates their outputs to produce a more accurate and robust prediction (Noi et al., 2017). RF is particularly effective in handling multicollinearity, high-dimensional datasets, and nonlinear interactions, making it suitable for environmental and agricultural applications.

Support Vector Machine (SVM), a supervised machine learning algorithm, was employed to predict crop yield affected due to LST and influencing parameters (Mandal & Saha, 2018). For regression tasks, Support Vector Regression (SVR) was used. The model constructs a hyperplane in high-dimensional space that best fits the data within a defined margin of tolerance (epsilon), balancing prediction accuracy and generalization. The kernel trick was applied to capture nonlinear relationships between predictors and yield.

The performance of each model was evaluated using standard regression metrics such as the coefficient of determination ($R^2$) and root mean square error (RMSE). A comparative analysis was conducted to assess the models' predictive accuracy, sensitivity to LST, and ability to generalize across kuruvai and samba seasons. Finally, the best performing algorithm was recommended for operational crop yield forecasting. This methodological framework not only enables detailed understanding of thermal dynamics in agriculture but also supports scalable, data-driven decision-making for climate-resilient farming

## 3. Results & Discussion

### 3.1 LST vs Yield

The analysis of LULC maps across the study years revealed a noticeable shift in land cover patterns, especially the reduction in agricultural land (4%) and the expansion of built-up areas and barren land was showed by overall accuracy 88% with kappa coefficient 82 in kuruvai period and 93% with kappa coefficient 90 for samba season. These land conversions were strongly correlated with rising Land Surface Temperature (LST). Spatial analysis revealed that regions with elevated LST values (>35°C) during the vegetative stage experienced substantial yield reductions in semi-arid regions. While areas where LST remained within a moderate range (28°C to 32°C) showed higher and more stable yields. Regression analysis between LST and yield demonstrated its correlation in critical growth stages. In areas where LST exceeded physiological thresholds, stress symptoms such as poor grain filling and yield reduction. The vegetative stage LST was consistently identified as the most critical phase affecting yield, confirming findings from the satellite data observations. These trends validate LST (Pavithrapriya et al., 2022) as a key environmental stress indicator for crop performance.

### 3.2 Vegetation Indices vs Yield

The relationship between yield and vegetation indices (BSI, NDVI, NDMI) further confirmed the stress impact of thermal dynamics on plant health. In thermally stressed zones (high LST), the NDVI values dropped significantly, indicating canopy temperature stress (Pavithrapriya et al., 2022), reduced chlorophyll content, and lower biomass accumulation. During the vegetative stage, areas with higher LST often exhibited reduced NDVI, suggesting moisture stress and inhibited leaf area development. In contrast, areas with optimal LST (<30°C) supported vigorous growth, reflected in high vegetation index values. NDMI provides the moisture level in farm fields, when used alongside LST, provided a complementary view of thermal and physiological crop status, enhancing early detection of heat, water stress, (Kannan et al., 2015) moisture stress, drought tolerance, and irrigation effectiveness. NDMI and BSI has moderate average importance to crop yield because of NDVI already captures much of the vegetative health. But still, it's biophysically meaningful, especially under semi-arid or water-variable conditions.

### 3.3 LST vs Yield vs ML Techniques

The predictive modelling of crop yield stress based on LST, vegetation indices, and rainfall was carried out using three machine learning algorithms including ANN, RF and SVM shown in Figure 3. Each model was trained and tested using input variables extracted from remote sensing data. Performance evaluation was conducted using standard regression metrics. The results indicate that all three models successfully captured the nonlinear relationships between crop yield and the input features. However, their predictive accuracy varied across ANN, RF and SVM. ANN performed well when data was abundant and continuous across all variables, particularly excelling in capturing complex interactions between LST and vegetation indices. The model achieved an $R^2$ of 0.84, with an RMSE of 2.1 (G Ravi Kumar, Getesh Challur, 2023). Random Forest (RF) showed the best overall performance, with a higher generalization ability and robustness to noise achieving the $R^2$ of 0.97 and RMSE of 0.4. The ensemble nature of RF allowed it to effectively handle feature redundancy and outliers present in satellite-derived LST datasets (Tiwari et al., 2024) SVM with an RBF kernel produced reasonable results, especially in well-separated data spaces, but its performance slightly declined for highly non-linear or imbalanced data (Mandal & Saha, 2018). The model reported an $R^2$ of 0.07, RMSE of 13.32. A visual comparison using predicted vs. observed yield scatterplots further confirmed that RF had the least dispersion, indicating superior accuracy and consistency across yield ranges. ANN, while close, slightly overestimated yields in high-stress (high LST) zones, whereas SVM tended to underpredict yields under extreme conditions. The integration of LST, vegetation indices, rainfall and machine learning models enabled accurate yield forecasting and stress zone identification. Eventually the feature importance Table 2 shows the significance of key factors with respect to ML models.

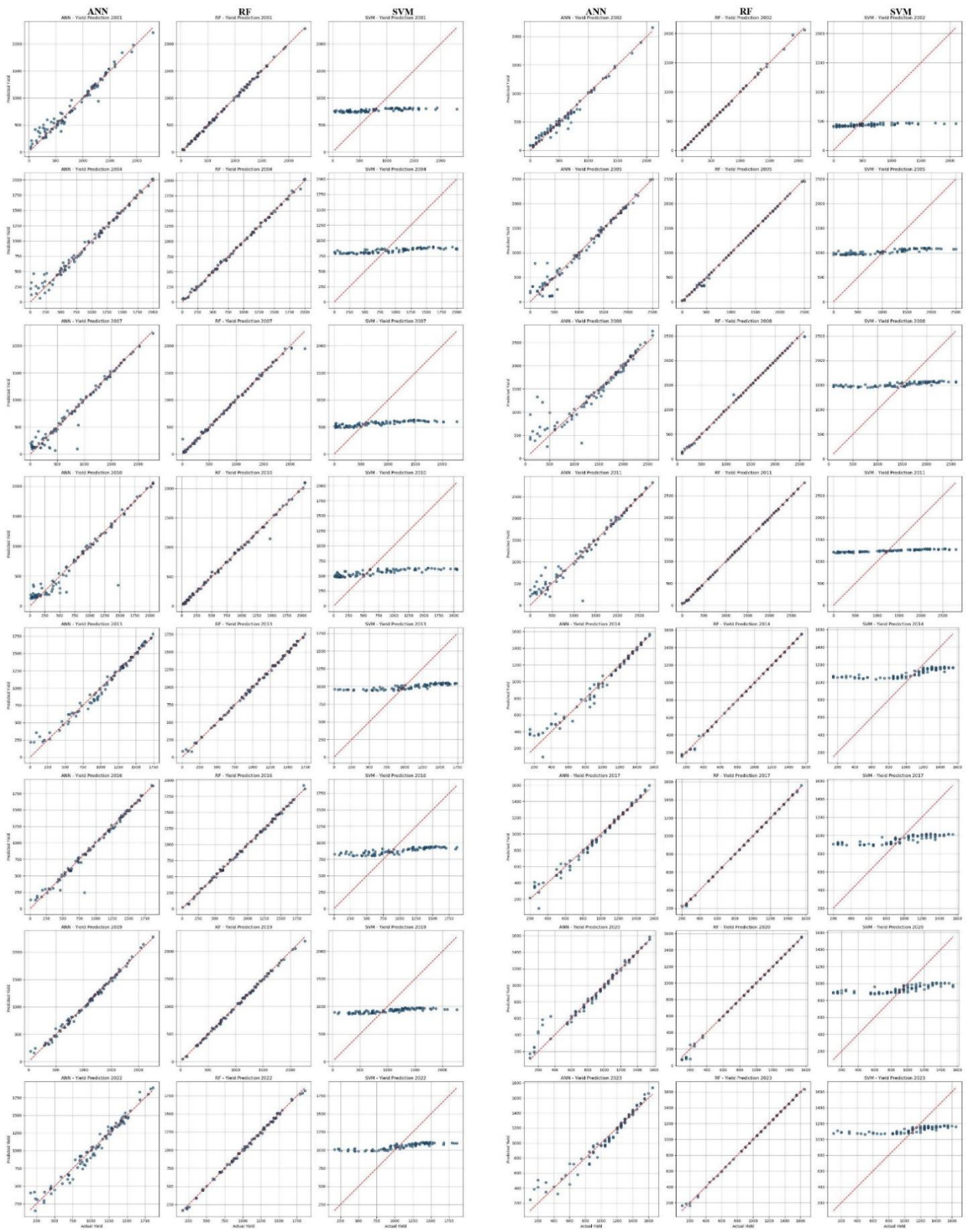


Figure 3. Performance of ANN, RF, and SVM Models for Paddy Yield Prediction (2001-2023) in Kuruvai and Samba seasons

| Models | BSI | NDMI | NDVI | RF | LST |
|---|---|---|---|---|---|
| ANN | Moderate | Low | High | Moderate | Moderate-High |
| RF | Low | Moderate | High | Moderate | Moderate-High |
| SVM | Moderate | Low | High | Low | High |

Table 2. Feature Importance ANN, RF, and SVM Models

## 4. Conclusion

This study highlights the critical role of LST in crop yield dynamics, particularly under increasing climate variability. The integration of LST with vegetation indices, rainfall and soil parameters using machine learning models including Random Forest (RF), Artificial Neural Network (ANN), and Support Vector Machine (SVM) provided valuable insights into the spatial and temporal patterns of thermal stress across the study region. Among the models tested, Random Forest outperformed others in accurately predicting yield, with the peak vegetative stage LST emerging as the most impactful variable. This underscores the importance of targeted thermal monitoring during sensitive phenological phases. The findings validate LST as a reliable stress indicator and a key input for real-time yield forecasting frameworks. Thermal bands are sensitive to cloud cover, atmospheric disturbances, and surface emissivity variations, potentially affecting data accuracy. Additionally, ground truth yield data for model training was limited in some regions, affecting model generalizability. While RF and ANN performed well, model retraining is required when applying to new crops, regions, or seasons, limiting plug-and-play scalability. Future studies could integrate real-time ground sensor data, crop management practices, and socio-economic variables to improve prediction accuracy. Moreover, extending the approach across multiple crop types and climatic zones will improve its scalability and utility in national yield monitoring programs. Thermal maps can guide agro-ecological zoning and help prioritize climate-resilient crops in areas prone to heatwaves or rising surface temperatures. Governments can deploy LST-driven monitoring platforms for early detection of heat stress and pre-emptive yield loss estimation. Integration of LST and ML outputs can support climate-smart insurance schemes, identifying yield loss zones more accurately (SDG-2). In summary, this study demonstrates that LST, when integrated with vegetation and soil metrics using robust machine learning models, offers a powerful and scalable solution for real-time yield prediction and thermal stress monitoring. It lays the foundation for smart agriculture systems that are both data-driven and climate-resilient (SDG-13).

## 5. Acknowledgements

We extend our sincere gratitude to the U.S. Geological Survey, Indian Meteorological Department, Geological Survey of India, and Joint Director of Agriculture-Thanjavur for providing necessary data for this research. We extend our special thanks to the management of SRM University, Kattankulathur Campus, for their continuous support and encouragement throughout this study. Additionally, we acknowledge all individuals whose efforts in data collection, and archiving have made this work possible.

## 6. References

Abdullah-Al-Faisal, Abdulla - Al Kafy, Foyezur Rahman, A. N. M., Rakib, A. Al, Akter, K. S., Raikwar, V., Jahir, D. M. A., Ferdousi, J., & Kona, M. A. (2021). Assessment and prediction of seasonal land surface temperature change using multi-temporal Landsat images and their impacts on agricultural yields in Rajshahi, Bangladesh. Environmental Challenges, 4(January),100147. https://doi.org/10.1016/j.envc.2021.100147

Badugu, A., Arunab, K. S., & Mathew, A. (2024). Predicting land surface temperature using data-driven approaches for urban heat island studies: a comparative analysis of correlation with environmental parameters.

In Modeling Earth Systems and Environment (Vol. 10, Issue 1). Springer International Publishing. https://doi.org/10.1007/s40808-023-01822-2

Do Nascimento, A. C. L., Galvani, E., Gobo, J. P. A., & Wollmann, C. A. (2022). Comparison between Air Temperature and Land Surface Temperature for the City of São Paulo, Brazil. Atmosphere, 13(3), 1–21. https://doi.org/10.3390/atmos13030491

G Ravi Kumar, Getesh Challur, P. B. T. (2023). Machine Learning Methods for Crop Yield Prediction. Communications in Computer and Information Science, 1866 CCIS(11), 195–209. https://doi.org/10.1007/978-3-031-43605-5_15

Gowri, L., & Manjula, K. R. (2019). Evaluation of various vegetation indices for multispectral satellite images. International Journal of Innovative Technology and Exploring Engineering, 8(10), 3494–3500. https://doi.org/10.35940/ijitee.J9195.0881019

Ilavarasan, N. (2022). Assessment of the Effects of Climate Change on Groundwater Fluctuations in Thanjavur District, Tamilnadu, India. https://www.researchsquare.com/article/rs-2308286/latest

Kannan, M., Beosha, B., Revanth, K., Pavatharini, P., & Nivethitha, N. S. (2015). Assessment of Groundwater Quality in Thanjavur District Using Geo-spatial Thanjavur District Using Geo-spatial. 3(04), 1–6. www.ijert.org

Kikon, N., Singh, P., Singh, S. K., & Vyas, A. (2016). Assessment of urban heat islands (UHI) of Noida City, India using multi-temporal satellite data. Sustainable Cities and Society, 22, 19–28. https://doi.org/10.1016/j.scs.2016.01.005

Mandal, S., & Saha, A. (2018). Support vector machines for monitoring land use dynamicity and temporal variation of land surface temperature in Kurseong and surrounding of Darjeeling Himalaya. Modeling Earth Systems and Environment, 4(2), 659–672. https://doi.org/10.1007/s40808-018-0430-4

Mansourmoghaddam, M., Rousta, I., Ghafarian Malamiri, H., Sadeghnejad, M., Krzyszczak, J., & Ferreira, C. S. S. (2024). Modeling and Estimating the Land Surface Temperature (LST) Using Remote Sensing and Machine Learning (Case Study: Yazd, Iran). Remote Sensing,16(3). https://doi.org/10.3390/rs16030454

Mohammadinia, A., Saeidian, B., Pradhan, B., & Ghaemi, Z. (2019). Prediction mapping of human leptospirosis using ANN, GWR, SVM and GLM approaches. BMC Infectious Diseases,19(1),1–18. https://doi.org/10.1186/s12879-019-4580-4

Noi, P. T., Degener, J., & Kappas, M. (2017). Comparison of multiple linear regression, cubist regression, and random forest algorithms to estimate daily air surface temperature from dynamic combinations of MODIS LST data. RemoteSensing,9(5). https://doi.org/10.3390/rs9050398

Pavithrapriya, S., Ramachandran, A., Ahamed Ibrahim, S. N., & Palanivelu, K. (2022). Climate variability trend and extreme indices for the Thanjavur Delta region of Tamil Nadu in South India. Mausam, 73(2), 237–250. https://doi.org/10.54302/mausam.v73i2.5475

Puppala, H., & Singh, A. P. (2021). Analysis of urban heat island effect in Visakhapatnam, India, using multi-temporal satellite imagery: causes and possible remedies. Environment, Development and Sustainability, 23(8), 11475–11493. https://doi.org/10.1007/s10668-020-01122-0

Sabaghy, S., Walker, J. P., Renzullo, L. J., & Jackson, T. J. (2018). Spatially enhanced passive microwave derived soil moisture: Capabilities and opportunities. Remote Sensing of Environment, 209(February), 551–580. https://doi.org/10.1016/j.rse.2018.02.065

Sánchez-Aparicio, M., Andrés-Anaya, P., Del Pozo, S., & Lagüela, S. (2020). Retrieving land surface temperature from satellite

imagery with a novel combined strategy. Remote Sensing, 12(2). https://doi.org/10.3390/rs12020277

Sarif, M. O., Gupta, R. D., & Murayama, Y. (2023). Assessing Local Climate Change by Spatiotemporal Seasonal LST and Six Land Indices, and Their Interrelationships with SUHI and Hot–Spot Dynamics: A Case Study of Prayagraj City, India (1987–2018). Remote Sensing,15(1). https://doi.org/10.3390/rs15010179

Sattari, F., & Hashim, M. (2014). A Breif Review of Land Surface Temperature Retrieval Methods from Thermal Satellite Sensors. Middle-East Journal of Scientific Research, 22(5),757–768. https://doi.org/10.5829/idosi.mejsr.2014.22.05.21934

Senay, G. B., Friedrichs, M., Singh, R. K., & Velpuri, N. M. (2016). Evaluating Landsat 8 evapotranspiration for water use mapping in the Colorado River Basin. Remote Sensing of Environment,185,171–185. https://doi.org/10.1016/j.rse.2015.12.043

Song, Y., Wang, C., Linderholm, H. W., Fu, Y., Cai, W., Xu, J., Zhuang, L., Wu, M., Shi, Y., Wang, G., & Chen, D. (2022). The negative impact of increasing temperatures on rice yields in southern China. Science of the Total Environment, 820, 153262. https://doi.org/10.1016/j.scitotenv.2022.153262

Tiwari, V., Thorp, K., Tulbure, M. G., Gray, J., Kamruzzaman, M., Krupnik, T. J., Sankarasubramanian, A., & Ardon, M. (2024). Advancing food security: Rice yield estimation framework using time-series satellite data & machine learning. PLoS ONE, 19(12), 1–22. https://doi.org/10.1371/journal.pone.0309982

Zhang, G., Xiao, X., Dong, J., Kou, W., Jin, C., Qin, Y., Zhou, Y., Wang, J., Menarguez, M. A., & Biradar, C. (2015). Mapping paddy rice planting areas through time series analysis of MODIS land surface temperature and vegetation index data. *ISPRS Journal of Photogrammetry and Remote Sensing*, *106*, 157–171. https://doi.org/10.1016/j.isprsjprs.2015.05.011

# Estimation of tropospheric water vapor from GNSS signals: applications and benefits of CORS stations in environmental management and sustainable development

Sarai Peña [a,b]

[a] *Universidad Distrital Francisco José de Caldas, Faculty of Environmental Sciences and Natural Resources, Bogotá, Colombia – nspenag@udistrital.edu.co*
[b] *Cuatro Conceptos S.A.S. Research, Development, and Innovation Unit R+D+i, Bogotá, Colombia - neyitspg@gmail.com; info@cuatroconceptos.com*

**Abstract**: As part of the National Multipurpose Cadastre policy led by the Agustín Codazzi Geographic Institute (IGAC), the project for the densification of the MAGNA-ECO National Geodetic Network (National Geocentric Reference Framework Continuous Stations) is being implemented through the installation of Continuous Operating Reference Stations (CORS) in various municipalities across the national territory. These GNSS stations are gaining growing relevance beyond their traditional applications in geodesy and surveying. One of their lesser known yet highly promising contributions lies in their ability to provide precise and continuous data for the estimation of precipitable water vapor (PWV), a key atmospheric variable in weather forecasting, risk management, and climate studies.This article presents the results of an applied study conducted as part of an undergraduate internship in Topographic Engineering, focusing on the estimation of PWV from GNSS observations recorded at a CORS station located in the municipality of Cumaribo, Vichada. The project is embedded within the broader effort to densify the MAGNA-ECO National Geodetic Network, under the leadership of IGAC and primarily executed by the Research, Development, and Innovation Unit (R+D+i) of the company Cuatro Conceptos S.A.S, officially recognized by resolution of the Ministry of Science and Technology.", which has played a pivotal role in deploying CORS infrastructure nationwide through an efficient industrial construction model. The findings, along with the development of an educational learning guide, and the implementation of a knowledge transfer process tailored to rural contexts, underscore how these technologies can empower rural, indigenous, and afrodescendant communities to better respond to contemporary environmental challenges.

***Keywords:*** National Geodetic Network MAGNA-ECO, Continuous Operation Reference Stations (CORS), Global Navigation Satellite System (GNSS), Tropospheric Water Vapor (PWV), Zenith Hydrostatic Delay (ZHD), Meteorology, Knowledge Transfer.

## 1. Introduction

Water vapor in the troposphere is a fundamental component of the climate system. It plays a critical role in cloud formation and precipitation processes, while also acting as a powerful greenhouse gas that amplifies global warming through positive feedback mechanisms. Consequently, real time monitoring of tropospheric water vapor is essential for enhancing the accuracy of weather forecasts, optimizing the management of water resources,

and strengthening early warning systems for extreme weather events.

In Colombia, the Agustín Codazzi Geographic Institute (IGAC), as the entity responsible for the national geodetic framework, has been implementing an ambitious plan to densify the CORS station network under the MAGNA-ECO system. This network provides high precision GNSS data in real time, which can be leveraged not only in topographic surveys but also in weather predictions and water resource management, as well as optimizing agricultural practices such as crop irrigation management.

As part of a university internship centered on geospatial knowledge transfer, a study was conducted with the objective of applying data generated by a CORS station to estimate atmospheric water vapor content using scientifically validated.

The project also involved the development of an educational booklet aimed at facilitating knowledge appropriation by rural communities prioritized by IGAC. The booklet highlights how the use of GNSS data can yield tangible benefits in areas such as agriculture, water resource management, public health, and climate change adaptation.

Throughout the material, the operation of CORS stations, their role in measuring tropospheric water vapor, and the practical applications of this information are explained in accessible terms. The goal is to empower communities to leverage this data to improve their quality of life, safeguard their environment, and contribute to the sustainable development of their municipalities.

## 2. Background and Justification

GNSS technology has revolutionized meteorology and climate monitoring through the implementation of CORS stations. From early studies to more recent research, the ability of these stations to accurately estimate tropospheric water vapor has proven useful in improving weather predictions and understanding climate patterns.

The study conducted by Bevis et al. (1992) represented a pivotal advancement in GNSS meteorology, as it was the first to demonstrate the feasibility of using GPS signals to remotely estimate atmospheric water vapor. The authors developed a model that enabled the conversion of tropospheric signal delay data into accurate measurements of precipitable water vapor (PWV), thereby laying the foundation for subsequent research in this domain. This work underscored the significance of GNSS technology in meteorological applications and opened new avenues for real time atmospheric monitoring.

In Europe, Guerova et al. (2005) conducted an evaluation of measured and modeled water vapor over Switzerland during the period 2001–2003. The study underscored the value of integrating GNSS derived water vapor data into numerical weather prediction models to enhance forecasting accuracy. The findings demonstrated that combining GNSS observations with other measurement techniques yields a more comprehensive and precise representation of atmospheric water vapor, an essential factor in improving the prediction of severe weather events.

In Latin America, Cioce et al. (2011) performed one of the first trials in Venezuela on the estimation of tropospheric water vapor through GPS observations. This study demonstrated that it is possible to adapt and use GNSS technologies in local contexts to obtain accurate data on water vapor. The results emphasized the importance of continuing local research to optimize the use of this technology in the region, highlighting its potential to improve weather predictions and water resource management.

One year later, in Colombia, Šverko Navarrete (2012) developed a method to estimate precipitable water vapor using the GPS system, with specific applications in Bogotá. This work demonstrated that GNSS techniques can be adapted to significantly improve local weather predictions, providing a clear example of how these technologies can benefit urban communities in the region.

Later in Argentina, Mackern Oberti et al. (2021) conducted a detailed analysis on the estimation of tropospheric water vapor using GNSS. This

work, presented at the XXIX Scientific Meeting of the Argentine Association of Geophysicists and Geodesists, explored methodologies for calculating tropospheric water vapor and evaluated its accuracy under different climatic conditions in the region. The research highlighted the need for locally adjusted models to improve the accuracy of weather predictions and supported the integration of GNSS data into weather forecasting systems.

A recent study in Indonesia by Wijaya et al. (2023) estimated precipitable water vapor using data from the Ina CORS network. This work is significant because it focuses on a tropical region where water vapor variability is high, presenting unique challenges for weather forecasting. The authors found that GNSS stations provide valuable data that can improve the understanding of local climate patterns and support natural disaster management.

Additionally, the study by Patel and Kuttippurath (2023) provided a global perspective on how the increase in tropospheric water vapor amplifies global warming and climate changes. This work highlighted the need for precise water vapor monitoring to better understand the effects of global climate change. The authors concluded that the increase in PWV is directly related to an increase in the intensity and frequency of extreme weather events, emphasizing the importance of GNSS stations in climate monitoring.

The Colombian Geological Survey (SGC) has been exploring the implementation of tropospheric water vapor monitoring using GNSS technology. The SGC's GNSS stations are equipped with integrated meteorological sensors that record variables such as temperature, atmospheric pressure, and relative humidity. They also have real time data transmisión systems and advanced software to calculate tropospheric water vapor content. This information is crucial for weather forecasting and climate research in the country (Colombian Geological Survey, 2023).

The development of an informational booklet on CORS stations and their role in tropospheric water vapor analysis is vital for empowering rural, agricultural, Indigenous, and afro descendant communities. Despite significant advances in GNSS technology and its meteorological applications, these communities often lack clear, accessible guidance on how to harness such tools to their advantage.

This booklet will bridge the gap between cutting edge geospatial science and the people who stand to benefit most. By clearly explaining how CORS stations operate and how GNSS signal delays are converted into precipitable water vapor (PWV) estimates, the material will demonstrate the direct relevance of these data to local challenges, such as optimizing crop irrigation, managing water resources, and preparing for extreme weather. Involving community members in interpreting and applying PWV information can foster more sustainable resource stewardship and enhance resilience to climate variability.

Furthermore, the booklet's educational design addresses the urgent need to boost geospatial technology literacy at the grassroots level. As a user friendly, didactic tool, it will demystify technical concepts and provide step by step guidance for using GNSS derived water vapor data in practical contexts, ranging from agricultural planning to early warning systems for floods and droughts. In doing so, it equips local stakeholders with the knowledge to integrate advanced environmental monitoring into their decision-making processes, thereby promoting sustainable development and more effective adaptation to climate change.

## 3. Objectives

### 3.1 General Objective

Apply GNSS derived data from CORS stations for the estimation of tropospheric water vapor in a case study of Cumaribo (Vichada) and to disseminate these methodologies among rural stakeholders, thereby promoting their integration into environmental management and territorial adaptation strategies.

### 3.2 Specific Objectives

- Estimate the value of tropospheric water vapor (PWV) from GNSS data obtained from

the CORS CUMA station using freely accessible services and formulas.

- Design and produce an educational learning guide that clearly conveys both the qualitative and quantitative advantages of CORS based PWV estimation, using language and visuals tailored to a diverse, nonspecialist audience for social appropiation of knowledge.
- Develop and implement a knowledge transfer process of the educational learning guide within a municipality prioritized by IGAC for CORS deployment and assess its effectiveness in enhancing local understanding and uptake of GNSS based environmental monitoring techniques.

## 4. Theoretical Framework

Tropospheric water vapor is one of the most dynamic and determining variables of the Earth's atmosphere. Its presence is essential for cloud formation, precipitation, and the transport of energy within the climate system. Although it constitutes a small fraction of the atmospheric air in terms of mass, its impact on the planet's thermal regulation is immense, as it acts as the most potent natural greenhouse gas (Error: Reference source not found), absorbing and emitting infrared radiation (Harries, 1997; Solomon et al., 2010). These characteristics make it a key factor in understanding both daily meteorological variability and long-term climate change processes.

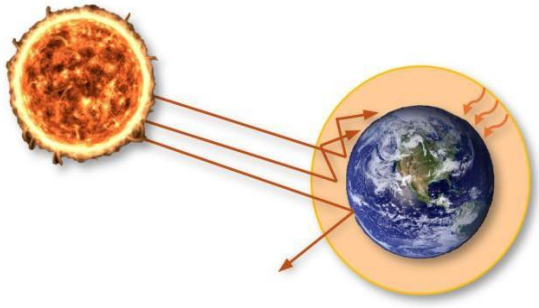

Figure 1. Water vapor as a greenhouse gas.

The concept of precipitable water vapor (PWV) refers to the total amount of water vapor contained in a vertical column of the atmosphere. Its measurement, especially in real time, provides critical information to improve weather forecasting, monitor extreme events such as intense storms or prolonged droughts, and design mitigation strategies for climate variability (Davis et al., 2016; Sherwood et al., 2010).

On the other hand, the global increase in water vapor content has been directly associated with global warming and the intensification of extreme phenomena. Patel and Kuttippurath (2023) analyzed this trend and warned that water vapor acts as an amplifier of climate change, making its monitoring a priority in environmental observation systems.

Traditionally, PWV measurement relied on the use of radiosondes, which, while accurate, have operational and spatial limitations. This scenario would change significantly with the incorporation of GNSS (Global Navigation Satellite System) technologies, which allow for continuous, automated estimation of tropospheric water vapor content without the need for additional meteorological devices.

The theoretical starting point for this approach was established by Bevis et al. (1992), who demonstrated that the delays experienced by satellite signals when passing through the atmosphere can be modeled to infer the amount of water vapor present. As the signal propagates from the satellite to the ground-based receiver, it suffers a total delay (ZTD) (Error: Reference source not found), which can be decomposed into two parts: the hydrostatic delay (ZHD), associated with pressure and dry gases, and the wet delay (ZWD), caused by the presence of water vapor. The latter is the one of interest for estimating the PWV.

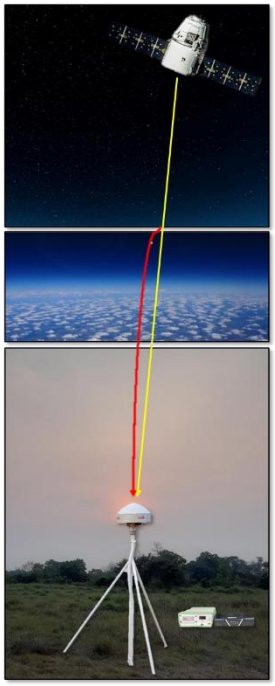

Figure 2. Tropospheric delay. Source: Own adaptation.

.

This approach offers several advantages: it allows continuous measurements, is independent of local weather conditions (such as cloud cover), and does not require complex or expensive instrumentation compared to other methods like radiosondes. Furthermore, the use of CORS station networks allows coverage of large areas and the generation of useful time series for atmospheric monitoring.

The conversion of ZWD to PWV relies on models that integrate GNSS data with meteorological variables. One of the most widely used models is Saastamoinen's, adjusted according to local parameters such as the average temperature and the altitude of the observation site. Currently, these calculations can be performed using freely available tools, such as the CSRS PPP service, which processes GNSS observation files and generates accurate estimates of the tropospheric delay.

The strategic value of these technologies is not limited to the scientific field. CORS stations are also key tools for risk management, climate change monitoring, agricultural irrigation optimization, and protecting vulnerable communities from extreme weather events. Cucurull et al. (2007) demonstrated that incorporating GNSS data into numerical models improves short term weather forecasting. Riccardi et al. (2021) showed its utility in volcanic regions prone to torrential rains, and Zhang et al. (2015) documented how they captured atmospheric signals prior to severe storms in Australia.

These technologies deliver reliable, real time estimates of precipitable water vapor (PWV), thereby strengthening climate monitoring capabilities and environmental management across scales. When paired with educational resources, such as the informational booklet developed in this study, they facilitate knowledge transfer and empower communities to address climate challenges proactively and with greater understanding.

Beyond purely scientific research, PWV data have numerous practical applications: they feed into numerical weather prediction models, support hydrological simulations, inform agricultural scheduling, guide the design of early warning systems, and underpin climate change monitoring efforts. The real time accessibility of PWV through CORS networks enables evidence-based decision making in climate sensitive sectors; agriculture, public health, water resource management, and disaster risk reduction, thereby enhancing resilience and sustainable development.

## 5. Methodology

The methodological development of this study combined an exploratory phase, aimed at identifying institutional and bibliographic sources related to the estimation of tropospheric water vapor using GNSS, with a technical and applied phase, in which the practical calculation of water vapor was carried out using real data from a CORS station. Additionally, a pedagogical component was integrated, aimed at the development of an accessible educational pamphlet designed to foster the social appropriation of geospatial knowledge by rural communities. The methodology executed is presented below:

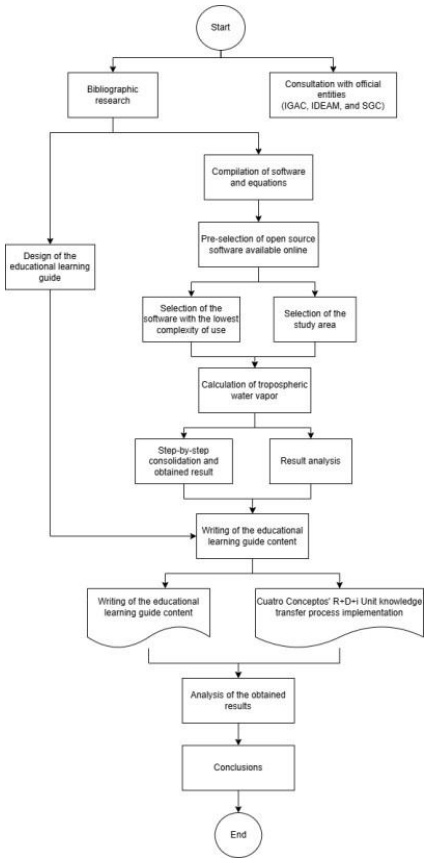


Figure 3. Tropospheric delay. Source: Own adaptation.

Initially, a formal inquiry was made to the Institute of Hydrology, Meteorology, and Environmental Studies (IDEAM) through written communication to establish whether this entity uses CORS stations to estimate meteorological variables such as tropospheric water vapor. The response from IDEAM, received via email, was documented and archived as part of the exploration process.

In parallel, telephone contact was made with the Agustín Codazzi Geographic Institute (IGAC), the entity responsible for the National Geodetic Network, without obtaining relevant results on the topic at that time. However, guidance was received to consult the Colombian Geological Survey (SGC), where it was identified that this entity has initiated the implementation of GNSS stations for meteorological purposes, as indicated on their institutional website.

To complement the search, a review of scientific literature and online academic repositories was conducted to identify the most widely used software, formulas, and methodologies for estimating PWV from GNSS data. A comparative compilation of available tools was made, prioritizing those that were freely accessible and had technical documentation available for nonspecialized users (Table 1).

| Document Name | Software Used | License | Formulas Used |
|---|---|---|---|
| Method for estimating precipitable water vapor, by remote detection, using the Global Positioning System (GPS) with application in improving the weather forecast in the city of Bogotá, D.C. | GIPSY-OASIS | License required | ZHD= 0.0022768 * P/ (1 - 0.00266 * cos(2φ) - 0.00028 * h) |
| Analysis of the calculation model used to obtain tropospheric water vapor from the delays in the GNSS signal in the central western region of Argentina | GIPSY-OASIS | License required | PWV=Π * ZWD, where Π is an empirical constant |
| Development of a correction model for the influence of tropospheric water vapor in DInSAR processing with the contribution of GNSS and ERA5 | GIPSY-OASIS, ERA5 | License required for GIPSY-OASIS, ERA5 Free | ZTD=ZHD+ZWD, PWV=Π * ZWD |
| Determination of Tropospheric Water Vapor Through GPS Observations: First Trials in Venezuela | GIPSY-OASIS | License required | ZHD= 0.0022768 * P/ (1 - 0.00266 * cos(2φ) - 0.00028 * h) |
| Tropospheric Delay in the Neapolitan and Vesuvius Areas (Italy) by Means of a Dense GPS Array: A Contribution for Weather Forecasting and Climate Monitoring | GIPSY-OASIS | License required | ZHD= 0.0022768 * P/ (1 - 0.00266 * cos(2φ) - 0.00028 * h) |
| Determination and assessment of GNSS-derived precipitable water vapor in Indonesia using Ina-CORS | RTKLIB | Free | ZHD= 0.0022768 * P/ (1 - 0.00266 * cos(2φ) - 0.00028 * h) |
| Variation of Precipitable Water Vapor derived from GNSSCORS Observations in Thailand | RTKLIB | Free | ZHD= 0.0022768 * P/ (1 - 0.00266 * cos(2φ) - 0.00028 * h) |
| Systematic Errors in Global Radiosonde Precipitable Water Data from Comparisons with Ground-Based GPS Measurements | GIPSY-OASIS | License required for GIPSY-OASIS | ZHD= 0.0022768 * P/ (1 - 0.00266 * cos(2φ) - 0.00028 * h) |
| An Integrated Assessment of Measured and Modeled Integrated Water Vapor in Switzerland for the Period 2001–03 | GIPSY-OASIS | License required | ZHD= 0.0022768 * P/ (1 - 0.00266 * cos(2φ) - 0.00028 * h) |
| GPS Meteorology: Remote Sensing of Atmospheric Water Vapor Using the Global Positioning System | GIPSY-OASIS | License required | ZHD= 0.0022768 * P/ (1 - 0.00266 * cos(2φ) - 0.00028 * h) |
| Integrated water vapour from GPS | RTKLIB | Free | ZHD= 0.0022768 * P/ (1 - 0.00266 * cos(2φ) - 0.00028 * h) |
| Assimilation of Global Positioning System Radio Occultation Observations into NCEP's Global Data Assimilation System | GIPSY-OASIS | License required | ZHD= 0.0022768 * P/ (1 - 0.00266 * cos(2φ) - 0.00028 * h) |
| Sensing Atmospheric Water Vapor With The Global Positioning System | GIPSY-OASIS | License required | ZHD= 0.0022768 * P/ (1 - 0.00266 * cos(2φ) - 0.00028 * h) |

Table 1. Compilation of most used software and equations.

Once the alternatives were identified, programs that were not available for download or did not allow easy access to tropospheric files were progressively discarded. As a result, the online service CSRS-PPP (Canadian Spatial Reference System – Precise Point Positioning), managed by Natural Resources Canada, was selected. This service allows the processing of RINEX files and provides key tropospheric parameters such as zenith wet delay (ZWD). (Figure 4)

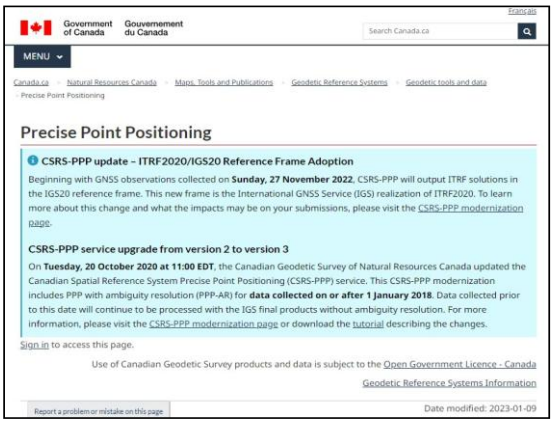


Figure 4. CSRS-PPP Service. Source: CSRS-PPP

To apply the methodology, the study area chosen was the municipality of Cumaribo, Vichada, specifically selecting the CORS CUMA station, which is part of the densification process of the National Geodetic Network (MAGNA-ECO), led by the IGAC and developed with support from the company Cuatro Conceptos S.A.S. Through the official platform "Colombia en Mapas," the RINEX observation file corresponding to July 20, 2024, was downloaded in order to perform a practical calculation (Figure 5).

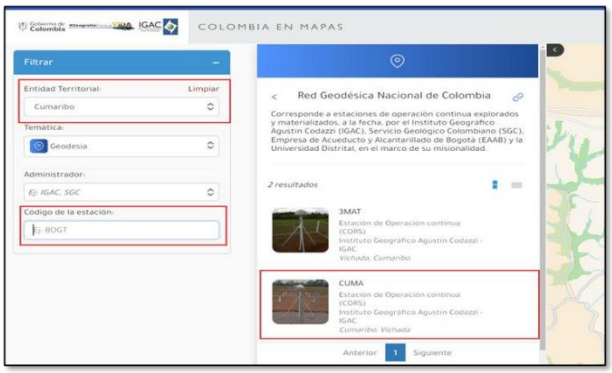


Figure 5. Selection of CORS CUMA station. Source: Colombia en Mapas IGAC.

The RINEX file was uploaded to the CSRS-PPP platform, where a tropospheric file was generated with the estimated values of ZTD, ZHD, and ZWD. To calculate the precipitable water vapor, the second 43200 of the GPS day, corresponding to noon, was selected, assuming atmospheric stability during that interval and optimal satellite visibility. (Figure 6)


Figure 6. Obtaining tropospheric file from CSRS-PPP. Source: own elaboration.

The PWV calculation was performed using a Python programming code, based on the empirical conversion formula derived from the Saastamoinen model, considering the conversion constant adjusted to the local average temperature. The formulation and procedure were based on the article “Variation of Precipitable Water Vapor derived from GNSS CORS Observations in Thailand” by Meunram and Satirapod (2019), adapting their method to the conditions observed in the Colombian region. (Figure 7)

```python
def calculate_PWV(ZWD, T_m):
    # Constantes
    p_w = 999.97  # Densidad del agua líquida en kg/m³
    R_v = 461.525  # Constante de gas para el vapor de agua en J/(K·kg)
    k_3 = 3739  # Constante física en K²/mb
    k_2 = 22.1  # Constante física en K/mb

    # Convertir temperatura a Kelvin
    T_m_k = T_m + 273.15

    # Constante de conversión Π en kg/m² por mm de ZWD
    Pi = (10**6) / (p_w * R_v * ((k_3 / T_m_k) + k_2))  # Resultado en kg/m² por mm de ZWD

    # Calcular PWV en mm
    PWV = Pi * ZWD

    return PWV

# Ejemplo de uso
ZWD = 326.2  # Retardo zenital húmedo en mm
T_m = 27  # Temperatura del aire en °C

PWV = calculate_PWV(ZWD, T_m)
print(f"PWV: {PWV:.2f} mm")
```

Figure 7. Programming code implemented in the calculation of tropospheric water vapor.

Subsequently, the step-by-step process for estimating water vapor was consolidated, structuring each stage clearly and sequentially. This systematization served as the basis for the creation of an educational learning guide aimed at spreading knowledge among rural, campesinos, indigenous, and afrodescendant communities as part of the social appropiation of knowledge.

The content of the educational learning guide was written in accessible and pedagogical language, accompanied by explanatory illustrations, local examples, and a participatory approach. Topics such as the functioning of CORS stations, the relationship between water vapor and climate, and the potential benefits this technology offers for agriculture, health, water management, and climate change mitigation were addressed. (Figure 8)

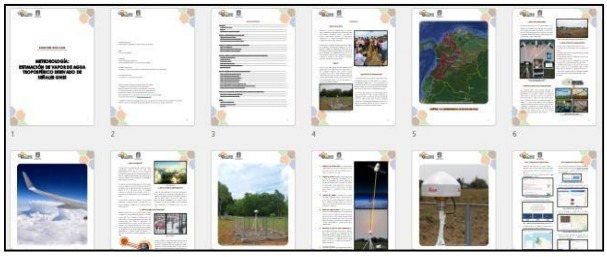

Figure 8. Writing and consolidation of the informational brochure.

Finally, the implementation of the knowledge transfer process was held by Cuatro Conceptos

S.A.S' Research, Development, and Innovation R+D+i Unit in the municipality of Vélez, Santander, at the SENA facilities. The event was attended by apprentices and instructors, who actively engaged with the content of the brochure and expressed interest in replicating and spreading the knowledge acquired. The activity was documented with photographic records and allowed the evaluation of the level of social appropriation achieved through this educational strategy. (Figure 9)

Figure 9. Community participation. Source: Cuatro Conceptos. (2024).

## 6. Results

### 6.1 Tropospheric Water Vapor Estimation

The result obtained for the estimation of tropospheric water vapor from the data of the CORS CUMA station, in Cumaribo, Vichada, was 20.45 mm, based on a RINEX file from July 20, 2024, calculated for the midday values.

```python
def calculate_PWV(ZWD, T_m):
    # Constantes
    p_w = 999.97 #Densidad del agua liquida en kg/m3
    R_v = 461.525 #Constante de los gases para el vapor de agua en J/(kg·K)
    k_3 = 3739 #Constante física en K2/mb
    k_2 = 22.1 #Constante física en K/mb

    #Convertir temperatura a Kelvin
    T_m_K = T_m + 273.15

    #Constante de conversión π en kg/m2 por mm de ZWD
    Pi = (10**6)/(p_w * R_v * (k_3/T_m_K + k_2)) #Resultado en kg/m2 por mm de ZWD

    #Calcular PWV en mm
    PWV = Pi * ZWD
    return PWV

# Ejemplo de uso
ZWD = 326.2  # Retardo zenital humedo en mm
T_m = 27   # Temperatura del aire en °C

PWV = calculate_PWV(ZWD, T_m)
print(f"El valor de PWV es: {PWV: .2f} mm")
```

```
PROBLEMS  OUTPUT  DEBUG CONSOLE  TERMINAL  PORTS
PS C:\Users\neyit.pena> & C:/Users/neyit.pena/AppData/Local/Programs/Python/Python312/python.exe "c:/Users/neyit.pena
/Documents/2_GENINVEST/1_PASANTIA/CARTILLA/ANALISIS DE DATOS/CUMA 20-07-24/Calculo PWV.py"
El valor de PWV es:  20.45 mm
PS C:\Users\neyit.pena>
```

Figure 10. Estimated troposheric wáter vapor from the CORS CUMA station, Cumaribo Vichada.

### 6.2 Educational Learning Guide for Social Appropiation of Knowledge

The outcomes of the learning guide effort are encapsulated in the publication titled "GNSS-CORS Benefits in Meteorology: Estimation of Tropospheric Water Vapor from GNSS Signals."

Interested readers may obtain the brochure directly by contacting the Geographic Institute Agustín Codazzi or Cuatro Conceptos S.A.S. via email at info@cuatroconceptos.com.

### 6.3 Cuatro Conceptos' R+D+I Unit Knowledge Transfer Process Implementation

The photographic record captured during the knowledge transfer process of the instalation and the benefits of the CORS stations in the municipality of Vélez, Santander, by the Research, Devolpment and Innovation Unit from Cuatro Conceptos S.A.S is shown below, highlighting the participation of Héctor Mauricio Ramírez Daza, Director of the unit and Francisco Javier Mora, Chief of Geosedy Department.

Figure 11. Knowledge transfer process, Vélez Santander. Source: Cuatro Conceptos (2024)

## 7. Analysis of Results

### 7.1 Tropospheric Water Vapor Estimation

The tropospheric water vapor estimation in Cumaribo, Vichada, revealed a value of 20.45 mm on July 20, 2024, at noon. This humidity level is indicative of cloud formation and frequent precipitation in the tropical region, which is crucial for water resource planning and anticipating adverse weather conditions.

In the agricultural field, this value allows farmers to optimize irrigation and crop management, improving water use efficiency and reducing the risk of plant diseases. Additionally, humidity information has health implications, as elevated levels can intensify heat and affect vulnerable people. It is also essential for risk management, as it enables the anticipation of extreme weather events and

improves preparedness and response to storms and floods.

### 7.2 Educational Learning Guide for Social Appropiation ff Knowledge

The educational learning guide developed for the social appropriation of GNSS-CORS knowledge effectively elucidates the operational advantages of CORS stations in a clear and accessible format, thereby serving a heterogeneous audience that includes rural farmers, Indigenous groups, and afrodescendant communities.

By incorporating the Cumaribo case study, the guide furnishes a concrete, practical illustration of how CORS derived tropospheric water vapor data can be processed and interpreted.

This methodological approach demystifies complex geodetic and meteorological concepts, thereby fostering the adoption of GNSS technology for optimized agricultural management, water resource planning, and early anticipation of extreme weather phenomena. Moreover, it stimulates active community engagement in both the dissemination and application of these technologies, ultimately strengthening local resilience and adaptive capacity in the face of climate variability.

### 7.3 Cuatro Conceptos' R+D+I Unit Knowledge Transfer Process Implementation

The knowledge transfer process implementation among SENA apprentices and instructors in the municipality of Vélez has catalyzed considerable interest in GNSS technologies. This collaborative exchange has established a foundation for broader adoption of these tools, thereby enhancing appreciation of CORS-station benefits across multiple disciplines and professional contexts.

Beyond its educational impact, the deployment of CORS stations yields tangible advantages for local communities, enhanced positional accuracy supports precision agricultural planning, optimizes water resource allocation, and boosts crop productivity. Furthermore, real time tropospheric water vapor data improves natural resource management and bolster preparedness for extreme weather events, thereby safeguarding community livelihoods. In sum, CORS station infrastructure not only cultivates the next generation of geospatial professionals but also underpins local sustainable development by equipping stakeholders with advanced tools for environmental management and strategic planning.

## 8. Conclusions

The data collection has confirmed that CORS stations are a valuable tool for analyzing the troposphere and estimating tropospheric water vapor, thereby improving the accuracy of weather forecasting and resource management.

An educational and informational guide was successfully created, explaining both the qualitative and quantitative benefits of CORS stations. As part of the quantitative findings, the study conducted in the municipality of Cumaribo, Vichada, estimated tropospheric water vapor at 20.45 mm on July 20, 2024, at noon. The educational guide was designed to be accessible to a broad and diverse audience, including rural populations, farmers (campesinos), indigenous peoples, and Afro-descendant communities.

The knowledge transfer process, implemented by Cuatro Conceptos in Vélez, Santander—a municipality prioritized by IGAC for the installation of CORS stations—engaged SENA apprentices and instructors, showing a high level of interest and understanding. This highlighted the relevance of CORS stations for the local community.

It is crucial to continue researching and leveraging GNSS data and CORS stations to maximize their potential in estimating precipitable water vapor and other meteorological parameters. These technologies improve the accuracy of weather forecasting, supporting water resource management and agricultural planning. Therefore, the implementation of CORS stations in rural, farming, indigenous, and Afro-descendant communities promote local development and strengthens resilience to extreme weather events.

The use of GNSS and CORS stations contributes to more efficient and sustainable natural resource management, benefiting both communities and the environment. Furthermore, promoting knowledge and use of these technologies will continue advancing science and innovation, generating a positive impact on society.

## 9. References


Arundel, A. V., Sterling, E. M., Biggin, J. H., & Sterling, T. D. (1986). Indirect health effects of relative humidity in indoor environments. Environmental Health Perspectives, 65, 351–361. https://doi.org/10.1289/ehp.8665351

Bevis, M., Businger, S., Herring, T. A., Rocken, C., Anthes, R. A., & Ware, R. H. (1992). GPS meteorology: Remote sensing of atmospheric water vapor using the global positioning system. Journal of Geophysical Research, 97(D14), 15787–15801. https://doi.org/10.1029/92jd01517

Cioce, V., Hoyer, M., Wildermann, E., Royero, G., & Díaz, A. (2011). Determinación del vapor de agua troposférico a través de observaciones GPS: primeros ensayos en Venezuela. Interciencia, 36(10), 721–730. https://www.redalyc.org/articulo.oa?id=33921449003

Cucurull, L., Derber, J. C., Treadon, R., & Purser, R.J. (2007). Assimilation of global positioning system radio occultation observations into NCEP's global data assimilation system. Monthly Weather Review, 135(9), 3174–3193. https://doi.org/10.1175/mwr3461.1

Davis, R. E., McGregor, G. R., & Enfield, K. B. (2016). Humidity: A review and primer on atmospheric moisture and human health. Environmental Research, 144, 106–116. https://doi.org/10.1016/j.envres.2015.10.014

Giri, R. K., Meena, L. R., Bhandari, S. S., & Bhatia, R.C.(2007).Integrated water vapour from GPS. Mausam, 58(1),101–106. https://doi.org/10.54302/mausam.v58i1.1139

Guerova, G., Brockmann, E., Schubiger, F., Morland, J., & Mätzler, C. (2005). An integrated assessment of measured and modeled integrated water vapor in Switzerland for the period 2001–03. Journal of Applied Meteorology, 44(7), 1033–1044. https://doi.org/10.1175/jam2255.1

Harries, J. E. (1997). Atmospheric radiation and atmospheric humidity. Quarterly Journal of the Royal Meteorological Society. Royal Meteorological Society (Great Britain), 123(544), 2173–2186. https://doi.org/10.1002/qj.49712354402

Mackern Oberti, M. V., Mateo, M. L., Camisay, M. F., & Rosell, P. A. (2021). Vapor de agua integrado troposférico estimado desde GNSS en Argentina. En Libro de resúmenes de la XXIX Reunión Científica de la Asociación Argentina de Geofísicos y Geodestas (Vol. 322, p. 323). Asociación Argentina de Geofísicos y Geodestas.

Mackern Oberti, M. V., Mateo, M. L., Camisay, M. F., Rosell, P. A., Weidmann, T., & Gonzalez Romo, A. (2021). Análisis del modelo de cálculo utilizado para obtener el vapor de agua troposférico desde los retardos en la señal GNSS en la región centro oeste de Argentina. Universidad Juan Agustin Maza; Investigación, Ciencia y Universidad, 5, 6; 3. https://ri.conicet.gov.ar/handle/11336/167417

Meunram, P., & Satirapod, C. (2019). Spatial variation of precipitable water vapor derived from GNSS CORS in Thailand. Geodesy and Geodynamics, 10(2), 140–145. https://doi.org/10.1016/j.geog.2019.01.003

Min Li, L. Q. (2014) Precise Point Positioning Using PANDA Software Package. GNSS Research Center,Wuhan University

Patel, V. K., & Kuttippurath, J. (2023). Increase in tropospheric water vapor amplifies global warming and climate change. Ocean-Land-Atmosphere.

Research. https://doi.org/10.34133/olar.0015

Riccardi, U., Tammaro, U., & Capuano, P. (2021). Tropospheric delay in the Neapolitan and Vesuvius Areas (Italy) by means of a dense GPS array: a contribution for weather forecasting and climate monitoring. Atmosphere, 12(9), 1225.

Rocken, C., Ware, R., Van Hove, T., Solheim, F., Alber, C., Johnson, J., Bevis, M., & Businger, S. (1993). Sensing atmospheric water vapor with the global positioning system. Geophysical Research Letters, 20(23), 2631–2634. https://doi.org/10.1029/93gl02935

Rosell, P. A. (20222). Desarrollo de un modelo de corrección de la influencia del vapor de agua troposférico en el procesamiento DInSAR con el aporte de GNSS y ERA5.

Rost, S., Gerten, D., Hoff, H., Lucht, W., Falkenmark, M., & Rockström, J. (2009). Global potential to increase crop production through water management in rainfed agriculture. Environmental research letters, 4(4), 044002. https://doi.org/10.1088/1748-9326/4/4/044002

Schneider, T., O'Gorman, P., y Levine, X. (2009). VAPOR DE AGUA Y DINÁMICA DE LOS CAMBIOS CLIMÁTICOS. Review of Geophysics, 48. https://doi.org/10.1029/2009RG000302

Servicio Geológico Colombiano. (2023). Monitoreo del vapor de agua troposférico utilizando tecnología GNSS. Recuperado de SGC https://geored2.sgc.gov.co/investigacion/metereologiaGNSS/Pa ginas/default.aspx

Sherwood, S. C., Roca, R., Weckwerth, T. M., & Andronova, N. G. (2010). Tropospheric water vapor, convection, and climate. Reviews of Geophysics (Washington, D.C.: 1985), 48(2). https://doi.org/10.1029/2009rg000301

Shivers, S. W., Roberts, D. A., McFadden, J. P., & Tague, C. (2019). An analysis of atmospheric water vapor variations over a complex agricultural region using airborne imaging spectrometry. PloS One, 14(12), e0226014. https://doi.org/10.1371/journal.pone.0226014

Shu-bo, Q. (2008). Concept,evolvement and tendency of CORS. Science of Surveying and Mapping.

Solomon, S., Rosenlof, K. H., Portmann, R. W., Daniel, J. S., Davis, S. M., Sanford, T. J., & Plattner, G.-K. (2010). Contributions of stratospheric water vapor to decadal changes in the rate of global warming. Science (New York, N.Y.), 327(5970), 1219–1223. https://doi.org/10.1126/science.1182488

Šverko Navarrete, M. (2012). Método de estimación del vapor de agua precipitable, por detección remoto, mediante el sistema de posicionamiento global (GPS) con aplicación en el mejoramiento del pronóstico del estado del tiempo en la ciudad de Bogotá, D.C.

Tackman, E. C., Higgins, D. N., Kerecman, D. E., Ott, E.-J. E., Johnston, M. V., & Freedman, M. A. (2023). The use of transmission electron microscopy with scanning mobility particle size spectrometry for an enhanced understanding of the physical characteristics of aerosol particles generated with a flow tube reactor. Aerosol Science and Technology: The Journal of the American Association for Aerosol Research, 57(4), 279–295. https://doi.org/10.1080/02786826.2023.2173999

Trenberth, K. E. (2011). Changes in precipitation with climate change. Climate Research, 47(1), 123–138. https://doi.org/10.3354/cr00953

Wang, J., & Zhang, L. (2008). Systematic errors in global radiosonde precipitable water data from comparisons with ground-based GPS measurements. Journal of Climate, 21(10), 2218–2238.https://doi.org/10.1175/2007jcli1944.1

Wijaya, D. D., Putri, N. S. E., Utama, A. K., Wibowo, S. T., & Sadarviana, V. (2024). Determination and assessment of GNSS-

derived precipitable water vapor in Indonesia using Ina- CORS. Advances in Space Research: The Official Journal of the Committee on Space Research (COSPAR), 73(1), 386–403. https://doi.org/10.1016/j.asr.2023.07.048

Zhang, K., Manning, T., Wu, S., Rohm, W., Silcock, D., & Choy, S. (2015). Capturing the signature of severe weather events in Australia using GPS measurements. IEEE journal of selected topics in applied earth observations and remote sensing, 8(4),1839–1847. https://doi.org/10.1109/jstars.2015.2406313

# Geoprocessing WorldClim Maps Using Python

José Luis Gutiérrez Ossio

*Adaptation to Climate Change Consultant, José Luis Gutiérrez Ossio - jl.gutierrez@gmx.net,*

**Abstract**: Meteorological information is used by countries for weather forecasting and warning, climate monitoring and research, agriculture and food security, disaster risk management, and water resource management, helping societies to stay safe, manage resources wisely, boost economies, and adapt to environmental changes. Unfortunately, that information is not available, especially in developing countries, which need to look for it in other sources, like WorldClim, which was developed by the Climatic Research Unit at the University of East Anglia. It is not advisable to directly use WorldClim datasets without knowing the strength and direction of the linear relationship with some source of information that is more reliable, like the meteorological information of ground stations managed by Bolivia's National Meteorological and Hydrological Service. To evaluate that correlation, a Python application was developed. With the help of that application, it was possible to conclude that for precipitation and the average minimum temperature, the correlation was strongly positive, while for the average maximum temperature, it was moderately positive.

***Keywords:*** WorldClim, GDAL, Pandas, Python, Geoprocessing

## 1. Introduction

Meteorological information is valuable because it supports decision-making in many sectors of society, economy, and science. It is used in several key areas, such as weather forecasting and warning, climate monitoring and research, agriculture and food security, disaster risk management, water resource management, and many more, helping societies stay safe, manage resources wisely, boost economies, and adapt to environmental changes (ChatGPT, 2025).

Historically around the world, meteorological information comes from observations that have been made on ground-based stations, which measure temperature, humidity, wind, pressure, and precipitation, among others, and were recorded mainly by meteorological services in each country. In some developed countries, there are stations that have been systematically recorded since the mid-19th century, but in developing countries, even today, it is not possible to use meteorological information coming from ground stations due to their low density of stations and gaps in the recorded data.

During the past decades, international institutions and universities have been working to overcome the problem of lack of weather data, developing methods and generating raster maps from remote sensing, radar systems, and data assimilation models that provide society with historical meteorological data.

## 2. Objective of the study

In order to overcome the lack of historical meteorological data, the objective of the present study is to evaluate the strength and direction of a relationship between the historical monthly weather data generated by WorldClim and data collected by ground

meteorological stations managed by the Bolivian National Meteorological and Hydrological Service in the area of Potosí[4] City.

To reach the mentioned objective, it was necessary to develop a geoprocessing application written in Python.

## 3. Geoprocessing application

### 3.1 Input data

The input data for the application comes from two sources.

#### 3.1.1 *WorldClim*

WorldClim is a database of high-resolution global climate data. It provides gridded datasets of historical and future climate conditions. This data is widely used for mapping, spatial modeling, and ecological studies. The key features of WorldClim are global coverage, high resolution, a variety of variables besides temperature and precipitation for climate data, and the fact that the data is freely available for academic uses and other non-commercial purposes.

For the present study, historical monthly weather data[5] for 1950-2024 was used in relation to the average minimum temperature (°C), average maximum temperature (°C), and total precipitation (mm) with a spatial resolution of 2.5 minutes (~21 km² at the equator). These data were downscaled from CRU-TS-4.09 by the Climatic Research Unit, University of East Anglia, using WorldClim 2.1 for bias correction. Each zip file downloaded contains 120 GeoTiff (.tif) files; each file corresponds to a month of the year (January is 1; December is 12) for a 10-year period.

In order to achieve the study objective, only data from 2000 to 2005 were used, because that is the period of data available from ground meteorological information to be compared with.

#### 3.1.2 *SENAMHI*

SENAMHI (National Meteorological and Hydrological Service) is Bolivia's national service for meteorology and hydrology, a technical and scientific institution under the Ministry of Environment and Water responsible for monitoring weather and water resources, maintaining the national network of weather stations, and issuing alerts and advisories on meteorological and hydrological phenomena.

SENAMHI, through its website[6] provides at no cost meteorological data, mainly for precipitation and temperature, collected in the network of ground stations. Unfortunately, that network, in most parts of the country, does not have a proper density and optimal distribution. The recorded data do not have a good historical record, and the freely available data for the study area have information from 2000 until 2024, with some gaps in the records.

For the study, eight meteorological stations were identified, but only five[7] has enough historical data to allow the objective of the research to be achieved.

### 3.2 Programming language

For developing the application, Python, a high-level, interpreted programming language, was selected due to its clear and readable syntax, its object-oriented capabilities, and a high number of libraries available to use for geoprocessing raster maps and data analysis.

Many Python libraries were used in the application, but some of them are the core of the application, which are mentioned below.

#### 3.2.1 *GDAL*

Geospatial Data Abstraction Library (GDAL) is a computer software library for reading and writing raster and vector geospatial data

[4] Potosí is a historic city and department in southern Bolivia, famous for its silver mines and colonial legacy, and was declared a UNESCO World Heritage Site. due to its cultural and historical significance. During the past decades, Potosi's population has been facing drinking water shortages.

[5] https://worldclim.org/data/monthlywth.html#google_vignette

[6] https://senamhi.gob.bo/index.php/sysparametros

[7] The five selected meteorological stations were Potosi Los Pinos, Tarapaya, Yocalla, Samasa, and Chaqui.

formats (e.g., shapefile, GeoTiff) and is released under the permissive X/MIT-style free software license by the Open-Source Geospatial Foundation. As a library, it presents a single abstract data model to the calling application for all supported formats. It may also be built with a variety of useful command-line interface utilities for data translation, projection, transformation, and processing.

GDAL/OGR[8] is considered a major free software project for its "extensive capabilities of data exchange" and also in the commercial GIS community due to its widespread use and comprehensive set of functionalities.

GDAL was used in the following modules:

- *WorldClim data loader,* using the `BuildVRT` command for the creation of a virtual dataset composed of WorldClim GeoTiff files. Its use was important in order to save disk space.
- *WorldClim to points*, where the `gdallocationinfo` command was used to extract the values of the bands of the virtual dataset corresponding to the meteorological ground station coordinates. It was necessary to use the NumPy library to properly arrange the output of the mentioned GDAL command.

#### 3.2.2 *Pandas*

Pandas ("Panel Data" and/or "Python Data Analysis") is an open-source Python library that is used for data manipulation and analysis. It consists of data structures and functions to perform efficient operations on data. It is well-suited for working with tabular data such as spreadsheets or SQL tables. It is used in data science because it works well with other important libraries. With Pandas it is possible to do data cleaning, merging, and joining; handling missing data; column insertion and deletion; group by operations; and data visualization.

Pandas were intensively used in all modules of the developed application, since SENAMHI's information came from tabular data, and the values of each raster map coming from WorldClim can be stored in DataFrames.

### 3.3 Application structure

The application has been developed in modules, one depending on the output of the previous one. It was programmed using the paradigm of object-oriented programming, which will allow, in the future, in an easy way, the updating, improving, and making more efficient of some methods without the need to change other parts of the code.

The modules are listed and explained below.

#### 3.3.1 *Senamhi data loader*

SENAMHI's data can be downloaded from its website as Excel files (more than one), which are saved in a directory. From that directory the data was loaded to a DataFrame using Pandas.

The output of this module is a csv file with meteorological information from the eight SENAMHI ground stations, cleansed and well organized for future use.

#### 3.3.2 *WorldClim data loader*

WorldClim GeoTiff maps were downloaded from its website as zip files and saved in a common directory. After their extraction, they were ready to be processed by the module.

The application read the directory and organized the GeoTiff to be processed as a DataFrame, where the file name included the month and year of the data, which was important to arrange in bands of the virtual dataset[9], which are the output of this module.

#### 3.3.3 *WorldClim to points*

In this module, the virtual dataset created in the previous module was used in conjunction with SENAMHI's meteorological ground station

[8] OGR library (Simple Features Library) is part of the GDAL source tree and provides a similar ability for simple features vector graphics data.

[9] A virtual dataset that contains 72 GeoTiff files has 1.6 megabytes. In contrast, if the virtual dataset is saved as a GeoTiff file, it has 10.7 gigabytes. It is important to mention that both have the same functionality.

coordinates. Using GDAL functionality, it was possible to extract the values of each band of the virtual dataset corresponding to each ground station, which was saved as a csv file, which is the output of this module.

#### 3.3.4 *WorldClim data evaluation*

Data from SENAMHI's ground station were used to evaluate the strength and direction of the relationship between the historical monthly weather data generated by WorldClim and data collected by ground meteorological stations in the area of Potosí City. For that, the Pearson standard correlation coefficient, which is one method of the Pandas library, was used.

The output of this module is a DataFrame that collects all the correlation coefficients organized by parameter and SENAMHI's ground station names.

### 3.4 Output data

The output of the application, besides the csv files with well-organized meteorological data and the virtual dataset, is a table (DataFrame) that presents all the correlation coefficients. The table is presented below.

| Senamhi's station | prec | tmax | tmin |
|---|---|---|---|
| Potosi Los Pinos | 0.91 | 0.58 | 0.91 |
| Tarapaya | 0.88 | 0.83 | 0.92 |
| Yocalla | 0.83 | 0.67 | 0.86 |
| Samasa | 0.88 | 0.55 | 0.87 |
| Chaqui | 0.92 | 0.58 | 0.88 |

Table 1. Correlation Coefficient by parameter and ground station

Where:

prec: Total precipitation

tmax: Average maximum temperature

tmin: Average minimum temperature

## 4. Conclusions

The WorldClim historical monthly weather data, used in the present study, has been generated by the Climatic Research Unit, University of East Anglia, and cannot be directly used without knowing the strength and direction of the correlation between the provided dataset compared with the more reliable data from the meteorological ground station for the specific part of the world.

On table 1, the values of the Pearson Correlation Coefficient are presented for five stations selected in this study. The closest station to the San Ildenfonso and Khari Khari Lakes that provide drinking water to Potosi City is the *Potosi Los Pinos* meteorological station.

For that station, the correlation coefficient for precipitation and average minimum temperature has a very strong positive correlation, and for the average maximum temperature, that value could be considered to have a moderate positive correlation. With those values, it is possible to use the WorldClim dataset in the Potosi Water Management, especially on the San Ildenfonso and Khari Khari Lakes watersheds.

## 5. References


ChatGPT. (2025, August 20). What are the uses of meteorological information? OpenAI. https://chat.openai.com/

GeeksforGeeks (2025). Pandas Introduction. Retrieved August 22, 2025, from https://www.geeksforgeeks.org/pandas/introduction-to-pandas-in-python/.

Harris, I., Osborn, T.J., Jones, P.D., Lister, D.H. (2020). Version 4 of the CRU TS monthly high-resolution gridded multivariate climate dataset. Scientific Data 7: 109

Wikipedia contributors. (2025, July 18). GDAL. In Wikipedia, The Free Encyclopedia. Retrieved 12:37, August 22, 2025, from https://en.wikipedia.org/w/index.php?title=GDAL&oldid=1301100983.

# Spatial Vulnerability Assessment Tools for Climate-Resilient Urban Planning: A Mixed-Methods GIS Framework

Michael Mutale [a, *], Oluibukun Gbenga Ajayi [b]

[a] *Department of Geomatics Engineering, Copperbelt University, Kitwe, Zambia – michael.mutale@cbu.ac.zm*

[b] *Department of Land and Spatial Sciences, Namibia University of Science and Technology, Windhoek, Namibia – oajayi@nust.na*

**Abstract**: Urban climate vulnerability assessment in African cities faces significant methodological challenges due to data scarcity, informal settlement complexity, and limited integration of spatial analysis tools with local contexts. This paper presents an innovative mixed-methods GIS framework for spatial vulnerability assessment, demonstrated through application in Windhoek's informal settlements. The methodology integrates Getis-Ord Gi* hotspot analysis with a novel Composite Climate Vulnerability Index (CCVI) and mixed-methods validation techniques. Applied across four informal settlements using 290 household surveys with GPS coordinates, the framework identified statistically significant vulnerability clusters and demonstrated strong methodological consistency across multiple validation measures. Key methodological innovations include adaptation of spatial clustering algorithms for informal settlement contexts, development of a scalable composite vulnerability index, and integration of quantitative spatial analysis with qualitative validation methods. The framework addresses critical gaps in existing vulnerability assessment tools by providing replicable, data-efficient methods suitable for resource-constrained African urban contexts. Results demonstrate the methodology's potential for supporting evidence-based climate adaptation planning and can be readily transferred to similar urban contexts across sub-Saharan Africa.

***Keywords:*** Vulnerability assessment, GIS methodology, spatial analysis, climate adaptation, urban planning, informal settlements

## 1. Introduction

Urban climate vulnerability assessment is a critical requirement for sustainable development planning, particularly in rapidly growing cities of sub-Saharan Africa, where informal settlements house significant proportions of urban populations (UN-Habitat, 2024). However, conventional vulnerability assessment methodologies face substantial limitations when applied to African urban contexts, including data scarcity, complex spatial patterns in informal settlements, and limited integration between quantitative spatial analysis and local contextual knowledge (Birkmann et al., 2022; Malaker & Meng, 2024).

Current approaches to urban climate vulnerability mapping predominantly rely on either coarse-resolution global datasets that fail to capture local variations or resource-intensive field-based assessments that lack spatial comprehensiveness (IPCC, 2023). The challenge is particularly acute in informal settlements, where conventional administrative boundaries, address systems, and infrastructure networks are absent or incomplete, making standard GIS analysis techniques less effective (Roy et al., 2024).

Recent advances in geoinformatics offer new opportunities for developing more robust and context-appropriate vulnerability assessment tools. Spatial clustering algorithms, particularly Getis-Ord Gi* statistics, have shown promise for identifying vulnerability hotspots, while composite index development provides mechanisms for integrating multiple vulnerability dimensions (Lanorte et al., 2024; Lapietra et al., 2024). However, these techniques have seremainted application in informal settlement contexts, and their integration with participatory validation methods remains underexplored.

The emergence of composite vulnerability indices represents a significant methodological advancement, allowing researchers to combine multiple indicators of exposure, sensitivity, and adaptive capacity into spatially explicit measures (Edmonds et al., 2020; Rabiei-Dastjerdi et al., 2025). Yet existing indices often lack validation against ground-truth data and may not capture the specific characteristics of informal urban environments in African contexts.

This paper addresses these methodological gaps by presenting an innovative mixed-methods GIS framework specifically designed for climate vulnerability assessment in African urban Windhoek provides an ideal testing ground due to its semi-arid climate, rapid urban growth, and well-documented challenges related to climate vulnerability and informal settlement development (City of Windhoek, 2022).

## 2. Methodological Framework

### 2.1 Study Area and Context

The methodology was developed and tested across four informal settlements in Windhoek: Havana, Hakahana, Okuryangava, and Otjomuise. These settlements were selected to represent diverse environmental and socio-economic conditions within the city's informal settlement landscape. Havana and Hakahana, located in northern areas, represent older and newer informal growth patterns, respectively. Okuryangava includes flood-prone eastern zones, while Otjomuise faces multiple climate contexts. The framework integrates three methodological innovations: (1) adaptation of Getis-Ord Gi* spatial clustering for informal settlement analysis, (2) development of a Composite Climate Vulnerability Index (CCVI) validated against local conditions, and (3) integration of quantitative spatial analysis with qualitative validation methods.

The methodology is demonstrated through application in Windhoek, Namibia, across four informal settlements (Figure 1) representing diverse topographic, climatic, and socio-economic conditions.

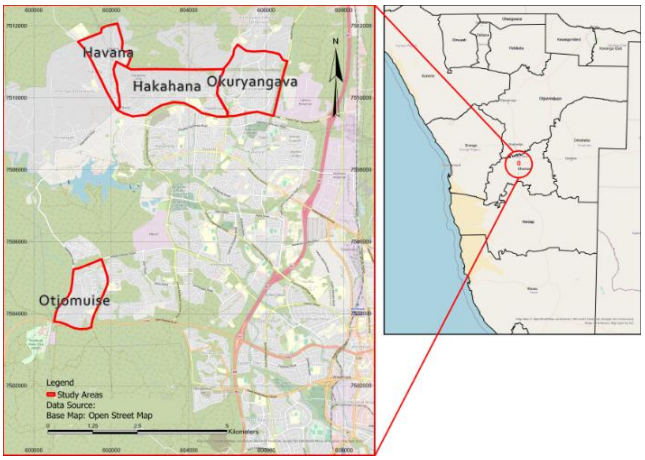


Figure 1. Study Area Map Showing Location of Four Settlements within Windhoek

risks, including heat exposure and erosion due to varied terrain and minimal vegetation cover.

Environmental challenges vary significantly across the study areas. Seasonal flooding affects low-lying regions, particularly in Okuryangava and parts of Hakahana. Heat stress is most pronounced in Otjomuise due to limited vegetation and challenging topography. All settlements face infrastructure deficits in drainage, water access, and sanitation systems, creating compound vulnerabilities that traditional assessment methods often fail to capture comprehensively.

### 2.2 Data Collection Strategy

The methodological framework (Fig. 2) employs a systematic multi-scale data collection approach designed to maximize spatial coverage while ensuring ground-truth validation.

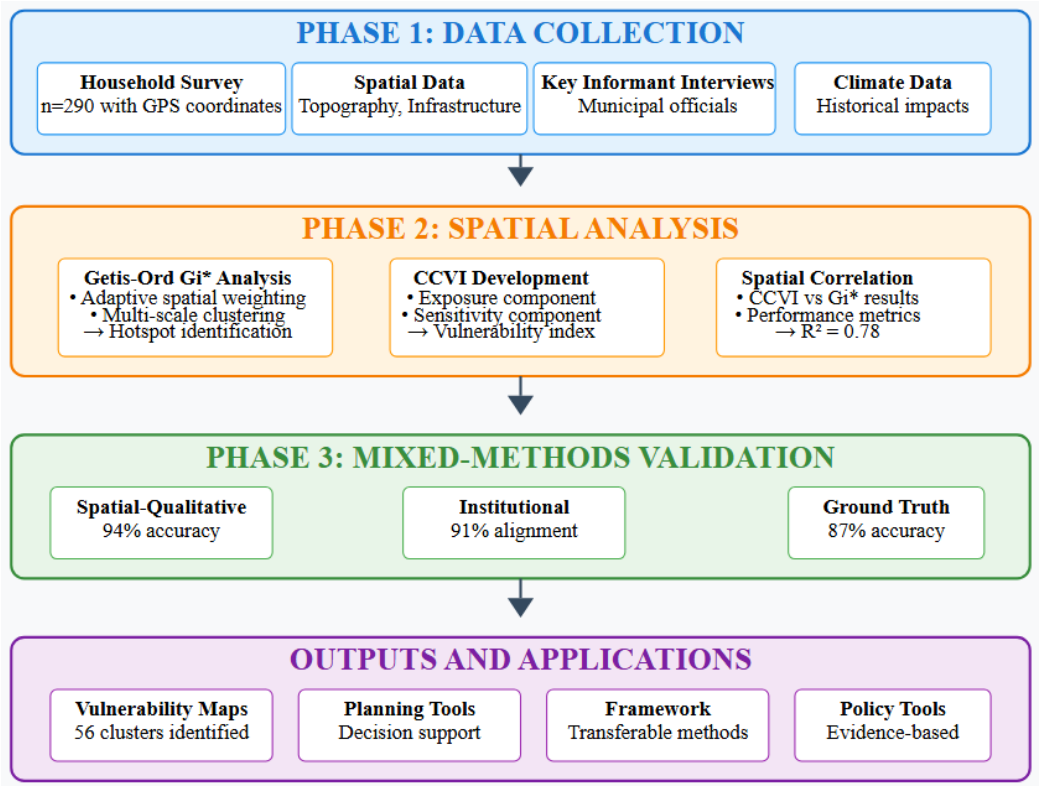


Figure 2. Mixed-Methods GIS Framework for Vulnerability Assessment

A household survey targeting 290 respondents was conducted across the four settlements, with GPS coordinates collected for each household to enable precise spatial analysis. Sample size calculation followed established protocols for spatial analysis studies, using a confidence level of 95% and a margin of error of 5%. The formula (Equation 1) for an infinite population yielded $n_0 = 384$, adjusted using the finite population correction () to arrive at the target sample size of 290 respondents distributed proportionally across settlements.

$$n_0 = \frac{Z^2 \, x p \, x (1-p)}{e^2} \qquad (1)$$

$$n = \frac{n_0}{1 + \frac{(n_0 - 1)}{N}} \qquad (2)$$

Where Z = 1.96 (95% confidence), p = 0.5 (maximum variability), e = 0.05 (margin of error), and N = estimated total population.

Five research teams were strategically deployed across settlements, with two teams assigned to Hakahana due to its larger geographic area and population density. This allocation strategy ensured comprehensive geographic coverage while optimizing data quality through team familiarity with local contexts.

Data collection employed mobile survey applications to ensure high data quality, real-time GPS coordinate capture, and offline functionality suitable for informal settlement conditions. The survey captured comprehensive information on climate impact experiences, adaptive capacity indicators, infrastructure access, and socio-economic characteristics necessary for vulnerability assessment.

### 2.3 Spatial analysis and index development

#### 2.3.1 *Getis-Ord Gi* Hotspot Analysis Adaptation*

The core spatial analysis methodology (Fig. 3) builds on Getis-Ord Gi* statistics, adapted specifically for informal settlement contexts where traditional spatial analysis assumptions may not hold. The Getis-Ord Gi* statistic identifies spatial clusters of high or low values by calculating standardized scores that indicate the degree to which similar values cluster spatially (Lester, 2024).

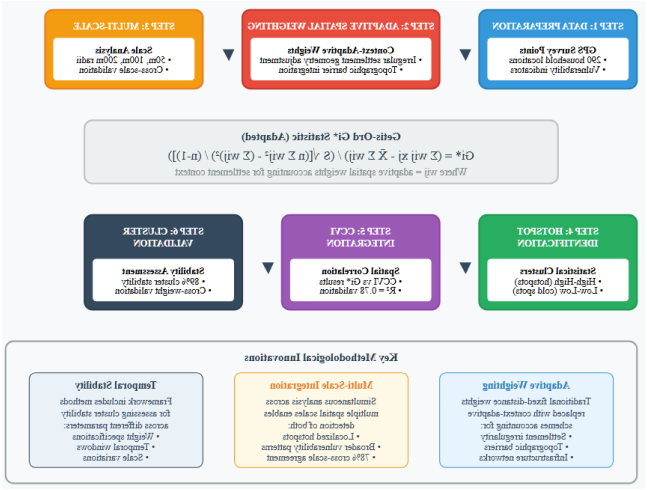

Figure 3. Spatial Analysis Workflow

The statistics are calculated using equation 3:

$$G_i^* = \frac{\sum_{j=1}^{n} w_{ij}x_j - \bar{X}\sum_{j=1}^{n} w_{ij}}{S\sqrt{\frac{\left[n\sum_{j=1}^{n} w_{ij}^2 - \left(\sum_{j=1}^{n} w_{ij}\right)^2\right]}{n-1}}} \quad (3)$$

Where $G_i^*$ *is the Getis-Ord Gi* statistic for location i, xj is the attribute value for feature j, wij is the spatial weight between features i and j, n is the total number of features, $\bar{X}$ is the mean of all attribute values, and S is the standard deviation of all attribute values.

Key adaptations for informal settlement analysis include adaptive spatial weighting, where traditional fixed-distance weights were replaced with adaptive weighting schemes that account for irregular settlement patterns and varying household densities. Multi-scale analysis was conducted at multiple spatial scales to capture different scales of vulnerability clustering. Topographic integration involved incorporating spatial weights with topographic factors (slope, elevation, drainage) that significantly influence vulnerability patterns in informal settlements.

### 2.3.2 *Composite Climate Vulnerability Index (CCVI) Development*

The CCVI (Fig. 4) integrates multiple dimensions of climate vulnerability following IPCC vulnerability frameworks while incorporating local context factors specific to informal urban environments. The index combines four primary components.

The exposure component measures direct climate hazard exposure, including flood risk, heat exposure, and water scarcity indicators.

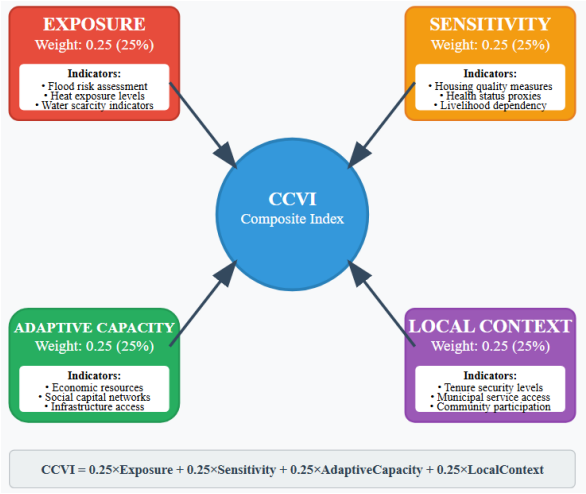


Figure 4. Composite Climate Vulnerability Index Structure

The sensitivity component captures factors that increase susceptibility to climate impacts, health status proxies (age composition, reported health impacts), and livelihood climate-dependency measures.

The adaptive capacity component encompasses the ability to respond to climate stressors, incorporating economic resources (income levels, asset ownership), social capital (community networks, institutional access), and infrastructure access.

Finally, the local context component incorporates factors specific to informal settlement environments, including tenure security levels, access to municipal services, and participation in community organizations.

The final CCVI (Equation 4) is calculated as a weighted composite:

$$CCVI = w_1 \times Exposure + w_2 \times Sensitivity + w_3 \times -Adaptive\ Capacity + w_4 \times Local\ Context \quad (4)$$

Component weights were determined through factor analysis and expert judgment, with equal weighting (0.25) applied to each

component to avoid bias toward any single dimension.

### 2.4 Mixed-Methods Integration

The framework integrates quantitative spatial analysis with qualitative validation through two mechanisms.

Spatial-qualitative triangulation involved validating hotspot analysis results through focused interviews with residents in identified high-vulnerability clusters to verify the accuracy of vulnerability predictions and understand local context factors.

Institutional validation employed semi-structured interviews with municipal planning officials, meteorological services, and urban

development practitioners to provide external validation of results and assessment of policy relevance.

## 3. Methodological Innovation and Framework Development

This research contributes several technical innovations to spatial clustering methodology specifically designed for informal settlement analysis in African urban contexts. The primary innovation lies in the development of adaptive spatial weighting schemes that replace traditional fixed-distance weights with context-adaptive approaches. These adaptive weights account for the irregular settlement geometry and varying household densities characteristic of informal settlements, while also incorporating topographic barriers that affect social and environmental connectivity and infrastructure networks that influence vulnerability transmission patterns.

The methodology demonstrates effective integration of analysis across multiple spatial scales, enabling simultaneous detection of both localized hotspots and broader vulnerability patterns. This multi-scale approach addresses a key limitation of single-scale analyses that often miss important vulnerability patterns operating at different geographic scales. Unlike static vulnerability assessments commonly used in urban planning, this framework includes systematic methods for assessing the temporal stability of identified clusters, which proves crucial for long-term planning applications and adaptive management strategies.

The Composite Climate Vulnerability Index development process introduces several methodological innovations that extend beyond traditional vulnerability assessment approaches. The inclusion of informal settlement-specific factors such as tenure security levels, differential service access patterns, and community organization participation addresses a significant gap in existing vulnerability indices that typically focus primarily on household-level characteristics without considering the unique spatial and social dynamics of informal settlements.

Component weights in the CCVI were determined through a systematic combination of statistical factor analysis and ground-truth validation procedures, ensuring both statistical rigor and practical relevance for local planning contexts. The index was deliberately designed for replication across different urban contexts through exclusive use of readily available data sources and standardized calculation procedures that can be implemented using common GIS software platforms.

The integration approach demonstrates several technical advances in mixed-methods spatial analysis. The research developed structured protocols for validating spatial analysis results through qualitative methods, directly addressing longstanding concerns about the reliability of purely quantitative approaches in complex social-environmental systems. Methods for systematically incorporating local knowledge into spatial analysis were developed without compromising analytical rigor, creating a template for participatory spatial analysis that maintains scientific validity while incorporating community perspectives.

Frameworks for translating complex spatial analysis results into actionable planning recommendations were established to bridge the persistent gap between technical analysis and policy implementation. This translation

mechanism proves particularly important in African urban contexts where technical capacity may be limited, and policy makers require clear, actionable insights rather than complex statistical outputs.

The framework demonstrates strong potential for transfer to other African urban contexts through several carefully designed features (Figure 5). The methodology relies primarily on household survey data and basic GIS datasets including topography and infrastructure networks that are either available or can be readily collected in most urban contexts across sub-Saharan Africa. Analysis procedures can be conducted using standard GIS software including both proprietary platforms like ArcGIS Pro and open-source alternatives like QGIS, with commonly available extensions, making the approach accessible to local planning agencies with varying technical resources.

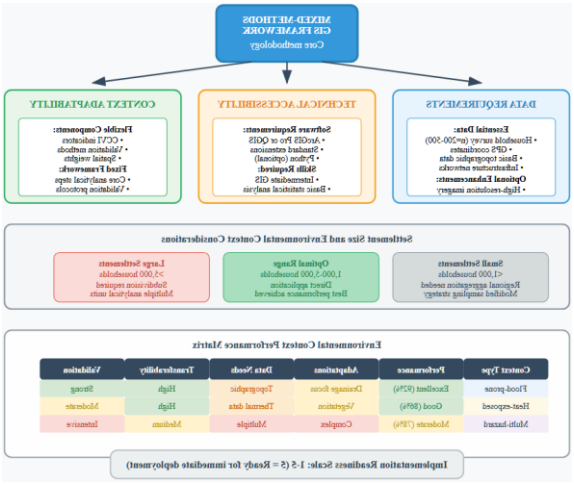

Figure 5. Framework Transferability Assessment for African Urban Contexts

The mixed-methods validation component (Figure 6) represents a particular strength in terms of transferability, as it allows systematic adaptation to local contexts and knowledge systems without requiring fundamental methodological changes. This flexibility enables the framework to accommodate different cultural contexts, linguistic diversity, and varying institutional arrangements while maintaining analytical consistency and comparability across different implementation contexts.

Testing across diverse settlement types revealed important scaling considerations that inform broader application strategies. The methodology performs optimally in settlements ranging from 1,000 to 5,000 households, though larger settlements can accommodate the approach through subdivision into manageable analytical units, while smaller settlements may require regional aggregation approaches to achieve sufficient statistical power for reliable clustering analysis.

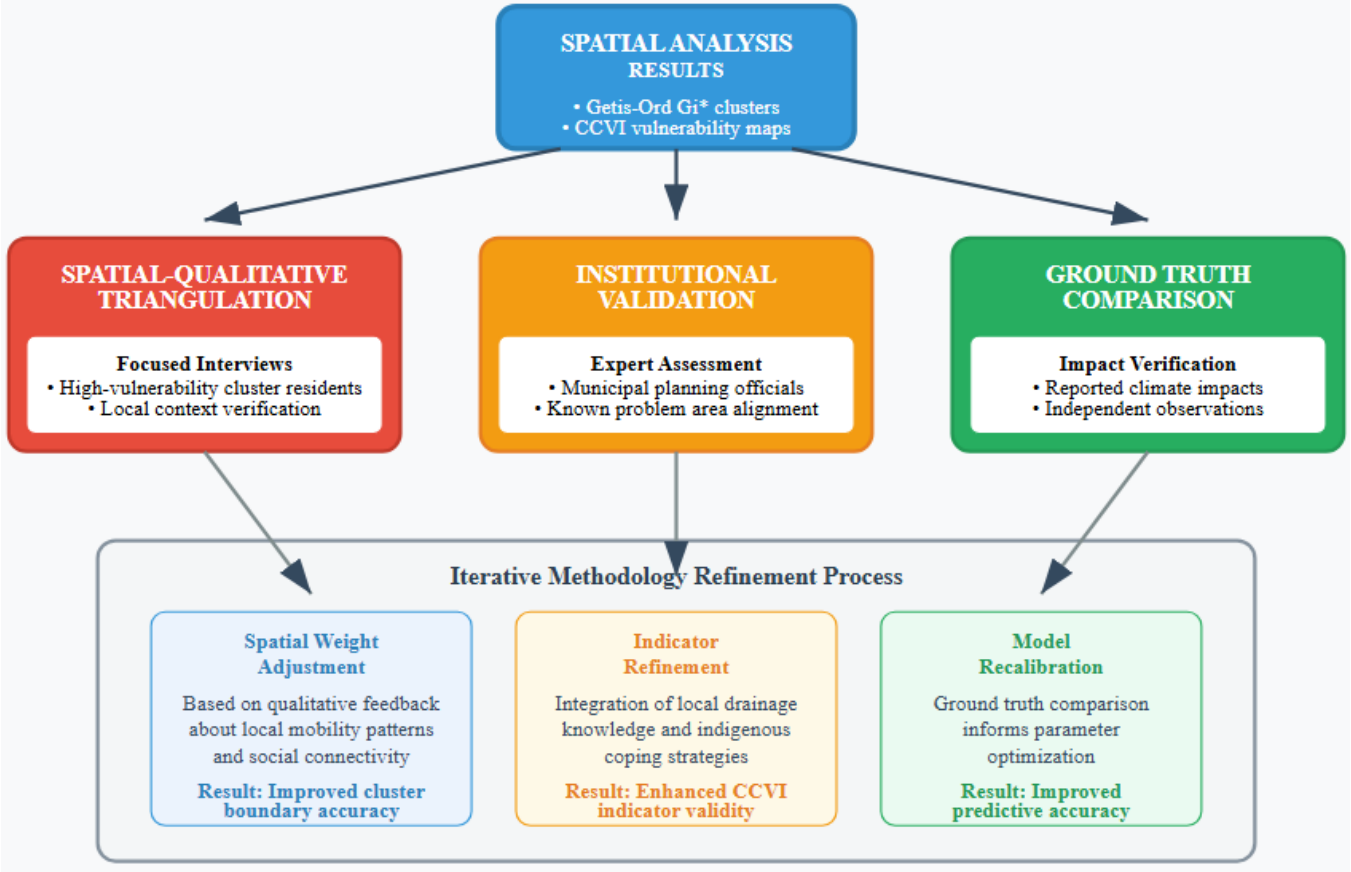


Figure 6. Mixed-Methods Validation Process for Spatial Analysis Results

The approach demonstrates remarkable effectiveness across varied environmental conditions, including flood-prone areas, heat-exposed zones, and complex multi-hazard environments, suggesting broad environmental transferability across the diverse climatic and topographic conditions found in African urban areas. Performance remains robust across different levels of infrastructure development, from areas with minimal municipal services to those with partial connections to formal infrastructure networks, indicating applicability across the full spectrum of informal settlement conditions.

The framework was explicitly designed for integration with existing urban planning processes and institutional arrangements. Results can be readily integrated with municipal GIS systems and standard planning software platforms commonly used in African cities. The methodology actively supports implementation of national urban policies, climate adaptation strategies, and Sustainable Development Goal monitoring requirements while building on widely available skillsets in African planning institutions rather than requiring extensive specialized training.

## 4. Technical Limitations and Future Development

Several technical limitations require acknowledgement. The current framework provides snapshot vulnerability assessment, while dynamic vulnerability assessment requires longitudinal data collection and modified analytical approaches. While multi-scale analysis is included, integration between household, neighborhood, and city scales requires further methodological development. The methodology captures infrastructure access but may miss nuanced service quality variations that affect vulnerability patterns.

The methodology provides several mechanisms for enhancing evidence-based urban planning. Hotspot analysis provides a clear geographic focus for resource allocation and intervention design. CCVI component analysis enables targeted interventions addressing specific vulnerability dimensions, including exposure reduction, sensitivity mitigation, and adaptive capacity enhancement. The framework provides baseline measures for monitoring the effectiveness of climate adaptation interventions over time, enabling adaptive management approaches that adjust strategies based on observed outcomes.

The methodology supports multiple aspects of urban climate adaptation. It provides spatially explicit risk assessment suitable for integration with climate adaptation plans and disaster risk reduction strategies. Vulnerability hotspots can guide infrastructure investment priorities, particularly for drainage, water systems, and housing upgrades. Mixed-methods validation (Figure 6) supports the identification of local knowledge and community-based adaptation strategies that can be scaled or supported through policy interventions. The framework facilitates integration between top-down planning processes and bottom-up community initiatives.

The framework contributes to policy development through regulatory integration, where results can inform updates to urban planning regulations, building codes, and land use policies to address identified vulnerability patterns. Spatial vulnerability maps provide common reference points for coordination between municipal departments, national agencies, and development partners, facilitating improved inter-agency coordination. Evidence-based vulnerability assessment supports resource mobilization from climate finance mechanisms and development funding sources, strengthening arguments for targeted investments in vulnerable communities.

## 5. Conclusions and Future Research

This research presents a robust mixed-methods GIS framework for spatial vulnerability assessment specifically designed for African urban contexts. The methodology successfully integrates Getis-Ord Gi* hotspot analysis with composite vulnerability index development and participatory validation methods,

demonstrating strong technical performance and practical applicability.

Key methodological contributions include: (1) adaptation of spatial clustering algorithms for informal settlement analysis, (2) development of a locally validated composite vulnerability index, and (3) systematic integration of quantitative spatial analysis with qualitative validation methods. The framework addresses critical gaps in existing vulnerability assessment tools by providing replicable, data-efficient methods suitable for resource-constrained environments.

The framework provides practical tools for evidence-based urban climate adaptation planning, enabling identification of vulnerability hotspots, targeted intervention design, and progress monitoring. Integration with existing planning processes is facilitated through compatibility with standard GIS platforms and alignment with policy frameworks.

Future research should focus on: (1) longitudinal studies tracking vulnerability changes over time, (2) machine learning integration for enhanced pattern recognition, (3) real-time data integration for dynamic vulnerability monitoring, and (4) comparative studies across multiple African cities to further validate transferability.

The methodology represents a significant advance in applied geoinformatics for climate adaptation, providing African cities with practical tools for addressing one of their most pressing challenges. As climate risks intensify and urban populations continue to grow, such methodological innovations become increasingly critical for sustainable urban development.

## 6. References


Birkmann, J., Jamshed, A., McMillan, J. M., Feldmeyer, D., Totin, E., Solecki, W., Ibrahim, Z. Z., Roberts, D., Kerr, R. B., Poertner, H.-O., Pelling, M., Djalante, R., Garschagen, M., Leal Filho, W., Guha-Sapir, D., & Alegría, A. (2022). Understanding human vulnerability to climate change: A global perspective on index validation for adaptation planning. Science of The Total Environment, 803, 150065. https://doi.org/10.1016/j.scitotenv.2021.150065

City of Windhoek. (2022). City of Windhoek Strategic Plan 2022-2027 (p. 34) [Strategic Plan]. City of Windhoek. https://www.windhoekcc.org.na/wp-content/uploads/2024/06/City-of-Windhoek-Strategic-Plan-2022-2027-1.pdf

Edmonds, H. K., Lovell, J. E., & Lovell, C. A. K. (2020). A new composite climate change vulnerability index. Ecological Indicators, 117, 106529. https://doi.org/10.1016/j.ecolind.2020.106529

IPCC. (2023). Climate Change 2022 – Impacts, Adaptation and Vulnerability: Working Group II Contribution to the Sixth Assessment Report of the Intergovernmental Panel on Climate Change (1st edn). Cambridge University Press. https://doi.org/10.1017/9781009325844

Lanorte, A., Nolè, G., & Cillis, G. (2024). Application of Getis-Ord Correlation Index (Gi) for Burned Area Detection Improvement in Mediterranean Ecosystems (Southern Italy and Sardinia) Using Sentinel-2 Data. Remote Sensing, 16(16), Article 16. https://doi.org/10.3390/rs16162943

Lapietra, I., Colacicco, R., Rizzo, A., & Capolongo, D. (2024). Mapping Social Vulnerability to Multi-Hazard Scenarios: A GIS-Based Approach at the Census Tract Level. Applied Sciences, 14(11), 4503. https://doi.org/10.3390/app14114503

Lester, K. (2024). Hot Spots and Getis-Ord Gi* Analysis. Geographic Information Science & *Technology Body of Knowledge*, *2024*(1). https://doi.org/10.22224/gistbok/2024.1.23

Malaker, T., & Meng, Q. (2024). Urban Disparity Analytics Using GIS: A Systematic Review. *Sustainability*, *16*(14), 5956. https://doi.org/10.3390/su16145956

Rabiei-Dastjerdi, H., Brereton, F., & O'Neill, E. (2025). Towards designing a comprehensive composite index for social vulnerability to natural hazards in the big data era: Potential challenges and partial solutions. Natural Hazards, 121(4), 3885–3913. https://doi.org/10.1007/s11069-024-06874-w

Roy, S., Majumder, S., Bose, A., & Chowdhury, I. R. (2024). Spatial heterogeneity in the urban household living conditions: A-GIS-based spatial analysis. Annals of GIS, 30(1), 81–104. https://doi.org/10.1080/19475683.2024.2304194

UN-Habitat. (2024). Gender equality and women's land and property rights strategy. UN-Habitat Gender Programme [Stategy]. UN-Habitat. https://unhabitat.org/topic/gender

# Assessing Long-Term Trends in Land Surface Temperature and Normalized Vegetation Index in Coastal Ecosystems: A Case Study of Kalpitiya Peninsula (1994–2024)

Senavirathne, M.K.G.A.N.*, Weerasinghe, V.P.A.

*Department of Zoology and Environmental Management, Faculty of Science, University of Kelaniya, Kelaniya, Sri Lanka, anushkha.sen29@gmail.com, primali@kln.ac.lk*

**Abstract**: Climate change and land-use modifications significantly impact local temperature dynamics, particularly in coastal ecosystems. The interaction between vegetation and land surface temperature (LST) is useful for understanding the effects of climate change and urbanization on ecosystem sustainability. The Kalpitiya Peninsula, known for its ecological diversity and human settlements, has experienced significant land-use changes over the past three decades. This study aims to investigate the temporal trends and correlations between LST and the Normalized Difference Vegetation Index (NDVI) from 1994 to 2024, providing insights into the impacts of vegetation changes on temperature dynamics. Landsat imagery from 1994, 2004, 2014, and 2024 was downloaded from the United States Geological Survey (USGS) platform and was processed using ArcGIS 10.8 software to derive LST and NDVI values. Statistical analyses, including Spearman's correlation and trend assessments, were conducted to quantify the relationship between these parameters. Results indicate a significant increase in average LST from 28.03°C in 1994 to 36.53°C in 2024, marking an 8.5°C rise over three decades. NDVI values initially increased from 0.178 (1994) to 0.240 (2014) but declined to 0.206 by 2024, reflecting changes in vegetation. The LST-NDVI correlation weakened from -0.48 in 1994 to -0.22 in 2024, suggesting that factors beyond vegetation loss, such as urbanization and land-use change, increasingly contribute to temperature rise. These findings highlight the urgent need for sustainable land management strategies, afforestation, and climate adaptation measures to mitigate surface warming in Kalpitiya. Future research integrating higher-resolution data and climate models could enhance the understanding of localized climate variability and inform conservation efforts.

***Keywords:*** Land Surface Temperature, NDVI, Correlation, Landsat, Kalpitiya

## 1. Introduction

Coastal ecosystems are highly dynamic and sensitive to both climatic and anthropogenic drivers. Land Surface Temperature (LST) and the Normalized Difference Vegetation Index (NDVI) are widely used remote sensing indicators for assessing the environmental impacts of land-cover changes on local climate patterns (Anbazhagan & Paramasivam, 2016; Zia Ur Rehman et al., 2015). Vegetation cover plays a critical role in regulating surface temperature by enhancing evapotranspiration and moderating the surface energy balance, while vegetation loss often leads to elevated LST (Kanjin and Alam, 2024).

In Sri Lanka, rapid urban expansion, agricultural intensification, and deforestation have altered land-cover patterns, influencing both NDVI and

LST (Fonseka et al., 2019). Studies in different regions of the country have reported significant spatial and temporal variations in LST linked to vegetation decline and urbanization, including in the Wilpattu Forest Complex (Dilini, M.M.G.S.and Wikramasooriya, 2019) Galle (Dissanayake, 2020), Colombo (Fonseka et al., 2019; Kaushalya, 2021) and Kandy Districts (Rashmika Nawarathna et al., 2023). Similar trends have been documented globally, such as in the Sundarbans mangrove forest (Kanjin and Alam, 2024) and the coastal zones of Pakistan (Zia Ur Rehman et al., 2015), where declining NDVI is strongly associated with increased LST.

The Kalpitiya Peninsula is an ecologically significant yet vulnerable coastal region in northwestern Sri Lanka. In recent decades, it has experienced substantial land-use changes due to tourism, settlement expansion, and agricultural conversion, leading to concerns about ecosystem degradation and microclimatic shifts (Indika et al., 2022; Ministry of Environment, 2011; Urban Development Authority, 2021).

### 1.1 Objectives

This study aims to analyze multi-temporal Landsat images from 1994 to 2024 to examine changes in NDVI and land surface temperature (LST) in the Kalpitiya area. It seeks to measure the strength and direction of the relationship between NDVI and LST and to assess how land-cover changes over the past 30 years have influenced surface temperature patterns. The findings will offer valuable insights to support sustainable land management and climate adaptation strategies in coastal environments.

## 2. Materials and Methods

### *2.1* Study Area

Kalpitiya Divisional Secretariat Division (DSD), which is in Puttalam District in the northwestern province of Sri Lanka, was selected as the major study area. Kalpitiya DSD is a low-laying sandy peninsula with approximately 160 km$^2$ located between 79° 40'– 79° 50' Easting longitude and 8° 20' – 8° 90' Northern latitude (Matharaarachchi et al., 2014). Geologically, the peninsula comprises Quaternary deposits, predominantly well-graded, dense dune sands near the surface (Katupotha and Dias, 2001). These sandy formations contribute to the development of unconfined aquifers, which are important for the region's groundwater resources (Wickramasinghe et al., 2021). Land use patterns of the study area consist of urban areas, agricultural lands, coconut cultivations, mixed cultivations, scrubs, coastal vegetations, mangroves, barren lands, sand dunes, active and abandoned shrimp farms, salt marshes, residential areas, and homesteads (Hitinayake, 2019). Kalpitiya, located within the DL3 dry zone agro-ecological region of Sri Lanka, experiences a tropical monsoon climate characterised by an average annual temperature of a maximum of 31°C and a minimum of 27°C and annual rainfall between 900 mm and 1,100 mm, primarily during the Northeast Monsoon from October to January (Matharaarachchi et al., 2014).

### 2.2 Data Acquisitions

Administrative boundary shape files of Divisional Secretariat Division (DSD) and Grama Nila Dhari Division (GNDs) of Kalpitiya were obtained from the Survey Department, Colombo. For the analysis of LST and NDVI, Landsat images from 1994, 2004, 2014, and 2024 were used, with 10-year gaps shown in Table 1. The images were obtained from the US Geological Survey (USGS) Earth Explorer platform[10].

| Sensor Type | Product ID | Acquisition date | Cloud Cover | Image Quality |
|---|---|---|---|---|
| TM | LT05_L2SP_142054_19940630_20200913_02_T1 | 1994.06.30 | 3.00 | 9 |
| TM | LT05_L2SP_142054_20041218_20200902_02_T1 | 2004.12.18 | 22.00 | 7 |
| OLI_TIRS | LC08_L1TP_142054_20140301_20200911_02_T1 | 2014.03.01 | 7.32 | 9 |

[10] https://earthexplorer.usgs.gov/

| | | | | |
|---|---|---|---|---|
| OLI_ TIRS | LC09_L2SP_142054_20240116_20240117_02_T1 | 2024.01.16 | 4.38 | 9 |

Table 1: Information about Landsat images used.

### 2.3 Computation of LST

The thermal infrared bands were extracted from Landsat 5, 7, 8, and 9, and LST was computed in a series of steps (Dissanayake, 2020; Fonseka et al., 2019; S. and C.R., 2016) using ArcGIS 10.8:

Step 1:

Conversion of Digital Numbers (DN) to Top-of-Atmosphere (TOA) Radiance using sensor-specific equations for Landsat 5, 7, 8, and 9.

For Landsat 5,7

$$L\lambda = \frac{(LMax - LMin)}{(QcalMax - QcalMin)} * (Qcal - QcalMin) + LMin \quad (1)$$

Lλ = TOA radiance (W $m^{-2}$ $sr^{-1}$ $\mu m^{-1}$)

LMax = Maximum TOA radiance

LMin = Minimum TOA radiance

QcalMax = Maximum quantized calibrated pixel value (DN = 255)

QcalMin = Minimum quantized calibrated pixel value (DN = 0)

Qcal = DN value of the pixel

For Landsat 8,9

$$L\lambda = ML \cdot Qcal + AL - O_i \quad (1)$$

Lλ = TOA spectral radiance (Watts $m^{-2}$ $sr^{-1}$ $\mu m^{-1}$)

ML = Radiance multiplicative scaling factor from metadata

AL = Radiance additive scaling factor from metadata

Qcal = Quantized and calibrated pixel value (DN)

Oi = Correction value for band 10

Step 2:

Conversion of TOA Radiance to Brightness Temperature (BT) using thermal calibration constants.

$$T_{BT} = \frac{K2}{\left(\frac{K1}{L\lambda} + 1\right)} \quad (2)$$

$T_{BT}$ = Brightness Temperature (Kelvin)

K1 = Thermal band calibration constant 1

K2 = Thermal band calibration constant 2

Lλ = TOA radiance

Step 3:

NDVI Calculation, derived from the near-infrared (NIR) and red bands, to quantify vegetation cover.

$$NDVI = \frac{(NIR - RED)}{(NIR + RED)} \quad (3)$$

NIR = Reflectance in the Near-Infrared band.

RED = Reflectance in the Red band

Step 4:

Surface Emissivity Estimation, based on NDVI-derived vegetation proportion.

$$\varepsilon = 0.004 \cdot PV + 0.986$$

ε = Surface emissivity

PV = Proportion of Vegetation

$$PV = \left[\frac{(NDVI - NDVI\,min)}{(NDVImax - NDVImin)}\right]^2 \quad (4)$$

NDVI = DN value from the NDVI image

NDVImax = Maximum DN value of the NDVI image

NDVImin = Minimum DN value of the NDVI image

Step 5:

LST Computation, incorporating emissivity and radiative transfer equations, followed by final conversion to Celsius (°C).

$$LST = \frac{T_{BT}}{1 + (\lambda * \frac{T_{BT}}{\rho} \in (\varepsilon)} \quad (5)$$

$T_{BT}$: Brightness Temperature (Kelvin)

λ = Wavelength of emitted radiance (μm)

ε = Surface emissivity

$$\rho = hc / \sigma$$

h: Planck's constant ($6.626 \times 10^{-34}$ J s)

c: Speed of light ($2.998 \times 10^{8}$ m/s)

σ: Boltzmann constant ($1.38 \times 10^{-23}$ J/ K)

$$LST_C = LST_K - 273.15$$

$LST_C$ = Land Surface Temperature (Celsius)

$LST_K$ = Land Surface Temperature (Kelvin)

The processed LST and NDVI data were used to generate spatial temperature maps for each study year, illustrating temporal changes in surface temperature and vegetation cover.

### 2.4 NDVI and LST Correlation Analysis

The relationship between LST and NDVI was analyzed using the Spearman Rank Correlation in R 4.4.2 software. Raster datasets for LST and NDVI were converted into point datasets using ArcGIS 10.8, where the 'Extract Values to Points' tool was applied. A total of 300 random points were generated across the study area to extract corresponding LST and NDVI values. The Spearman correlation was then computed to assess the strength and direction of the relationship between vegetation cover and surface temperature over time.

## 3. Results

### 3.1 Changes in LST and NDVI in Kalpitiya

Table 2 summarizes the temporal variation in mean LST and NDVI across the Kalpitiya Peninsula from 1994 to 2024. Average LST increased steadily from 28.03 °C in 1994 to 36.53 °C in 2024. NDVI showed a moderate increase from 0.178 in 1994 to 0.240 in 2014, followed by a decline to 0.206 in 2024.

| Year | Average LST | Average NDVI |
|---|---|---|
| 1994 | 28.03 | 0.178 |
| 2004 | 30.14 | 0.192 |
| 2014 | 32.29 | 0.240 |
| 2024 | 36.53 | 0.206 |

Table 2: Average LST and NDVI of 300 points covering the peninsula.

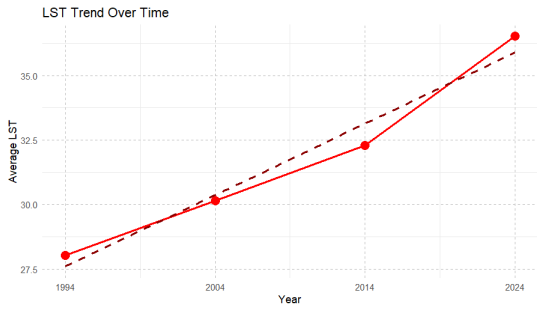


Figure 1: LST changes from 1994 to 2024

Figure 1 illustrates the temporal progression of LST, highlighting a consistent upward trajectory over the 30 years, with the steepest rise between 2014 and 2024.

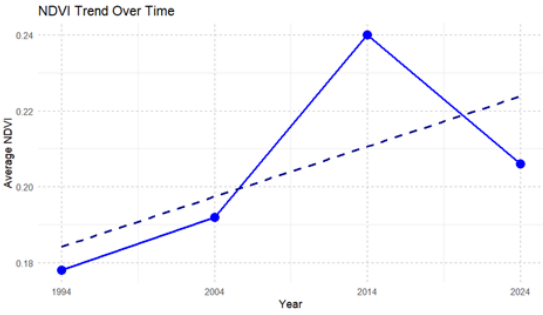


Figure 2: NDVI changes from 1994 to 2024

Figure 2 shows NDVI changes, where initial gains are evident between 1994 and 2014, followed by a notable decrease by 2024.

### 3.2 Spatial Distribution Maps of LST and NDVI

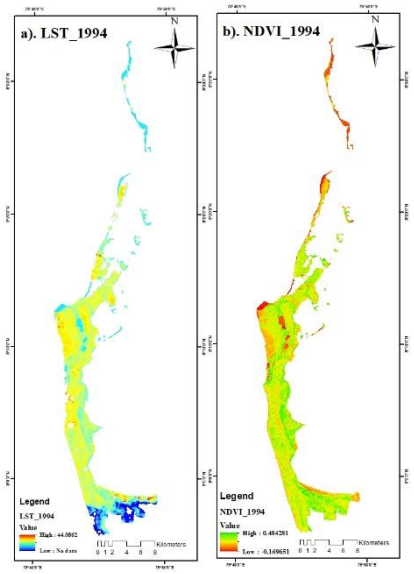


Figure 3: a) LST 1994 and b) NDVI 1994

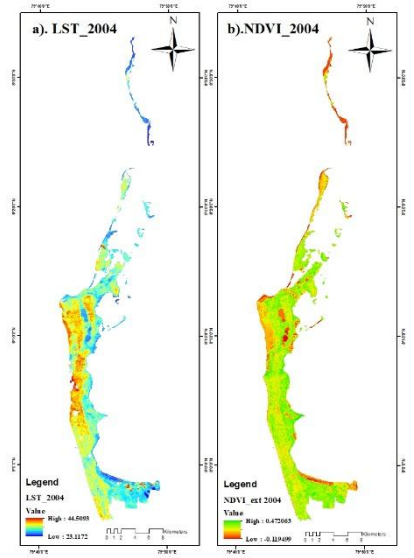


Figure 4: a) LST 2004 and b) NDVI 2004

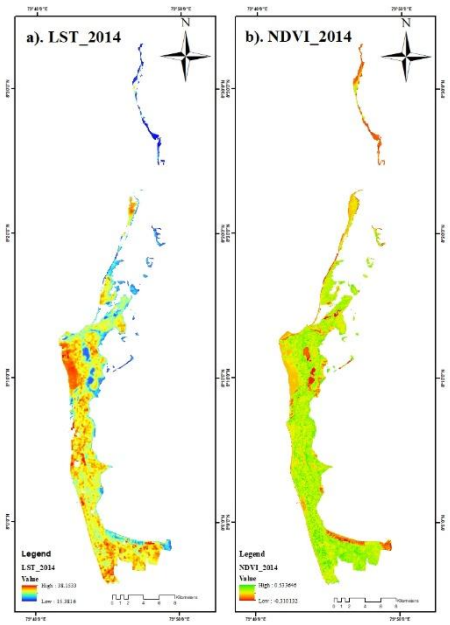


Figure 5: a) LST 2014 and b) NDVI 2014

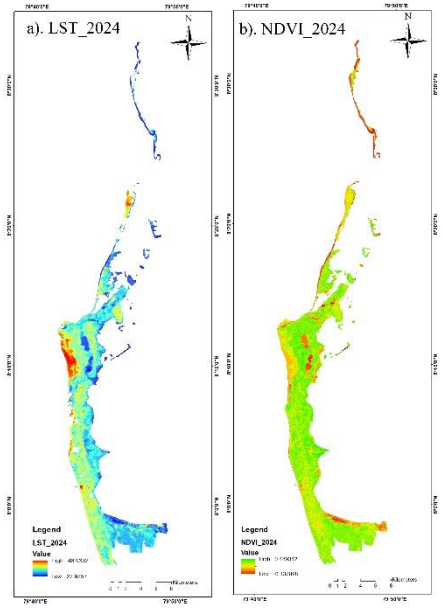


Figure 6: a) LST 2024 and b) NDVI 2024

Figure 3, Figure 4, Figure 5, Figure 6 present spatial distribution maps of LST along with corresponding NDVI maps for 1994, 2004, 2014, and 2024. LST maps reveal progressive expansion of high-temperature zones, particularly in urbanized, deforested, and sandy areas. Corresponding NDVI maps show the vegetation cover changes.

### 3.3 Relationships between NDVI and LST in the Kalpitiya

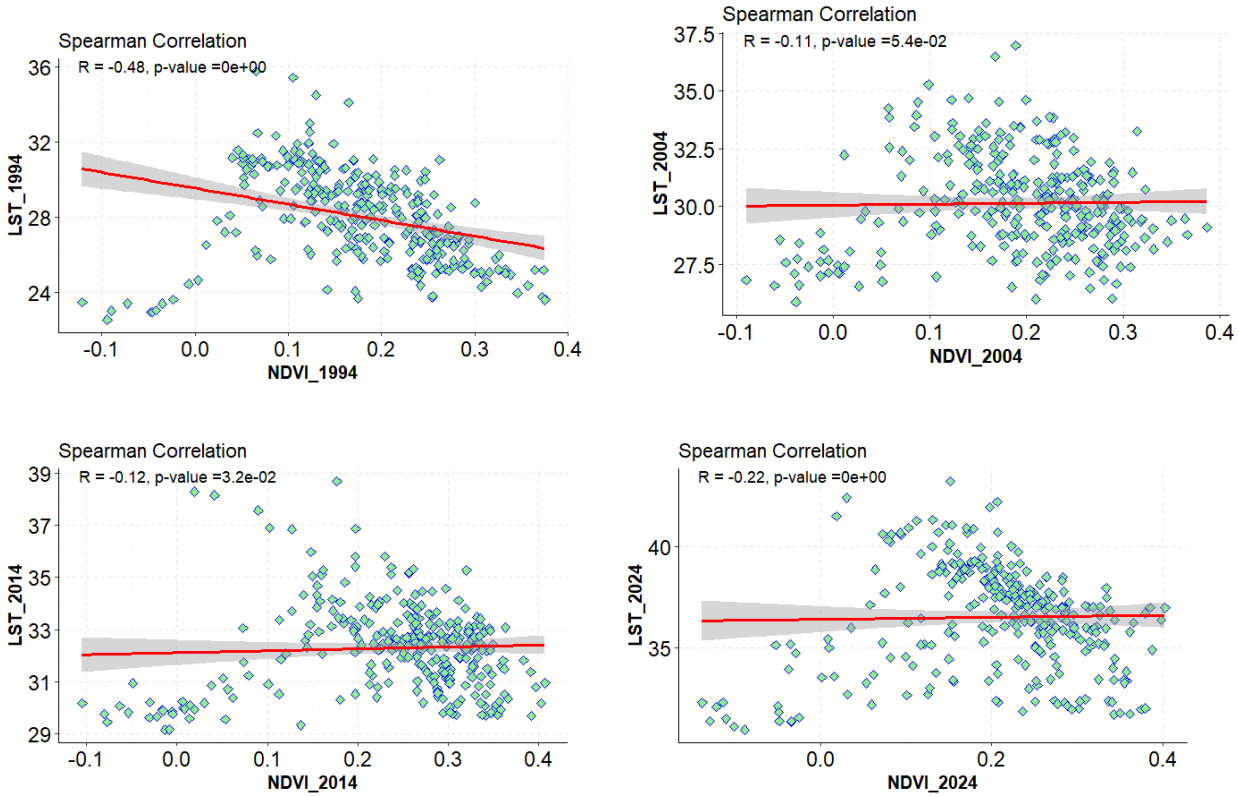


Figure 7: Correlation of LST and NDVI in the Kalpitiya from 1994 to 2024

Figure 7 display the results of the Spearman correlation analysis between LST and NDVI for each study year. In 1994, a moderate negative correlation ($r = –0.48$, $p < 0.001$) was observed. This relationship weakens progressively, with $r = –0.22$ ($p < 0.001$) in 2024, suggesting that non-vegetative factors such as bare sand exposure, urban expansion, and land-cover change have become increasingly important drivers of LST variation.

## 4. Discussion

Land Surface Temperature (LST) serves as a key indicator of the Earth's surface thermal dynamics, with its variation strongly influenced by different land-cover types and alterations in land-use patterns (Kanjin and Alam, 2024). The results of this study indicate a clear upward trend in LST over the past three decades in the Kalpitiya Peninsula, with an overall increase of 8.5°C from 28.03°C in 1994 to 36.53°C in 2024. The most significant rise occurred between 2014 and 2024, a period likely influenced by intensified land-use change, rapid tourism-related development, and deforestation in the area(Urban Development Authority, 2021). Similar patterns of accelerated warming linked to recent urbanization and vegetation loss have been documented in other regions of Sri Lanka, such as Colombo (Fonseka et al., 2019) and selected urban areas studied by Sanjeewani and Manawadu (2016).

NDVI is a widely used remote sensing index that quantifies vegetation cover and is derived by measuring the difference between reflected near-infrared and red light, making it a reliable indicator of vegetation health and density(Kanjin and Alam, 2024; S. and C.R., 2016). The peninsula transitions from extensive coastal sand/dune fields with moderate vegetation to a matrix of more sparse vegetation, mainly due to intensive agricultural development in the region. In a dry coastal system like Kalpitiya, such vegetation is typically a low-stature, discontinuous canopy

with limited leaf area index and shallow roots(Hitinayake, 2019). It boosts NDVI modestly but provides limited evapotranspirative cooling compared with dense canopies or wetlands.

These LULC changes strongly influenced both vegetation indices and land surface temperature (LST). The average normalized difference vegetation index (NDVI) showed an initial increase from 0.178 in 1994 to 0.240 in 2014, reflecting the expansion of vegetated cover. However, by 2024, NDVI declined slightly to 0.206, possibly due to vegetation stress, seasonal variability, or partial clearance. In contrast, LST exhibited a consistent and substantial rise. This divergence indicates that the increase in vegetation area was insufficient to mitigate thermal loading in the region. The dominance of sparse vegetation(Weragodatenna, 2022), which has low canopy density and limited evapotranspiration capacity, and continued exposure of sandy and built-up surfaces, likely contributed to this thermal amplification.

The correlation analysis between LST and NDVI revealed a weakening negative relationship over time, with Spearman correlation values declining from -0.48 in 1994 to -0.22 in 2024. While a moderate negative correlation in 1994 suggests that vegetation played a significant role in temperature regulation (Dissanayake, 2020; Kanjin and Alam, 2024), the decreasing correlation implies that other factors, such as land-use modifications, urban and agricultural expansion, and soil moisture changes, may increasingly influence LST patterns (Fonseka et al., 2019). This trend aligns with global observations (Kanjin and Alam, 2024; Zia Ur Rehman et al., 2015) where urbanization and deforestation reduce the cooling effects of vegetation, leading to localized warming. Spatial analysis further highlights that urbanized and deforested regions experienced the most significant LST increases, reinforcing the Urban Heat Island (UHI) effect and the critical role of dense vegetation in temperature mitigation (Rashmika Nawarathna et al., 2023; Sanjeewani and Manawadu, 2016). As LST continues to rise, the implications for biodiversity, agriculture, and human settlements in the Kalpitiya Peninsula become increasingly concerning.

In Kalpitiya, rapid expansion of high-intensity, rotational cash-cropping on sandy soil sustained largely by groundwater-fed tube wells and agro-wells (Hitinayake, 2019) has increased in the past decades. The spatial extent of cultivated land typically leaves fields frequently bare between rotations, lowering canopy density and surface moisture despite intermittent greening during crop growth (Hitinayake, 2019). This production model is well documented for the peninsula and the wider Northwestern coastal belt, where agriculture relies on shallow, highly vulnerable aquifers and broader groundwater stress in the porous coastal sands (Jayasekera et al., 2011; Matharaarachchi et al., 2014; Phok et al., 2021). These conditions can influence the LULC changes. Our findings of dominant sparse vegetation, only modest gains in average NDVI (peaking in 2014 then dipping by 2024), and a substantial rise in LST (≈ +8.5 °C), as sparse, water-limited canopies offer weak evapotranspirative cooling. Concurrent settlement growth and tourism-oriented development (Urban Development Authority, 2021) further fragment vegetated buffers and convert coastal land, reinforcing the thermal signal by reducing dense, moisture-rich cover. Together, these land and water-use trajectories help explain the persistently negative but weakened NDVI–LST coupling observed.

This study faced several limitations that may have influenced the accuracy and generalizability of its findings. A major constraint was the presence of cloud cover in optical satellite imagery, which is particularly challenging in equatorial regions like Sri Lanka (Fonseka et al., 2019), where frequent cloud formation is common throughout the year. Landsat thermal bands cannot penetrate thin clouds, potentially introducing errors in LST estimation(Fonseka et al., 2019). Another limitation is the spatial resolution of Landsat data (30 m) (S. and C.R., 2016), which may not capture fine-scale variations in land surface

characteristics, especially in heterogeneous coastal landscapes with narrow vegetation strips, small water bodies, and scattered built-up areas. Temporal resolution is also a factor(Dissanayake, 2020); using decadal intervals may overlook seasonal variations or short-term changes in LST and NDVI caused by weather events or land-use shifts.

## 5. Conclusion

This study demonstrates a significant rise in LST alongside notable changes in NDVI in the Kalpitiya Peninsula over the past three decades, highlighting the combined effects of vegetation change, urbanization, and land surface characteristics on local thermal dynamics. The weakening LST–NDVI correlation indicates that non-vegetative factors are increasingly influencing surface warming. Implementing targeted reforestation, sand dune stabilization, and sustainable land-use planning will be essential to mitigating further temperature increases and preserving coastal ecosystem resilience. Future research integrating higher-resolution, cloud-free datasets and additional climatic variables will enhance understanding and support informed climate adaptation strategies. Furthermore, to improve the robustness of the analysis, future studies should integrate agricultural pattern tracking with in-situ measurements, including plant evapotranspiration and field temperature, to strengthen the reliability and accuracy of the findings.

## 6. Acknowledgement:

We would like to acknowledge the University of Kelaniya research grant No: RP/03/02/07/03/2023 for facilitating the research work.

## 7. References

Dilini, M.M.G.S.and Wikramasooriya, A.K., 2019. Land Surface Temperature Volatilities with the Recent Forest Cover Changes Land Surface Temperature Volatilities with the Recent Forest Cover Changes in Wilpattu Forest Complex , Sri Lanka. https://doi.org/10.2312/yes19.17

Dissanayake, D.M.S.L.B., 2020. Land use change and its impacts on land surface temperature in Galle city, Sri Lanka. Climate 8. https://doi.org/10.3390/CLI8050065

Fonseka, H.P.U., Zhang, H., Sun, Y., Su, H., Lin, H., Lin, Y., 2019. Urbanization and its impacts on land surface temperature in Colombo Metropolitan Area, Sri Lanka, from 1988 to 2016. Remote Sens (Basel) 11, 1–18. https://doi.org/10.3390/rs11080926

Hitinayake, G., 2019. Kalpitiya Farming System: its Characteristics and Emerging Challenges.

Indika, W.A.K., Matharaarachchi, H., Silva, Y. de, 2022. Kalpitiya Socioeconomic and Ecological Profile Kalpitiya Socioeconomic and Ecological Profile 2022. Environmental Foundation (Guarantee) Ltd.

Jayasekera, D.L., Kaluarachchi, J.J., Villholth, K.G., 2011. Groundwater stress and vulnerability in rural coastal aquifers under competing demands: A case study from Sri Lanka. Environ Monit Assess 176, 13–30. https://doi.org/10.1007/s10661-010-1563-8

Kanjin, K., Alam, B.M., 2024. Assessing changes in land cover, NDVI, and LST in the Sundarbans mangrove forest in Bangladesh and India: A GIS and remote sensing approach. Remote Sens Appl 36, 101289. https://doi.org/10.1016/j.rsase.2024.101289

Katupotha, J., Dias, P., 2001. The geological evolution correlated to the stratigraphy of the Kalpitiya peninsula.

Kaushalya, G.N., 2021. Spatial Variability of NDVI and LST in Colombo District, Sri Lanka.

Matharaarachchi, S., Piyadasa, R.U.K., Wickramasinghe, D., 2014. Groundwater Quality Variation in Kalpitiya Peninsula -Sri Lanka.

Ministry of Environment, 2011. Climate Change Vulnerability Data Book Maps and Data. Ministry of Environment, Sri Lanka.

Phok, R., Kosgallana Duwage Wasantha, N., Sumana Bandara, W., Herath

Mudiyanselage Thalapitiye Gedara Amarasooriya, P., Hingure Arachchilage, D., 2021. Using intrinsic vulnerability and anthropogenic impacts to evaluate and compare groundwater risk potential at northwestern and western coastal aquifers of Sri Lanka through coupling DRASTIC and GIS approach. Appl Water Sci 11, 1–18. https://doi.org/10.1007/s13201-021-01452-y

Rashmika Nawarathna, B.N., Nianthi, R., Subasinghe, S.I.S., 2023. Spatial and temporal variation of land surface temperature (LST) in the Kandy District of Sri Lanka. IOP Conf Ser Earth Environ Sci 1266. https://doi.org/10.1088/1755-1315/1266/1/012074

Anbazhagan S., Paramasivam C.R., 2016. Statistical Correlation between Land Surface Temperature (LST) and Vegetation Index (NDVI) using Multi-Temporal Landsat TM Data. International Journal of Advanced Earth Science and Engineering 5, 333–346. https://doi.org/10.23953/cloud.ijaese.204

Sanjeewani, R.M.S.S., Manawadu, L., 2016. Spatial trends of land surface temperature variation over selected urban regions in Sri Lanka using remote sensing. 37th Asian Conference on Remote Sensing, ACRS 2016 3, 2351–2360.

Urban Development Authority, 2021. Kalpitiya Urban Development Plan. Urban Development Authority Ministry of Urban Development & Housing.

Weragodatenna, D., 2022. GIS Atlas for Puttalam Lagoon As an Assistance for Natural Resource Management.

Wickramasinghe, B.N.B., Jayasena, H.A.H., Perera, K.V.G.S., Rajapakse, R.R.G.R., 2021. Assessment of hydrogeological scenario in a cross-section from Anamaduwa to Kalpitiya in Northwest Sri Lanka. Ceylon Journal of Science 50, 83–96. https://doi.org/10.4038/cjs.v50i1.7850

Zia Ur Rehman, Syed Jamil H. Kazmi, Farheen Khanum, Zuber Ali Samoon, 2015. Analysis of Land Surface Temperature and NDVI Using Geo-Spatial Technique: A Case Study of Keti Bunder, Sindh, Pakistan. Journal of Basic & Applied Sciences 11, 514–527. https://doi.org/10.6000/1927-5129.2015.11.69

# Modelling Future Streamflow under Climate and Land Use Scenarios in the Lower Okavango River Basin

Kaleb Gizaw Negussie[a], Daniel Wyss[b] and Martin Kappas[c]

[a] *Department of Land and Spatial Sciences; knegussie@nust.na,*
[b] *Namibia University of Science and Technology,*
[c] *Department of Cartography, GIS and Remote Sensing, Georg-August University Göttingen*

This study investigates the long-term impacts of climate change and land use/land cover (LULC) dynamics on streamflow within a transboundary section of the lower Okavango River Basin, spanning northeastern Namibia and southern Angola. Employing the SWAT+ hydrological model, we simulated historical and future hydrological responses under combined scenarios of climate and LULC change using four CMIP6 general circulation models (GFDL-ESM4, IPSL-CM6A-LR, MPI-ESM1-2-HR, NorESM2-MM) and 1-km resolution global land projection datasets. The model was calibrated and validated with historical streamflow data at Rundu, achieving reliable performance statistics. Future scenarios—spanning the periods 2025–2040, 2041–2070, and 2071–2100—were run under moderate (SSP2-4.5) and high (SSP5-8.5) emission trajectories.

Results indicate a consistent decline in precipitation and an amplified reduction in streamflow, with peak runoff periods significantly shortened and dry-season flows nearing collapse by 2100. Model projections show strong agreement in the direction of change, particularly in the latter half of the century. Parallel LULC projections reveal a rapid loss of wetland and natural vegetation, coupled with an expansion of cropland and urban areas—particularly around Rundu. These land use transitions further intensify hydrological losses by reducing infiltration capacity and enhancing surface runoff.

Water yield simulations reflect this compounding impact, with historically high-yield zones gradually shrinking and nearly disappearing by the end of the century. The study highlights the disproportionate sensitivity of streamflow to both upstream rainfall and local land management, underscoring the urgent need for coordinated adaptation strategies. Findings provide critical insight for water resource managers and policymakers aiming to address long-term water security and ecological stability in one of Southern Africa's most vulnerable transboundary river systems.

***Keywords:*** Climate change, Land use land cover change, Streamflow simulation, SWAT+ model, Okavango River Basin, CMIP6, Water yield, SSP scenarios, Semi-arid hydrology

# Tracking Climate Variability for Rainfed Agriculture in Ghana Using Google Earth Engine: A Multi-Year Analysis (2015–2025)

Naa Dedei Tagoe[a*] and Edward Martey[b]

[a] *University of Mines and Technology; ndtagoe@umat.edu.gh,*
[b] *CSIR-Savanna Agricultural Research Institute*

Ghana's agricultural sector remains highly dependent on rainfed cultivation due to the limited reach of irrigation infrastructure. As a result, farmers are increasingly vulnerable to shifting rainfall patterns and unpredictable weather conditions, which threaten crop yields and food security. This study presents the development and application of a cloud-based climate monitoring tool, built on Google Earth Engine (GEE), to analyse spatiotemporal climate dynamics across Ghana from 2015 to 2025. The system focuses on tracking rainfall onset and cessation, soil moisture suitability, temperature variation, and rainfall variability to support climate-resilient agriculture and early warning systems.

The tool integrates multi-source geospatial datasets, including Climate Hazards Group InfraRed Precipitation with Station (CHIRPS) data for precipitation, TerraClimate for temperature, MODIS Normalized Difference Vegetation Index (NDVI) for vegetation dynamics, and NASA's Soil Moisture Active Passive (SMAP) for soil moisture. Rainfall onset and cessation are computed annually using agro-meteorological thresholds.

The system further analyses monthly maximum and minimum temperatures, diurnal temperature range (DTR), and computes the coefficient of variation (CV) for annual rainfall to detect areas with high climatic instability. Soil moisture was assessed using an HWSD-based suitability index and NASA SMAP-derived surface moisture trends, allowing the identification of periods of moisture stress or retention, which is particularly useful in near-real-time monitoring for rainfed zones.

Additional data layers on elevation provide localized context for climate risk assessments. The platform includes an interactive dashboard where users can click on a point or upload shapefiles to generate detailed time series charts for selected clusters. Drop-down filters support custom exploration of rainfall and temperature trends by year or variable, while export features allow downloading of cluster-level statistics for further analysis or integration into decision support systems.

Findings from selected clusters confirm strong seasonal and interannual climate variability. Maximum temperatures regularly exceed 38°C in northern zones, while DTR values above 14°C persist throughout the year. Rainfall charts reveal delayed onset, sharp seasonal peaks, and high CV values in the northern interior, indicating elevated climate risk. Cluster-specific visualisations also highlight spatial differences in thermal stress and moisture availability, which are critical for planning resilient, rainfed agricultural interventions. This paper aligns with the AGSE 2025 Theme Day on "Climate Change Monitoring through Remote Sensing Imagery and Processing", demonstrating the

application of Earth observation data for monitoring rainfall, temperature variability, and soil moisture in support of climate-resilient planning in rainfed agricultural systems.

***Keywords:*** Rainfed Agriculture, Climate Variability, Rainfall Onset and Cessation, Soil Moisture Monitoring, Google Earth Engine, Diurnal Temperature Range, Spatiotemporal Analysis

---

# Technical Session: Geoinformation and Artificial Intelligence – Current Trends and Applications

# Does AI plus Geoinformatics equal GeoAI ?

Dietrich Schröder

*University of Applied Sciences, Stuttgart, Germany, dietrich.schroeder@hft-stuttgart.de*

The concept of artificial intelligence can be traced back to our ancestors thousands of years ago. As with other cultures, the ancient Greeks introduced the concept of autonomous, human-like robots in their mythology. It was a long way from those ancient times to autonomous, AI-supported robots like the robot dog. Nowadays, AI applications are state of the art in the geoinformatics domain too – but can we really call it GeoAI?

This talk will first provide a brief overview of the key milestones in the development of AI and introduce the main concepts. Geoinformatics encompasses non-machine learning AI concepts such as cellular automata and agent-based models, particularly for simulation and prediction. Shallow machine learning concepts, such as ensemble decision trees (e.g. random forest) and boosting concepts (e.g. XGBoost), are also widely used for classification. For feature extraction and object detection in remote sensing, concepts of deep learning, such as Convolution Neural Networks (particularly as pre-trained models for standard tasks such as land cover classification or tree detection), are widely used. Geographic information systems (GIS), such as Esri's ArcGIS Pro or open-source GIS, such as QGIS, have integrated, user-friendly tools for preparing data for machine learning and accessing these models. However, the additional installation of Python-based libraries such as PyTorch, Fast.ai, TensorFlow, Torchvision or Keras is still required, and as each GIS version requires specific deep learning library versions, installation remains challenging.

But do the models actually utilise spatial concepts? In machine learning, in particular, incorporating the well-known characteristics of geographic phenomena — autocorrelation, heterogeneity, and similarity — remains challenging. While non-machine learning AI concepts make extensive use of neighbourhoods, which play a crucial role in cellular automata and agent-based models, machine learning models only make implicit use of them by using spatial data as input.

Machine learning concepts in geoinformatics also pose other challenges, such as hardware and GPU requirements, processing times and the need for large training data sets. Natural phenomena are often poorly defined and biased training data sets can result in features being overlooked or machine learning results being inexplicable.

General "Geo Foundation Models" or "Large Geo Models" similar to those in other fields are not at the horizon.

# Fuzzy Logic and Deep Learning for susceptibility zoning related to volcanic eruptions

Valbuena G. Martha P [a,*], Hernandez Rodrigo [b], Doncel David [c]

[a] *Research, Development and Innovation Procalculo Prosis- mvalbuena@procalculo.com,*
[b] *Universidad Nacional de Colombia – rhernandez@unal.edu.co,*
[c] *Research, Development and Innovation Procalculo Prosis- ddoncel@procalculo.com*

**Abstract**: The 2024 eruption of Colombia's Los Aburridos mud volcano affected 109 families, highlighting the urgent need for advanced risk management strategies. This study integrates multicriteria analysis (AMC), hydrological modelling, and geospatial data using fuzzy logic and deep learning to identify vulnerability zones. Fuzzy logic quantifies uncertainties in risk factors, while the U-Net deep learning model processes satellite imagery for land cover classification. The methodology produced a vulnerability that matched a 93% of the areas impacted by the eruption. These results validate the approach, offering a robust framework for assessing volcanic risks and enhancing disaster preparedness and mitigation strategies.

***Keywords:*** U-Net, Multicriteria Analysis (AMC), Streams modeling, Vulnerability, Satellite Imagery

## 1. Introduction

Volcanic eruptions in Colombia have been studied with greater rigor since 1985, when the Nevado del Ruiz Volcano recorded the most destructive eruption in the country (Florez & Ochoa, 1986).

This event marked a milestone in the history of risk management in Colombia due to the lack of planning and monitoring that existed in the face of a phenomenon of this magnitude, which led the government and institutions to focus on preventing these disasters. The laws and regulations on risk management adopted after this date focused on the study of the social, economic, and environmental conditions of the risk areas, as the strengthening of these factors reduces the existing vulnerability to these inevitable impacts and constitutes a fundamental element for the development of the territory (Lavell, 2001).

The constant monitoring of volcanoes plays a crucial role in risk management in Colombia, as there are several human settlements in volcanic threat areas and most of the population is unaware of this threat. This, combined with the limited understanding of the vulnerability generated by volcanoes, represents a challenge for local and national authorities (Hernández-Peña et al., 2021). Thus, volcanic risk management, with a focus on evacuation and protection of the population, emerges as a necessary tool for the control and reduction of damage caused by a possible eruption.

Currently, most countries with high volcanic activity use technological tools, such as specialized programs to better monitor the activity of their volcanoes (Deligne et al., 2017). Therefore, in Colombia, new methodologies and tools for volcanic monitoring are also required to strengthen risk management strategies.

Based on this need, it has been decided to use the AMC as a tool for the development of the study. The AMC is known as a methodology used in different professional fields, based on the evaluation and comparison of scenarios considering different factors associated with the phenomenon under study, regardless of their nature, whether qualitative or quantitative. Some methodologies implement Geographic Information Systems (GIS) for the AMC, determining the most appropriate location for human settlements, considering the vulnerability generated by the ecosystem (Cruz et al, 2018).

Today, the methodology implemented by the Colombian Geological Service (SGC) is based on the characterization of the threat to establish the intensity pattern that will be considered to analyse the vulnerability and thus establish impact scenarios of the phenomenon, identifying the loads produced. With these scenarios, the weights of the factors to be considered for the subsequent development of cartography are determined. The SGC also recommends considering reports of volcanic eruptions and the threat map to establish these scenarios (Biass et al., 2016). Although this methodology has been adopted and implemented in the country, the absence of current technological tools that could be used is identified.

Fuzzy logic offers great advantages in establishing vulnerability zones, considering the factors that determine a volcanic eruption. It consists of approximating the computational process to human decision-making, allowing machines to manipulate complex problems. This is achieved in such a way that a machine's decision is not encoded only with a “yes” or a “no” but generates more nuanced responses such as “a little more” or “maybe”. It is a model that manages uncertainties by expressing terms with a degree of certainty in a numerical format in the range of 0 to 1. Therefore, a fuzzy relevance vector is also referred to as a possibility vector or a possibility distribution (Juvanhol, 2021).

In 2024, the Colombian mud volcano Los Aburridos (also known as El Aburrido or Cacahual) erupted, affecting 109 families. This research seeks to determine the vulnerability zones of Los Aburridos by developing a risk assessment methodology based on AMC, fuzzy logic, and Deep Learning—a model capable of quantifying the weight of vulnerability factors (physical, geological, and geographic) inherent to this phenomenon (Torres Corredor, 2020).

## 2. Methods and Materials

### 2.1 Zoning of volcanic eruptions vulnerability

A volcano is a rupture on the earth’s crust through which hot lava, volcanic ash, and gases are spewed out during the eruption from a magma chamber underneath the surface. Most of them are found near the tectonic plate boundaries, where they converge and subduct or diverge. Volcanism can be caused by diapirs 3000 km deep within the earth forcing their way from the core–mantle boundary, with impacts far away from plate boundaries (Yadav et al., 2022)

Colombia is in an area with high susceptibility to natural phenomena such as earthquakes, floods, landslides and volcanic eruptions, which have significantly affected human life, infrastructure and the economy. According to data from the National Unit for Disaster Risk Management (UNGRD), between January 1998 and December 2021, a total of 21.5 million people were affected in the country, 3,690 died, 675 were missing and 6,173 were injured by natural disasters (Ayala & Ospino, 2023).

The second major event in Colombia is related to the eruption of the Nevado del Ruiz volcano on 19 February 1845 when a massive lahar with logs, “stinky” mud, sand, large rocks and even ice killed about 1000 tobacco plantation workers at the outlet of the Lagunillas River catchment. The 1845 lahar was the second deadliest volcanically related event recorded in the same area and the same stream, the Lagunillas River, along with the 1985 Armero lahar (H. Garcia-Delgado et al., 2022). This event in the risk management scenario establishes the need to understand, the location of the population and its economic activities related to the volcano eruption track, which could be extracted based on stream modelling using a Digital Elevation Model (DEM).

Hundreds of mud volcanoes characterize the north-western part of Colombia can pose serious hazard for people living in the surrounding area and can cause serious damage to neighbouring infrastructures. The frequent emission of toxic gases also severely threatens the neighbouring colonial cities (Di Luccio et al., 2021). In 2024, an eruption of the mud volcano named Los Aburridos registered an eruption that affected 109 families.

### 2.2 Topographic analysis for susceptibility zoning related to volcanic eruptions

Hydrological analysis is a process by which, based on a DTM, depression zones are classified in the terrain through which liquid material could flow in the form of drainage around a study area. Hydrological analysis is the process of studying and evaluating the water cycle, including precipitation, runoff, infiltration and evaporation, to understand the availability and behavior of water in a specific region (Chow et al., 2021). At the volcanological level, this tool allows modeling the accumulation and distribution of volcanic material generated in an eruption. Flow modeling allows the identification and zoning of areas most likely to be affected and, based on Euclidean distances, understand the level of susceptibility that exists around eruptive activity.

### 2.3 Fuzzy logic and deep learning in vulnerability zoning of volcanic eruptions

Vulnerability is composed of two components: (1) elements potentially at risk (population, networks, and assets) and their susceptibility to damage, i.e., the parameters that influence the damaging effects of a threat; and (2) the response capacity or resilience of an individual, household, or community, which includes both the coping capacity to face the event and the adaptive capacity to absorb disturbances and reorganize into a fully functional system (Michellier et al, 2016).

Deep Learning is a branch of Artificial Intelligence that has been growing to improve the results derived of image processing to extract information. This technique requires a considerable amount of high-resolution training data to learn and predict with the highest accurate results (Sawant & Ghosh, 2024). For land cover classification, in this project the U-Net model was implemented based on convolution operations to learn global semantic information, which has produced good results, which makes such methods unable to completely meet the accuracy requirements of semantic segmentation (Tang, 2024).

Fuzzy set theory facilitates the analysis of non-discrete natural processes as mathematical formulas. Membership in a classical set is defined as true or false, 1 or 0, while in the fuzzy set, membership is expressed on a continuous scale from 1 to 0. The membership function describes the membership of the factor to the fuzzy set of A and consists of the quantification of the effect of factor X on the event to be predicted (Baharvand et al., 2020).

For multicriteria analysis at the geographic level, two membership functions are proposed based on the Sine and Cosine functions, which are applied to direct and indirect variables of the phenomenon under study (Valbuena & Ferrucho, 2024). In this case, variables such as distance to the flow accumulation and distance to buildings and roads will generate greater social vulnerability in the event of a possible volcanic eruption, so they are normalized from the cosine membership function. Similarly, variables such as the presence of forest biomass and crops correspond to factors correlated with the vulnerability analysis at the ecosystem and economic level.

All variables must be normalized due to the similar weight in the assessment of vulnerability to volcanic eruptions, so having all variables in the same range allows the assessment of different types of vulnerability, which are key tools within Disaster Risk Management for decision-making.

The integration of multiple criteria is based on the foundations of fuzzy logic, which establish different functions associated with overlapping based on Geographic Information Systems - GIS, such as the algebraic operators OR, AND, SUM, Product and Gamma. The fuzzy Gamma operator ($\gamma$) is the most widely implemented for spatial modelling and is estimated based on the multiple between the fuzzy algebraic product

and the fuzzy algebraic sum. The value of Gamma (γ) varies between 0 and 1 (Baharvand et al., 2020).

## 3. Results

A pair of images captured by Sentinel 1 satellite was implemented in the generation of DEM based on the interferometric theory. Each image was captured with different angle. The processing was generated in SNAP, a software provided by the European Space Agency.

Thus, the flow accumulation was calculated which simulates the flow of the mad or magma derived from the volcanoes. This allows the quantification of susceptibility based on the Euclidean distance from the flow accumulation to the different points.

Subsequently, the population vulnerability was calculated with the extraction of buildings and roads using Deep Learning techniques, specifically U - Net. Table 1 presents the configuration implemented on each of the coverages extracted from the Planet Scope images with the deep learning methods.

| Land Cover | Model | Backbone | Learning Rate |
|---|---|---|---|
| Forest | UnetClassifier | ResNet34 | 3.02e-06 a 3.02e-05 |
| Crops | PSPNetClassifier | ResNet50 | 3.63e-04 a 3.63e-03 |
| Buildings | PSPNetClassifier | ResNet34 | 1.45e-04 a 1.454e-03 |
| Roads | MultiTaskRoadExtractor | ResNet50 | 9.12e-05 |

Table 3. Deep Learning Models Configuration

The accuracy of the extraction of buildings was around 70%, and the road extraction achieved an accuracy of 78%. A postprocessing methodology was applied getting the results presented in Figure 1.

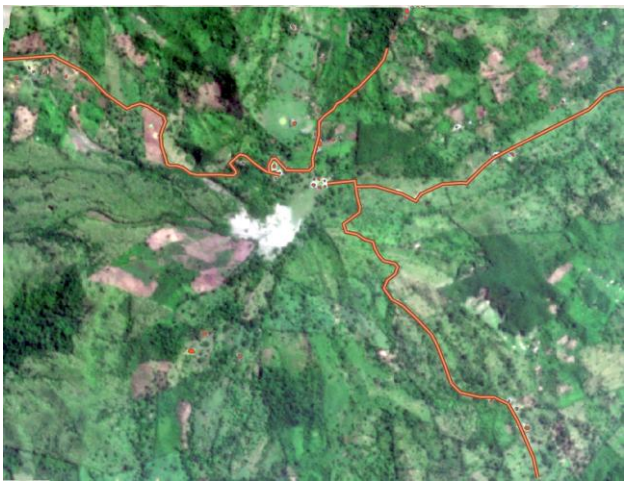

Figure 1. Road and Building extraction with postprocessing

Based on these results, the susceptibility was crossed with the areas correlated with population, using the fuzzy logic methodology.

A normalized model is obtained where values close to zero correspond to the areas with the greatest vulnerability associated with the eruption of the Los Aburridos Volcano. The results are compared with the eruption recorded in 2024 and it is determined that 93% of the affected area is recorded in the model derived with Fuzzy Logic and Deep Learning. Figure 2 shows the phenomena and the susceptibility.

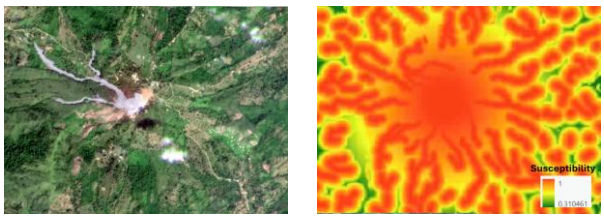


Figure 2. Comparison of volcanic eruptions with susceptibility

This comparison allows the validation of the methodology to be applied to other volcanic bodies, facilitating risk management associated with the evaluation, mitigation and prevention of social impacts resulting from volcanic eruptions.

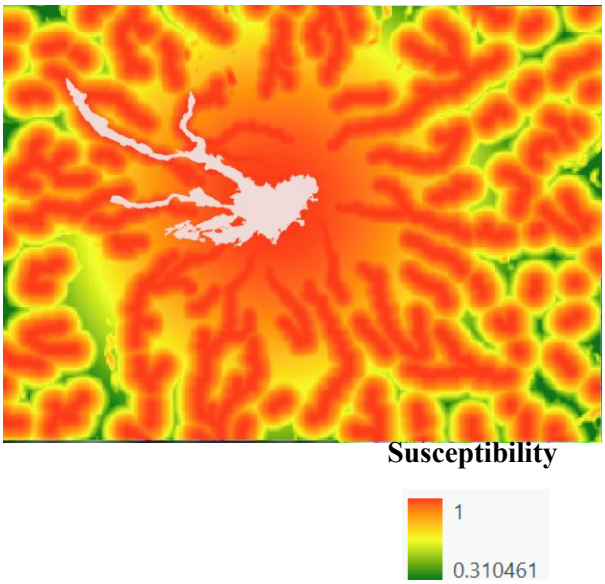


Figure 3. Overlay volcanic eruption with susceptibility

Finally, roads and buildings were crossed with susceptibility with the main objective of identifying the vulnerability of anthropic elements related to volcanic eruptions. The results are presented in Figure 4.


Figure 4. Length of Roads classified by Vulnerability


Figure 5. Buildings count classified by Vulnerability

Results are alarming due to the vulnerability that roads and buildings present during the volcanic eruption. In the eruption presented in 2024, many families were affected by this phenomenon, and it is necessary to identify alternatives to locate population and decrease vulnerability.

## 4. Conclusions

For decision-making at the risk management level, social vulnerability is the main input required to carry out the relocation work of the main vulnerable populations in the face of a volcanic threat. An analysis based on fuzzy logic and multicriteria is carried out to superimpose the geographic layers extracted from hydrological modelling and deep learning, identifying the vulnerability around volcanic eruptions.

Deep Learning methods allow a high precision extraction of the land covers based on the digital numbers, the shape, and the size of geographic elements derived from satellite imagery. Due to the daily monitoring of Planet Scope Imagery, it was possible to identify and quantify the area affected by the mud volcano eruption, understanding the territorial impacts based on the dynamics before the event.

In conclusion, this methodology could be applied to other volcanoes to forecast the areas, roads and buildings that could be affected for an eruption event in the future.

## 5. References

Ayala, A., & Ospino, J. (2023). Desastres naturales en Colombia: un análisis regional. Centro de Estudios Económicos Regionales (CEER), Cartagena, Colombia.

Baharvand, S., Mohammady, M., & Khaledi, N. (2020). Landslide susceptibility zoning in a catchment of Zagros Mountains using fuzzy logic and GIS. *Environmental Earth Sciences, 79*(10), 204. https://doi.org/10.1007/s12665-020-08957-w

Biass, S., Smith, V. C., Miller, T. P., & Johnson, E. R. (2016). Probabilistic evaluation of the physical impact of future tephra fallout events for the Island of Vulcano, Italy. *Bulletin of Volcanology, 78*(37). https://doi.org/10.1007/s00445-016-1028-1

Chow, V. T., Maidment, D. R., & Mays, L. W. (1988). *Applied Hydrology*. McGraw-Hill.

Cruz, N., Torres, J., & Calderón, A. (2018). Análisis multicriterio como herramienta de toma de decisiones en las ciencias de la tierra. CIATEC, Centro de Innovación Aplicada en Tecnologías Competitivas, México.

Deligne, N. I., Smith, J. D., Thompson, R. A., & Martínez, L. R. (2017). Evaluating the impacts of volcanic eruptions using RiskScape. *Journal of Applied Volcanology, 6*, Article 18. https://doi.org/10.1186/s13617-017-0069-2

Di Luccio, D., Salamone, F., & Escobar, F. (2021). Physical and geochemical characteristics of land mud volcanoes along Colombia's Caribbean coast and their societal impacts. *Science of The Total Environment, 759*, 144225. https://doi.org/10.1016/j.scitotenv.2020.144225

Flórez, A., & Ochoa, F. (1986). La erupción del volcán del Ruíz. *Revista Colombia Sus Gentes y Regiones*, Instituto Geográfico Agustín Codazzi.

Garcia-Delgado, H., Pérez, M., & Rodríguez, J. (2022). Fatal landslides in Colombia (from historical times to 2020) and their socio-economic impacts. *Landslides, 19*(7), 1689–1716. https://doi.org/10.1007/s10346-022-01870-2

Hernández-Peña, Y. T., Vargas-Cuervo, G., & Zafra-Mejía, C. A. (2021). Percepciones sobre fenómenos volcánicos: elementos para la gestión del riesgo en Colombia. *Perspectiva Geográfica, 25*(1), 99–119. https://doi.org/10.19053/01233769.9488

Juvanhol, R. S., Silva, M. T., Andrade, L. T., & Pereira, A. M. (2021). GIS and fuzzy logic applied to modelling forest fire risk. *Anais da Academia Brasileira de Ciências, 93*, e20190726. https://doi.org/10.1590/0001-3765202120190726

Lavell, A. (2001). Sobre la gestión del riesgo: apuntes hacia una definición. Recuperado de https://desastres.unanleon.edu.ni/pdf/2004/mayo/PDF/SPA/DOC15036/doc15036-contenido.pdf

Michellier, C., Tchatchueng, L., & Ngnikam, E. (2016). Contextualizing vulnerability assessment: A support to geo-risk management in central Africa. *Natural Hazards, 82*(S1), 27–42. https://doi.org/10.1007/s11069-016-2295-z

Sawant, S., & Ghosh, J. K. (2024). Land use land cover classification using Sentinel imagery based on deep learning models. *Journal of Earth System Science, 133*(2), 101. https://doi.org/10.1007/s12040-024-02298-z

Tang, Y., Li, J., Wang, Z., & Chen, X. (2024). A Siamese Swin-Unet for image change detection. *Scientific Reports, 14*(1), 4577. https://doi.org/10.1038/s41598-024-54096-8

Torres Corredor, R. A., Hernández, F. J., Ramírez, M., & Puerta, L. (2020). Guía metodológica para la evaluación de la vulnerabilidad y riesgo por caídas de material piroclástico transportado por el viento. Servicio Geológico Colombiano. https://doi.org/10.32685/9789585279483

Valbuena, M., & Ferrucho, C. (2024). Fuzzy Logic, Artificial Intelligence, and Planet Scope Imagery for the Zonification of Wildfire Vulnerability. En *2024 IEEE International Geoscience and Remote Sensing Symposium (IGARSS)* (pp. 3971–3975). https://doi.org/10.1109/IGARSS53475.2024.10642446

Yadav, R. K., Singh, A., & Patel, M. (2022). Volcanic Emissions: Causes, Impacts, and Its Extremities. Department of Atmospheric Science, School of Earth Sciences, Central University of Rajasthan, India.

# Enhancing Vertical Accuracy of SRTM DEMs in Undulated Terrain Using LiDAR-Derived GCPs and Multiple Linear Regression

G.S.N. Perera *, H.A. Nalani , D.M.A.G.A.S. Senavirathna

*Faculty of Geomatics, Sabaragamuwa University of Sri Lanka, P.O. Box 02, 70140, Belihuloya, Sri Lanka*
*sanka@geo.sab.ac.lk, nalani@geo.sab.ac.lk, avintha.geo@gmail.com*

**Abstract**: Digital Elevation Models (DEMs) such as SRTM are widely used in geospatial applications but often exhibit vertical errors due to terrain complexity and vegetation cover. This study aimed to improve the vertical accuracy of SRTM DEMs over the Gin River Basin in Sri Lanka using a Multiple Linear Regression (MLR) approach. Ground Control Points (GCPs) derived from high-resolution LiDAR DEMs were used to model elevation errors as a function of terrain attributes including slope, aspect, curvature, elevation, and land cover. Three training datasets of different sizes (418, 88, and 50 GCPs) were evaluated to assess the influence of training data on model performance. The MLR-corrected DEMs demonstrated substantial improvements over the original SRTM DEM, with $R^2$ values of 0.9773, 0.9561, and 0.9466, and corresponding MAE values of 3.44 m, 5.26 m, and 4.67 m for the three datasets. Independent validation using 22 sparsely distributed GCPs confirmed that the corrections generalized well, reducing RMSE from 5 m to 6.4 m across datasets. Analysis of individual test point errors showed consistent spatial performance, indicating that the MLR model effectively captured terrain-induced SRTM errors. These results highlight that MLR, combined with sufficient and well-distributed GCPs, provides an effective, scalable approach for correcting global DEMs in regions with complex topography.

***Keywords:*** DEM, SRTM, Multiple Linear Regression, RMSE, Machine Learning

## 1. Introduction

Digital Elevation Models (DEMs) are fundamental to geospatial applications such as hydrological modeling (Liang and Xie, 2011), flood risk assessment (Teng et al., 2017), landslide susceptibility mapping (Guzzetti et al., 2006), and infrastructure planning (Shahabi et al., 2015). Despite their importance, the quality of DEMs varies depending on the acquisition method and terrain complexity. Freely available global DEMs, including the Shuttle Radar Topography Mission (SRTM; USGS, 2023), ASTER GDEM (NASA/METI, 2011), and Copernicus DEM (European Space Agency, 2020), provide near-global coverage but often exhibit reduced vertical accuracy due to their relatively coarse resolution and the inability of their measuring signals to penetrate to the bare earth. Resolution effects are common to both optical and radar missions used for generating global DEMs (Farr et al., 2007; Gesch et al., 2016). Low resolution often smooths sharp changes, ridges, and slope breaks in terrain, leading to shifts in elevation values.

For radar-based DEMs, canopy structure, wavelength, and moisture conditions further limit the penetration of radar signals to the

ground surface (Carabajal and Harding, 2006; Hofton et al., 2009). Conversely, DEMs derived from optical stereo imagery often deviate due to shadows, cloud cover, and poor image correlation in homogeneous areas (Tachikawa et al., 2011). As a result, the vertical accuracy of DEMs in hilly and forested regions can significantly deviate from reality, limiting their suitability for high-precision applications.

In contrast to freely available global DEMs, many countries have produced centimetre-level accurate DEMs at the national scale, primarily from airborne laser scanning point clouds. However, the substantial financial investment required for such data acquisition often restricts access in developing countries. This highlights the necessity of improving the vertical accuracy of global DEMs to support a wider range of applications.

Previous approaches to DEM correction include co-registration techniques (Nuth and Kääb, 2011), bias removal using ground control points (Wessel et al., 2018), and geostatistical interpolation (Li et al., 2013). However, these methods can be resource-intensive and difficult to apply at scale. Machine learning has emerged as a powerful alternative, capable of capturing nonlinear error relationships between elevation discrepancies and terrain attributes (Hengl et al., 2018). Random Forest regression, in particular, has been shown to perform well in spatial prediction tasks (Breiman, 2001; Belgiu and Drăguţ, 2016).

This study aims to enhance the vertical accuracy of the SRTM DEM covering a subset of the Gin River Basin by leveraging ground control points acquired from LiDAR point clouds and Multiple Linear Regression. The proposed approach is designed to be scalable while effectively addressing terrain-induced DEM errors.

## 2. Study Area and Data

The study area is located within the Gin River Basin of Sri Lanka, encompassing elevations ranging from approximately 0 m to over 228 m above sea level. The terrain is characterized by steep slopes, rugged topography, and dense tropical forest cover—conditions under which global DEMs typically demonstrate poor performance (Weerasinghe et al., 2018). For this research, a subset of the Gin River Basin was selected where a LiDAR-derived DEM was made available through the Climate Resilience Improvement Project in 2017. The selected study area covers an extent of 430 km².

Figure 1. Study Area

The following datasets were used in this study:

SRTM DEM: The Shuttle Radar Topography Mission (SRTM) DEM with 1 arc-second (~30 m) resolution, freely available from the USGS Earth Explorer, was used as the base dataset.

Ground Control Points (GCPs): For training the MLR model, ground control points were extracted from a highly accurate DEM derived from aerial LiDAR data. One point was sampled from each 1 km × 1 km grid cell of the DEM, ensuring uniform spatial representation. The vertical accuracy of these control points is within ±15 cm.

Terrain Attributes: Ancillary variables including slope, aspect, curvature and height corresponding to each GCP location were derived during the pre-processing stage.

Land Cover Data: Land cover information was obtained from Sentinel-2 imagery and the ESA Climate Change Initiative (CCI) land cover dataset.

## 3. Methodology

The workflow comprised four stages — pre-processing, error modelling, training the MLR model, and validation — and is illustrated step-by-step in Figure 2.

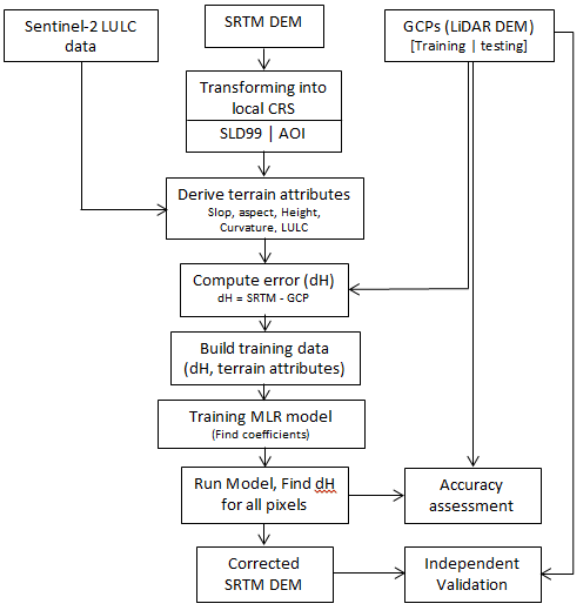


Figure 2. schematic diagram of the workflow

### 3.1 Pre-processing

The SRTM DEM is referenced to the WGS84 coordinate reference system (CRS), which differs from the CRS of the GCPs. Therefore, the SRTM DEM was re-projected into the Sri Lankan local CRS (SLD99), and a sea surface topography (SST) correction was applied to align DEM heights with the mean sea level (MSL) heights of the GCPs. Terrain attributes such as slope, aspect, height, and curvature were derived from the DEM, as these variables are known to influence deviations between DEM elevations and actual topography (see Section 1). The area of interest (AOI) was clipped from the DEM tiles to match the extent covered by the available GCPs, since no GCPs were available outside the selected region.

### 3.2 Error Modelling

Elevation differences (Δh) were computed at GCP locations as:

$$\Delta h = SRTM_H - GCP_H$$

Where $SRTM_H$ is the SRTM elevation and $GCP_H$ is the LiDAR-derived ground control elevation. Predictor variables included slope, aspect, curvature, elevation, and land cover type, which together capture the spatial heterogeneity of DEM errors. The dataset was split into training (80%) and validation (20%) subsets.

### 3.3 Multiple Linear Regression (MLR)

MLR was used to model the elevation errors of the SRTM DEM using predictor variables such as slope, aspect, curvature, elevation, and land cover type (Li et al., 2013; Hengl et al., 2018). Regression coefficients ($\beta s$) were estimated to define the linear relationship between these predictors and Δh as shown in equ_1.

$$\Delta h = \beta_0 + \beta_0 . slope + \beta_1 . aspect + \beta_2 . curvature + \beta_3 . height + \beta_4 . LU\ types + \in \quad \text{.....(equ\_1)}$$

The trained MLR model produced a spatially continuous error surface, which was subtracted from the original DEM to generate the corrected DEM. Models were trained on different subsets of GCPs to assess the effect of training data size, and validation was performed using an independent set of GCPs to evaluate improvements in vertical accuracy (Li et al., 2013).

### 3.4 Accuracy Assessment

Validation was conducted using independent checkpoints derived from the LiDAR DEM of the same area. Accuracy metrics included the Root Mean Square Error (RMSE) and Mean Absolute Error (MAE). Results were reported for the three corrected DEMs generated from different training dataset sizes.

## 4. Results and Analysis

The main feature attributes required for training the MLR model, derived from the re-projected SRTM DEM and LULC data obtained from the Copernicus Data Space Ecosystem over the study area, are shown in Figure 3.

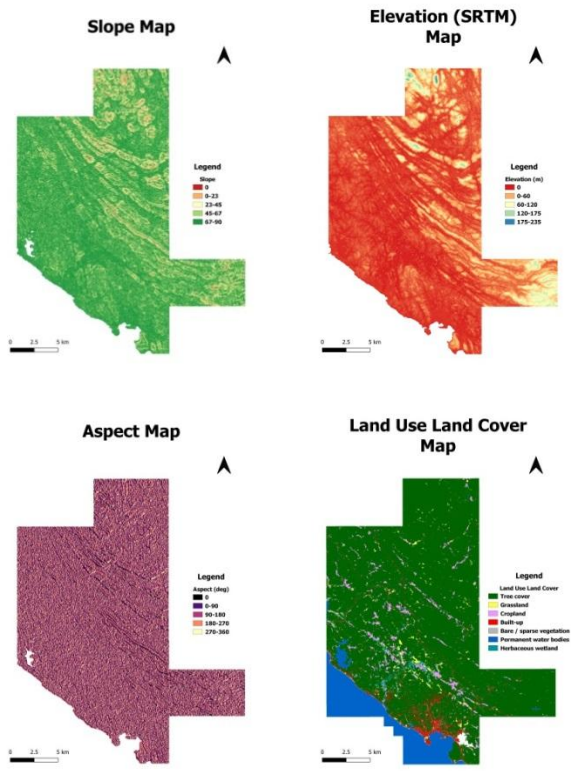


Figure 3: Feature maps – (a) slope,(b) elevation (c) aspect, (d) LULC maps

To obtain a detailed picture of the quality of the SRTM DEM, GCPs were selected near the center of each 1 km × 1 km grid cell within the study area. During the selection, points located on hilltops, slopes, valleys, and other varying terrain conditions were included, while water bodies were excluded. In total, 415 GCPs were chosen, of which 80% were used for model training and the remaining 20% for testing model accuracy.

Elevation errors at the GCP locations were calculated, and the original RMSE of the SRTM DEM was found to be 8.953 m.

To investigate the influence of the number of GCPs on model training and the generation of corrected DEMs, three training datasets were prepared, containing 418, 88, and 50 records, respectively, and were spatially distributed across the study area. Correspondingly, the test datasets included 84, 18, and 10 points in each case.

To ensure sufficient iterations and proper model training, a ceiling of 500 iterations was set. For each data set, the following training matrices were obtained.

| Feature | Coefficient_beta Data Set1 | Coefficient_beta Data Set2 | Coefficient_beta Data Set3 |
|---|---|---|---|
| Aspect | -0.154224311 | 0.236588963 | 0.465727562 |
| SRTM_Height | 27.66107524 | 24.42993624 | 32.68854528 |
| Slope | 0.644845241 | 0.986060201 | 1.060767445 |
| WorldCover_10 | -1.428305986 | -1.239319624 | -0.729116274 |
| WorldCover_30 | 0.938895592 | 2.04024127 | |
| WorldCover_40 | 0.494368356 | | |
| WorldCover_50 | -0.682837807 | -3.486054692 | -2.900776249 |
| WorldCover_60 | -0.943604434 | | |
| WorldCover_90 | 1.621484279 | 2.685133046 | 3.629892523 |
| Intercept | 26.07902159 | 23.58495472 | 26.51127405 |

Table 1. MLR Coefficient Matrix

The large positive coefficient for SRTM height reflects the systematic difference between the SRTM DSM and the DTM-based GCPs, primarily caused by vegetation canopy and built structures. This indicates that higher SRTM elevations are associated with larger positive elevation errors, which the MLR model corrects.

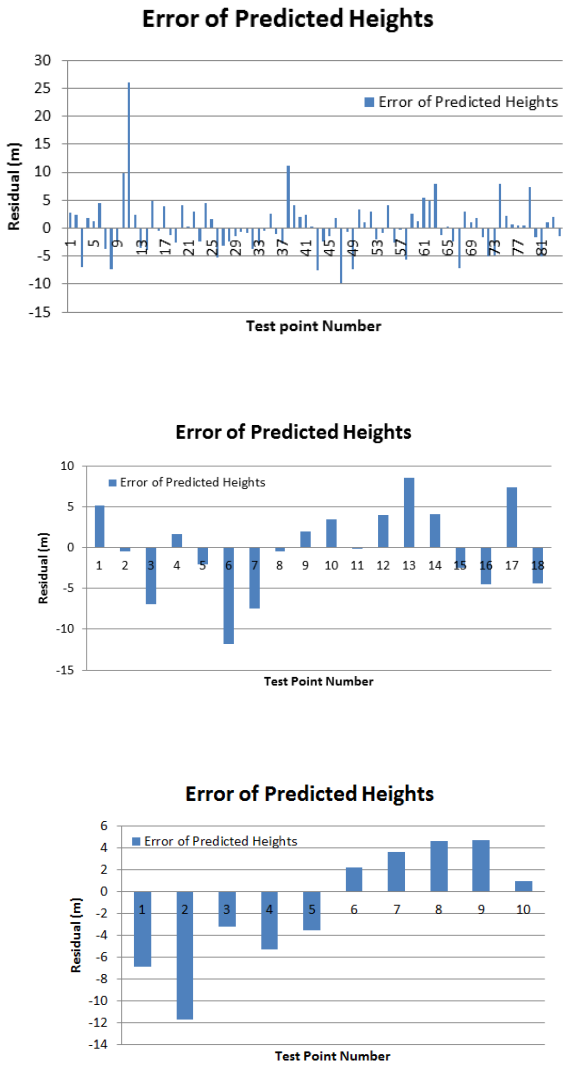


Figure 4. Individual test point errors of three datasets (top-dataset1, middle-dataset2, and bottom-dataset3)

Analysis of individual test point errors shows (figure 4) that Dataset 1, with the largest GCP set, exhibits small and consistent deviations across the study area, while Datasets 2 and 3, with fewer GCPs, show larger variability. This pattern aligns with the summary metrics (MAE and RMSE), highlighting that sufficient and spatially well-distributed training points are essential for achieving accurate and stable DEM corrections.

| Dataset | Test_R2 | Test_MAE | Test_RMSE |
|---|---|---|---|
| Data set 1 | 0.9773 | 3.4428 | 4.8903 |
| Data set 2 | 0.9561 | 4.2562 | 5.2594 |
| Data set 3 | 0.9466 | 4.6726 | 5.4658 |

Table 2. Summary statistics of Testing

The performance of the MLR-corrected DEMs was evaluated using three different training datasets of varying sizes. Dataset 1, with the largest number of GCPs, achieved the highest accuracy, with an $R^2$ of 0.9773, MAE of 3.44 m, and RMSE of 4.89 m, indicating excellent agreement between predicted and true elevations. Dataset 2 and Dataset 3, with fewer GCPs, showed slightly lower performance ($R^2$ = 0.9561 and 0.9466; MAE = 4.26 m and 4.67 m; RMSE = 5.26 m and 5.47 m, respectively), demonstrating that model accuracy decreases as the number of training points is reduced. Overall, these results highlight that a sufficiently large and well-distributed set of GCPs is crucial for robust MLR-based correction of SRTM DEMs, effectively capturing spatial patterns of elevation errors across diverse terrain conditions.

Figure 5 shows the elevation errors at test points for each case, illustrating how model accuracy varies with the amount of training data.

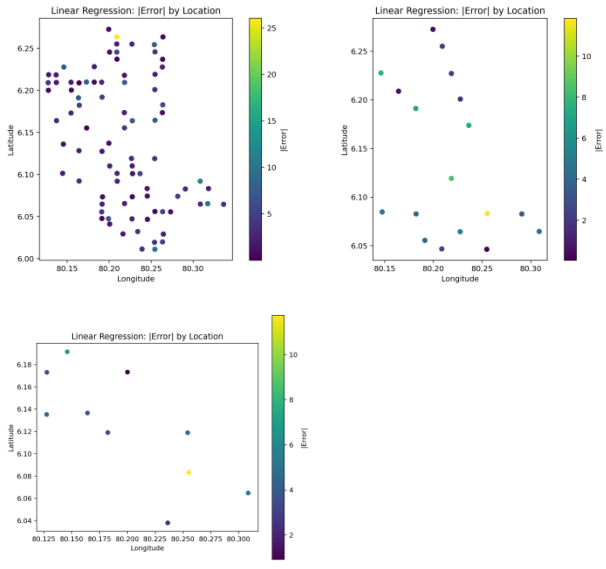


Figure 5: spatial distribution of errors at test points for the three datasets

The elevation errors at the test points, which were evenly distributed throughout the study area, show no large deviations, as illustrated in Figure 5. This uniform distribution of small

errors suggests that the MLR model effectively captured the spatial patterns of SRTM elevation errors across diverse terrain conditions, including hilltops, slopes, and valleys. The results indicate that the model provides consistent and reliable corrections throughout the study area, demonstrating its robustness and suitability for improving DEM accuracy in regions with complex topography.

Figure 6 presents the predicted versus true elevation errors at the test points for the MLR-corrected DEMs. The points closely follow the 1:1 line, indicating that the model predictions match the observed errors well and that the MLR model effectively captures the spatial variation of SRTM elevation errors

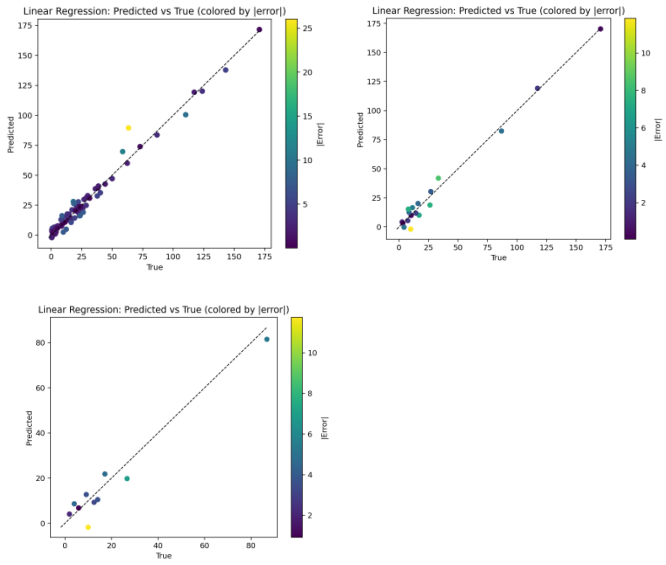


Figure 6: predicted vs true plot showing 1:1 line

Independent validation was performed using 22 sparsely distributed GCPs across the study area to assess the generalization of the MLR-corrected DEMs. Comparison of elevations at these points demonstrates that the MLR correction reduced systematic and local errors. The RMSE values for Dataset 1, Dataset 2, and Dataset 3 were 5.023 m, 5.734 m, and 6.427 m, respectively, slightly higher than those obtained from the testing datasets. This is expected because the independent GCPs cover locations not used during training, reflecting the model's generalization performance across diverse terrain conditions.

## 5. Conclusion

This study demonstrated that Multiple Linear Regression (MLR) can effectively correct elevation errors in SRTM DEMs using high-accuracy LiDAR-derived GCPs and terrain attributes as predictors. The MLR-corrected DEMs showed significant improvements in vertical accuracy, with RMSE and MAE reduced across all datasets compared to the original SRTM DEM. Larger and well-distributed training datasets yielded better performance, highlighting the importance of sufficient GCP coverage for robust model training. Independent validation confirmed that the corrections generalize well beyond the training data, accurately capturing spatial error patterns across diverse terrain conditions. Overall, the results indicate that MLR provides a simple, interpretable, and scalable approach for improving global DEMs, making them more suitable for hydrological modeling, infrastructure planning, and other high-precision geospatial applications.

## 6. References


Belgiu, M., & Drăguţ, L., 2016. Random forest in remote sensing: A review of applications and future directions. ISPRS Journal of Photogrammetry and Remote Sensing, 114, 24–31.

Breiman, L.,b., 2001. Random forests. Machine Learning, 45(1), 5–32.

Dubayah, R., et al. (2020). The Global Ecosystem Dynamics Investigation: High-resolution laser ranging of the Earth's forests and topography. Science of Remote Sensing, 1, 100002.

European Space Agency. 2020. Copernicus Global DEM. Retrieved from [https://spacedata.copernicus.eu]

Farr, T. G., et al. , 2007. The Shuttle Radar Topography Mission. Reviews of Geophysics, 45(2).

Guzzetti, F., Carrara, A., Cardinali, M., & Reichenbach, P., 2006. Landslide hazard

evaluation: A review of current techniques. Landslides, 3(2), 85–99.

Hengl, T., et al., 2018. Machine learning in geospatial analysis: Applications in soil mapping and beyond. Environmental Modelling & Software, 109, 111–123.

Li, J., Zhu, A. X., & Gold, C., 2013. DEM error correction based on terrain feature constraints. Computers & Geosciences, 54, 19–27.

Li, Z., Zhu, Q., & Gold, C., 2013. Digital Terrain Modeling: Principles and Methodology. CRC Press.

Liang, X., & Xie, Z., 2011. A new surface runoff parameterization with subgrid-scale soil heterogeneity for land surface models. Advances in Water Resources, 34(6), 727–738.

NASA/METI., 2011. ASTER Global Digital Elevation Model (GDEM) Version 2. Retrieved from [https://asterweb.jpl.nasa.gov/gdem.asp]

Neuenschwander, A., & Pitts, K., 2019. The ATL08 land and vegetation product for the ICESat-2 Mission. Remote Sensing of Environment, 221, 247–259.

Nuth, C., & Kääb, A., 2011. Co-registration and bias corrections of satellite elevation data sets for quantifying glacier thickness change. The Cryosphere, 5, 271–290.

Shahabi, H., et al., 2015. Landslide susceptibility mapping using GIS and statistical models: A case study. Environmental Earth Sciences, 74, 1017–1037.

Teng, J., Jakeman, A. J., Vaze, J., Croke, B. F. W., Dutta, D., & Kim, S., 2017. Flood inundation modelling: A review of methods, recent advances and uncertainty analysis. Environmental Modelling & Software, 90, 201–216.

USGS., 2023. Shuttle Radar Topography Mission (SRTM) User Guide. Retrieved from [https://www.usgs.gov/national-geospatial-program/ned]

Weerasinghe, K. D. N., et al., 2018. DEM-based terrain analysis for landslide susceptibility in Sri Lanka's hill country. Natural Hazards, 90, 1001–1021.

Wessel, B., et al., 2018. TanDEM-X global DEM: Methods and accuracy analysis. ISPRS Journal of Photogrammetry and Remote Sensing, 139, 171–182.

# MapBiomas Ecuador: Applying Machine Learning to Monitor Land Cover and Land Use Changes from 1985 to the Present

Wagner Holguin

*EcoCiencia Foundation, Ecuador; weholguin@gmail.com*

MapBiomas Ecuador is the first spatiotemporal monitoring system of remaining natural cover and land use in Ecuador, covering the period from 1985 to present. The initiative used all cloud-free scenes from the Landsat image catalog (including TM onboard Landsat 4 and 5, ETM+ onboard Landsat 7, OLI-TIRS onboard Landsat 8, and OLI-2 TIRS-2 onboard Landsat 9), along with machine learning algorithms—particularly the Random Forest classifier—and cloud computing to generate annual thematic land cover and land use maps.

As of 2023, Ecuador retains 58.48% of its territory under forest cover (both primary and secondary). An additional 8.33% is covered by other natural non-forest formations (e.g., grasslands, shrublands, and others). In terms of net change, at least 1.1 million hectares of natural cover were lost between 1985 and 2023. By 2023, 32% of the country had been transformed into anthropogenic land uses, mainly agricultural mosaics. Other land uses such as aquaculture (0.6%), forestry (0.16%), and mining (0.05%) were also mapped and show expansive temporal dynamics.

Although dense forest experienced the largest absolute reduction in area (-981,000 ha), mangroves declined by 9,000 ha—significant losses considering their already limited distribution and high degree of ecological transformation. In terms of glaciers, Ecuador went from having 7,949 hectares in 1985, to 5,019 in 2023. This is a significant loss of 37%, considering that glaciers do not recover.

In contrast, agricultural areas increased by 16% over the 39-year period, while forestry and aquaculture expanded by 46% and 151%, respectively—nearly doubling their extent since 1985. Mining, which was undetectable by satellite in 1985, has now emerged prominently; in the Amazon biome alone, it has reached an area of 9,0000 hectares, of which 1,405 ha (15.7%) were added in a single year between 2021 and 2022—marking the most rapid expansion detected.

The monitoring system analyzes land cover change trends at a biogeographical level by dividing the country into five biomes: Amazon, Andes, Galápagos, Pacific Tropical Rainforest, and Equatorial Dry Forest. The Amazon biome recorded the largest loss of natural cover and also experienced a 154% increase in anthropogenic land uses compared to 1985 levels.

This annual thematic mapping effort constitutes the most comprehensive reconstruction of land cover transformation in Ecuador over nearly four decades. It is designed as a continuously improving and updatable tool to support land use evaluation and planning across various sectors of society.

***Keywords:*** Satellite monitoring, Natural cover, Land use, Change detection, Ecuador, Remote sensing, Land cover classification, Climate Change

# AI-Enhanced 3D Landcover Classification Using Fused LiDAR and UAV Images

Hetti Arachchige Nalani

*Sabaragamuwa University, Sri Lanka, nalani@geo.sab.ac.lk*

Accurate landcover classification is essential for a wide range of applications including precision agriculture, environmental monitoring, forest resource management, and urban planning. Traditional classification methods using only 2D spectral data (RGB or multispectral) often fail to capture the complexity of land surface features in heterogeneous terrains such as urban-rural fringes, mountainous areas, and dense forests. LiDAR data, acquired via UAVs, provide detailed 3D structural information but lack spectral context. This research aims to overcome these limitations by integrating UAV-based LiDAR point clouds with UAV imagery using advanced AI techniques. Specifically, we propose a dual-stream deep learning architecture that utilizes PointNet++, a hierarchical point-based neural network for classifying 3D point clouds, and DeepLabv3+ with Xception backbone, a state-of-the-art semantic segmentation model for 2D imagery. The outputs of the two streams were fused through a late fusion strategy to enhance classification accuracy. The innovation of this approach lies in the synergistic use of both geometric and spectral data, which enables more robust and accurate landcover classification. The study area is located in Sabaragamuwa university premises, Sri Lanka. The overall classification accuracy exceeded 95%, demonstrating that semantically rich 3D landcover maps can be generated with substantial accuracy improvements over single-modality approaches. Some misclassifications were observed among certain classes. Despite these challenges, the results are promising surpassing those obtained using more complex geometric feature sets.

***Keywords:*** Landcover Classification, UAV LiDAR, UAV Images, Deep Learning

# Assessing land suitability for leguminous crops in the Okavango River basin: A multicriteria and machine learning approach

Kaleb Gizaw Negussie [a] *, Bisrat Haile Gebrekidan [b], Daniel Wyss [c] and Martin Kappas [c]

[a] *Department of Land and spatial sciences, Namibia University of Science and Technology, Windhoek, Namibia; knegussie@nust.na*
[b] *International Maize and Wheat improvement Center (CIMMYT), Addis Ababa, Ethiopia;*
[c] *Department of Cartography, GIS and Remote sensing, Georg-August University Goettingen, Germany.*

This study aimed to create a model to identify land suitable for growing sunn hemp (*Crotalaria juncea*) and pigeon pea (*Cajanus cajan*) in the Okavango River basin of the Kavango East region of Namibia. Advanced tree-based ensemble learning models, including Random Forest, Extra Trees, Gradient Boosting, XGBoost and multivariate regression analysis, were employed to enhance analytical accuracy. The Random Forest and XGboost models exhibited outstanding performance, as evidenced by their respective accuracy values of 0.97 and 0.96. In addition, this study proposed an innovative approach through the integration of subjective and objective analytical methods, which are independent of one another. The subjective component of the analysis employed a Multi-Criteria Decision Making-Analytic Hierarchy Process (MCDM-AHP). On the other hand, the objective component used a data-driven multivariate approach supported by tree-based learning algorithms. Twenty-two variables were considered, encompassing climatic conditions, hydro-geomorphologic features, soil characteristics, vegetation patterns, and socio-economic factors. These variables played a crucial role to identify the most suitable areas for growing the selected leguminous crops. The MCDM-AHP method utilised expert evaluations to rank the importance of variables, identifying water sources, slope, and soil properties as key factors. A suitability mapping analysis revealed that 17.63% of the area was highly suitable and 62.77% moderately suitable, while 10% was less suitable and 9.59% unsuitable for growing these two legumes. According to the data driven methodology, soil fertility and nitrogen content emerged as key determinants for land suitability. This is particularly relevant for nitrogen-fixing leguminous crops such as sunn hemp and pigeon pea, which play a central role in improving soil quality and ensuring food security.

***Keywords:*** MCDM, Ensemble Learning Models, Leguminous Crops, Land suitability, Okavango River, Namibia

# Integrated Analysis of Groundwater Responses to Climate Change and Agricultural Water Demand Using AI and Geographic Modeling

Jorge Alberto Valero-Fandiño[a] and Josue Medellin-Azuara [b]

[a] *Universidad Distrital Francisco Jose de Caldas; javalerof@udistrital.edu.co*
[b] *University of California; jmedellin@ucmerced.edu*

This research analyzes the potential effects of climate change and land use dynamics on groundwater in highly productive agricultural regions dependent on water imports and groundwater regulation. Before focusing on the research topic, solving a series of conceptual, operational, and computational challenges, such as having reliable, integrable, and fast models, was necessary. Initially, we evaluate the performance of three emulators of the sophisticated hydrology model known as the Fine Grid California Central Valley Groundwater-Surface Water Simulation Model (C2VSimFG) to estimate how climate and agriculture affect groundwater levels. Once the best emulator was identified, we assessed the hypothesis that groundwater levels in the Greater Kern County Region would exhibit a more rapid decline with projected climate change scenarios compared to historical climate resembling 1995 and 2015. Finally, we focus on determining economically and environmentally optimal operational policies for the Shafter-Wasco irrigation district by considering the conjunctive water use approach and identifying the best policies through Bayesian Optimization Programming. The findings suggest groundwater levels will likely decline unless agricultural water demand is reduced and recharge is increased, with climate scenarios exacerbating this decline compared to historical conditions. Our findings underscore the balance between profit and aquifer recovery, indicating farmers' need to curtail profits to achieve groundwater sustainability. Ultimately, our method can potentially integrate water and agricultural systems facing various uncertainties, providing valuable insights into optimal operational policies and tradeoffs.

***Keywords:*** Groundwater, Climate Change, Agricultural Water Demand, AI, Geographic Modeling

# Technical Session: Application of Geoinformation

# Remote sensing applied to spectral, soil and morphological characterization for archaeological prospecting purposes. A comparative study about Cerro Tusa and Morro de Tulcán, Colombia.

Rafael Rebolledo Wueffer

*Universidad Militar Nueva Granada, Colombia.- rafael.rebolledo@unimilitar.edu.co.edu.co*

**Abstract**: Remote sensing is a discipline oriented to observe the Earth's surface in order to know physical-chemical properties of matter. This technology is an attractive option for archaeological exploration and prospecting. In this article, two study areas were selected: One to represent slightly disturbed archaeological relics (*Morro de Tulcán* in *Popayán*, COLOMBIA); and other that is taken as a natural monument, usually confused with archaeological ruins (*Cerro Tusa* in *Venecia, Antioquia* COLOMBIA). For both areas, the potential of some freely accessible remote sensing options to improve preliminary archaeological exploration was evaluated. Four options of satellite data were analysed coming from specialized satellite data portals (SoilGrids-WoSIS, ASF Vertex Data Search, NASA-Gionanni and USGS-GLOVIS). From these services, 13 indicators were derived and measured for those study areas; These indicators take into account: data-quality of the data, archaeological relic expected characteristics and the usual characteristics of natural monuments. After that, a comparative analysis was done, including two strategies: internal comparison, to compare the study areas and their context regions (in order to determine how distinguishable, they are from their surroundings); and external comparison, to match study areas each other; in order to determine differentiable indicators (between archaeological remains from natural monuments). The results showed that ground surface temperature (LST) and bare soil index (BSI) were the best indicators for preliminary archaeological exploration.

***Keywords:*** Archaeology, remote sensing, archeological relicts, spectral indicators, morphological indicators, soil indicators.

## 1. Introduction

Remote sensing is the discipline that focuses on the observation of the Earth's surface with the aim of interpreting the physical-chemical properties of matter (Chuvieco, 1995). This framework gives this technology interesting qualities to contribute to archaeological exploration and prospection work, proof of which is the current recognition of specialties such as archaeological remote sensing (Deodato et al 2021). For the archaeologist, the possibility of accessing information through technological means specific to remote sensing are an ally in the task of prospecting for previously ignored, unknown, or difficult-to-access remains and evidence (Palacios and Martin 2004). Antonio Montufo, in his article "Applications of Archaeological Remote Sensing," identifies three applications of remote sensing to archaeology: analysis of the territory (physiographic, ecological, and

geological), infrared spectral studies, and radar-based studies (Montufo 1992). Rejas and Burillo, in 2016, highlight the non-invasive diagnostic qualities of a broad spectrum that remote sensing has for exploratory archaeology.

In this line of thought, having remote sensing tools that allow for a preliminary evaluation of particularities of the territory that help guide future archaeological exploration work would offer a great advantage to traditional archaeology: on the one hand, it would significantly expand search areas, considering remote or poorly accessible regions to anthropogenic infrastructure; on the other hand, it would significantly improve the precision of the search by considering only those areas that potentially present qualities that, in terms of the signals perceived by the remote sensor, can be associated with the presence of archaeological remains. This could significantly reduce the logistical costs of archaeological exploration. In this case, a comparative study will be developed of some aspects that can be measured by freely accessible remote sensors, over a recognized archaeological zone (*Morro de Tulcán*), versus a singular landscape natural element (*Cerro Tusa*). *Morro Tulcán*, located in municipality of *Popayán*, a pre- Columbian archaeological pyramidal relict (Cubillos 1959). The *Cerro Tusa* is a natural monument, in the municipality of *Venecia*, *Antioquia*, whose peculiar shape is frequently confused as pyramid (Ruta regions 2023). Both sites are in Colombia.

This study will compare spectral, soil and geomorphological characteristics for both sectors in order to identify features that make able distinguish the relics of sightly disturbed human settlements from natural elements of singular landscape value.

## 2. Data and Methods

### 2.1 Data

For this study, freely available satellite data in open format was used. In this regard, four sources were utilized: ISRIC's SoilGrids and WoSIS, NASA's GIOVANNI-Earth Data, ASF Vertex Data Search, and USGS GLOVIS portal.

### 2.2 Methodological strategy

The objective of this study is to establish, through a comparative analysis, key factors to differentiate potential archaeological relicts from monuments of natural with singular shape, using remote sensed data.

To develop this study, three independent sources of information were considered: multi-spectral imagery for spectral characterization; digital elevation models for textural and relief characterization; and re-sampled volumetric moisture as an indirect indicator of density.

The information sources were sectioned in terms of the context region of each study area: *Venecia* for *Cerro Tusa* and *Popayán* for *Morro de Tulcán*. Pre-processing tasks were completed with the geo-statistical downscaling of the volumetric moisture data and the atmospheric correction of the satellite images.

Following pre-processing, for each context region and from each information source, specific indicators were derived according to their characteristics. Spectral indices: NDVI and BSI; and land surface temperature (LST) were obtained from multispectral images. Relief thematic indicators: topographic irregularity (TI), slope, and aspect; and texture indicators: correlation, contrast, entropy, variance, homogeneity, and regularity; were derived from the Digital Elevation Models. Finally, indicators of remnant soil intervention (IRS) were obtained from the volumetric moisture raster and soil properties.

The study completed 13 indicators, for which statistical descriptors were calculated: average, range, maximum, minimum, and standard dev. This process was done for the study areas (*Cerro Tusa* and *Morro*) and their context regions (*Venecia* and *Popayán*) *Tulcán*). Based on these descriptors different and similar aspects were identified; both in terms of each study area with respect to its context region; and for the study areas between themselves. Based on the differences and similarities of the statistical descriptors, the

characteristic aspects of *Morro Tulcán* were determined with respect to *Cerro Tusa*. As a result of this analysis, the best indicators (spectral, morphological, and intervention-related) for the exploration of potential archaeological sites in the future were identified.

## 3. Relevant Results

### 3.1 Results of Statistical Characterization

To avoid bias and subjectivity in a comparative analysis based on similarities and differences is to systematize the comparison process and measure parametrically similar characteristics. In this sense, for this study, it was decided to base the comparisons on the following statistical descriptors: average, maximum, minimum, range, and standard deviation. These statistical values were calculated both for the context regions (*Popayán* and *Venecia*) and for the study areas (*Morro Tulcán* and *Cerro Tusa*) respectively. The following tables summarize these results (see Tables 3, 4, 5, and 6).

**Table 3: Statistical Descriptors of Popayán, Cauca.**

| POPAYAN | Max | Min | Average | Range | STD |
|---|---|---|---|---|---|
| NDVI | 1,000 | -1,000 | 0,715 | 2,000 | 0,292 |
| BSI | 1,000 | 1,000 | -0,132 | 2,000 | 0,196 |
| VARIANCE | 3,998 | 0,000 | 1,326 | 3,998 | 0,778 |
| CORRELATION | 0,792 | -0,129 | 0,408 | 0,921 | 0,242 |
| UNIFORMITY | 1,000 | 0,032 | 0,482 | 0,968 | 0,279 |
| CONTRAST | 10,578 | 0,000 | 0,262 | 10,578 | 0,235 |
| HOMOGENEITY | 1,000 | 0,217 | 0,876 | 0,783 | 0,090 |
| ENTROPY | 5,011 | 0,000 | 1,572 | 5,011 | 0,944 |
| SLOPE | 73,025 | 0,000 | 12,939 | 73,025 | 8,827 |
| ASPECT | 359,582 | 0,000 | 189,111 | 359,582 | 109,231 |
| T. IRREGULARITY | 109,000 | 0,000 | 7,660 | 109,000 | 5,740 |
| IRS | 2,846 | 1,857 | 2,384 | 0,988 | 0,182 |
| LST | 36,670 | -2,252 | 23,056 | 38,922 | 6,185 |

Table 1. Statistical Descriptors of Popayán, Cauca.

**Table 4: Statistical Descriptors of Venecia, Antioquia.**

| VENECIA | Max | Min | Average | Range | STD |
|---|---|---|---|---|---|
| NDVI | 1,000 | -0,785 | 0,803 | 1,785 | 0,137 |
| BSI | 0,665 | -0,587 | -0,218 | 1,252 | 0,130 |
| VARIANCE | 25,696 | 0,000 | 25,696 | 9,114 | 0,525 |
| CORRELATION | 0,794 | -0,123 | 0,554 | 0,918 | 0,191 |
| UNIFORMITY | 1,000 | 0,104 | 0,456 | 0,896 | 0,267 |
| CONTRAST | 35,688 | 0,000 | 0,576 | 35,688 | 0,745 |
| HOMOGENEITY | 1,000 | 0,070 | 0,780 | 0,930 | 0,147 |
| ENTROPY | 3,292 | 0,000 | 1,515 | 3,292 | 0,820 |
| SLOPE | 77,014 | 0,000 | 19,773 | 77,014 | 11,756 |
| ASPECT | 359,712 | 0,000 | 198,165 | 359,712 | 109,476 |
| T. IRREGULARITY | 141,000 | 0,000 | 12,353 | 141,000 | 8,806 |
| IRS | 2,904 | 1,999 | 2,527 | 0,905 | 0,177 |
| LST | 26,350 | 2,503 | 15,763 | 23,847 | 4,364 |

Table 2. Statistical Descriptors of Venecia, Antioquia.

**Table 5: Statistical Descriptors of Morro de Tulcán**

| Morro Tulcán | Max | Min | Average | Range | STD |
|---|---|---|---|---|---|
| NDVI | 0,737 | 0,442 | 0,628 | 0,295 | 0,071 |
| BSI | 0,222 | 0,015 | 0,091 | 0,207 | 0,047 |
| VARIANCE | 2,658 | 0,000 | 1,417 | 2,658 | 0,952 |
| CORRELATION | 0,742 | 0,059 | 0,562 | 0,683 | 0,127 |
| UNIFORMITY | 0,590 | 0,000 | 0,171 | 0,590 | 0,125 |
| CONTRAST | 0,694 | 0,000 | 0,287 | 0,694 | 0,204 |
| HOMOGENEITY | 0,930 | 0,705 | 0,803 | 0,225 | 0,044 |
| ENTROPY | 3,251 | 1,165 | 2,395 | 2,086 | 0,399 |
| SLOPE | 35,351 | 0,810 | 19,646 | 34,540 | 7,078 |
| ASPECT | 358,531 | 0,000 | 209,327 | 358,531 | 104,818 |
| T. IRREGULARITY | 24,000 | 2,000 | 11,658 | 22,000 | 4,661 |
| IRS | 2,529 | 2,457 | 2,480 | 0,072 | 0,021 |
| LST | 31,151 | 28,128 | 29,562 | 3,023 | 0,690 |

Table 3. Statistical Descriptors of Morro de Tulcán

**Tabla 6: Statistical Descriptors of Cerro Tusa**

| Cerro Tusa | Max | Min | Average | Range | STD |
|---|---|---|---|---|---|
| NDVI | 0,963 | 0,451 | 0,828 | 0,512 | 0,065 |
| BSI | 0,139 | -0,276 | -0,447 | 0,585 | 0,076 |
| VARIANCE | 9,114 | 0,000 | 0,809 | 9,114 | 1,071 |
| CORRELATION | 0,793 | -0,076 | 0,609 | 0,870 | 0,175 |
| UNIFORMITY | 1,000 | 0,104 | 0,374 | 0,896 | 0,257 |
| CONTRAST | 12,854 | 0,000 | 1,198 | 12,854 | 1,499 |
| HOMOGENEITY | 1,000 | 0,174 | 0,690 | 0,826 | 0,197 |
| ENTROPY | 3,292 | 0,000 | 1,856 | 3,292 | 0,889 |
| SLOPE | 69,650 | 0,000 | 27,605 | 69,650 | 16,418 |
| ASPECT | 359,519 | 0,000 | 185,570 | 359,519 | 96,992 |
| T. IRREGULARITY | 91,000 | 0,000 | 19,116 | 91,000 | 14,390 |
| IRS | 2,585 | 2,288 | 2,410 | 0,296 | 0,075 |
| LST | 18,546 | 5,496 | 11,522 | 13,050 | 2,668 |

Table 4. Statistical Descriptors of Cerro Tusa

### 3.2 Results of the Comparative Analysis.

The comparative analysis was based on two criteria: the comparison of the context regions and their study areas (internal comparison) and the comparisons of the study areas each other (external comparison).

#### 3.2.1 *Internal Comparison for Cerro Tusa - Venecia:*

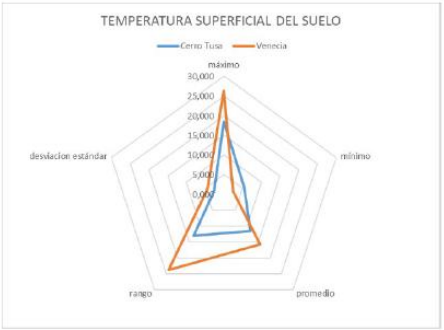


Figure 1. Internal Comparison LST Cerro Tusa vs. Venecia.

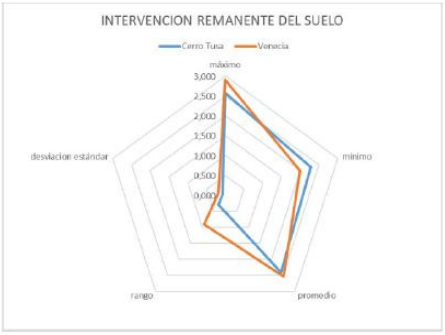


Figure 2. Internal Comparison IRS Cerro Tusa vs. Venecia.

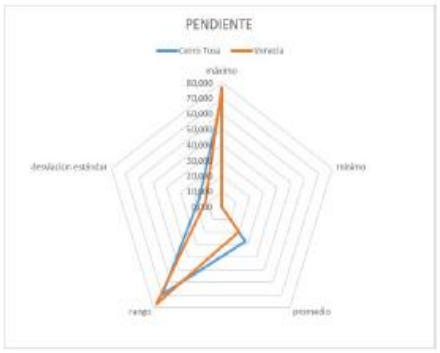


Figure 3. Internal Comparison Slope Cerro Tusa vs. Venecia.

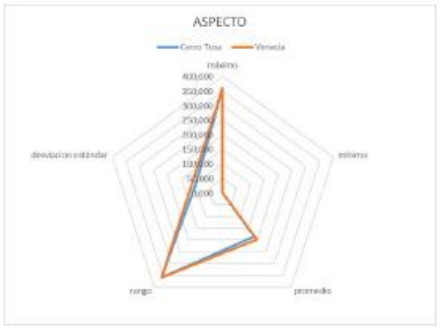


Figure 4. Internal Comparison Aspect Cerro Tusa vs. Venecia.


Figure 5. Internal Comparison TI Cerro Tusa vs. Venecia.

.

The next set of graphs for the location of *Cerro Tusa* and its surrounding region (*Venecia*) considers the perspective of mayor textural features: Variance, Correlation and Contrast (see Graph series 3).

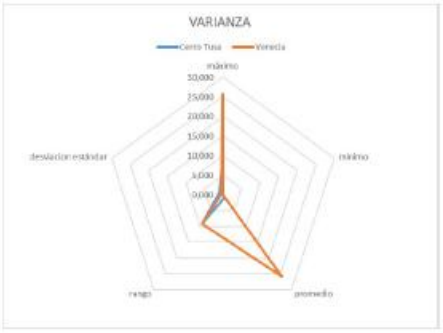


Figure 6. Internal Comparison TI Cerro Tusa vs. Venecia.

.

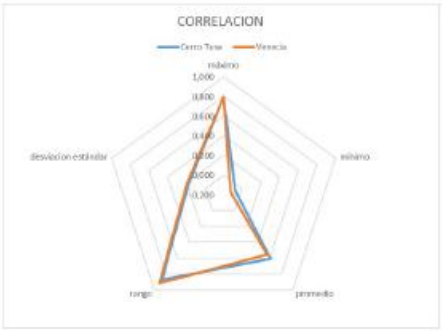


Figure 7. Internal Comparison TI Cerro Tusa vs. Venecia.

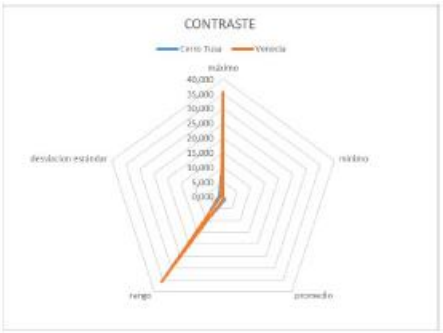


Figure 8. Internal Comparison TI Cerro Tusa vs. Venecia.

Finally, for this location, the last perspective of analysis aims to study spectrality, using to spectral indexes NDVI a BSI. The next graph series shows this result.

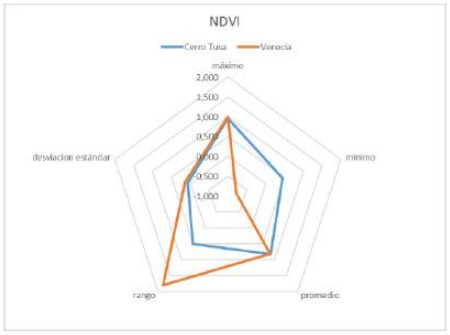


Figure 9. Internal Comparison NDVI Cerro Tusa vs. Venecia.

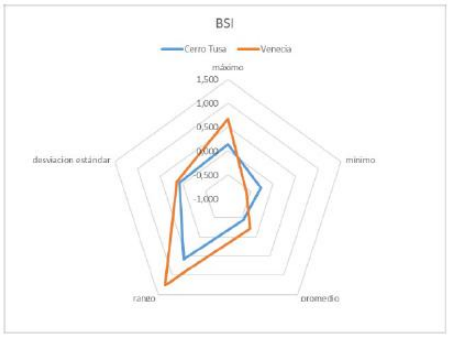


Figure 10. Internal Comparison BSI Cerro Tusa vs. Venecia.

3.2.2 . *Internal Comparison for Morro Tulcán - Popayán:*

In addition, the systematization of the internal comparison process for *Morro Tulcán* regarding to *Popayán* is shown in graphs.

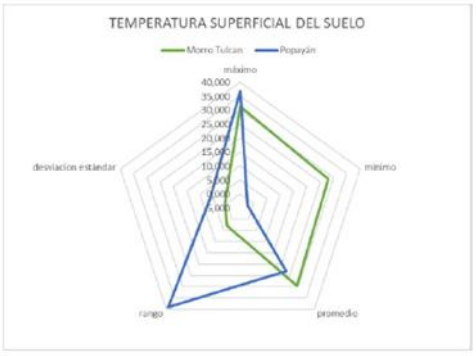


Figure 11. Internal Comparison LST Morro Tulcán Popayan.

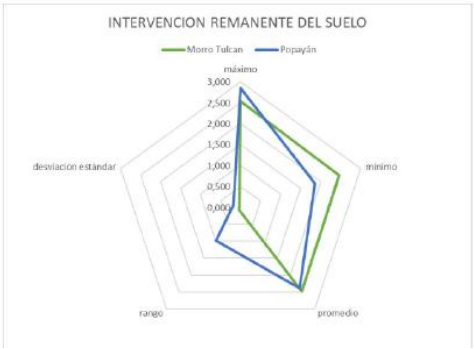


Figure 12. Internal Comparison IRS Morro Tulcán Popayan.

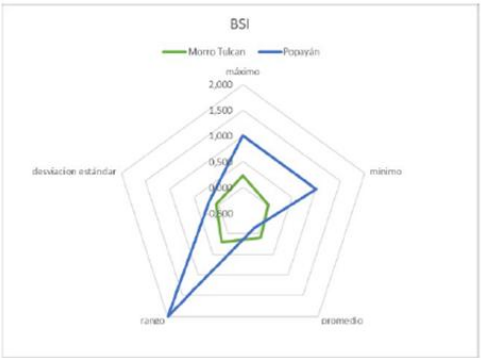


Figure 13. Internal Comparison BSI Morro Tulcán Popayan.

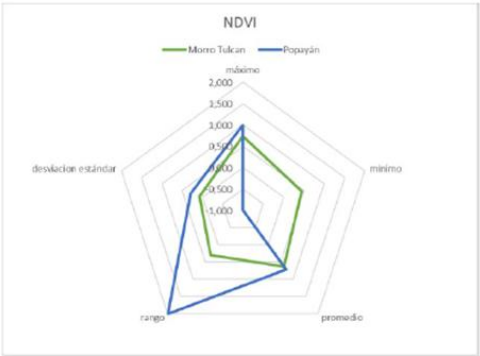


Figure 14. Internal Comparison NDVI Morro Tulcán Popayan.

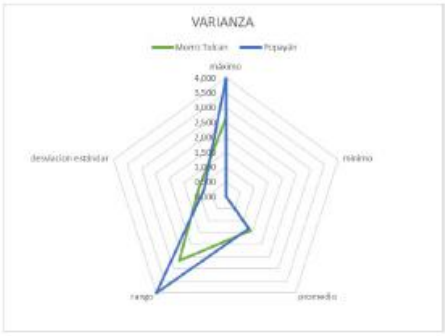


Figure 15. Internal Comparison Variance Morro Tulcán Popayan.


Figure 16. Internal Comparison Correlation Morro Tulcán Popayan.

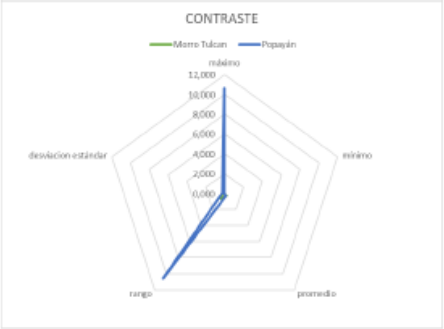


Figure 17. Internal Comparison Contrast Morro Tulcán Popayan.

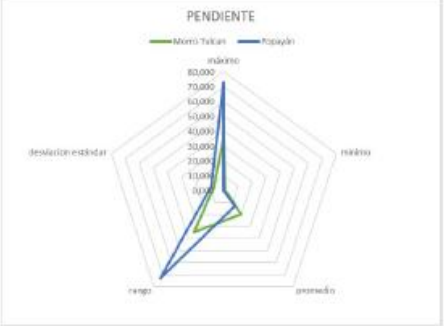


Figure 18. Internal Comparison slope Morro Tulcán Popayan.


Figure 19. Internal Comparison Aspect Morro Tulcán Popayan.


Figure 20. Internal Comparison TI Morro Tulcán Popayan

The results of the internal comparison process had two objectives: first to identify how different the study areas are from their respective context regions (singularity); and on the other hand, to determine the most characteristic indicators of this singularity.

Considering the shape of radial diagrams, variables as: remnant soil intervention, slope, aspect, and topographic irregularity; variance, correlation, contrast, and uniformity; did not show sufficient differentiation between the study area and its surroundings. Just the two spectral indices (NDVI and BSI) were relatively different between the study areas with respect to their surroundings. This condition was present for both cases. The sightly disturbed archaeological relic (*Morro Tulcán*) and the natural monument (*Cerro Tusa*). The variables: Land Surface Temperature (LST), homogeneity, and entropy were more differentiating for the case of *Morro Tulcán* with respect to its surroundings than for the case of *Cerro Tusa* with respect to its surroundings.

### 3.2.3 *Results of the External Comparison:*

To systematize the external comparison process, it was decided to develop scatter plots for each descriptor, using the values of each descriptor in study areas (*Cerro Tusa* and *Morro Tulcán*) as inputs. The following graphs show these results.

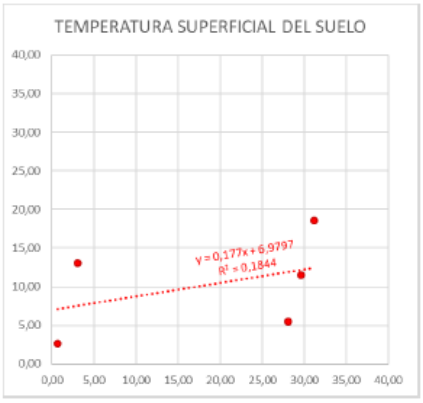


Figure 21. External Comparison of LST M. Tulcán vs C. Tusa.


Figure 22. External Comparison of IRS M. Tulcán vs C. Tusa.

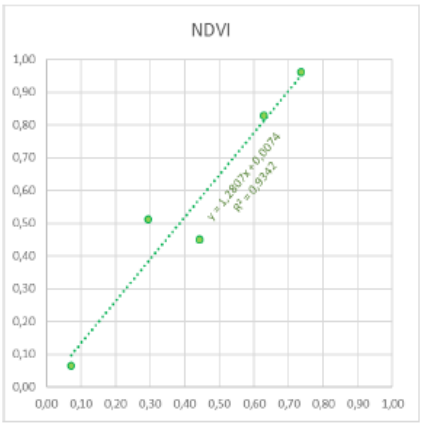


Figure 23. External Comparison of NDVI M. Tulcán vs C. Tusa.

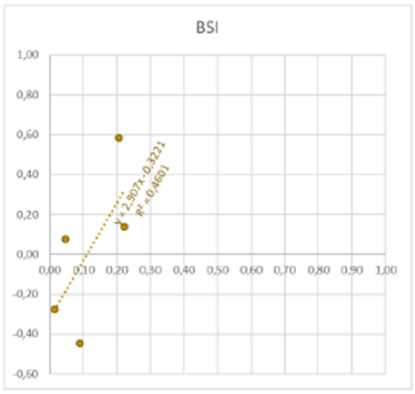


Figure 24. External Comparison of BSI M. Tulcán vs C. Tusa.

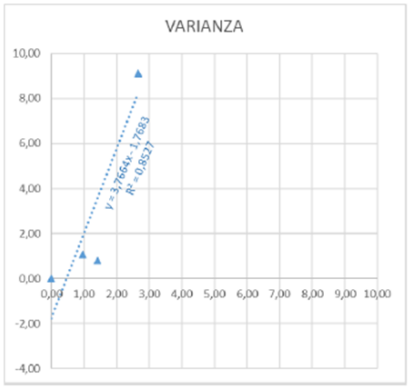


Figure 25. External Comp. of variance M. Tulcán vs C. Tusa.

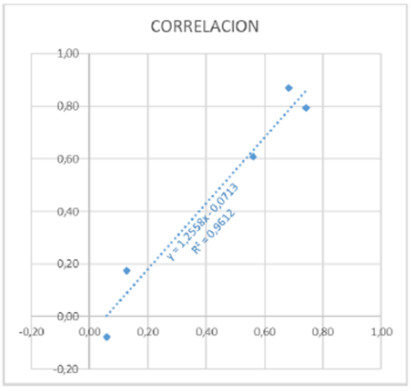


Figure 26. External Comp. correlation M. Tulcán vs C. Tusa.

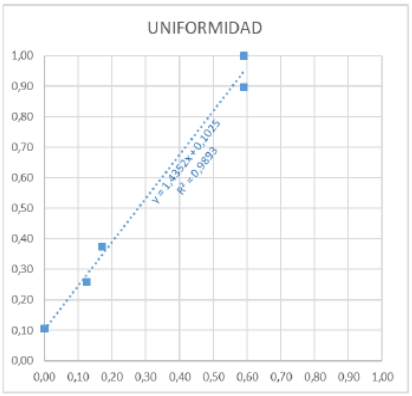


Figure 27. External Comp. of uniformity M. Tulcán vs C. Tusa.

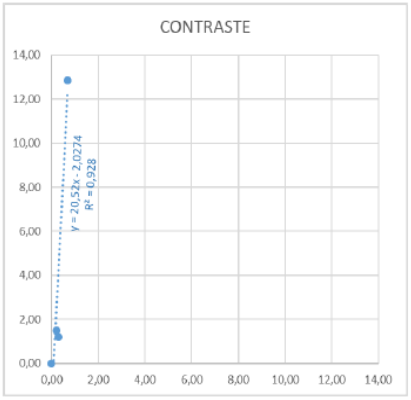


Figure 28. External Comp. contrast M. Tulcán vs C. Tusa.

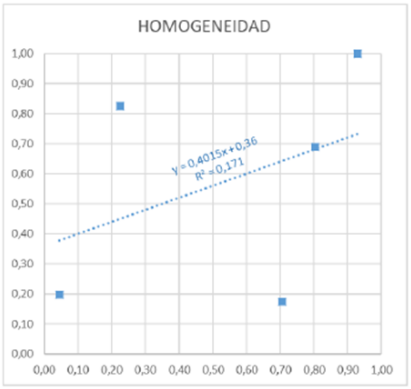


Figure 29. External Comp. homogeneity M. Tulcán vs C. Tusa

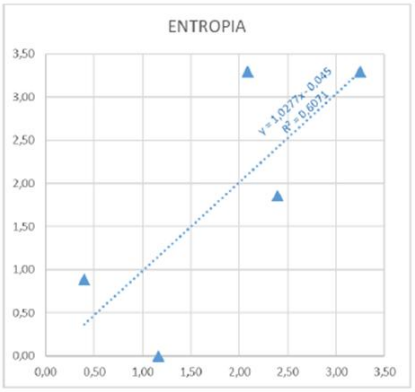


Figure 30. External Comp. entropy M. Tulcán vs C. Tusa.


Figure 31. External Comp. slope M. Tulcán vs C. Tusa

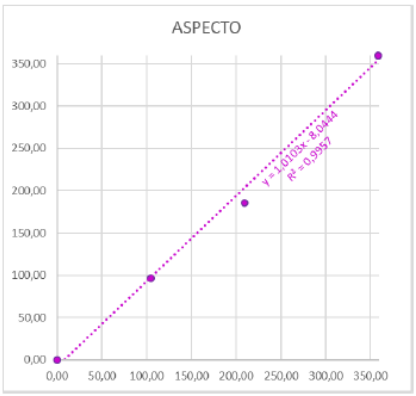


Figure 32. External Comp. of aspect M. Tulcán vs C. Tusa.

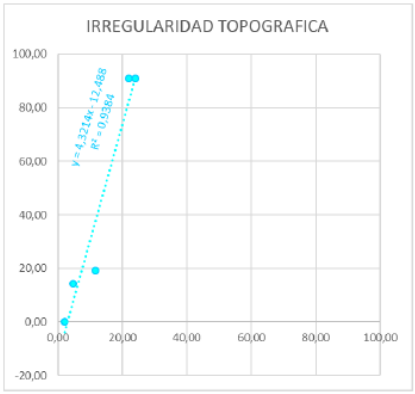


Figure 33. External Comp. of TI M. Tulcán vs C. Tusa

Considering the type of graph chosen for this comparison (scatter plot), any representative linear trend of which the slope close to 45° would be an unequivocal sign of similarity between the archaeological relic and the natural monument. In this sense, for the purpose of promoting effective archaeological exploration, the exact opposite situation would be sought, that is, scatter plots that deviate from this trend. 6 indicators do not show sufficient differentiation between the little-disturbed archaeological relic and the natural monument: NDVI, correlation, aspect, entropy, IRS, and homogeneity. Textural indicators such as variance, uniformity, and contrast; as well as the thematic indicators of aspect, slope, and topographic irregularity; are better as differentiating factor. The best indicators were Land Surface Temperature (LST) and the Bare Soil Index (BSI). These indicators are good differentiators in terms of internal and external comparison.

## 4. Conclusions

The objective in this study was to evaluate the possibility that certain remote sensing options could contribute to improve the effectiveness of preliminary archaeological exploration work. In this regard, four types of satellite data available for public access through specialized services and geo-portals of satellite data and models were explored.

13 indicators were measured in the study areas, considering the quality of the available data, the expected qualities of the object of observation (slightly disturbed archaeological relicts), and the characteristics of natural monuments whose singularity could lead to their confusion with archaeological vestiges. These indicators were: Land Surface Temperature, Remnant Soil Intervention, the

Normalized Difference Vegetation Index, the Bare Soil Index, the slope, aspect, and topographic irregularity of the relief, and the textural variables as variance, contrast, correlation, entropy, homogeneity, and uniformity. Finally, based on statistical descriptors, Bare Soil Index and Land Surface Temperature demonstrated be the best indicators to apply in a preliminary archaeological exploration. For this scenario, obtaining values close to the expected condition for elements of this nature could lead to the definition of search areas with a higher probability of success than the definition of search areas unaided by this technology. However, it would be necessary to develop a subsequent phase of the study that puts these findings into practice to demonstrate their effectiveness.

## 5. Acknowledgements

This article was made possible thanks to *Universidad Militar Nueva Granada*, which promotes spaces and dedicated time for the creation of academic outputs. These outputs stem from pedagogical and investigative experiences, in this specific case, those linked to the preparation of remote sensing lectures.

## 6. References

Cubillos Chaparro, Julio. (1959). El Morro Tulcán (Pirámide Prehispánica) Instituto Colombiano de Antropología.

Chuvieco, Emilio. (1995). Fundamentos de Teledetección Espacial, segunda edición. Ediciones Rialp, S.A. Alcalá, 290. 28027 Madrid.

Deodato Tapete, Arianna Traviglia, Eleonora Delpozzo y Francesca Cigna. (2021). Regional-Scale Systematic Mapping of Archaeological Mounds and Detection of Looting Using COSMO-SkyMed High Resolution DEM and Satellite Imagery.

Remote Sensing 2021, 13, 3106. Doi 10.3390.

Montufo Martin, Antonio M. (1992). Aplicaciones de la Teledetección en Arqueología. una Revisión Crítica. Cuadernos Preh. GR. 16-17, 1991-92. pp. 425-451.

Palacios Helena y Manuel Martin-Bueno. (2004). La teledeteccion arqueología: El Instrumento SAR. Saldvie nro. 4 2004. Pp.331-361.

Rejas Ayuga, Juan Gregorio y Francisco Burillo Mozota. (2016). Manual de Tecnologías de la Información Geográfica aplicadas a la Arqueología. Editores María del Carmen Mínguez García y Enrique Capdevila Montes, 2016, ISBN 978-84-451-3539-6, págs. 241-270.

Ruta Regiones (2023). La pirámide natural más grande del mundo está en Colombia: así puede visitarla. Mayo 15, 2023, Ruta Antioquia.

# Approaches for measuring the accuracy of landscape metrics derived from remote sensed data in small scale agricultural areas of sub-Sahara Africa

Gillie Cheelo

*Copperbelt University, Zambia, gillie.cheelo@gmail.com*

Small scale agricultural cultivated area expansion is one of the main drivers of forest fragmentation in sub-Saharan Africa (SSA), which creates numerous small single tree forest fragments inside and around the agricultural fields. Forest fragments impact the ecosystem provision and biodiversity loss in the region. Studies on forest fragmentation in SSA mainly use freely available coarse spatial resolution Landsat imagery. The use of coarse spatial resolution such as Landsat imagery misses, exaggerating, oversimplify and generalizing the small forest fragments which dominate small scale agricultural landscapes in the region. This causes accuracy concerns on the determined forest fragmentation results. Despite these inaccuracy concerns, studies in SSA rarely measure the accuracy of the landscape metrics used to measure forest fragmentation. Therefore, this study firstly reviews theoretical approaches to guide how to measure and account for uncertainty in forest fragmentation measurements. Then develops novel approaches which measure the accuracy of landscape metrics and ways of reducing errors in forest fragmentation analysis relevant in small-scale agricultural landscapes of SSA. The proposed approach uses high-resolution imagery (UAV-generated orthophotos and WorldView-2) as reference data to determine accuracy of landscape metrics derived from landcover maps classified from satellite imagery such as Planet Scope, Landsat, and Sentinel-2 imagery. The level of uncertainty and accuracy of each imagery will be determined using Root Mean Square Error (RMSE), standard deviation (SD), Monte Carlo analysis, sensitivity analysis, and Bayesian analysis. The proposed approach will account for the unique characteristics of small-scale agriculture landscapes, the main driver of forest fragmentation in SSA, hence contributing towards more credible determination of forest fragmentation and its related effects on biodiversity in the region.

***Keywords:*** Landscape metrics, uncertainty, small-scale agriculture, satellite data, forest fragmentation, biodiversity, landcover, Sub-Sahara Africa

# Interpreting ENVI-met Simulated Microclimate Data with Measured Observations in HFT Stuttgart

Muhtasimul Islam Rushdi [a,*], Angela Blanco-Vogt[a], Sourav Karmaker [b]

[a] *Hochschule für Technik Stuttgart, muhtasimul.rushdi@hft-stuttgart.de, angela.blanco-vogt@hft-stuttgart.de*
[b] *Technische Universität Darmstadt, souravkm021@gmail.com*

**Abstract**: This study investigates the impact of green surface areas on urban microclimates using ENVI-met simulation software, focusing on Hochschule für Technik Stuttgart (HFT Stuttgart). The study validates ENVI-met's accuracy in predicting microclimatic conditions and recommends urban design strategies to mitigate the Urban Heat Island (UHI) effect. Findings show significant temperature reductions in areas converted from paved to green surfaces, with decreases of up to 1.15°C in Block 1, 0.70°C in Block 2, and 1.00°C in Block 3. Statistical analysis reveals strong correlations between measured and simulated data, with maximum $R^2$ values of 0.81 for temperature and 0.93 for humidity, confirming the model's reliability. The study emphasizes the importance of integrating green surfaces into urban planning to enhance thermal comfort and sustainability, validating ENVI-met as a robust tool for micro-climate analysis.

***Keywords:*** Microclimate Simulation, Green Surfaces, ENVI-met, Germany

## 1. Introduction

Urban microclimates, shaped by local features such as buildings, vegetation, and water bodies, strongly influence thermal comfort, energy use, and air quality. Poor microclimatic conditions can intensify the Urban Heat Island (UHI) effect, reduce outdoor comfort, and increase energy demand for cooling (Tsoka et al., 2020; Fan et al., 2021). With more than half of the world's population living in cities (UN-Habitat, 2013), understanding microclimatic dynamics has become essential for sustainable urban planning.

Urban design interventions, such as vegetation, green roofs, and high-albedo materials, are widely applied to mitigate UHI effects (Ali-Toudert & Mayer, 2007; Lindberg & Grimmond, 2011; Santamouris, 2014). Vegetation is particularly effective in reducing local air temperatures and providing shade, though it faces challenges of cost, irrigation, and maintenance. Computational modeling offers a cost-effective way to evaluate such strategies before implementation (Ambrosini et al., 2014; Taleghani et al., 2015).

Among available models, ENVI-met is one of the most widely used due to its balance of sophistication, usability, and relatively low computational cost (Ali-Toudert, 2007; Chow & Brazel, 2012; Singh & Laefer, 2015; Roth & Lim, 2017). It integrates wind, radiation, vegetation, soil, and pollutants (Bruse & Fleer, 1998) and is applied in studies on outdoor thermal comfort (Blocken, 2015), air quality (Wang et al., 2018), and UHI mitigation (Wang et al., 2016; Berardi & Graham, 2020).

Stuttgart, Germany, exemplifies the challenges of UHI due to its valley topography, low wind

speeds, and high industrial and traffic activities. The city has developed a Climate Atlas and zoning regulations to expand green infrastructure and preserve ventilation corridors (Climate-ADAPT, 2024). Within this context, the Hochschule für Technik Stuttgart (HFT) campus provides an ideal site for microclimate analysis.

This study aims to evaluate the influence of landcover, particularly green surfaces, on urban microclimates using ENVI-met simulations validated with field observations. The research objectives are:

- To validate ENVI-met results against measured air temperature and relative humidity data within the area of interest.
- To assess the effect of enhanced green surfaces on local microclimate conditions.

Accordingly, the research addresses two main questions:

- Are simulated and measured air temperature and humidity distributions consistent across different times of the day?
- How does increasing green surface coverage affect microclimatic conditions in the study area?

## 2. Literature Review

ENVI-met has become one of the most widely used microclimate simulation tools in urban climate research over the past two decades (Singh & Laefer, 2015). ENVI-met is a Computational Fluid Dynamics (CFD) model that applies the Reynolds-Averaged Navier-Stokes (RANS) equations to simulate atmospheric flow, heat transfer, and radiation exchange in urban environments (Bruse and Fleer, 1998). It has been employed extensively to assess strategies for mitigating the Urban Heat Island (UHI) effect, including street trees, roof gardens, building form modifications, and high-albedo materials (Ng et al., 2012; Taleghani et al., 2016; Umberto & Wang, 2016; Bonggeun & Kyunghun, 2015). Its plant database, which defines parameters such as leaf area density, height, albedo, and transpiration capacity, has been expanded by researchers to better represent local vegetation (Declet-Barreto et al., 2013; Hedquist and Brazel, 2014; Middel et al., 2014). While the model's versatility and visualization capabilities make it popular, studies have noted limitations such as misaligned radiation flux calculations and overestimation of turbulence (Acero & Herranz-Pascual, 2015; Toparlar et al., 2017).

Early validation efforts (Lahme & Bruse, 2003; Emmanuel & Fernando, 2007) found only moderate agreement between measured and simulated conditions. Later studies reported mixed outcomes depending on climate and site context. For instance, Song et al. (2014) in South Korea observed large discrepancies in net radiation and temperature, while Elnabawi et al. (2015) in Cairo reported good overall agreement between monitored and simulated data. More recent validations have shown correlation coefficients ($R^2$) ranging from 0.3–0.8 for air temperature and humidity, with ENVI-met often overestimating peak temperatures and underestimating relative humidity (Toparlar et al., 2017; Tsoka et al., 2018).

In parallel, research highlights the crucial role of vegetation in reducing UHI impacts through evapotranspiration and shading, which improve outdoor thermal comfort (Anyanwu & Kanu, 2006; Yu & Hien, 2006). Quantitative studies confirm cooling effects of 0.5–2.0 °C in areas with increased vegetation cover (Qaid & Ossen, 2015; Morakinyo et al., 2017). ENVI-met's vegetation module allows simulation of these dynamics, though the accuracy strongly depends on reliable plant parameters and careful scenario design (Yang & Lan, 2019).

## 3. Methodology

This study followed a structured workflow (Figure 1) combining field measurements, weather data, ENVI-met simulations, and comparative analysis.

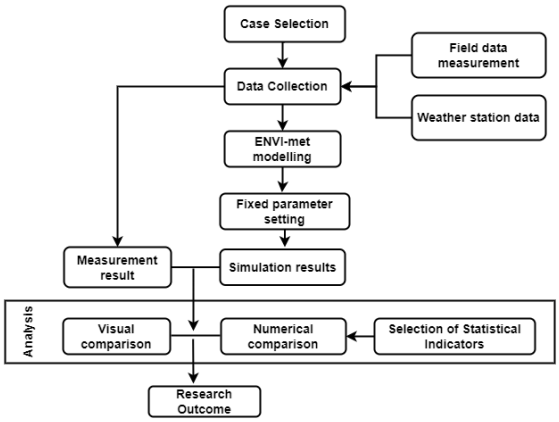


Figure 1. Workflow of the study.

### 3.1 Study Area

The research was conducted at the Hochschule für Technik (HFT) Stuttgart campus (Figure 2) located in the city center (48.7831°N, 9.1770°E). The site represents a dense urban environment with educational buildings, paved courtyards, and patches of vegetation, making it suitable for assessing the influence of green surfaces on local microclimates.

### 3.2 Data Collection

Air temperature and relative humidity were measured on 4 June 2024 using HOBO MX2302 data loggers placed at 1.75 m height across five locations (Figure 2) on campus.

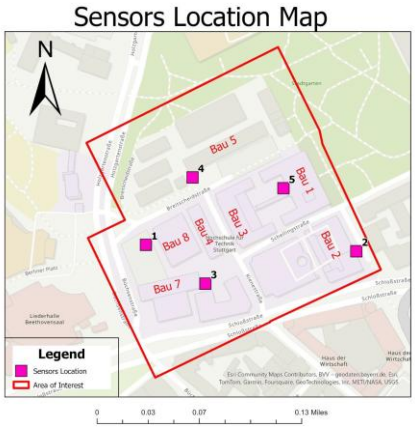


Figure 2. Study Area and Location of Sensors

Data were recorded at 30-minute intervals between 08:00 and 21:00, capturing daily variations. Complementary meteorological observations (temperature, RH, wind speed) were obtained from the Cannstatt weather station operated by Agrarmeteorologie Baden-Württemberg. These datasets provided the boundary conditions for the simulations.

### 3.3 Modelling Tools

The ENVI-met software was used to simulate microclimate dynamics, supported by QGIS for spatial data preparation, ArcGIS Pro for mapping, and Excel for data analysis. ENVI-met allows the integration of buildings, surfaces, and vegetation to represent urban form and evaluate thermal interactions (Bruse & Fleer, 1998; Acero & Herranz-Pascual, 2015).

### 3.4 Model Setup

The campus was digitized into three simulation blocks (~20,000 m² each) due to computational constraints (Figure 3). The defined resolution of the model along the x, y, and z is 1.5m. Land uses (buildings, streets, grass, trees, paved areas) were represented with appropriate surface and material parameters. Vegetation was included using simple grass layers and 3D tree models to capture shading and evapotranspiration effects (Yang & Lan, 2019). Meteorological inputs (temperature, RH, wind speed, wind direction) were set according to measurements from 08:00–21:00.

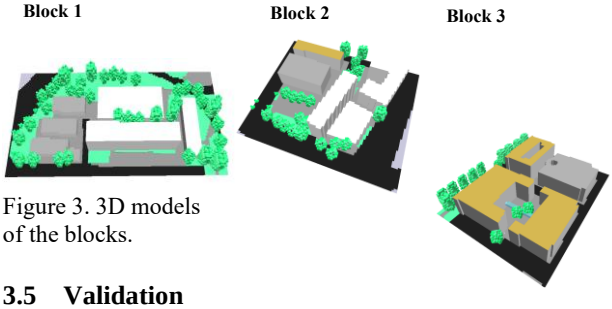


Figure 3. 3D models of the blocks.

### 3.5 Validation

Model outputs for air temperature and relative humidity were compared with field measurements through visual inspection (spatial maps and diurnal curves) and statistical evaluation. The coefficient of determination ($R^2$) was calculated to quantify agreement between measured and simulated values, following approaches used in earlier validation studies (Tsoka et al., 2018; Wang et al., 2019).

### 3.6 Scenario Testing

To assess the cooling potential of vegetation, additional simulations were conducted where selected paved surfaces were converted into grass (Figure 4). For example, paved courtyards between campus buildings were replaced with 25 cm grass cover. This allowed evaluation of how expanded green surfaces influence local temperature and humidity patterns, contributing to urban heat mitigation strategies (Yu & Hien, 2006; Morakinyo et al., 2017).

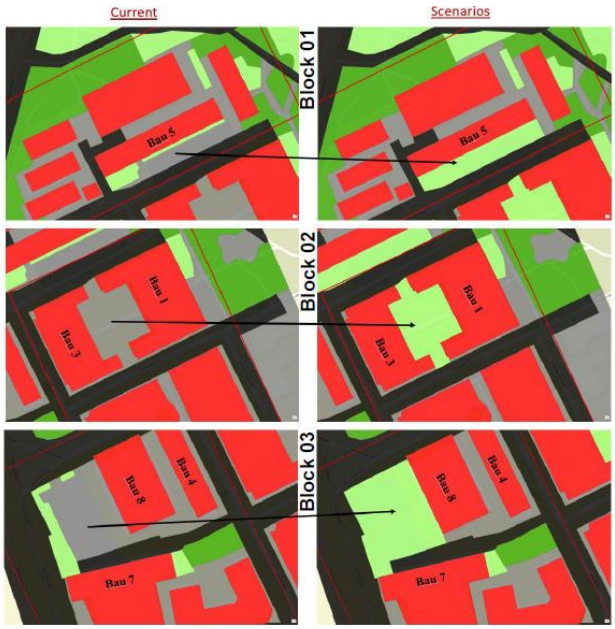


Figure 4. Paved surfaces converted into grass.

## 4. Result

### 4.1 Measurement Result

The field campaign at the HFT Stuttgart campus revealed the typical diurnal cycle of an urban microclimate. Air temperature increased steadily from around 15 °C at 08:00 in the morning to 23–25 °C in the late afternoon, before declining again in the evening (Figure 5).

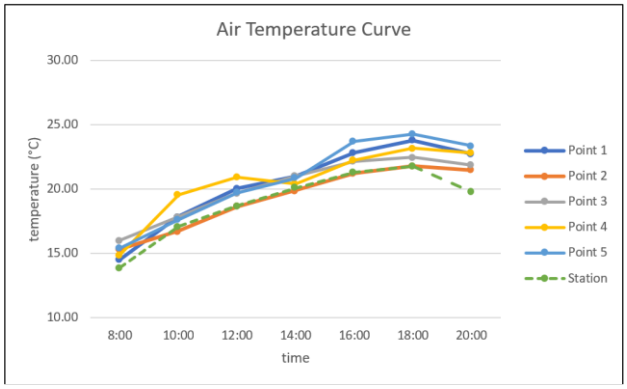


Figure 5. Air Temperature Measurement of Study Area

In contrast, relative humidity displayed an inverse pattern, with initial morning values of 70–80% that decreased to 40–50% at the afternoon minimum, followed by a gradual increase to approximately 55% by 20:00 (Figure 6). Spatial variations between the measurement points further illustrated the influence of local urban features. Points located closer to paved surfaces and roads recorded slightly higher peak temperatures, while those positioned near shaded or vegetated areas maintained comparatively lower values throughout the day.

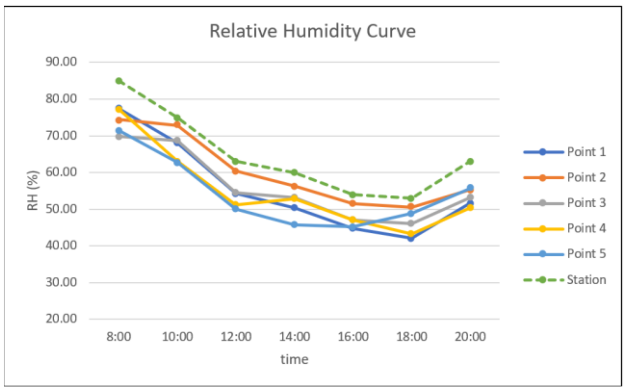


Figure 6. Relative Humidity Measurement of Study Area

### 4.2 ENVI-met Simulated Results

The ENVI-met simulations at 16:00 (height 1.35 m) provided insight into the spatial distribution of air temperature and relative humidity across the three study blocks. In Block 01 (Figure 7), simulated air temperatures ranged between 23.1 °C and 28.2 °C. Hotspots appeared around Bau 5 and the northeast asphalt road, where paved surfaces and streets elevated local temperatures to 27–28 °C. In contrast, adjacent green areas

remained cooler, with values closer to 23–25 °C. Relative humidity displayed the opposite tendency, decreasing to 35–37% near paved surfaces while remaining between 46% and 49% in green areas.

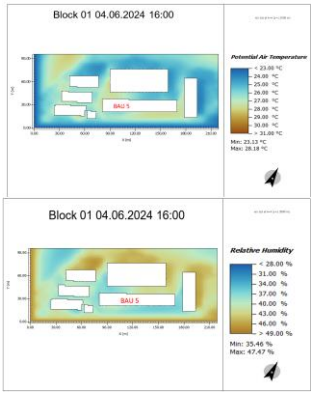


Figure 7. Simulated Air Temperature and Relative Humidity distribution of Block 1

In Block 02 (Figure 8), temperatures varied from 24.1 °C to 29.5 °C. The street between Bau 1 and Bau 2 emerged as the warmest area, exceeding 29 °C, whereas the courtyard surfaces between Bau 1 and Bau 3 showed relatively moderate conditions around 24–25 °C. Relative humidity patterns again mirrored these trends: the lowest values of 31–34% occurred on the streets, while higher levels of 43–49% were observed near the vegetation surrounding Bau 2.

Block 03 (Figure 9) recorded the widest thermal range, from 23.8 °C to 31.4 °C. The streets around Bau 7 produced the highest temperatures above 29 °C, while the areas near Bau 4 and Bau 8 were significantly cooler, averaging between 23 °C and 25 °C. Relative humidity levels fell as low as 31–34% near the exposed paved areas, but remained between 40% and 49% where shading or vegetation was present. Overall, the simulation results confirmed that built form and material characteristics strongly influence the microclimate: paved areas amplify heating and reduce humidity, whereas vegetation and shaded zones buffer these extremes.

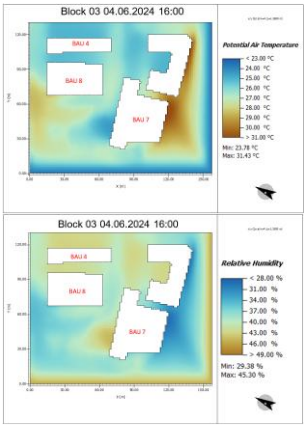


Figure 8. Simulated Air Temperature and Relative Humidity distribution of Block 3

### 4.3 Statistical Analysis

The statistical comparison of measured and simulated values showed mixed levels of agreement (Figure 10). For air temperature, the coefficients of determination ($R^2$) ranged from 0.24 at Point 2 to 0.81 at Point 3. Points 1 and 5 recorded $R^2$ values of 0.76 and 0.61 respectively, while Point 4 showed a moderate correlation of 0.50. In all cases, ENVI-met tended to overestimate peak afternoon temperatures by 1–2 °C.

Relative humidity correlations were generally stronger. $R^2$ values reached 0.93 at Point 1, 0.90 at Point 3, and 0.76 at Point 4. Points 2 and 5 showed lower but still acceptable agreement, with $R^2$ values of 0.36 and 0.75 respectively. Simulated RH values were slightly underestimated at most points but captured the diurnal trend well. These validation outcomes are consistent with previous studies, which have reported mixed but generally acceptable agreement between ENVI-met and field observations in diverse urban climates.

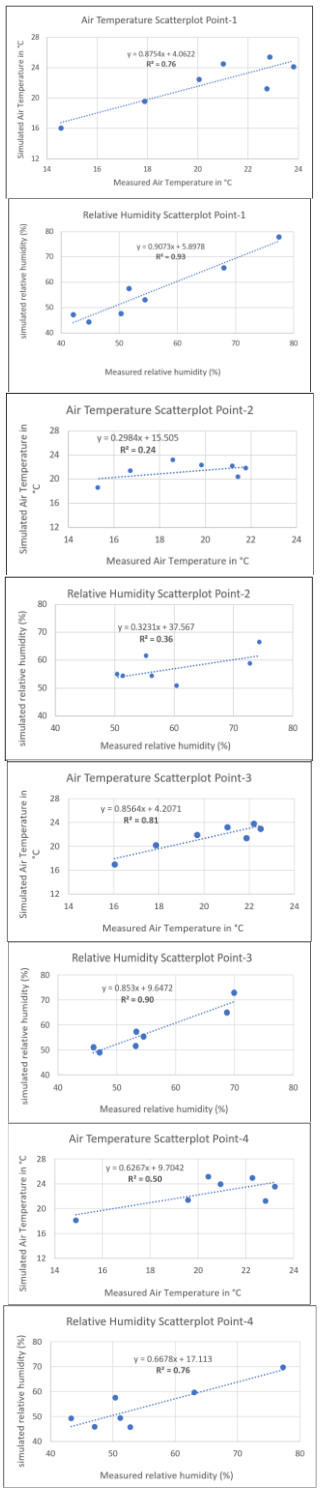


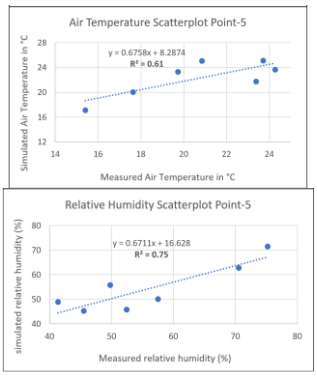


Figure 9. Air Temperature and Relative Humidity Scatterplot.

### 4.4 Scenario Results: Green Surface Conversion

The result image shows a noticeable decrease in temperature in the green area (Figure 11). In Block 1, the replacement of 774 m² of paved surface in front of Bau 5 led to temperature reductions of up to 1.15 °C. The cooling was strongest within the converted area but extended slightly into adjacent zones, reflecting the combined effects of evapotranspiration and reduced heat storage.

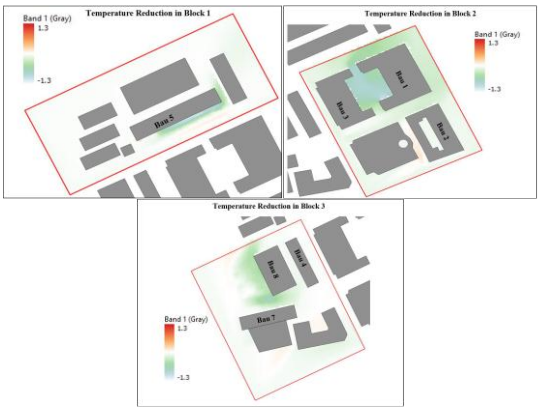


Figure 10. Air Temperature decreases across all blocks.

In Block 2, the conversion of 1,661 m² between Bau 1 and Bau 3 led to a more moderate cooling effect, with temperatures dropping by up to 0.70 °C. Nonetheless, the results indicate localized improvement in thermal comfort and a slight spillover of cooling into surrounding paved zones. Block 3 showed reductions of up to 1.00 °C after converting 1,630 m² in front of Bau 8. The decrease was most visible directly in the modified area but also spread to nearby streets, suggesting that vegetation improves airflow and mitigates heat accumulation.

## 5. Discussion

### 5.1 Site Design and Microclimate

The comparative analysis of Blocks 1, 2, and 3 revealed clear links between planning layouts and microclimatic outcomes. Block 1, with the highest greening rate (29.3%) and lowest building density (27.5%), maintained the most favourable conditions, with air temperatures ranging between 23.1–28.2 °C and relative humidity between 35–47%. By contrast, Block 2, with the highest density (44.3%) and lowest greening rate (3.5%), experienced higher peak temperatures (up to 29.5 °C) and greater humidity fluctuations (31–49%). Block 3, though less dense (26.1%), had the highest road coverage (47.6%), resulting in the highest recorded temperatures (up to 31.4 °C). These findings confirm that both vegetation cover and the extent of impervious surfaces strongly influence local thermal conditions.

### 5.2 Validation of ENVI-met.

Comparison with field data showed that ENVI-met successfully reproduced the diurnal trends of both air temperature and relative humidity but displayed systematic biases. Simulated air temperatures were consistently higher by about 1–2 °C, while relative humidity was slightly underestimated. Statistical analysis demonstrated moderate-to-strong correlations across the five points ($R^2$ ranging from 0.24 to 0.81 for temperature and 0.36 to 0.93 for relative humidity). These results suggest that while ENVI-met requires careful parameter calibration, it remains a reliable tool for assessing relative scenario differences.

### 5.3 Impact of Enhanced Green Surfaces

Scenario testing showed that replacing paved areas with grass reduced local air temperatures by up to 1.15 °C in Block 1, 0.70 °C in Block 2, and 1.00 °C in Block 3. Beyond the immediate sites, the cooling effect also extended to adjacent areas, reflecting the influence of evapotranspiration and reduced heat storage. These results highlight the effectiveness of even modest greening interventions in mitigating localized Urban Heat Island effects and enhancing outdoor comfort.

## 6. Conclusion

This study validated ENVI-met simulations with field data and demonstrated that green surfaces measurably reduce urban air temperatures by 0.7–1.15 °C in the HFT Stuttgart campus. The results confirm that higher greening rates and lower impervious surface coverage are linked to cooler, more humid microclimates. Although the model showed systematic overestimation of temperature and underestimation of humidity, the correlations were sufficiently strong to establish ENVI-met as a reliable tool for urban microclimate analysis. The findings highlight the value of green infrastructure as a strategy for mitigating the Urban Heat Island effect and improving outdoor comfort in urban areas.

### 6.1 Limitations and Outlook

The research was limited to a single study site and one-day measurement period, which restricts broader generalization. Nighttime data were not collected, and some parameter settings relied on researcher judgment. Future work should expand validation across different seasons, larger sample sizes, and varied urban typologies. Additional scenario testing—such as increasing tree cover or green roofs—would provide further insights for sustainable urban planning in Stuttgart and beyond.

## 7. References


Acero, J.A. and Herranz-Pascual, K., 2015. A comparison of thermal comfort conditions in four urban spaces by means of measurements and modelling techniques. Building and Environment, 93, pp. 245–257.

Ali-Toudert, F. and Mayer, H., 2007. Effects of asymmetry, galleries, overhanging facades and vegetation on thermal comfort in urban street canyons. Solar Energy, 81, pp. 742–754.

Ambrosini, D., Galli, G., Mancini, B., Nardi, I. and Sfarra, S., 2014. Evaluating mitigation effects of urban heat islands in a historical small center with the ENVI-Met climate model. Sustainability, 6, pp. 7013–7029.

Anyanwu, E.C. and Kanu, I., 2006. The role of urban forest in the protection of human environmental health in geographically prone unpredictable hostile weather conditions. International Journal of Environmental Science and Technology, 3(2), pp. 197–201.

Berardi, U. and Graham, J., 2020. Investigation of the impacts of microclimate on PV energy efficiency and outdoor thermal comfort. Sustainable Cities and Society, 62, 102402.

Blocken, B., 2015. Computational fluid dynamics for urban physics: Importance, scales, possibilities, limitations and ten tips and tricks towards accurate and reliable simulations. Building and Environment, 91, pp. 219–245.

Bonggeun, S. and Kyunghun, P., 2015. Contribution of greening and high-albedo coatings to improvements in the thermal environment in complex urban areas. Advances in Meteorology, Article ID 814680, pp. 1–14.

Bruse, M. and Fleer, H., 1998. Simulating surface-plant-air interactions inside urban environments with a three-dimensional numerical model. Environmental Modelling & Software, 13(3–4), pp. 373–384.

Chow, W.T.L. and Brazel, A.J., 2012. Assessing xeriscaping as a sustainable heat island mitigation approach for a desert city. Building and Environment, 47, pp. 170–181.

Declet-Barreto, J., Brazel, A.J., Martin, C.A., Chow, W.T. and Harlan, S.L., 2013. Creating the park cool island in an inner-city neighborhood: heat mitigation strategy for Phoenix, AZ. Urban Ecosystems, 16, pp. 617–635.

Elnabawi, M., Hamza, N. and Dudek, S., 2015. Numerical modelling evaluation for the microclimate of an outdoor urban form in Cairo, Egypt. HBRC Journal, 11, pp. 246–251.

Emmanuel, R. and Fernando, H.J.S., 2007. Urban heat islands in humid and arid climates: Role of urban form and thermal properties in Colombo, Sri Lanka and Phoenix, USA. Climate Research, 34, pp. 241–251.

Fan, C.J., Gai, Z.Y., Shen, S.G. and Sun, S., 2021. An implementation evaluation framework of ecological spatial planning based on multi-dimensional data: A case study in China. Urban Forestry & Urban Greening, 64, 127264.

Hedquist, B.C. and Brazel, A.J., 2014. Seasonal variability of temperatures and outdoor human comfort in Phoenix, Arizona, USA. Building and Environment, 72, pp. 377–388.

Lahme, E. and Bruse, M., 2003. Microclimatic effects of a small urban park in densely built-up areas: Measurements and model simulations. In: ICUC5, Lodz.

Lindberg, F. and Grimmond, C.S.B., 2011. Nature of vegetation and building morphology characteristics across a city: Influence on shadow patterns and mean radiant temperatures in London. Urban Ecosystems, 14, pp. 617–634.

Middel, A., Häb, K., Brazel, A.J., Martin, C. and Guhathakurta, S., 2014. Impact of urban form and design on microclimate in Phoenix, AZ. Landscape and Urban Planning, 122, pp. 16–28.

Morakinyo, T.E., Dahanayake, K.W.D.K.C., Ng, E. and Chow, C.L., 2017. Temperature and cooling demand reduction by green-roof types in different climates and urban densities: A co-simulation parametric study. Energy and Buildings, 145, pp. 226–237.

Ng, E., Chen, L., Wang, Y. and Yuan, C., 2012. A study on the cooling effects of greening in a high-density city: An experience from Hong Kong. Building and Environment, 47, pp. 256–271.

Qaid, A. and Ossen, D.R., 2015. Effect of asymmetrical street aspect ratios on microclimates in hot, humid regions. International Journal of Biometeorology, 59(6), pp. 657–677.

Roth, M. and Lim, V.H., 2017. Evaluation of canopy-layer air and mean radiant temperature simulations by a microclimate model over a tropical residential neighborhood. Building and Environment, 112, pp. 177–189.

Singh, M. and Laefer, D.F., 2015. Recent trends and remaining limitations in urban microclimate models. Demography Journal, 1, pp. 1–12.

Song, B.-G., Park, K.-H. and Jung, S.-G., 2014. Validation of ENVI-met model within situ measurements considering spatial characteristics of land use types. Journal of the Korean Association of Geographic Information Studies, 17(2), pp. 156–172.

Stuttgart: Combating the heat island effect and poor air quality with ventilation corridors and green-blue infrastructure, 2024. Web site: https://climate-adapt.eea.europa.eu/en/metadata/case-studies/stuttgart-combating-the-heat-island-effect-and-poor-air-quality-with-green-ventilation-corridors

(accessed July 21, 2024).

Taleghani, M., Kleerekoper, L., Tenpierik, M. and Van Den Dobbelsteen, A., 2015. Outdoor thermal comfort within five different urban forms in the Netherlands. Building and Environment, 83, pp. 65–78.

Taleghani, M., Sailor, D.J. and Banweiss, G., 2016. Micrometeorological simulations to predict the impacts of heat mitigation strategies on pedestrian thermal comfort in a Los Angeles neighborhood. Environmental Research Letters, 11(2), 024003.

Toparlar, Y., Blocken, B., Maiheu, B. and Van Heijst, G.J.F., 2017. A review on the CFD analysis of urban microclimate. Renewable and Sustainable Energy Reviews, 80, pp. 1613–1640.

Tsoka, S., Tsikaloudaki, A. and Theodosiou, T., 2018. Analyzing the ENVI-met microclimate model's performance and assessing cool materials and urban vegetation applications – a review. Sustainable Cities and Society, 41, pp. 55–76.

Tsoka, S., Tsikaloudaki, K., Theodosiou, T. and Bikas, D., 2020. Urban warming and cities' microclimates: Investigation methods and mitigation strategies – a review. Energies, 13(6), 1419.

Umberto, B. and Wang, Y., 2016. The effect of a denser city over the urban microclimate: The case of Toronto. Sustainability, 8(8), 782.

UN-Habitat, 2013. State of the world's cities 2012/2013: Prosperity of cities. Web site: http://unhabitat.org/books/prosperity-of-cities-state-of-the-worlds-cities-20122013 (accessed April 18, 2013).

Wang, J., Lu, C.D., Niu, L.W. and Zhang, F.F., 2018. Simulation and verification of the influence of road vegetation structure on the diffusion of atmospheric inhalable particulate matter. Transactions of the Chinese Society of Agricultural Engineering, 34(20), pp. 225–232.

Wang, Y., Berardi, U. and Akbari, H., 2016. Comparing the effects of urban heat island mitigation strategies for Toronto, Canada. Energy and Buildings, 114, pp. 2–19.

Wang, Y., Zhou, D., Wang, Y., Fang, Y., Yuan, Y. and Lv, L., 2019. Comparative study of urban residential design and microclimate characteristics based on ENVI-met simulation. Indoor and Built Environment, 28(9), pp. 1200–1216.

Yang, Y.J. and Lan, H.N., 2019. A review of the application of numerical simulation tools in the field of urban microclimate research – taking ENVI-met software as an example. In: International Green Building and Building Energy Conservation Conference and New Technology and Product Expo, pp. 697–701.

Yu, C. and Hien, W.N., 2006. Thermal benefits of city parks. Energy and Buildings, 38(2), pp. 105–120.

# Analysis tool for sustainable Land resource management: Case study Of Palmira, Valle Del Cauca

Edwin Alvaro Cortés Cerón

*Universidad La Gran Colombia, Master in Planning and Management of Sustainable Territorial Habitat*
*ecortesc1@ulagrancolombia.edu.co*

**Abstract**: This paper presents an analysis tool for the sustainable management of land resources, with Palmira, Valle del Cauca, as a case study. The research addresses conflicts generated by intensive land use and its spatial distribution, which affect environmental, social, and economic dynamics. The conceptual basis relies on authors such as Brundtland (1987), Soil Survey Staff (1994), and Bocco (2007), who define territory as a strategic space where human activities converge. The methodology was developed in four phases: literature review, diagnosis of land-use conflicts through geographic information, analysis of impacts from environmental, sociocultural, and economic perspectives, and definition of the tool's key characteristics. As a result, three impact management records were produced, along with a final record containing the proposed analysis tool. Once implemented, this instrument could help mitigate territorial conflicts within Palmira's boundaries and provide decision-makers with a comprehensive framework for sustainable land management. The tool is designed to be replicable in similar contexts, strengthening territorial planning and governance.

***Keywords:*** Territorial Conflict, Management instrument, Geographic Information, Soil Resource

## 1. Introduction

Land-use changes are identified through various techniques, and as Pedroza del Toro (2015) explains, technical and administrative processes allow for the assessment of the impacts of projects, works, or activities carried out in a territory. These require prior information to be provided to communities so that they can participate in decision-making. Therefore, the analysis proposed in this research serves as an informational foundation for territorial decision-making. Its social relevance lies in identifying land-use changes caused by the implementation of territorial planning regulations, offering a global vision of the behavior of environmental phenomena and geographic, economic, and social components, thus enabling relationships with the environment to be established and raising awareness for the sustainable use, utilization, and protection of natural resources.

Amid the environmental issues related to land resource exploitation in the municipality of Palmira, and the 2016 implementation of the national policy on sustainable soil management, it becomes necessary to establish the characteristics that an analysis tool for sustainable land resource management should have. This tool should help identify the relationships established at the social, cultural, economic, and environmental levels in this geographic area, as well as the interaction with impacts caused by economic activities in the sugarcane cultivation sector and the various protected area declarations, including national forest reserves, 14 civil society nature reserves,

Las Hermosas National Natural Park, the Nima Regional Natural Park, and Las Hermosas páramo, all of which fall within the jurisdiction of Palmira and are crucial for land-use planning.

This proposal for designing a tool for sustainable land resource management is essential due to the land-use change conflicts observed in the rural areas of this municipality. These are driven by overexploitation of land resources, current regulations, and the latest structural modification of the Land Use Plan (POT) from 2001—formulated for the first time and unchanged in over 22 years. Therefore, this work analyzes sociocultural, environmental, and economic conflicts caused by land-use changes, based on the authors referenced in the Ministry of Environment and Sustainable Development's 2016 Land Management Policy, Soil Survey Staff, and experts in the field such as Raffino, Echeverri, Bocco, Castree, Clout, and Renalul Adib. It identifies transformations experienced by Palmira's territory and proposes the characteristics of an analysis tool for sustainable land resource management. This is achieved by defining analytical categories that guide strategy formulation, aligned with national, departmental, regional, and local policies on sustainable land resource management in Palmira, to overcome existing policy conflicts.

This research adopts a mixed-methodological approach that includes both quantitative and qualitative data processing, distributed across four phases. The initial or preparation phase involves a preliminary literature review based on the project's conceptual framework. Phase one provides a diagnosis of conflicts and analysis of secondary geographic data sources. Phase two analyzes the conflicts from environmental, sociocultural, and economic perspectives through impact evaluation. Phase three establishes the characteristics that an analysis tool for sustainable land management should have, resulting in the creation of three conflict management records and a fourth record outlining parameters for a proposed analysis tool aimed at identifying and reducing territorial conflicts within the political-administrative boundaries of Palmira, offering an integrated territorial perspective.

Following this introductory section, the project is structured as follows:

Section one includes the referential frameworks, covering the normative and political framework, the institutional framework, and the conceptual framework used for the development of this research. Section two outlines the methodological aspects, organized into four phases: a preparation phase that defines the categories and variables used in the analysis; phase one, which identifies and diagnoses conflicts from land-use changes; phase two, which analyzes sociocultural, environmental, and economic conflicts caused by such changes; and phase three, which establishes the characteristics that an analysis tool for sustainable land management should possess in the study area. Section three presents the results obtained through the identification and diagnosis of land-use change conflicts in Palmira, including the development of comparative environmental, sociocultural, and economic categories of analysis, and the consolidation of a geographic database for the study area. This section also describes the analysis of conflicts from each category and highlights those with the greatest impact, identifying critical points through impact evaluation and geographic data overlay. It concludes by defining the characteristics of the proposed tool for reducing territorial conflicts in Palmira through the design of an analysis tool for sustainable land resource management. Section four contains the conclusions and bibliographic references.

## 2. Referential Frameworks

The normative and political framework in Colombia establishes the soil as a strategic resource. Table 1 summarizes the key laws and regulations, while Table 2 outlines policies and guidelines relevant to sustainable land management. Together, they provide the legal and political basis for this research.

| Legal Type | Topic | Title | Date |
|---|---|---|---|
| Political Constitution of Colombia | Chapter 3: Collective Rights and the Environment | Article 79: Everyone has the right to enjoy a healthy environment. It is the duty of the State to protect the diversity and integrity of the environment, conserve areas of special ecological importance, and promote education to achieve these objectives. | 1991 |
| Law 388 de 1997 | Land Development Law | Chapter V, Article 21: Land Classification. In addition to the provisions of Article 33 of Law 388 of 1997, land use plans shall indicate the physical boundaries and general conditions for the use of rural land that must be maintained and preserved for agricultural, livestock, forestry, or natural resource exploitation purposes, considering urban growth needs and appropriate agrological use. | 1997 |
| Law 1728 de 2014 | Allocation of Public Lands | Provisions for the distribution of vacant lands to poor families in the country for social and productive purpose and other related provisions. | 2014 |
| Decree 1299 | Natural Resources | Regulates the establishment of environmental management departments in industrial companies and other related provisions. | April 22, 2008 |
| Decree 2041 | Environmental Licenses | Regulates Title VIII of Law 99 of 1993 on environmental licenses. | October 15, 2014 |

Table 1. Description of the Normative Framework

| Policy | Topic | Guideline | Date |
|---|---|---|---|
| Policy for Sustainable Soil Management | Soil Management | Promotes the sustainable management of soil in Colombia, considering the convergence of biodiversity conservation, water and air quality, land-use planning, and risk management. | 2016 |
| CONPES Document 3510 | Biofuel Production | Policy guidelines for promoting sustainable biofuel production in Colombia. | March 31, 2008 |
| CONPES Document 3624 | Environmental Management | Program for sanitation, management, and environmental recovery of the upper Cauca River basin. | November 20, 2009 |
| Environmental Guide for the Sugarcane Subsector | Environmental Management | Association of Sugarcane Growers of Colombia. | December 30, 2010 |

Table 2. Description of the Political Framework

## 3. Methodological Aspects

A mixed-method approach was applied in four phases: (1) literature review, (2) diagnosis of land-use conflicts, (3) analysis of conflicts from environmental, sociocultural, and economic perspectives, and

(4) definition of tool characteristics. Figure 1 illustrates the research phases and Table 3 describes the methodological structure:


Figure 1. Research Phases

| Phase | Specific Objective | Activities | Methodological Tool | Result |
|---|---|---|---|---|
| Preparation | Identify and diagnose conflicts caused by land-use change in the municipality of Palmira, Valle del Cauca. | Definition of analysis categories and variables of the land resource. | Based on the construction of the conceptual framework | Matrix for identifying categories and variables |
| 2 | | Establish comparative analysis categories.<br>Compilation of geographic data layers for analysis. | Identification matrix of categories, components, effects, impacts, and land-use conflicts in Palmira.<br>Geographic | Matrix of categories, components, effects, impacts, and land-use conflicts in Palmira.<br>GBD[11] compiled with spatial information layers. |

[11] GDB: Geographic database generated using the ArcMap module of the ArcGIS software by ESRI, for the storage of geospatial and alphanumeric information.

| Phase | Specific Objective | Activities | Methodological Tool | Result |
|---|---|---|---|---|
| 3 | Analyze sociocultural, environmental, and economic conflicts caused by land-use changes in Palmira. | Establish the relationship between conflicts with the greatest impact due to land-use changes.<br>Determine critical points[12] in the conflict relationships identified through analysis. | Map algebra (cartography and spatial overlays).<br>Matrix for spatial data overlay analysis.<br>Matrix for identifying critical points and territorial conflicts using CONESA´s[13] impact evaluation method. | Analysis by means of:<br>Comparative and percentage maps with geographic elements of analysis.<br>Environmental impact assessment matrix and overlay of geographic information and analysis categories.<br>Conflict identification maps and critical point mapping. |
| 4 | Establish the characteristics of an analysis tool for sustainable land resource management in the study area as a proposal to | Define the components and indicators that an analysis tool for the sustainable management of the soil resource should include. | Development of templates describing conflict relationships and proposed management approaches. | Proposed hierarchical template: soil management policy / component / analysis category / relationship / indicator. |

Table 3. Methodological Structure

[12] Identification of critical points based on the following indicators: Sociocultural and environmental relationship: Geographic space. Sociocultural and economic relationship: Production practices. Economic and environmental relationship: Land use and exploitation.

[13] CONESA: Vicente Conesa. Methodological Guide for Environmental Impact Assessment. (1993).

## 4. Results

Based on the data and results from the chapters on the identification and diagnosis of land-use change conflicts, the analysis of conflicts from environmental, sociocultural, and economic categories, and the definition of the characteristics that an analysis tool for sustainable land management should have in Palmira, this research proposes the parameters and contents of such a tool through the development of a hierarchical template. This template consists of five parts:

1) The vision, management component, and considerations from the national policy for sustainable soil management.

2) The analysis categories addressed in previous chapters and the outcomes of management programs as show in Figure 2.

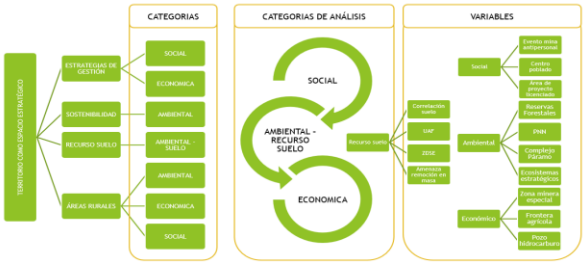


Figure 2. Conceptual Synthesis and Definition of Categories and Variables for Soil Resource Analysis, Including Social, Environmental, and Economic Variables

3) The municipality's location and area.

4) Identified strategic lines and their strategic relationships.

5) The spatial distribution of the proposed strategies and their cartographic scale of application.

The first part of the instrument considers a comprehensive vision of sustainable management, as it must be based on the development of knowledge about the processes that govern territorial dynamics, in order to support decision-making from an integrated perspective for the sustainable management of the same resource. The management component addressed in this work is the soil resource in rural areas, drawing upon the Soil Sustainable Management Policy developed by MADS (2016), which recognizes that "soil plays a fundamental role in supporting society and individuals; therefore, its degradation affects the well-being of the population" (p. 10). It also highlights considerations such as "the conservation and sustainable management of soil are essential to achieving population well-being and are interrelated with the success or failure of numerous public policies (...) where sustainable management is key to consolidating peace processes in the country" (p. 29), as shown in Figure 3.

| INSTRUMENTO DE ANÁLISIS PARA LA GESTIÓN SOSTENIBLE DEL RECURSO SUELO (FICHA ESTRATÉGICA) | | |
|---|---|---|
| VISIÓN | **Integral de la Gestión Sostenible:** La gestión del territorio se debe basar en el desarrollo de conocimiento de los procesos que rigen el comportamiento del territorio para la toma de decisiones desde una perspectiva integral para la gestión sostenible del mismo. Medio natural y medio construido. | PARTE 1 |
| COMPONENTE DE GESTIÓN | **RECURSO SUELO EN ÁREAS RURALES** | |
| A PARTIR DE | **Política para la gestión sostenible del suelo (MADS, 2016):** "La cual reconoce que el suelo desempeña un papel fundamental en el sustento de la sociedad y las personas, por tanto, su degradación afecta el bienestar de la población". | |
| CONSIDERACIONES | La conservación y el manejo sostenible del suelo son indispensables para lograr el bienestar de la población y está interrelacionado con el éxito o el fracaso de numerosas políticas públicas, entre estas, las relacionadas con los sectores agropecuario, minero, de vivienda, desarrollo urbano y agua potable, de industria y comercio, de transporte y, salud, entre otros. Adicionalmente, la gestión sostenible del suelo es fundamental para consolidar los procesos de paz en el país. | |

Figure 3. Part 1 of the Proposed Strategic Sheet

This section should clearly describe the vision to be achieved and the proposed analysis variable (e.g., environmental category, soil resource variable, sustainable management). In the management component, a specific and concrete description should be provided—that is, the component that requires analysis in accordance with the defined variable (e.g., the soil resource).

In the row titled "based on", the regulatory and/or policy framework related to the variable under analysis and its corresponding information source should be described (e.g., Policy for the Sustainable Management of Soil). In the considerations section, the identified issue should be mentioned and described, oriented toward the proposal and analysis variables, in order to define the relationship among the analysis categories.

The second part of the instrument proposes a review of the analysis categories and the outcomes of the identified conflicts.

From the environmental category, it was found that there is a conflict arising from changes in soil characteristics due to overexploitation of the resource. This indicates the need for new

areas dedicated to protection, conservation, and agricultural production, resulting in the generation and implementation of an environmental management program for soil and vegetation cover protection.

From the sociocultural category, the identified aspects include community participation, where conflicts are observed in relation to the registration of sugarcane growers in the association, as well as shifts in production activities due to the introduction of new production technologies. These changes have led to population displacement within the municipality as people seek new job opportunities.

This links directly with the economic category, which highlights a shift in employment dynamics, alterations in the availability of labor for agricultural activities, and the need to redefine the boundaries of mining exploitation zones and transition toward new productive sectors, as illustrated in Figure 4.

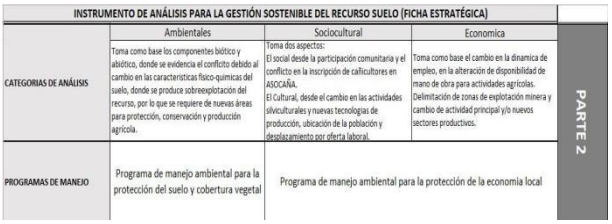

| INSTRUMENTO DE ANÁLISIS PARA LA GESTIÓN SOSTENIBLE DEL RECURSO SUELO (FICHA ESTRATÉGICA) | | | | |
|---|---|---|---|---|
| | Ambientales | Sociocultural | Economica | PARTE 2 |
| CATEGORIAS DE ANÁLISIS | Toma como base los componentes biótico y abiótico, donde se evidencia el conflicto debido al cambio en las características físico-químicas del suelo, donde se produce sobreexplotación del recurso, por lo que se requiere de nuevas áreas para protección, conservación y producción agrícola. | Toma dos aspectos:<br>El social desde la participación comunitaria y el conflicto en la inscripción de cañicultores en ASOCAÑA.<br>El Cultural, desde el cambio en las actividades silviculturales y nuevas tecnologías de producción, ubicación de la población y desplazamiento por oferta laboral. | Toma como base el cambio en la dinamica de empleo, en la alteración de disponibilidad de mano de obra para actividades agrícolas.<br>Delimitación de zonas de explotación minera y cambio de actividad principal y/o nuevos sectores productivos. | |
| PROGRAMAS DE MANEJO | Programa de manejo ambiental para la protección del suelo y cobertura vegetal | Programa de manejo ambiental para la protección de la economía local | | |

Figure 4. Part 2 of the Proposed Strategic Sheet

This section should describe the analysis categories, detailing the selected category based on the study variables that compose it and the topics of interest. It is recommended to include environmental, social, and economic aspects. In the management programs row, based on the selected categories and the analysis of the variable, and grounded in the impact assessment, a proposal for management programs is developed in accordance with the template adapted from the Ministry of Environment and Sustainable Development.

The third part of the instrument describes the geographic location of the study area, which in this case corresponds to the political-administrative boundary of the municipality of Palmira and its location within the department of Valle del Cauca, as well as the calculation of its area, as presented in Figure 5.


Figure 5. Part 3 of the Proposed Strategic Sheet

This part of the instrument provides a detailed description of the geographic location and the area of interest for the analysis (it is considered that this can be any territorial entity with available base cartographic and geographic information; for example, the political-administrative boundary of a municipality in the country or another territorial entity). It is also recommended to include a graphic output or spatial figure describing the location or area of interest.

The fourth part of the instrument proposes the definition of four strategic lines, based on the analyses developed in previous chapters.

The first strategic line focuses on the conservation and protection of natural resources in the high mountain areas of the municipality of Palmira, with indicators such as the calculation of areas designated for conservation and protection, and the percentage relationship of these areas with respect to the total area within the political-administrative boundary of the municipality. This line is related to the prospective scenario of managing a legally protected territory, based on the official declaration of protected areas in this sector.

The second strategic line proposes the expansion of supply to new productive sectors through an environmental economic valuation, based on the availability of resources in protected areas and the special mining zone. Indicators include the calculation of areas identified as new productive sectors for environmental economic valuation and their percentage relationship with the declared areas and the municipality's political-administrative boundary. This scenario is seen as a negotiated

territory, shaped through prior consultations and the public policies established in Palmira's development plan.

The third strategic line is oriented toward the redefinition and delimitation of the special mining zone, based on the calculation of its area with respect to the zone already declared by the National Mining Agency. This could be achieved through participatory agendas with residents of Palmira involved in these activities.

The fourth proposed strategic line is based on the implementation of good production practices in the sugarcane sector, aiming to protect the soil resource and vegetative cover. As an indicator, workshops and training sessions are proposed, aligned with the program for soil and vegetation cover protection. In this case, the prospective scenario is based on a territory that is envisioned and lived, since the people of Palmira identify themselves as producers of sugar and as part of the country's sugar industry.

As part of the strategic framework, all institutional actors are considered, as well as the environmental, sociocultural, and economic analysis categories, taking into account the components of production practices, geographic space, and the use and exploitation of the soil resource, as illustrated in Figure 6.

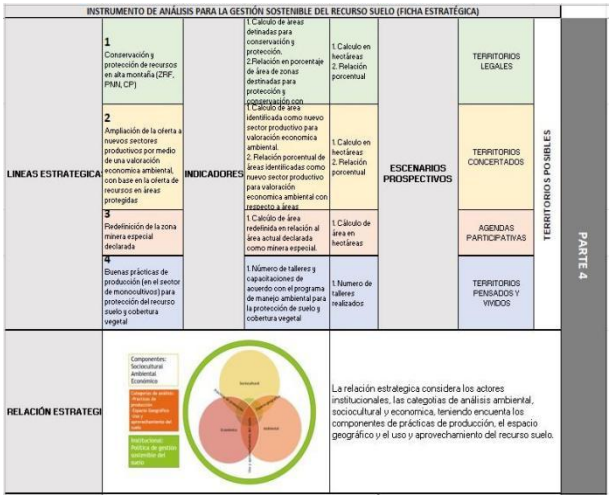

Figure 6. Part 4 of the Proposed Strategic Sheet

In this part of the instrument, based on the analysis of geographic information overlays, strategic lines of interest are proposed in accordance with the selected variables and the suggested management programs. These lines must be coherent with the variables and categories of analysis. Likewise, indicators should be developed based on the study area and the percentage relationship in accordance with the coverage of the proposed strategic line.

According to the proposed strategic line, a prospective scenario is indicated depending on the nature of the proposal. For instance, if it involves area delimitation, it must be subject to an administrative act or legal framework; if the strategic line proposes social or economic valuation, it must be agreed upon or consulted with the target population; if the line proposes the redefinition of declared areas or aligns with the territorial entity's vision, prospective scenarios involving participatory agendas with the inhabitants of the area or study zone are recommended; and if the strategic line envisions future scenarios (e.g., good production practices), it should align with the management programs and suggest prospective scenarios as envisioned and lived territories, built from the community's or communities' own knowledge within the area or study zone.

In the "strategic relationship" row, the connection between the proposed strategic lines and the analysis categories must be described, as well as the relevant components and variables. This relationship should be expressed both graphically and textually.

The fifth part of the instrument proposes the spatial distribution of the strategic lines, that is, a redistribution of the territory based on the identified conflicts. It provides guidance for the possible implementation or development of public policies in Palmira, as proposed in Figure 7.

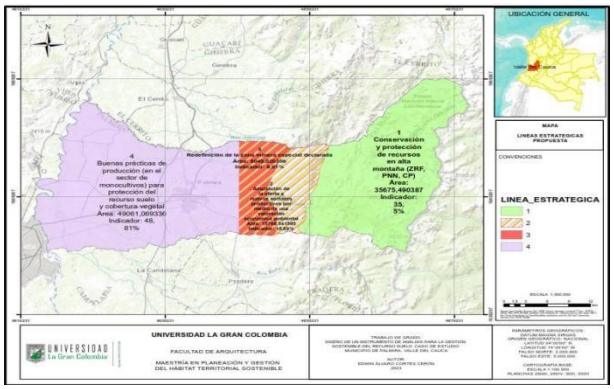


Figure 7. Spatial Distribution of the Strategic Lines Resulting from the Analysis

Therefore, the new spatial interpretation of the municipality is shown through a map and a geographic database, redefining:

1) Conservation and protection of resources in high mountain areas, with an approximate area of 35,675 hectares, representing 35.5%, to generate protection programs in addition to those already established in these protected areas.

2) Expansion of the offer to new productive sectors through environmental economic valuation, with an estimated area of 15,768 hectares, equivalent to 15.7% of the municipality.

3) Redefinition of the special mining zone, covering an area of 8,049 hectares, equivalent to 8%, which is compatible with environmental economic valuation as it is an extraction sector and will require control, mitigation measures, and redefinition of compensation areas.

4) Generation of good production practices programs for soil and vegetation cover protection, with an approximate area of 49,061 hectares, equivalent to 48.8% of the municipality, as shown in Figure 8.


Figure 8. Part 5 of the Proposed Strategic Sheet

In this part of the instrument, an annex is proposed with a graphic output that allows the graphic and spatial visualization of the proposal according to the strategic lines and the coverage area in hectares over the defined study area or territorial entity. It should be described based on the proposed strategic lines resulting from the analysis, the spatial distribution of the strategic lines based on the result of the indicator calculations (area calculated in hectares covered by the strategy within the study area and its respective percentage indicator in relation to the total study area or the boundary of the territorial entity of interest).

Likewise, it is proposed to define the cartographic scale of the strategic lines, where the scale of application of the strategic lines according to the study area and/or territorial entities must be mentioned (e.g., municipal scale defined by the political-administrative boundary of a municipality). The cartographic scale of application of the proposed strategic lines should be established in accordance with the cartographic scales of the country's highest authority in technical matters (IGAC) related to cartography, geography, territorial planning, territorial entity boundaries, and geographic names, among others (standardized and in accordance with the official base cartography available and open databases in the country).

Thus, this chapter concludes that, through the identification of conflicts and the application of methodologies established and proposed in this thesis, a proposal for the design of an analysis instrument for the sustainable management of the soil resource was created, with the municipality of Palmira, Valle del Cauca, as a case study. This proposal, based on the creation of a strategic sheet, suggests elements of analysis and possible implementation with a comprehensive vision of the municipality, guiding the management and planning of the territory as a strategic space where various activities converge from social, environmental, and economic components.

## 5. Conclusions

Based on the results obtained in this thesis, it is concluded that the generation of methodologies and processes, the analysis of categorized variables from different components, and the development of a proposal that consisted of designing an analysis instrument for the sustainable management of the soil resource, are relevant for the analysis of territorial entities in the country that may have characteristics similar to the case study, the municipality of Palmira, Valle del Cauca. This is because, at present, there are no similar instruments that allow the consolidation of information and the execution of comparative analysis with geographical variables to determine territorial conflicts and propose management solutions for them.

Management Instruments such as those from CEPAL, MADS, and DNP, only consider some aspects and variables aimed at providing support for environmental management, the generation of management programs, or intervention and monitoring, respectively. However, the instrument proposed in this thesis considers all three categories of analysis—social, environmental, and economic—through a cross-sectional approach to the variable of soil resources for its sustainable management. This promotes an integrated vision of the territory for its protection, conservation, use, and sustainable exploitation.

The diagnosis of territorial conflicts due to land-use change in the study area, the municipality of Palmira, Valle del Cauca, was developed based on the definition of categories and analysis variables derived from the construction of the conceptual framework, such as the social, environmental, and economic categories.

The main territorial conflicts due to land-use changes in the municipality of Palmira, Valle del Cauca, from the environmental category, are mainly related to the changes in the physical-chemical characteristics of the soil. These include soil overexploitation, which requires new areas or the redefinition of already established areas for protection, conservation, and agricultural production. There has also been a loss of species, which highlights the need to delimit reserve zones, create, review, and/or modify existing management plans.

From the sociocultural category, the territorial conflict is identified due to the municipality's production practices, where the participation offer for the people of Palmira is limited to registration in ASOCAÑA, overlooking the variety of organizations present in Palmira and public management policies. Moreover, it was identified that due to monocultures and the spatial distribution of the municipality, the delimitation of production areas, urban areas, reserve zones, and environmental protection areas creates linear displacement zones for the population, moving from the municipal center to populated areas and rural labor supply zones.

From the economic category, territorial conflict is identified due to the spatial distribution of the municipality's urban areas, rural areas, monoculture zones, and forest reserve zones, where employment dynamics change and alterations in the employment rate depend on the geographic location of monocultures.

Thanks to the analysis of conflicts in the defined environmental, social, and economic categories caused by land-use change in the municipality of Palmira, it is concluded that the relationship between these conflicts could be established through the cross-referencing of geographic information (geographic layers compiled in the BDG), and through the corresponding algebra of maps, comparative graphic outputs were obtained that contain area calculations and conflict territorial impact percentages.

Furthermore, by determining critical points, the most significant impacts and conflicts in the municipality of Palmira were established using Professor Vicente Conesa's methodology, which allows for impact evaluation. It became evident that in Palmira, the activities that generate the greatest

environmental impact in relation to soil resources are the increase of monocultures, which leads to the overexploitation of the resource, showing that new areas for protection, conservation, and sustainable agricultural production are required, as proposed by the country's soil management policy.

Also, from the social and economic aspects, the evaluated impacts show that Palmira could experience a change in employment dynamics due to the shift in the primary productive activity. Monocultures occupy nearly 48% of the territory, while the municipality also has a special mining zone covering almost 10% of the territory and around 36% of protected areas, which calls for designing an analysis instrument oriented to sustainable management of soil resources, highlighting key aspects in decision-making and in the construction of instruments and methodologies for territorial planning.

The characteristics that an analysis instrument for sustainable soil management should have been established as part of the proposal for managing and reducing territorial conflicts. These characteristics include describing the relationship of the identified conflicts, with a problem and study area vision, including a management component, a policy or regulation, the proposed analysis categories, management programs, geographical localization, strategic lines identified in the conflicts, the strategic relationship, spatial distribution of the strategy, and its cartographic application scale.

By establishing the characteristics for an analysis instrument for sustainable soil management, it is concluded that, for the study area, the municipality of Palmira, the components, and parameters for designing an analysis instrument were defined. This is supported by the adaptation of environmental management forms used by MADS in environmental studies, with the result being the proposal of three management programs for soil resource protection, based on the analysis of the environmental, social, and economic categories.

Thanks to this proposal, a strategic form was constructed as an analysis instrument, which guides the proposal of strategic management lines based on the analysis of geographic information for soil resources in rural areas of the municipality of Palmira. The main conclusion is that this form is useful for identifying territorial conflicts and is composed of five parts, considering an integral vision of sustainable management, the management component of soil resources, based on sustainable soil management policies, passing through analysis categories, management programs, localization, and concluding with the definition of four strategic lines, their strategic relationship, and the spatial distribution and cartographic application scale.

Thus, this research work becomes a contribution to territorial planning and management from the perspectives of sustainability and habitat. It considers hierarchical analysis categories and proposes a methodology that can be applied to the evaluation and analysis of any environmental, social, and economic component using geographic information. This methodological proposal can also be applied to any municipality in the country, taking into account secondary source variables, categories, components, aspects, impacts, and identification of territorial conflicts, proposing the application of the strategic form from territorial planning and public policy generation, which allows any municipality to obtain the territorial vision they wish to have based on their own territorial capacities and potentialities.

## 6. References

Adib, A. R. (Ed.). (2010). Guide for the formulation and management of sustainable rural development plans: A participatory approach with a territorial focus. IICA. https://acortar.link/kKzYiN

Alcaldía Municipal de Palmira. (2013). Action plan for the incorporation of risk

prevention and reduction in the territorial planning plan. Palmira, Valle del Cauca. https://bit.ly/3mKEaEM

ANLA, M. (2018). General methodology for the preparation and presentation of environmental studies. Ministry of Environment and Sustainable Development, National Authority of Environmental Licenses. https://acortar.link/x0VeHM

Asociación de Cultivadores de Caña de Azúcar de Colombia. (2010). Environmental guide for the sugarcane subsector. Valle del Cauca, Colombia. https://bit.ly/3JypcuB

Borrero, A. P. (1956). Some chemical properties of nine soils from Valle del Cauca. Acta Agronómica, 6(3), 135–141. https://acortar.link/sP8olE

Bozzano, H. R. (2017). Possible territories and territorial intelligence: A formula between people, science, and public policies. Geographical Analysis. https://acortar.link/4ON1tV

Conesa, V. (1993). Methodological guide for environmental impact assessment (2nd ed.). MUNDI-PRENSA Publishing.

Constitución política de Colombia [Political Constitution of Colombia]. (1991). Retrieved February 15, 2019, from http://bit.ly/3Fm9AYv.

Cortés Ortiz, B. T. (2010). Socio-environmental description of soil in the geographical valley of the Cauca River: The case of the sugar agroindustry. Luna Azul, (31), 41–57. https://bit.ly/3ZO8VYg

Decree 2041/14, October 15, 2014. Ministry of Environment and Sustainable Development (Colombia). Retrieved March 10, 2023, from https://onx.la/a2c64.

National Planning Department (DNP). (2012). Instruments for results-based territorial public management (Guides for territorial public management). Bogotá D.C., Colombia: DNP. https://acortar.link/ec1N8A

Durand-Lasserve, A. (2003). City and land: Land ownership, debate, and perspectives. CEPAL Notebooks. https://repositorio.cepal.org/handle/11362/27820

Echeverri, R., & Sotomayor Echenique, O. (2010). Strategies for rural territorial management in public policies in Ibero-America. https://repository.eclac.org/handle/11362/3847

FEDESARROLLO. (2010). Socioeconomic impact of the Colombian sugar sector on the national and regional economy. January. Bogotá D.C., Colombia. https://acortar.link/l5bfu9

IDEAM & U.D.C.A. (2015). Synthesis of the national study on soil degradation by erosion in Colombia – 2015. IDEAM – MADS. https://onx.la/21a2e

Geographic Institute Agustín Codazzi (IGAC) & CORPOICA. (2002). Current land cover and use in Colombia. Agrology Subdirectorate, Bogotá D.C., Colombia. Unpublished.https://www.igac.gov.co/es/ide/estrategia-y-gobierno-geoespacial/estandares/agrologia

Ministry of Environment and Sustainable Development. (2016). Policy for the sustainable management of soil. Bogotá D.C., Colombia. https://bit.ly/400D8CZ

Morales, M. M. B., & Caetano, C. M. (2013). Inventory and valuation of flora used in the Santa Teresa village, Palmira (Valle del Cauca). Journal of Agrarian and Environmental Research, 4(1), 89–99. https://hemeroteca.unad.edu.co/index.php/riaa/article/view/985

Polidori, L. (2017). Contributions of remote sensing to building peace with sustainable development: Successes and limitations over the past 25 years. Geographical Analysis, 52, 17–34. https://revistas.unal.edu.co/index.php/rcg/article/view/70766

United Nations Environment Programme (UNEP). (2010). Environmental Outlook: Latin America and the Caribbean. Panama. https://acortar.link/0mrBGd

Sepúlveda, S. (2008). Sustainable development management in rural

territories: Methods for planning. Inter-American Institute for Cooperation on Agriculture (IICA). http://repiica.iica.int/docs/B0712E/B0712E.pdf

United Nations. (2015). Sendai framework for disaster risk reduction 2015–2030. UN Office for Disaster Risk Reduction. https://acortar.link/rDdF4v

Victoria Russi, A. M., Ramírez Galvis, M. A., Vallejo Cabrera, F. A., Salazar Villarreal, M. D. C., Arana Gutiérrez, A. D., Marín Velásquez, P. A., & Panesso Jiménez, F. (2020). Socio- environmental conflicts in Valle del Cauca, Colombia. https://hdl.handle.net/10901/19193.

# Multiscale Monitoring of Urban Green Space Dynamics and Heat Stress

HA Nalani [a,*], GSN Perera [a], IAB Saubhagya[a], WWHN Waduge[a]

[a] *Dept. of Remote Sensing & GIS, Faculty of Geomatics, Sabaragamuwa University of Sri Lanka – nalani@geo.sab.ac.lk, sanka@geo.sab.ac.lk, saubhagya@geo.sab.ac.lk, nipuni@geo.sab.ac.lk*

**Abstract**: Urban green spaces play a vital role in mitigating the impacts of climate change by regulating urban temperatures, enhancing air quality, and reducing the Urban Heat Island (UHI) effect. However, rapid urbanization and climate shifts are causing significant green space loss, leading to increased urban heat stress in cities. This study presents an integrated assessment of urban green space dynamics and associated heat stress using both Unmanned Aerial Vehicle (UAV) imagery and satellite remote sensing data. High-resolution UAV imagery were used to map the current distribution of urban green spaces, while historical changes were analysed using vegetation indices (NDVI) derived from Sentinel-2 and Landsat imagery. Land Surface Temperature (LST) data extracted from Landsat thermal bands were utilized to map heat stress patterns over time. The study focuses on Colombo urban area, Sri Lanka, experiencing rapid development and climate challenges. The results provide valuable insights for urban planners and policymakers to design climate-adaptive strategies and promote sustainable urban growth. By integrating UAV and satellite data at multiple scales, the study offers a practical, data-driven approach to monitor and manage urban environmental health. On average, 86% of the urban area exhibited a surface urban heat island (HI), while most surface urban freshness islands were located near watercourses, parks, slopes, and valley bottoms, highlighting the influence of green areas and topography on the creation of microclimates. The HI demonstrated significant seasonal variability.

***Keywords:*** Remote Sensing Data, UAV, Urban Green Space Dynamics, Heat Stress

## 1. Introduction

Urbanization is rapidly reshaping the Earth's surface, replacing vegetated land with impervious materials like concrete and asphalt. This transformation amplifies the Urban Heat Island (UHI) effect—where urban areas experience significantly higher temperatures than their rural surroundings—leading to heightened heat stress, energy demand, and health risks. Urban green spaces (UGS), including trees, parks, and vegetated corridors, play a crucial role in mitigating these effects through shading and evapotranspiration. The World Health Organization highlights green spaces as important to physical and mental well-being, and they also contribute to temperature moderation and pollution reduction. Green infrastructure plays a critical role in mitigating the adverse effects of climate change, particularly by reducing the urban heat island (UHI) effect, enhancing thermal comfort, and improving urban sustainability (Zhou et al., 2022; Li et al., 2023). Monitoring urban green space dynamics associated thermal patterns is therefore essential for designing strategies to maintain ecological balance and improve urban resilience.

Traditional methods such as ground surveys offer high accuracy but are labour-intensive and spatially constrained. Remote sensing (RS) assists broader spatial and temporal monitoring: satellite platforms like Landsat and Sentinel-2 support vegetation mapping (via indices such as NDVI) and estimation of Land Surface Temperature (LST). These tools have been widely used to trace trends in green cover and thermal landscapes across cities (Imatrakul et al., 2024; Jumari et al., 2023; Li et al., 2022). However, while these datasets offer regional insights, they often fail to capture micro-scale heterogeneity of urban environments—especially small streetscapes, scattered trees, or rooftop gardens due to their coarse resolution compared to urban structures (Peng et al., 2023).

Recent studies have demonstrated the potential of Unmanned Aerial Vehicles (UAVs) to fill this gap by providing ultra-high-resolution (centimeter-level) data that enable detailed mapping of urban green spaces and fine-scale validation of satellite-derived products (Mantey et al., 2023; Ranjan et al., 2024). Unmanned Aerial Vehicles (UAVs) provide ultra-high-resolution imagery (at centimetre-scale), enabling detailed land cover mapping of micro-urban environments. UAV photogrammetry produces orthophotos and land cover maps that reveal small parks, street trees, and other vegetation features that are often undetectable in satellite images. When integrated with multispectral and thermal satellite data, UAV data supports a multiscale monitoring framework that can capture both long-term trends and fine-scale variations in urban green and thermal environments. UAV-based studies, such as the work by Gibril et al. (2020), successfully combine UAV imagery with digital surface models to classify heterogeneous urban landscapes with advanced segmentation techniques (Gibril et al., 2020).

Despite UAVs offering exceptional detail and several advancements, their coverage is limited in time and extent, and purely UAV-based approaches struggle to capture long-term trends due to operational constraints. This underscores the need for an integrated multiscale monitoring framework that merges UAV-derived spatial detail with the historical and thermal capabilities of satellite data.

Several studies have attempted to assess UHI using satellite-derived thermal and vegetation indices. In Kuala Lumpur, RS-based LST and NDVI analysis revealed widening temperature differences between urban and rural regions, emphasizing that vegetation restoration can help reduce urban heat islands (Jumari et al., 2023). In Bangkok, long-term LST trends showed rising urban temperatures paired with decreased green cover—highlighting the inverse correlation between vegetation and surface heat (Thanvisitthpon et al., 2023).

Many previous works have relied solely on either coarse-resolution satellite imagery (30 m Landsat) or medium-resolution Sentinel imagery (10 m), missing the potential to validate and downscale LST at finer scales (Weng et al., 2021). Others have assessed vegetation indices but did not incorporate combined metrics of urban heat stress, such as the Urban Thermal Field Variance Index (UTFVI) and Heat Stress Index (HSI), which offer stronger links to human thermal comfort (Chen et al., 2022; Yang et al., 2023). Moreover, few studies have employed UAV-derived orthophotos as a validation and enhancement tool in SUHI analysis.

Yet, research gaps remain. Most studies rely on either satellite data for large-scale temporal analysis or UAV imagery for micro-scale mapping, rarely integrating both approaches in a single framework. Temporal continuity is often missing in UAV-based studies, while satellite-only methods miss micro-variability. Moreover, validation with ground truth data is frequently limited.

There is thus a compelling need for a multiscale integration strategy that leverages spatial precision from UAVs and temporal, thermal depth from satellite data to monitor UGS changes and heat stress dynamics. This approach can fill critical gaps in urban environmental assessment by capturing both

fine-scale spatiotemporal complexity and trends.

The present study addresses these gaps by adopting a multiscale approach combining UAV-based orthophotos with Sentinel-2 and Landsat. The main objectives of this study were to:

- Map current green space distribution at high resolution;
- Analyze historical changes in vegetation through satellite-derived NDVI trends;
- Evaluate urban heat stress;
- Correlate green space changes with heat patterns across scales;
- Validated satellite-based classifications and indices using UAV orthophotos.

This integrative methodology provides new insights into urban heat dynamics at multiple scales, demonstrating the value of UAV–satellite fusion for environmental monitoring in rapidly urbanizing cities. It also contributes significantly to revitalizing urban green infrastructure in the face of rising heat.

## 2. Materials and Methodology

This study integrates UAV-based ultra-high-resolution imagery and multi-temporal satellite data (Sentinel-2 and Landsat series) for assessing urban green space dynamics and their relationship with heat stress patterns. The methodology consists of five major stages: (i) Data Acquisition, (ii) Data Pre-processing, (iii) Land Cover Classification and Change Detection, and (iv) Heat Stress Assessment and Validation. The overall workflow for the entire process is shown in Figure 1.

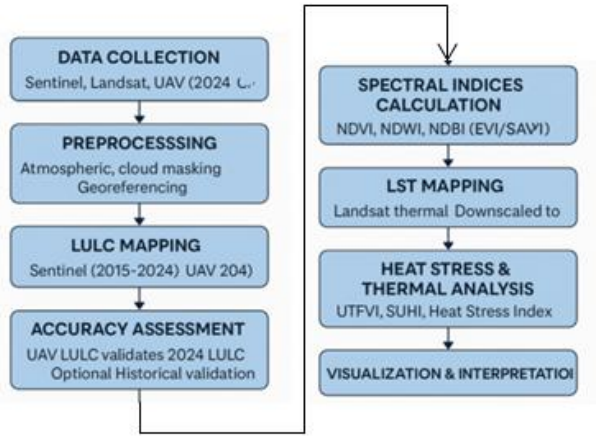


Figure 1. Workflow of analysis of urban green space dynamics and heat stress

### *2.1* Study Area

The study focuses on Colombo City Region, Sri Lanka, which has experienced rapid urbanization in recent decades leading to significant transformations in land cover patterns and green space loss and intensifying urban heat. Colombo is the capital of Sri Lanka. The area is characterized by a tropical climate, dense built-up zones, fragmented green spaces, and increasing susceptibility to urban heat stress.

### 2.2 Data Sources

Two primary datasets were utilized in this study:

Satellite Data: Sentinel-2 MSI (10–20 m) and Landsat 8–9 OLI/TIRS (30 m, with thermal bands) images covering the period from 2015 to 2024 were used. Sentinel-2 was primarily used for vegetation mapping, while Landsat thermal bands were processed to derive Land Surface Temperature (LST) for heat stress analysis.

UAV Data: High-resolution RGB imagery was captured in 2024 using a UAV platform equipped with a consumer-grade camera. The flight missions were planned to provide centimeter-level spatial resolution suitable for micro-scale land cover classification and validation of satellite-based observations.

### 2.3 UAV Image Classification

The acquired UAV images were processed using Structure-from-Motion (SfM) photogrammetry in Agisoft Metashape to generate an orthomosaic image. Radiometric and geometric corrections were applied prior to further analysis.

The orthomosaic was then classified into nine major land cover classes: dense vegetation, lo vegetation, built-up (roof), bare lands, roads, metal roofs, water bodies, impervious surfaces, and concrete roofs. A supervised classification approach using the Random Forest (RF) algorithm was implemented due to its robustness in handling high-dimensional datasets and its superior performance in previous studies (Belgiu & Drăguț, 2016). Training samples were collected from the orthomosaic based on visual interpretation, and vegetation indices such as the Excess Green Index (ExG) were computed to enhance vegetation detection (Gupta et al., 2023) using:

$$ExG = 2G - R - B \quad (1)$$

Where R, G, B are the red, green, and blue reflectance values, respectively.

The classification was validated using an independent set of reference points, and accuracy assessment was performed using a confusion matrix and Kappa coefficient.

$$OA = \frac{\sum_{i=1}^{k} nii}{N} \quad (2)$$

$$k = \frac{N\sum_{i=1}^{k} n_{ii} - \sum_{i=1}^{k} n_{i+}n_{+i}}{N^2 - \sum_{i=1}^{k} n_{i+}n_{+i}} \quad (3)$$

Where $n_{ii}$ represents correctly classified pixels, N is total pixels, and $n_{i+}, n_{+i}$ are row and column sums.

### 2.4 Satellite Image Analysis

#### 2.4.1 *Satellite image Classification*

Geometric corrections and resampling were applied to both Sentinel-2 and Landsat imagery, which were also corrected for atmospheric effects to standardize spatial resolution and projection across datasets. Cloud masking was performed using Fmask to exclude cloudy pixels, and all images were subset to the study area boundary for further analysis. Supervised classification was performed on Sentinel-2 data using the Random Forest classifier, following the same thematic classes as UAV classification from 2015 to 2024. Accuracy was validated using UAV-derived maps.

#### 2.4.2 *Land Surface Temperature (LST) Analysis*

The LST in Kelvin was estimated from Landsat 8/9 thermal bands using the radiative transfer equation method (Weng et al. 2021). The calculation involved deriving the Top of Atmosphere (TOA) Radiance($L$ ), Brightness Temperature ($T_B$), and NDVI-based Emissivity ($\varepsilon$ ), which were then used to compute the LST for each pixel using the following equations:

$$L = M_L \times Q_{cal} + A_L \quad (4)$$

$$T_B = \frac{K_2}{ln\left(\frac{K_1}{L} + 1\right)} \quad (5)$$

$$\varepsilon = -0.004 \times PV + 0.986 \quad (6)$$

$$PV = \left(\frac{NDVI - NDVI_{min}}{NDVI_{max} - NDVI_{min}}\right)^2 \quad (7)$$

$$LST = \frac{T_B}{1 + \left(\frac{T_B}{\rho}\right) ln\varepsilon} \quad (8)$$

#### 2.4.3 *Spectral Indices Analysis*

Urban heat can be identified using the feasibility of RS-based different spectral indicators. Sentinel-2 images were used to derive NDVI, NDWI, and NDBI indices to monitor vegetation dynamics in the study area for each year used to calculate LST.

For vegetation detection, the Normalized Difference Vegetation Index (NDVI) as computed:

$$NDVI = \frac{NIR - RED}{NIP + RED} \quad (9)$$

Urban areas were identified using the Normalized Difference Built-up Index (NDBI), calculated as follows:

$$NDBI = \frac{SWIR\text{-}NIR}{SWIR + NIR} \quad (10)$$

The Normalized Difference Water Index (NDWI) is used to map and monitor surface water and vegetation moisture using satellite imagery. It is calculated as follows:

$$NDWI = \frac{Green\text{-}NIR}{Green + NIR} \quad (11)$$

where NIR , GREEN and RED represent near-infrared, green, red, and short-wave infra-red band reflectance, respectively.

### 2.5 Change Detection and Correlation Analysis

A post-classification comparison approach was employed to analyze green space dynamics over the ten-year period (2015–2025). Change detection maps highlighted zones of vegetation loss, expansion, and conversion to built-up areas. Furthermore, correlation analysis was performed to examine the relationship between LULC map and LST, as well as to assess the associations between each spectral index and LST.

### 2.6 Heat Stress Analysis

Heat stress assessment was conducted using Land Surface Temperature (LST) derived from Landsat thermal bands. LST was estimated using the Single Channel Algorithm after converting digital numbers to spectral radiance and subsequently to brightness temperature. The LST data were analyzed in relation to land cover classes, demonstrating that regions with reduced vegetation exhibited higher temperatures, indicating an intensified Urban Heat Island (UHI) effect.

Heat Stress Analysis was conducted by integrating Surface Urban Heat Island (SUHI) evaluation, heat stress assessment, and urban thermal field analysis using remote sensing-derived Land Surface Temperature (LST). The UHI effect was quantified by calculating the temperature difference between urban and non-urban as:

$$SUHI = \frac{(LST_S - LST_{mean})}{STD} \quad (12)$$

where $LST_s$ represents the LST (K) of a specific pixel, $LST_{mean}$ is the mean LST (K) of the entire study area and STD denotes the standard deviation of the LST values across the study area.

This formula is employed to standardize the LST values, effectively transforming them into a Z-score. The z-score indicates how many standard deviations a particular pixel's temperature is from the mean temperature of the study area. The primary reason for using this approach was to identify thermal anomalies, normalize data and enhance spatial analysis. Then, the SUHI effect was quantified by:

$$SUHI = T_{urban} - T_{non\text{-}urban} \quad (13)$$

Where, $T_{urban}$ = mean LST of urban pixels and $LST_{nonurban}$ = mean LST of all non-urban pixels.

This comparison helps in understanding the intensity of the urban heat island effect by assessing the temperature differences urban and rural area.

To assess localized heat stress, the Heat Stress Index (HSI) was derived by normalizing pixel-wise LST against the minimum and maximum LST values within the study area:

$$HSI = \frac{T_S - T_{min}}{T_{max} - T_{min}} \quad (14)$$

where Ts is the surface temperature at a given pixel, and Tmin and Tmax are the minimum and maximum LST values.

Furthermore, the Urban Thermal Field Variance Index (UTFVI) was calculated to capture deviations of individual pixels from the mean thermal field:

$$UTFVI = \frac{T_S - T_{mean}}{T_{max} - T_{min}} \quad (15)$$

where $T_{mean}$ is the mean LST of the study area. These indices together provide a comprehensive understanding of urban thermal dynamics, enabling the identification of heat-vulnerable zones and their relationship with vegetation, water bodies, and built-up

areas. The combined UHI, HSI, and UTFVI approach supports sustainable urban planning by providing evidence-based insights into heat mitigation strategies, such as enhancing urban greening, optimizing land use, and improving climate resilience.

## 3. Results and Discussion

### 3.1 Land Use/Land Cover (LULC) Dynamics

The multi-temporal classification of Sentinel-2 imagery for 2015, 2018, 2021, and 2024 revealed significant shifts in the spatial extent of major land use categories, particularly vegetation, built-up areas, and water bodies (Figure 2).

Vegetation cover demonstrated a gradual decline over the study period, primarily due to urban expansion, while built-up areas increased markedly between 2015 and 2024. Water bodies remained relatively stable but showed minor seasonal fluctuations linked to rainfall patterns.

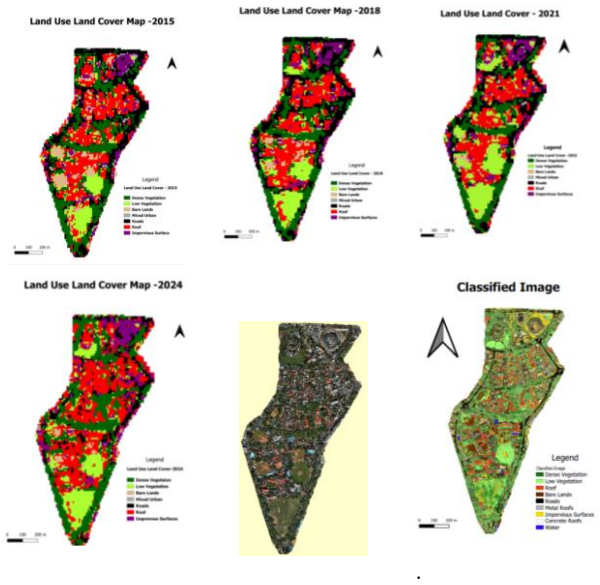


Figure 2. Sentinel-based LULC classification in 2015, 2018, 2021, and 2024 and UAV-based orthophoto & LULC classification in 2024

The UAV-derived orthophoto (0.05 m resolution) further validated the Sentinel-based classifications, providing fine-scale insights into small green patches, roadside vegetation, and fragmented urban greenery that were not captured in the coarser Sentinel imagery.

By integrating UAV data, this study reduces the uncertainty in detecting micro-scale vegetation dynamics that often remain undetected in 10–30 m satellite imagery. The accuracy assessments of four different year images were 93%, 94.2%, 94%, and 93.6%, respectively. The Kappa coefficients were 0.925, 0.932, 0.92, and 0.918 for same years.

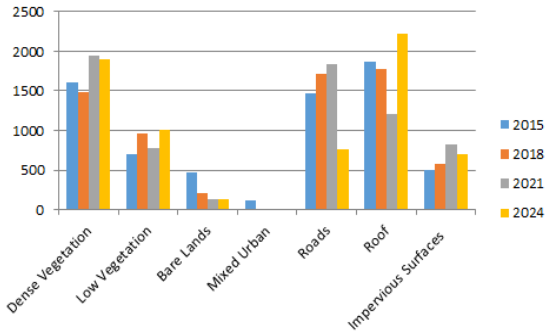


Figure 3. LULC change analysis form 2015 to 2024

### 3.2 Land Surface Temperature (LST) Patterns

LST derived from Landsat imagery showed a clear increasing trend from 2015 to 2024 (Figure 4). The average LST in built-up areas rose by approximately X °C, whereas vegetated areas exhibited significantly cooler temperatures. The downscaling of LST to 10 m resolution improved spatial matching with Sentinel-derived indices and enabled pixel-level correlation analysis.

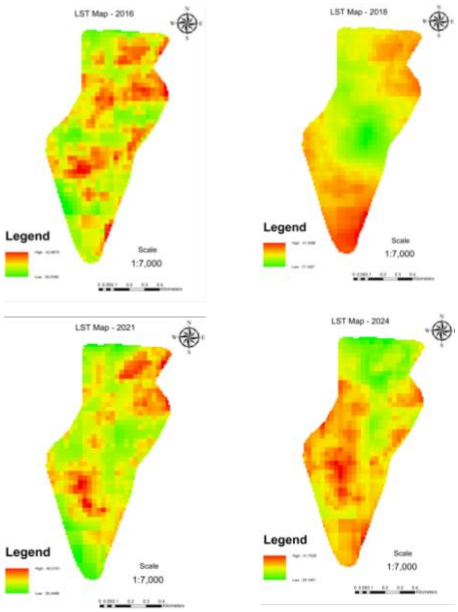


Figure 4. The LST variation over the years 2015, 2018, 2021, and 2024 for Colombo area.

Correlation analysis between LULC classes and LST confirmed that built-up areas had the highest mean LST, while dense vegetation exhibited the lowest.

### 3.3 Spectral Indices Analysis

Spectral indices, including NDVI, NDWI, and NDBI, were derived for all study years. NDVI trends indicated a continuous decline in healthy vegetation, while NDBI values increased over time, reflecting intensifying urbanization. NDWI highlighted seasonal variations in surface water retention. The combination of NDVI and NDBI provided a reliable indication of the vegetation–urbanization trade-off.

### 3.4 Urban Green Space Patterns

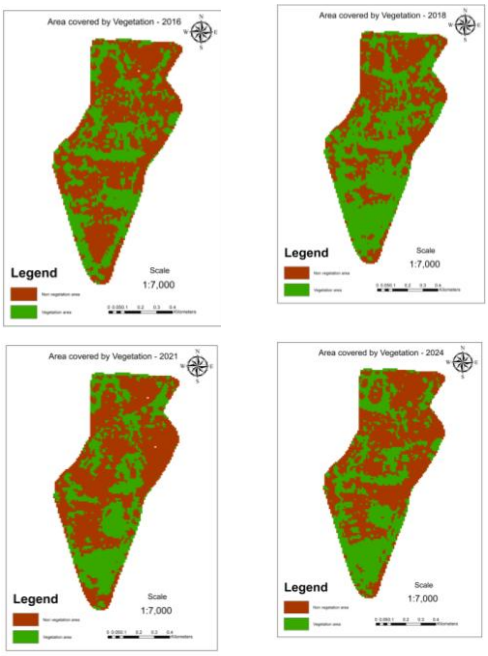


Figure 5. Green space dynamics in 2015, 2018, 2021, and 2024.

### 3.5 Urban Thermal Field Variance Index (UTFVI) and Surface Urban Heat Island (SUHI)

The UTFVI results revealed that areas with dense built-up land were classified under "strong heat stress" categories, whereas urban green areas were in the "no–weak heat stress" class. The SUHI intensity maps further demonstrated a progressive intensification of UHI effects, particularly between 2021 and 2024. The overall urban heat intensity is 1.108, 0.139, 1.058, and 0.577 for each year's respectively.

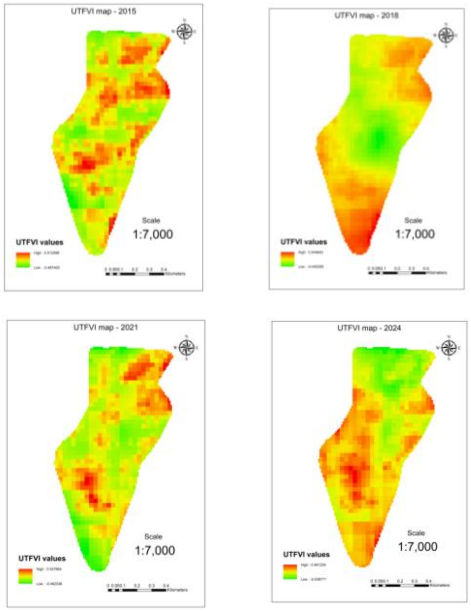


Figure 6. UTFVI variation in 2015, 2018, 2021, and 2024.

### 3.6 Heat Stress Index

The HSI maps (Figure. 13) revealed that populations residing in highly built-up and poorly vegetated neighborhoods are exposed to significant heat stress risks. When cross-referenced with UAV-derived micro-green patches, it was evident that even small-scale vegetation contributed to localized cooling effects, reducing HSI scores in otherwise high-stress zones.

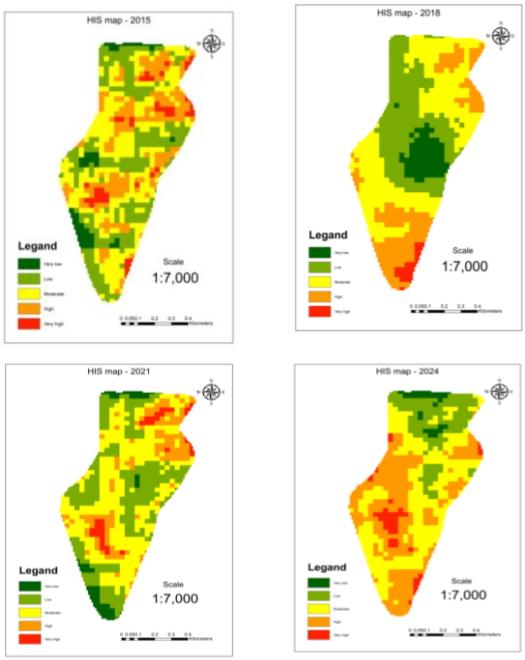


Figure 7. Heat Stress Index maps in 2015, 2018, 2021, and 2024.

## 4. Conclusions and Recommendation

This study presented a multiscale framework for assessing urban green space dynamics and heat stress through the integration of UAV-based ultra–high-resolution imagery and multi-temporal satellite datasets. The results demonstrate that urban green cover in the study area declined significantly between 2015 and 2024, accompanied by an expansion of built-up land and a corresponding rise in land surface temperatures. The derived vegetation and urbanization indices (NDVI, NDWI, NDBI, SAVI, and EVI) clearly highlighted the progressive loss of vegetation and intensification of urban expansion, while UAV orthophotos provided critical fine-scale validation of fragmented green patches that were not captured by Sentinel imagery alone.

Thermal analysis revealed increasing land surface temperatures across urbanized zones, with built-up areas consistently showing the highest heat intensities. The application of UTFVI and SUHI indices further confirmed that recently urbanized areas are particularly vulnerable to heat stress. Importantly, the integration of UAV data showed that even small-scale vegetation, such as roadside trees and pocket parks, exerts a measurable cooling effect, reducing local heat stress levels. This finding underscores the necessity of incorporating micro-green infrastructure into urban planning policies.

By validating satellite-derived classifications with UAV-based data, the study enhances the reliability of urban climate monitoring frameworks. The combined approach advances beyond previous studies limited to medium-resolution imagery, offering both regional trends and localized insights into urban environmental dynamics. These findings contribute to global discussions on urban resilience and climate adaptation, emphasizing the role of fine-scale vegetation management in mitigating the impacts of urban heat islands.

Future work should expand the use of UAV data across multiple time periods to capture temporal dynamics at fine resolution, as well as explore machine learning–based data fusion techniques for more accurate heat stress modeling. Overall, this research provides an evidence-based foundation for policymakers and urban planners to promote sustainable green infrastructure development and reduce heat-related risks in rapidly urbanizing cities.

## 5. References


Chen, X., Zhou, W., Pickett, S.T.A., and Li, W., 2022. Urban vegetation and heat stress: A multi-scale remote sensing approach. Remote Sensing of Environment, 280.

Li, X., Xu, H., and Guo, B., 2023. Downscaling land surface temperature using Sentinel-2 and machine learning. ISPRS Journal of Photogrammetry and Remote Sensing, 198, pp.47–61.

Mantey, S., Opoku, G., and Forkuo, E.K. ,2023. UAV-based mapping of urban vegetation: Implications for thermal comfort. Urban Forestry & Urban Greening, 84.

Peng, J., Wang, X., Chen, Y., and Liu, Y.,2023. Multiscale analysis of urban heat island intensity using UAV and Landsat data. Science of The Total Environment, 865.

Ranjan, R., Kumar, P., and Sharma, A.,2024. UAV–satellite data fusion for urban heat stress assessment. International Journal of Applied Earth Observation and Geoinformation, 129.

Weng, Q., Fu, P., and Gao, F., 2021. Generating daily land surface temperature at Landsat resolution by fusing Landsat and MODIS data. Remote Sensing of Environment, 264.

Xu, L., Zhou, W., and Huang, G.,2022. Evaluating urban heat stress with UTFVI and land cover dynamics. Ecological Indicators, 142.

Yang, J., Yu, Z., and He, C.,2023. Evaluating heat stress in global cities using remote sensing and urban indices. Urban Climate, 49.

Yao, R., et al. (2022). Monitoring urban heat island dynamics using Landsat and Sentinel data. Remote Sensing, 14(3), 637.

Zhou, D., Zhao, S., & Zhang, L. (2022). Urbanization and heat stress in Asian megacities. Environmental Research Letters, 17(11).

Iamtrakul P., Padon, A., Chayphong, S.,2024. Quantifying the Impact of Urban Growth on Urban Surface Heat Islands in the Bangkok Metropolitan Region. Thailand, Atmosphere 2024, 15(1), 100.

Jumari, N. A. S. K., Ahmed, A., Huang, Y., Ng, J., Koo, C.H., Chong, K.L., Sherif, M., Elshafie, A., 2023. Analysis of urban heat islands with landsat satellite images and GIS in Kuala Lumpur Metropolitan City. Heliyon, Volume 9, Issue 8, August 2023, e18424

Li, Y., Ren, B., Chen Y., Huang L., and Sun C., 2022. Multiscale spatiotemporal dynamics analysis of urban green space: Implications for green space planning in the rapid urbanizing Hefei City, China. Journal of Urban Ecology, Volume 10 – 2022.

Gibril, M.B.A., AI-Ruzoug, R., Ueda, N., Saeidi, V., Shanableh, A., Mansor, S., Shafri, H. M., 2020. Mapping Heterogeneous Urban Landscapes from the Fusion of Digital Surface Model and Unmanned Aerial Vehicle-Based Images Using Adaptive Multiscale Image Segmentation and Classification. Remote Sens. 2020, 12(7), 1081.

Thanvisitthpon, N. Nakburee, A., Khamchiangta, D., Saguansap, V., 2023.Climate change-induced urban heat Island trend projection and land surface temperature: A case study of Thailand's Bangkok metropolitan. Urban Climate, Volume 49, May 2023, 101484.

Trzeciak, M., Sikorska, D. 2024. Application of UAV and ground measurements for urban vegetation cooling benefits assessment, Wilanów Palace case study. Scientific Review Engineering and Environmental Sciences (SREES) 33(1):1-14

Arunima KAR, 2025.India Is Using AI and Satellites to Map Urban Heat Vulnerability Down to the Building Level. Wired, NESLETTERS

# Webinar

# From Blueprints to Digital Twin – A GIS-Based Smart Campus

Nicolas Luna[a] and Joaquin Huerta[a,*]

[a] *Universitat Jaume I, Spain; fluna@uji.es*

The development of a Smart Campus application at Universitat Jaume I (Spain) integrated 3D modeling, geospatial databases, and indoor navigation technologies to improve spatial management and accessibility. The project used Blender to generate high-quality 3D models of campus buildings from AutoCAD blueprints, providing a realistic and data-rich representation of university facilities. These models were integrated into ArcGIS Indoors within ArcGIS Pro, where a structured geospatial database was created to manage spatial units using unique identifiers.

Beyond building structures, the database was enriched with external data, many from OSM, incorporating points of interest such as waste bins, information kiosks, faculty and staff office locations, banking services, and printing services.

A key component of the project is multimodal navigation, implemented through 3D Network Analysis. This feature enables optimized routing for vehicles, bicycles, and pedestrians, facilitating efficient movement across the campus. Additionally, indoor navigation was deployed by publishing services in ArcGIS Enterprise and configuring the system using ArcGIS Online templates. This allows users to seamlessly transition between outdoor and indoor navigation, ensuring accessibility and efficient wayfinding inside university buildings.

The final result is a first version of a dynamic digital twin of the university campus, integrating 3D visualization, real-time spatial analysis, and interactive navigation. The next step is to connect to real-time building and exterior sensors to facilitate monitoring and analytics. This digital twin enhances decision-making processes, improves facility management, and provides students, faculty, and visitors with an intuitive tool to navigate and interact with campus spaces. The combination of ArcGIS Indoors, other GIS services, and 3D modeling establishes a smart campus framework that supports future expansions and innovations in university infrastructure. Multiple graduate students participated in its creation, providing them with a realistic digital twin experience that might later be applied to careers involving smart city projects that utilize similar software stacks.

***Keywords:*** 3D modeling, ArcGIS Indoors, Digital twin, GIS, Indoor navigation, Smart Campus

# Harnessing Deep Learning and Remote Sensing for Water Segmentation

Amina Said

*Dublin City University, Ireland; am.omarsaid@gmail.com*

Water is an important resource that occupies about 70% of the Earth's surface. However, the ongoing climate change has led to significant spatial variation of water bodies. Remote sensing has proven to be an effective tool in the study of water extent, which relies on the traditional approach of using spectral indices such as normalized difference water index (NDWI). With the advancement of technology and improved computational resources, deep learning models like U-NET have been adopted in segmentation of the water bodies. There is a rich amount of freely accessible satellite data with good spatial resolution, which facilitates the integration of deep learning techniques with remote sensing. This will improve the water body extraction accuracy, scalability and enable effective monitoring of water body changes.

***Keywords:*** deep learning, remote sensing, segmentation, water

# Stand age diversity (and more than climate change) affects forests' resilience and stability, although unevenly

Elia Vangi[a*], Daniela Dalmonach[a], Elisa Clocolo[b], Gina Marano[c], Leonardo Bianchini[b], Paulina Puchi[a], Elisa Grieco[a], Alessandro Cescatti[d], Andrea Colantoni[b], Gherardo Chirici[e], Alessio Collati[a]

[a] *CNR-ISAFOM, Italy,* elia.vangi@unifi.it*
[b] *University of Tuscia, Italy,*
[c] *ETH Zürich Switzerland,*
[d] *JRC,*
[e] *University of Florence, Italy*

Stand age significantly influences the functioning of forest ecosystems by shaping structural and physiological plant traits, affecting water and carbon budgets. Forest age distribution is determined by the interplay of tree mortality and regeneration, influenced by both natural and anthropogenic disturbances. Unfortunately, human driven alteration of tree age distribution presents an underexplored avenue for enhancing forest stability and resilience. In our study, we investigated how age impacts the stability and resilience of the forest carbon budget under both current and future climate conditions. We employed a state–of–the–science biogeochemical, biophysical, validated process–based model on historically managed forest stands, projecting their future as undisturbed systems, i.e., left at their natural evolution with no management interventions (i.e., forests are left to develop undisturbed). Such a model, forced by climate data from five Earth System Models under four representative climate scenarios and one baseline scenario to disentangle the effect of climate change, spanned several age classes as representative of the current European forests' context, for each stand. Our findings indicate that Net Primary Production (NPP) peaks in the young and middle-aged classes (16- to 50-year-old), aligning with longstanding ecological theories, regardless of the climate scenario. Under climate change, the beech forest exhibited an increase in NPP and maintained stability across all age classes, while resilience remained constant with rising atmospheric CO2 and temperatures. However, NPP declined under climate change scenarios for the Norway spruce and Scots pine sites. In these coniferous forests, stability and resilience were more influenced.

These results underscore the necessity of accounting for age class diversity –lacking in most, if not all, the current Global Vegetation Models – for reliable and robust assessments of the impacts of climate change on future forests' stability and resilience capacity. We, therefore, advocate for customized management strategies that enhance the adaptability of forests to changing climatic conditions, taking into account the diverse responses of different species and age groups to climate.

***Keywords:*** carbon cycle, climate change, forest resilience, forest age, forest management, modeling

# AI-Based Enrichment of Building Data for Urban Planning through Demographic Predictions

Fatemeh Rafiei [a,b,*], Robert Hecht [b,c], Angela Blanco Vogt [a]

[a] *Stuttgart University of Applied Sciences, 1st Author – fatemehrafiei1996@gmail.com, 3rd Author - angela.blanco-vogt@hft-stuttgart.de*
[b] *Leibniz Institute of Ecological Urban and Regional Development, 2nd Author - r.hecht@ioer.de*
[c] *Center for Scalable Data Analytics and Artificial Intelligence (ScaDS.AI) Dresden/Leipzig, Germany*

**Abstract:** Accurate demographic predictions at fine spatial resolution play a critical role in helping urban planners allocate resources efficiently for diverse populations. Traditional demographic data collection methods, such as censuses and surveys, suffer from limitations in frequency, spatial resolution, and cost, which make it difficult to capture dynamic demographic changes in urban areas. This research proposes a solution to address this gap by leveraging machine learning (ML) models to enrich building data with predicted demographic characteristics at the building level. The study uses Random Forest (RF) and EXtreme Gradient Boosting (XGBoost) as machine learning models for training the model in Stuttgart, Germany and testing in Dresden, Germany to examine the generalizability of the models across cities with different urban structures. The indicators for the training models were provided through feature engineering of various datasets, primarily using two-dimensional building data derived from 3D CityGML data, 100-meter grid census data, and OpenStreetMap points of interest (POI). The results show Random Forest (RF) outperformed XGBoost, being less affected by errors despite slightly different $R^2$ values. The population model performed very good ($R^2 \approx 0.75$), while residents' age predictions were weaker due to disaggregating demographic data from grids to buildings without building-level reference data. The POI data shows a minor effect on age pattern predictions and not the population itself. This research highlights potential of integrating ML with urban data as an alternative to traditional demographic data collection but enhancing building data quality and feature engineering could improve accuracy and better assess of POI impact.

***Keywords:*** Machine learning, Random Forest, EXtreme Gradient Boosting, Demographic prediction, Building data enrichment

## 1. Introduction

Different groups from different extents could be characterized by demographic data through categories such as age, gender, marital status, level of education and so on (Nettleton, 2014). The effective formulation, implementation, and evaluation of national master plans and social impact assessments, are dependent on the collection and analysis of such detailed socio-demographic data, particularly for large-scale projects (Tey et al., 2021). Traditionally, demographic data collection has been done through methods such as censuses, surveys and public records to provide the key insights which are required for data-driven decision-making (Fernandez et al., 2016). However, these conventional methods present significant drawbacks such as long-time intervals between data collection (e.g. census data is usually collected every 10 years), low levels of spatial resolution (Kunze & Hecht, 2015), the high costs associated with conducting surveys, uncertain accuracy due to declining response rates during the time (Sturgis & Luff, 2021), limitations in methodology (such as small sample sizes) and variations in data coding in each region (Tetzlaff et al., 2024). Furthermore, these drawbacks are also vulnerable to human errors (Fitzgerald & FitzGibbon, 2014), limit their utility in rapidly evolving environments (Sturgis & Luff, 2021). Moreover, in this rapidly changing situation, the integration of building datasets with demographic data is getting more essential for developers and decision-makers, as contextual indicator or neighbourhood level demographic data, often does not show the true distribution of people within a city. This makes it challenging for them to design services that meet the needs of specific groups, such as families having children. Predicting demographic data at the building level helps solve this issue by providing more precise insights into where different groups live and what they need (Georgati et al., 2024). Understanding who lives in a building also helps cities to manage resources efficiently, and create better policies for sustainability and urban development (Hecht et al., 2018). For instance, estimating the number of retirement homes needed in the future based on the capacity of existing homes and the current population of seniors (Burian et al., 2018). Also, building data only cover the physics and operation of buildings, so it needs demographic data to understand the socio-economic aspects for helping in decision making. Current methods for enrichment building data are often costly and time-consuming, highlighting the need for efficient solutions that decrease the required expertise (De Paoli et al., 2024). Considering these limitations, the interest in leveraging the more advanced technologies is increasing. Artificial Intelligence (AI), particularly Machine Learning (ML), is such an advanced technology used to enhance accuracy efficiency while enriching the data. Compared to traditional methods, machine learning algorithms can process large datasets more quickly and, when trained using comprehensive and high-quality datasets, have the potential to predict complex patterns with greater accuracy (Krasteva et al., 2023). Additionally, machine learning can continuously improve its predictions over time as it learns from new data, making it a valuable tool for adapting to changing conditions and needs. This study aims to develop and test an AI/ML-based approach to estimate population figures and the proportion of people over 65 and under 18 at individual building level. This data is crucial for urban planning as they influence infrastructure needs, service accessibility, and housing demand. By leveraging AI/ML models, we can incorporate external factors such as proximity to healthcare, public facilities, and other POIs to improve the accuracy of demographic predictions at the building level. For finding these trends, having an enriched dataset with indicators is essential. These indicators take two aspects of the buildings into account. One aspect is the morphological characteristics of the building itself, such as area, height, and volume, while the other is the contextual characteristics defined by the surroundings of the buildings (Biljecki & Chow, 2022) which will affect the demographic patterns. For

example, closeness to the park could make a zone more popular for elderly people. Various datasets, such as building data and Point Of Interest (POI) data, which cover the buildings and amenities in their surroundings, will be integrated as predictive indicators to enhance the accuracy of demographic predictions within the German context. This research structured as follows. After the introduction, problem statements, and defining the goal of this thesis in Section 1, Section 2 provides a review of relevant studies and presents the indicators used in this research. Section 3 defines the data used. Section 4 outlines the methodology. Section 5 presents the research results and discussions. Section 7 concludes the study by summarizing the findings and challenges.

## 2. Literature review

The distribution of statistical data from larger scales, such as the municipal level or grid systems, to smaller scales, such as individual buildings, is referred to as spatial disaggregation or dasymetric mapping (Eicher & Brewer, 2001). Recently, these approaches have been enhanced through machine learning (ML) methods, which learn patterns from data instead of relying on fixed assumptions and utilize ancillary information from various sources, leading to more accurate predictions (Georgati et al., 2024). Among ML techniques RF is a robust method that builds multiple decision trees from random subsets of training data, each considering a specific feature (Baccari et al., 2024). The final prediction is the average of all tree decisions, making RF reliable and resistant to noise. XGBoost, on the other hand, is a tree-based model that builds trees sequentially, each correcting the previous errors, which by learning noises from training data, is at risk of the overfitting (Chen et al., 2024). Both RF and XGBoost have shown high accuracy in uncovering relationships between building features and demographic patterns. In one study, Szarka & Biljecki (2022) applied the RF model to estimate demographic characteristics such as population, average age and the distribution of the senior population, achieving an accuracy of around 80%. They used the real estate data, POI data and demographic data. Their study in Singapore revealed that while real estate data alone produced strong predictions, POI data did not significantly improve results. However, they acknowledged that the impact of POI data may vary by region, as the result that they achieved was based on their specific study region, with similar patterns. In the German context another study, Reiter et al. (2024) developed an XGBoost machine learning method for population estimation, using LoD2 buildings and 2011 census demographics data. They find the relationships between building features and the number of inhabitants. The trained model was then used to estimate the population for 2022. After the estimation, a correction factor was applied to align the estimated municipal populations with the official figures. Then the accuracy was validated against 2023 reference data available for Munich, showing only a 3.3% difference in the total estimated population, which was quite well for them but they also report that the difference between the estimation year and reference data could also introduce some errors to the model. Our study aims to incorporate POI data to evaluate its effectiveness in predicting demographic characteristics in a German urban environment. This will provide insights into whether the inclusion of service and amenity data improves prediction accuracy in various urban contexts.

## 3. Methodology

### 3.1 Data

Several datasets were used in this research. Combining these various sources opens up opportunities for more precise analysis and improves the training process: 1. Building data (Zentrale Stelle Hauskoordinaten und Hausumringe) 2022, formatted to 2D by the Leibniz Institute of Ecological Urban and Regional Development (IÖR) includes 187583 buildings for Stuttgart and 162169 buildings for Dresden and structural details such as building volume, height, area, perimeter, usage, roof type and roof area.

2. Administrative boundaries (Bundesamt für Kartographie und Geodäsie) 2022, a 1 km pairwise buffer around Stuttgart and Dresden borders to ensure complete coverage of cities.

3. POI data (OpenStreetMap) 2024, extracted for areas within 1 km buffer of city borders, includes types for public services as key-value pair format. Key represents a category (e.g., "amenity") and the value provides specific details (e.g., "cinema" as a type of amenity).

4. Demographic data on grid level (Statistisches Bundesamt) 2022, includes population figures and age group proportions, which were collected at address level and aggregated at 100-meter grid cell level via the address coordinates.

5. House Coordinates data (Zentrale Stelle Geotopographie) 2022, consists of point data that provides the geographic location of buildings in easting/northing coordinates.

6. Block data (Zentrale Stelle Geotopographie) 2022, including the type of land use for each spatial unit containing the buildings (e.g., residential, Industrial and commercial).

7. Proximity and Accessibility data, created using the open source routing engine OpenRouteService (HeiGIT, 2024). The Directions API calculates the shortest distance and time between two positions. The Isochrones API generates accessibility regions.

### 3.2 Methods

This section describes the methodology of the study, detailing the processes of data preprocessing, information enhancement, model development and validation.

#### 3.2.1 *Pre-processing*

Preparing the dataset for the ML models carried out using Python programming language. To ensure consistency, all datasets projected to the ETRS89 / LAEA Europe coordinate reference system, which is suitable for analysis covering whole Germany. The datasets filtered using administrative boundaries to focus on the study areas. The demographic data was provided at the grid level, so each building had to be assigned to its corresponding grid to obtain the associated demographic values. The house coordinates (address points) used for this assignment; for buildings without address points, the assignment was based on the largest overlap between the building's footprint and a grid cell (Reiter et al., 2023). Overlay analysis revealed that some buildings had multiple address points, sometimes across different grids. Therefore, a combined method was applied. First, each building was initially assigned to the grid cell containing the largest portion of its footprint. Then, for buildings with a single address point, in cases of mismatch, the building was assigned to the address point's grid. Then the buildings filtered based on their usage, available in building dataset, to residential (including mixed-use) and non-residential buildings, to ensure that population data would be assigned only to residential buildings. Additionally, buildings with areas smaller than 10 m², likely representing balconies, garages, or similar structures, excluded, following the approach of Hartmann et al. (2016), noting that very small polygons often do not represent actual buildings.

#### 3.2.2 *Feature development*

Various characteristics are used as indicators for this study. These characteristics reflect the properties of the buildings, but also their proximity to POIs that may influence people's choice of place of residence. The indicators were selected based on previous studies, notably the work of Biljecki & Chow (2022). They were differentiated into two categories: building-level indicators and contextual indicators.

#### 3.2.3 *Building level indicators*

At the building level, the following building indicators were used to describe the morphology of the building: footprint area (A), roof area (RF_A), roof type (RF_TYPE), perimeter (C), height (H), volume (V), number of vertices (Vertices), number of floors (Floors), Minimum Bounding Rectangle Area (MBRA), wall area (WA), height to footprint area ratio (H2A), total building area (b_area), building complexity through the Equivalent Rectangular Index (ERI), evaluating how

much a polygon is different from a rectangle shape (Basaraner & Cetinkaya, 2017) and compactness using the Proximity Index (PI) (Angel et al., 2010). These indicators describe the shape and size of buildings, regardless of being residential or non-residential. However, according to Kunze & Hecht (2015) many residential buildings contain non-residential spaces, so by incorporating POI data, the area and volume of non-residential spaces can be deducted from the total building area and volume to have residential area (Res_area) and residential volume (Res_Vol) of the buildings as residential specific indicators.

#### 3.2.4 *Contextual indicators*

Contextual indicators refer to factors that describe different characteristics of the neighbourhood and on a higher scale, the form of the whole city. These indicators include: proximity or walking distance to the city centre (d2center) which reflects the compactness of the city (Angel et al., 2010), walking time to the city centre (t2center) which is the time required to walk to the city centre, fullness of built-up area (full_built), showing the share between the built-up areas and open space in a small neighbourhood (one percent of the total area) (Angel et al., 2010), fullness of residential area (full_res), which is the share between the residential areas and open space in a small neighbourhood (one percent of the total area). Additionally, three buffer zones of 50m, 100m, and 500m based on previous studies (Milojevic-Dupont et al., 2020; Zhang et al., 2020) used for generating some indicators based on them. While Biljecki & Chow (2022) defined various statistical measures (e.g., minimum and maximum), in this research only the average values are computed to have a general insight into these features behaviours: number of neighbouring residential buildings (NN_Xm), average distance from a residential building to its neighbouring residential buildings (AD_Xm), average height-to-distance ratio of neighbouring residential buildings (H2D_Xm), number of neighbouring residential and non-residential buildings (2NN_Xm), average distance from the residential building to its neighbouring residential and non-residential buildings (2AD_Xm) and average height-to-distance ratio of neighbouring residential and non-residential buildings (2H2D_Xm). Biljecki & Chow (2022) also utilized some indicators in the grid basis to analyse the urban morphology. In this research 100m grid cells from demographic data used as the reference for calculating the total area of buildings (area_grid), average height of buildings (avg_h_grid) and total residential volume of buildings (vol_grid). The mentioned indicators in the grids also calculated for each block of buildings, as described in Hecht (2014), blocks are essential spatial units for structuring urban areas and serve as a reference for calculating settlement patterns, making them a valuable basis for demographic data estimation. These indicators include total area of residential buildings (Ablock), average height of residential buildings (Hblock), total volume of residential buildings (Vblock), total area of buildings (residential and non-residential) (Ablock2), average height of buildings (residential and non-residential) (Hblock2) and total volume of buildings (residential and non-residential) (Vblock2). Finally, based on the study by Vale & Lopes (2023), an essential urban structure consideration is ensuring that different types and numbers of POIs are accessible within a 15-minute walk. This can influence population density patterns. They categorized OpenStreetMap POI data into ten types for their analysis. In this research, the same categorization was applied to the POIs data to assess the building accessibility to POIs including: supermarkets, markets, food shops (N_markets), sports and recreation (N_ Sports), retail (N_ Retail), parks and other green areas (N_ Parks), public service (N_ Public), culture and leisure (N_ Culture), eating & drinking establishments (N_ Eating), education (N_ Educate), healthcare (N_ Health) and religious (N_ Religion). Also, the total number of accessible POIs (Sum_poi) calculated.

#### 3.2.5 *Feature extraction and feature engineering*

Feature extraction and feature engineering are essential steps in the machine learning process,

which transform raw data into meaningful representations to enhance model performance. Feature extraction includes the process of deriving relevant indicators, such as area, directly from raw data to use in the model, while feature engineering involves processing extracted features to create new ones out of them. Feature extraction and technical processes in this study begin with the residential building dataset, which already contains volume, height, area, perimeter, roof type, and roof area. The dataset is supplemented with additional processed indicators (e.g., ERI). Number of floors was estimated by dividing the building height by an average floor height of 3 m. This value is based on Kunze & Hecht (2015), who reported that among different types of the buildings, most of them had floor heights of 3 m, with fewer at 3.5 m, and as the type of buildings in this research was not available, the 3 m was chosen. MBRA calculated by extracting the geometry of residential building, creating a rectangular polygon from these coordinates, and computing its area. Wall area is calculated by multiplication of perimeter and height. Height-to-distance ratio is calculated by dividing the height by footprint area. Total building area is calculated by multiplication of number of floors and footprint area. Equivalent Rectangular Index indicator is computed using the following formulas from Basaraner & Cetinkaya (2017):

$$k = \sqrt{A_{PN} / A_{MBRA}} \quad (1)$$

where $A_{PN}$ is the area of the polygon and $A_{MBRA}$ is the area of MBRA.

$$P_{EAR} = k \times P_{MBRA} \quad (2)$$

where $P_{EAR}$ is the perimeter of the equal-area rectangle and $P_{MBRA}$ is the perimeter of the MBRA.

$$ERI = P_{EAR} / P_{PN} \quad (3)$$

where $P_{EAR}$ is the perimeter of the equal-area rectangle and $P_{PN}$ is the perimeter of the polygon.

Proximity Index indicator based on Angel et al. (2010) determined by calculating the radius of an equal-area circle, extracting building corner points, measuring their distances to the building centroid and using following formulas:

$$PI = \frac{2}{3} R / \overline{d} \quad (4)$$

$$R = \sqrt{A_{PN} / \pi} \quad (5)$$

where $\overline{d}$ is the average distance from the building corner points to the centroid, R is the radius, and $A_{PN}$ is the area of the polygon.

Fullness was defined by creating a small neighbourhood area equal to 1% of the city boundary's area. Then, built-up area fullness calculated using dividing the area of all buildings in the neighbourhood by the total area of the neighbourhood, and residential area fullness calculated similarly, but ignoring non-residential areas. The other neighbouring metrics were derived from buffer analysis. Buffers of 50 m, 100 m, and 500 m were generated around each residential building. All buildings inside the created buffer, excluding the residential building itself, were counted as the number of neighbours. The average of the minimum Euclidean distance from the residential building to all neighbours in the buffer created the average distance indicator and the average height-to-distance ratio, considering all the neighbours in the buffer, produced the other indicator. The same procedures were repeated in the buffers, considering only residential neighbours to have the three other indicators. Proximity analysis involved measuring walking distance and time from each residential building as starting points to the commercial centre (common destinations for daily activities) of the two cities as destination points and using the ORS Directions endpoint to have the shortest path metric. Accessibility measures were obtained using the ORS Isochrones endpoint to generate 15-minute (900 s) isochrones around residential buildings. Following Vale & Lopes (2023), the number of POIs from ten mentioned categories within each isochrone was counted and stored as indicators. The total number of accessible POIs in each isochrone was then counted as another

indicator. POI data also helped identify partial non-residential usage within residential buildings, adapting the approach of Kunze & Hecht (2015). Their list of OSM key-value pairs includes the number of non-residential floors allocated to the different types of POIs, usage category, and a priority level. Their original list was updated to include newer pairs documented in the OSM Wiki and for some modifications, for example, "power"="generator" was treated as fully non-residential in the original study in Dresden, but here only one floor was assigned to this category. Based on Google Maps, verified that many such buildings in Stuttgart were primarily residential, with a small portion allocated for a generator. Categorizing the entire volume of these buildings as non-residential would exclude a significant portion of residential buildings from dataset. To account for positional inaccuracies, a 2 m buffer was applied to each POI before spatial joining with residential building data (Kunze & Hecht, 2015). Detected POIs were then linked to floors, avoiding overestimation. The calculated non-residential floor area and volume were subtracted from the total to obtain the residential area and volume. Based on the residential buildings in the grids, the grid-based metrics were also calculated, including: the total residential building area, average residential building height and total residential building volume, per grid. Finally, based on each building's residential volume, the population assigned to them using the following formula:

$$P_b = (V_b / V_g) \times P_g \quad (6)$$

where $P_b$ is the residential building population, $V_b$ is residential volume of the residential building, $V_g$ is the total grid residential volume, and $P_g$ is the grid population.

Based on the estimated population of each residential building and the shares of the population ages, the number of residents over 65 and under 18 was also allocated. Since no additional information on age distribution at the building level is available, it was assumed that all residential buildings within the same grid share the same proportions. Since the population at building level was also computed in this study, and age group shares were derived directly from the population, acknowledging potential error propagation. Additionally, based on Hecht (2014), ATKIS DLM blocks used in this study were five area codes of 41001: Residential, 41002: Industrial and commercial, 41006: Mixed-use, 41007: Special functional, 41008: Sports, recreation, and leisure. For each block, three metrics of total area, total volume, and average height were calculated twice, once for residential buildings only and once for both residential and non-residential buildings and then assigned to all buildings in the same block.

#### 3.2.6 *Model development*

Once all indicators generated, model development was conducted in the R programming language, following the approach of Szarka & Biljecki (2022), using the package called Caret (Classification And Regression Training), facilitated the model training, saved time, and employed the cross-validation method (Kuhn, 2008). In this method, the same model was run for 10 resamples of the dataset (folds), which are training/validation pairs with the lowest overlap, and the proportion of special data among each resample should be the same as the proportion of that data among the whole data (Stratification) (Alpaydin, 2014).

#### 3.2.7 *Model validation*

The focus of this study was to understand whether building and contextual features are related to demographic patterns and to explore the potential of using this methodology as a replacement for traditional methods. Model performance was assessed using the coefficient of determination ($R^2$) value. Metrics such as Mean Absolute Error (MAE) focus on quantifying the average size of errors, but do not indicate whether the features are useful for predictions. $R^2$ shows how well the input data explains the variance of the predictions. This value ranges from 0 to 1, where a value closer to 1 indicates a better fit of the model to the data. To investigate the contribution of individual characteristics, feature importance

analyses were conducted to more effectively evaluate their usefulness. In RF, the importance measured by the drop in accuracy when a feature is permuted, while in XGBoost, frequency and information gain measured the importance of features (Kuhn, 2008; Wang et al., 2021). Finally, for an additional validation, building-level predictions in Dresden were aggregated to grids and compared with official demographic data at grid level from the statistical office (Statistisches Bundesamt).

## 4. Results and discussion

In this chapter, the results of the analysis for two cities, Stuttgart and Dresden explained. The results are based on the prepared data, as explained in detail in section 4.3. To predict the total population, the proportion of the population over 65, and under 18. RF and XGBoost are trained in each case.

### 4.1 Population prediction model

Population prediction models trained on 94,332 residential (including mixed-use) buildings in Stuttgart and the average $R^2$ of the cross-validation folds of all indicators was 0.85 for RF and 0.87 for XGBoost. Reducing to 15 most important indicators (Figure 1) maintained performance (RF: 0.84, XGBoost: 0.88) while simplifying the model. Applying to Dresden (69,632 buildings), RF showed $R^2$ of 0.78, and XGBoost had $R^2$ of 0.75. RF demonstrated greater robustness to errors, exhibited lower error rates, and performed better in generalization; therefore, it was used for further validation with official statistical data at the grid level. Aggregated predictions showing that about 60% of grids had errors below 10 persons.

Figure 2 shows the difference between predicted values and reference data based on the Natural Breaks method, which groups the data, so that the values in the same group are similar, and different groups are as different as possible. Using land use classes from Dresden's open data portal (Dresden, 2025), the best performance was in single-family housing areas, including almost one-third of all buildings with a prediction error of maximum 2 persons, while the second-best performance was observed for multi-family houses (8%). The model had a stronger emphasis on structural attributes, but also captured contextual indicators, and residential volume and wall area were most important indicators. POI-related features do not play a role. Overall, high-quality building data proved crucial for population prediction. However, despite relying on several assumptions in distributing population across the grids, such as assigning non-residential uses, the prediction model still achieved an explained variance of over 70%.

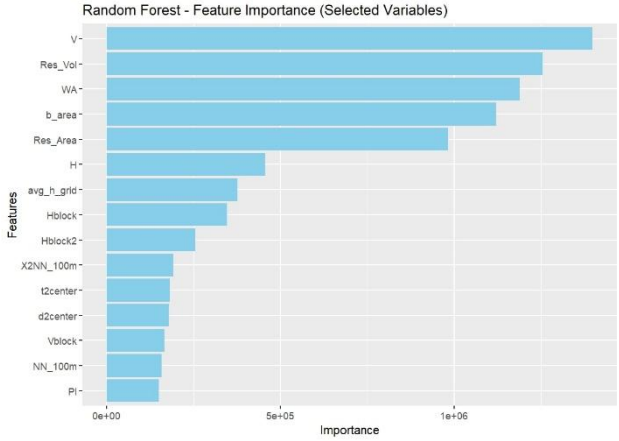


Figure 1. The top 15 important indicators for RF population prediction model of Stuttgart

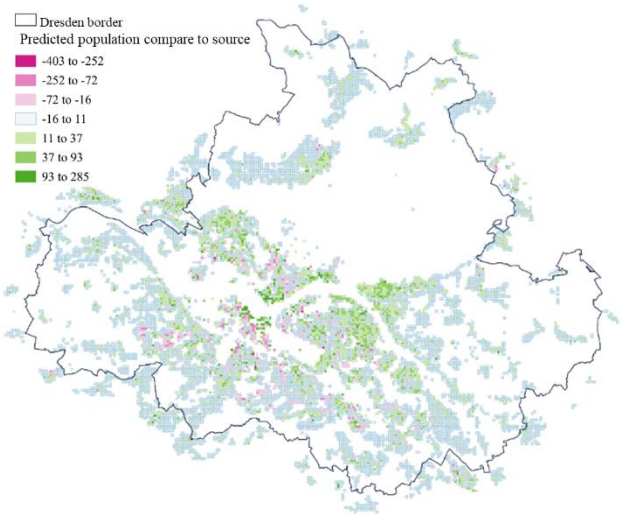


Figure 2. Population Difference Between Source Data and RF Model Predictions at the Grid Level in Dresden

#### 4.1.1 *Population prediction model for people over the age of 65*

For the over-65 population prediction models, residential buildings with zero elderly residents were included in the training to

enable the model to recognize that some buildings lack elderly occupants. Models utilizing all indicators achieved $R^2$ of 0.64 (RF) and 0.71 (XGBoost). Both showed lower accuracy compared to the population prediction models, with wall area and residential volume identified as the most important indicators. Two POI categories of eating and drinking establishments, as well as culture and leisure, were among the 15 most important indicators. Applied to Dresden, $R^2$ dropped considerably (RF: 0.36, XGBoost: 0.29), though RF generalized better, with almost 70% of buildings predicted within one person error (compared to the number of elderly calculated in this research). Grid-level validation revealed the reason for the low $R^2$ values. Large prediction errors primarily affected this metric, mainly due to buildings with unusually high elderly populations, such as retirement homes. Further feature engineering measures or special treatment of these particular buildings could help reduce errors. Another source of error stems from assuming a uniform age distribution when disaggregating grid data to buildings. Differences between real population shares and assigned shares especially in large buildings, can thus inflate prediction errors at the grid level. The best performance of this model was observed for single-family housing. Combining accurate building with detailed POI data could improve the results.

#### 4.1.2 *Population prediction model for people under the age of 18*

For the under-18 population prediction models, residential buildings with zero values were also included to ensure the model considers buildings without residents under 18. Training in Stuttgart with all indicators yielded $R^2$ of 0.67 (RF) and 0.75 (XGBoost), lower than the population prediction models. Key indicators were residential volume and wall area, while POIs had no effect. Applied to Dresden, the $R^2$ value dropped (RF: 0.35, XGBoost: 0.26), though RF performed better. Over 70% of buildings had an error of only one young person (compared to the number of young people calculated in this research). Same as over 65 population prediction model, high prediction for larger populations likely reduced $R^2$ and affected the grid-level validation, but overall accuracy was better than that model, due to fewer extreme values. The top-performing land use type was still single-family class. The precise building data remains key for assigning population correctly and the lack of POI suggests youth distribution is not tied to them.

## 5. Conclusion

The study underscores the potential of leveraging machine learning models to enhance demographic predictions at fine spatial resolutions, highlighting the effectiveness of using building-level and contextual indicators for population prediction, as well as the limitations and sensitivities of age-related models to data precision. The results indicate that, compared to the work of Szarka & Biljecki (2022), which was the primary reference for this research, key differences emerged: While their precise real estate dataset produced robust results, the models in this research relied on hypothesized building attributes, especially residential volume, reducing accuracy. Furthermore, their analysis incorporated significant indicators, such as building age, which were not available in this research. Although their results indicated that RF is robust to outliers, our models for age groups (under 18 and over 65) produced extreme residuals. They also suggested POIs are crucial for population prediction, but not age prediction, whereas this research showed the opposite. POIs influenced age-related models but not population prediction. Although these findings may change with more precise building data. During training, XGBoost performed slightly better, but RF outperformed it in testing using data from the other city. Despite dataset limitations, the population prediction model achieved high accuracy, indicating the methodology's potential for population estimation. However, age-related models are more sensitive to data precision and could be significantly enhanced with more accurate

building data and indicator values. To ensure robustness and generalizability, precise datasets should not be limited to areas with uniform housing structures: First, Szarka & Biljecki (2022) noted that their research was successful with data from a specific region provided by the Singapore's Housing and Development Board, suggesting that their approach may not be applicable to other areas due to differing housing structures and demographic data. Second, this research confirmed that errors predominantly occur in heterogeneous land uses, while more uniform structures, such as single-family housing, yield better results.

## 6. References


Alpaydin, E. (2014). Introduction to Machine Learning. MIT Press. https://books.google.de/books?id=NP5bBAAAQBAJ

Angel, S., Parent, J., & Civco, D. L. (2010). Ten compactness properties of circles: Measuring shape in geography. Canadian Geographies / Géographies Canadiennes, 54(4), 441–461. https://doi.org/10.1111/j.1541-0064.2009.00304.x

Baccari, N., Hamza, M. H., Slama, T., Sebei, A., & Rebai, N. (2024). Evaluation of SVM and RF Machine Learning Algorithms in Land Use/Land Cover Change Assessment: Tessa Watershed Case Study (Northwest of Tunisia). In Review. https://doi.org/10.21203/rs.3.rs-4359112/v1

Basaraner, M., & Cetinkaya, S. (2017). Performance of shape indices and classification schemes for characterising perceptual shape complexity of building footprints in GIS. International Journal of Geographical Information Science, 31(10), 1952–1977. https://doi.org/10.1080/13658816.2017.1346257

Biljecki, F., & Chow, Y. S. (2022). Global Building Morphology Indicators. Computers, Environment and Urban Systems, 95, 101809. https://doi.org/10.1016/j.compenvurbsys.2022.101809

Burian, J., Zimmermannová, J., & Macků, K. (2018). Urban Planner as a tool for demographic development planning in the cities.

Chen, C.-Y., Koch, F., & Reicher, C. (2024). Developing a two-level machine-learning approach for classifying urban form for an East Asian mega-city. Environment and Planning B: Urban Analytics and City Science, 51(4), 854–869. https://doi.org/10.1177/23998083231204606

De Paoli, F., Ciavotta, M., Avogadro, R., Hristov, E., Borukova, M., Petrova-Antonova, D., & Krasteva, I. (2024). An interactive approach to semantic enrichment with geospatial data. Data & Knowledge Engineering, 153, 102341. https://doi.org/10.1016/j.datak.2024.102341

Dresden. (2025). Open data portal of the administration of Dresden. https://opendata.dresden.de/informationsportal/?open=1&result=B227E19161714861B33B65D3548385E2#app/mainpage////

Eicher, C. L., & Brewer, C. A. (2001). Dasymetric Mapping and Areal Interpolation: Implementation and Evaluation. Cartography and Geographic Information Science, 28(2), 125–138. https://doi.org/10.1559/152304001782173727

Fernandez, T., Godwin, A., Doyle, J., Verdin, D., Boone, H., Kirn, A., Benson, L., & Potvin, G. (2016). More Comprehensive and Inclusive Approaches to Demographic Data Collection. 2016 ASEE Annual Conference & Exposition Proceedings, 25751. https://doi.org/10.18260/p.25751

Fitzgerald, G., & FitzGibbon, M. (2014). A Comparative Analysis of Traditional and Digital Data Collection Methods in Social Research in LDCs—Case Studies Exploring Implications for Participation, Empowerment, and (mis)Understandings. IFAC Proceedings Volumes, 47(3), 11437–

11443. https://doi.org/10.3182/20140824-6-ZA-1003.02796

Georgati, M., Monteiro, J., Martins, B., Keßler, C., & Hansen, H. S. (2024). Modeling population distribution: A visual and quantitative analysis of gradient boosting and deep learning models for multi-output spatial disaggregation. Transactions in GIS, 28(2), 130–153. https://doi.org/10.1111/tgis.13130

Hartmann, A., Meinel, G., Hecht, R., & Behnisch, M. (2016). A Workflow for Automatic Quantification of Structure and Dynamic of the German Building Stock Using Official Spatial Data. ISPRS International Journal of Geo-Information, 5(8), 142. https://doi.org/10.3390/ijgi5080142

Hecht, R. (2014). Automatische Klassifizierung von Gebäudegrundrissen: Ein Beitrag zur kleinräumigen Beschreibung der Siedlungsstruktur. Rhombos-Verl.

Hecht, R., Herold, H., Behnisch, M., & Jehling, M. (2018). Mapping Long-Term Dynamics of Population and Dwellings Based on a Multi-Temporal Analysis of Urban Morphologies. ISPRS International Journal of Geo-Information, 8(1), 2. https://doi.org/10.3390/ijgi8010002

HeiGIT. (2024). Open Route Service. https://openrouteservice.org/

Krasteva, I., Petrova-Antonova, D., Paoli, F. D., Hristov, E., Borukova, M., Ciavotta, M., & Avogadro, R. (2023). Geospatial Enrichment of Urban Data for Advanced City Planning: A Pilot Study. 2023 IEEE International Conference on Big Data (BigData), 3139–3143. https://doi.org/10.1109/BigData59044.2023.10386822

Kuhn, M. (2008). Building Predictive Models in R Using the caret Package. Journal of Statistical Software, 28(5). https://doi.org/10.18637/jss.v028.i05

Kunze, C., & Hecht, R. (2015). Semantic enrichment of building data with volunteered geographic information to improve mappings of dwelling units and population. Computers, Environment and Urban Systems, 53, 4–18. https://doi.org/10.1016/j.compenvurbsys.2015.04.002

Milojevic-Dupont, N., Hans, N., Kaack, L. H., Zumwald, M., Andrieux, F., De Barros Soares, D., Lohrey, S., Pichler, P.-P., & Creutzig, F. (2020). Learning from urban form to predict building heights. PLOS ONE, 15(12), e0242010. https://doi.org/10.1371/journal.pone.0242010

Nettleton, D. (2014). Incorporating Various Sources of Data and Information. In Commercial Data Mining (pp. 17–47). Elsevier. https://doi.org/10.1016/B978-0-12-416602-8.00003-0

Reiter, D., Hecht, R., & Jehling, M. (2024). Mapping access to medical service provision at micro-scale: Dynamics in supply and demand in Germany. Raumforschung Und Raumordnung | Spatial Research and Planning, 82(4), 322–337. https://doi.org/10.14512/rur.2278

Reiter, D., Jehling, M., & Hecht, R. (2023). Benefits of using address-based dasymetric mapping in micro-level census disaggregation. AGILE: GIScience Series, 4, 1–7. https://doi.org/10.5194/agile-giss-4-38-2023

Sturgis, P., & Luff, R. (2021). The demise of the survey? A research note on trends in the use of survey data in the social sciences, 1939 to 2015. International Journal of Social Research Methodology, 24(6), 691–696. https://doi.org/10.1080/13645579.2020.1844896

Szarka, N., & Biljecki, F. (2022). Population estimation beyond counts—Inferring demographic characteristics. PLOS ONE, 17(4), e0266484. https://doi.org/10.1371/journal.pone.0266484

Tetzlaff, F., Sauerberg, M., Grigoriev, P., Tetzlaff, J., Mühlichen, M., Baumert, J., Michalski, N., Wengler, A., Nowossadeck,

E., & Hoebel, J. (2024). Age-specific and cause-specific mortality contributions to the socioeconomic gap in life expectancy in Germany, 2003–21: An ecological study. The Lancet Public Health, 9(5), e295–e305. https://doi.org/10.1016/S2468-2667(24)00049-5

Tey, N. P., Talha, R., Abdul Rahman, E. N., & Ismail, M. F. (2021). SPATIAL DEMOGRAPHIC DATA FOR PLANNING AND RESEARCH. PLANNING MALAYSIA, 19. https://doi.org/10.21837/pm.v19i15.927

Vale, D., & Lopes, A. S. (2023). Accessibility inequality across Europe: A comparison of 15-minute pedestrian accessibility in cities with 100,000 or more inhabitants. Npj Urban Sustainability, 3(1), 55. https://doi.org/10.1038/s42949-023-00133-w

Wang, J., Luo, H., Li, W., & Huang, B. (2021). Building Function Mapping Using Multisource Geospatial Big Data: A Case Study in Shenzhen, China. Remote Sensing, 13(23), 4751. https://doi.org/10.3390/rs13234751

Zhang, J., Cui, P., & Song, H. (2020). Impact of urban morphology on outdoor air temperature and microclimate optimization strategy base on Pareto optimality in Northeast China. Building and Environment, 180, 107035. https://doi.org/10.1016/j.buildenv.2020.107035

# Mapping Climate Memory: Climate Justice, Indigenous Counter-Mapping, and OpenSource Empowerment in Arabic and Welsh Multi-Ethnic Language Outsider Communities

Rupert Allan

*Royal Scientific Society (Jordan), Cambridge University (UK); mail@rupertallan.com*

This paper examines evidence from multi-ethnic indigenous participatory OpenStreetMapping work as community-designed place-making practice. OpenStreetMap has been called 'the wikipedia of maps', one of the OpenSource 'liberation technologies' increasingly populating thinking in GIS, public policy and human rights. Comparing multi-ethnic precarious groups in the Black Desert of the Levant (Jordan) with indigenous historically displaced communities in the Green Desert of the Cambrian Ucheldir/Uplands (Wales), this paper looks to discuss these parallels in the context of OpenStreetMap community-led participatory mapping, where Community Archive is generated by the local people themselves as auto-ethnography in their own language. Here, not only the survey answers are decided by the community, but the questions themselves.

In the drying-out desert oasis of Al Azraq, Jordan, Bedouin, Druze, Palestinian, Syrian and Chechen groups have cohabitated since it served as the headquarters of T.E.Lawrence and before. This land has progressed from wetland to arid desert within living memory as a result of localised water extraction and global climate change. Even the younger generation remember fish and wildlife in what are now arid dusty plains.

In the Cambrian Mountains communities carry clearly remembered childhood memories of dwellings in thriving mountain settlements which now stand in ruins, forested-over by over-enthusiastic policy-makers less than two generations ago. Community life has witnessed withdrawal of public transport, schools and social infrastructure from this once central heartland of cultural heritage, now designated an area of mass deprivation.

Findings across each of these projects reveal many parallels: land-features are prominent; the connections with practical, rural horseback life are strongly evident, still-used, and very 'mappable' in both landscapes. Abandoned villages litter both of these deserts, standing in ruins as testimony to multiple forced/voluntary displacements. These settings carry stories of mining, dynamite, camel-racing and community toponymy. In each context, intergenerational memory is bound-up in the practices, coping mechanisms and adaptations of multiple cultural approaches and languages.

How do people invisage their place-based lived experiences of climate and cultural change on this scale, and at this speed? What geospatial indicators can communities now devise in the OpenSource revolution to express climate memory in the Arabian Peninsula and in the Green Desert in new ethnographic ways? And how can displacement, livelihoods and wider determinants of well-being be visualised in the universal spatial language of the wiki-map?

# ML Insights for Climate Change and Snow-melt Dynamics in Pakistan

Dawood Ahmed[a], Muhammad Shees Saleem[a], Saira Bano[b], *Shahid Parvez[a]

[a]*Institute of Space Science,*
[b]*College of Earth & Environmental Sciences, University of the Punjab, Lahore, Pakistan, shahid.spsc@pu.edu.pk*

Glacial melt and snow cover changes in Northern Pakistan are more than just environmental shifts. They are powerful signals of how climate variability is reshaping this region. These changes directly affect water availability and the resilience of ecosystems that depend on seasonal snow and ice. In this study, we used a data-driven approach to predict Snow Melt (SM) and Snow Cover Area (SCA), combining remote sensing derived datasets like GLDAS and MODIS with advanced machine learning techniques. We tested five predictive models (Random Forest, Support Vector Machine, K-Nearest Neighbors, Gradient Boosting, and Linear Regression) across historical data spanning 1948 to 2014 for SM, and 2001 to 2014 for SCA. Before modeling, we applied rigorous preprocessing steps to clean and transform the data, including outlier removal and statistical normalization. We also addressed multi-collinearity to ensure more reliable predictions. Gradient Boosting and Random Forest performed best for SM prediction, with high accuracy ($R^2$ = 0.9254 and 0.9233). SCA prediction was less robust due to limited long-term data ($R^2 \leq 0.20$), yet trends were revealing. From 2001 to 2014, SCA declined steadily, with notable variability in 2004, 2009, and a sharp drop in 2012. Monthly climatology showed snow cover peaking in March–April (~$3.8 \times 10^{12}$ km²) and reaching a minimum in July–August (~$9.0 \times 10^{11}$ km²). SM followed a similar seasonal pattern, peaking in April (0.104 kg/m²) and dropping to near-zero in winter. By combining machine learning with remote sensing and climate data, this study offers a scalable and robust framework for cryosphere monitoring and water management in Northern Pakistan.

***Keywords:*** Machine Learning, Remote Sensing of Environment, Climate Change, Snow Melt, Snow Cover Area.

# Temporal Monitoring to Track the Health of Olive Trees and Increase Their Productivity Under Global Climate Change for the Assessment of Biophysical Parameters and Soil and Water Properties in the Tabarjal/ Al-Bassita Area (Al-Jouf Region-Kingdom of Saudi Arabia) Using Medium- and High-Resolution Satellite Imagery (Sentinel-1, Sentinel-2, and WorldView-3).

N. I. Abd El Hamed [a],*, Ali A. Aldosari [b]

[a] *Department of Physical Geography, J. W. Goethe-University Frankfurt a.M., Germany.*
**National Authority for Remote Sensing and Space Sciences (NARSS) , Cairo, Egypt; Nabila_gis@hotmail.com*
*b Geography Department, King Saud University, Building 16, Ground Floor, Office AA 106, 11451 Riyadh, Saudi Arabia. Email: adosari@ksu.edu.sa*

**Abstract**: This study investigates the temporal monitoring—monthly, annually, and occasionally daily—of olive tree growth, focusing on intensive olive plantations known for their rapid growth, unique morphology, denser planting arrangements, and increased annual yields compared to traditional methods. The research is conducted in the Tabarjal and Al-Bassita regions of Al-Jouf Province, Saudi Arabia. Monitoring utilises freely accessible medium- and high-resolution satellite images from Sentinel-1 (radar) and Sentinel-2 (optical), which are provided by the European Space Agency's Copernicus program. Sentinel-2 imagery significantly improves Earth observation services by offering essential data for land cover change mapping and assessing vital biophysical parameters, such as Leaf Area Index (LAI), Leaf Chlorophyll Content (LCC), and Leaf Cover (LC). The main goal is to provide accurate, up-to-date land cover information to aid environmental monitoring, climate change research, and the management of extensive agricultural operations, especially where on-ground monitoring faces labor constraints. Major agricultural companies like Al-JOUF and NADEC are increasingly adopting advanced technologies, including ground-based meteorological stations, to oversee their operations. This research enhances such efforts by offering digital geospatial monitoring services, particularly for pinpointing areas with poor soil conditions that could impact crop health and productivity. The results also support broader applications in spatial planning, forestry management (for olive, palm, and fruit trees), regional water resource management, agriculture, and food security.

***Keywords:*** Olive Trees (Arbosana, Arbequina), Sentinel 1& 2, Leaf Area Index (LAI), Leaf Chlorophyll Content (LCC), Leaf Cover (LC), Land Cover Monitoring, Climate Change, Precision Agriculture, Tabarjal, Al-Bassita, Al-Jouf, NADEC, Saudi Arabia.

## 1. Introduction

The Al-Jawf region is one of the most fertile areas in the Kingdom of Saudi Arabia. Basita Center, in the Al-Jawf region of Tabarjal Governorate, is known as the "breadbasket of the Kingdom" due to its fertile soil e.g. Torrifluvents/Entisols, calcaric fluvisols (Fine-loamy, mixed, superactive, calcareous, Typic Torrifluvents, irrigated soils in desert regions) and flood terraces, moderate summer climate, and abundant fresh groundwater. The region is famous for its olive tree cultivation, producing 67% of the Kingdom's domestic olive oil and 150,000 tonnes of dates annually. Al-Jawf is also a significant agricultural hub, growing dates, grains, fruits, and vegetables. Its olive cultivation, which started in 2007 and has expanded to become the largest organic olive grove in the Middle East, now accounts for 2% of the world's olives. With over 15 million olive trees spread across 12,000 farms and 3,000 agricultural projects (Rabeh et al., 2017), Al-Jawf produces approximately 100,000 litres of oil and 15,000 kg of table olives.

The region's success is attributed to its adoption of "intensive olive farming," a modern technique enabling the cultivation of 1,600 trees per hectare, in contrast to the 200 trees per hectare typically grown under traditional methods. The number of trees planted in this way in Al-Jouf is about 5 million trees. With the great demand for olive products, residents of the region have expanded their investments in the olive tree and its many derivatives, such as the manufacture of soap and cosmetics, as well as the manufacture of charcoal from the residues of olive pressing, known as "peat".

The aim of this study is to develop a methodology for the mapping of olive farms on a sub-tree scale. For this purpose, multispectral images were acquired for the Basta'a region, where most of the olive farms and crops are concentrated.

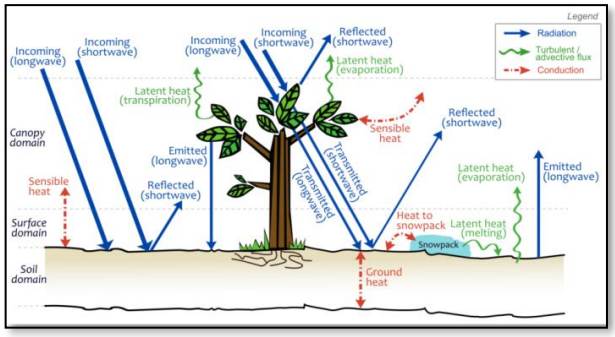


Figure 1: Energy balance cycle (reflections and emissions) and its effect on plants (Source: Manita and Silverman, 2013).

The study's comprehensive processing series of satellite visualisations can be considered as suitable for operational olive tree monitoring in order to address potential stresses, which for example may occur in a part of the tree rather than the whole tree, as a result of local climate change, ‘increased’ drought years, high temperatures and heat waves affecting flowering, fruit formation and ripening, disease characteristics, or inappropriate agricultural practices such as lack of fertilizers.

SENTINEL-2 imagery is currently making a significant contribution to land monitoring services through its frequent and regular coverage every 10 days, providing the necessary data (Figure ) that are used to map land cover and its changes, and supporting the assessment of biophysical parameters such as leaf area index (LAI), leaf chlorophyll content (LCC) and leaf cover (LC) (Figure 2).

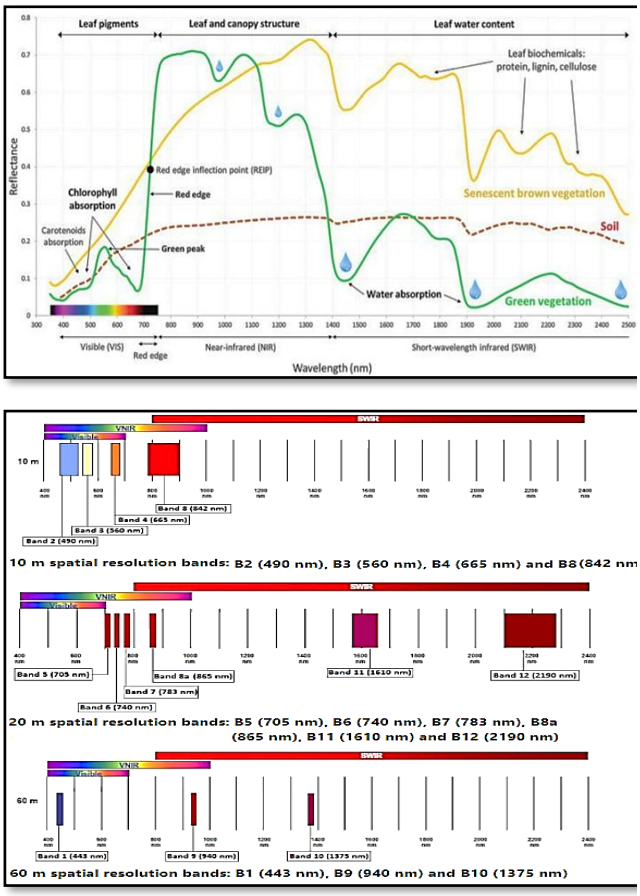


Figure 2: Spatial resolution and spectral bands of SENTINEL-2 (Spectral Vegetation Signatures).

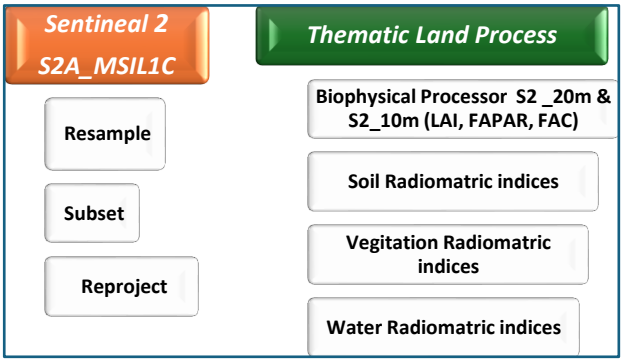


Figure 3: Methods for processing and analyzing multispectral SENTINEL-2 images to infer olive tree characteristics

## 2. Biophysical Processor (S2 (20m-10m))

To some extent, empirical statistical methods are used to extract vegetation information from spectral indices and reflectance, such as using specific wavelengths of the electromagnetic spectrum known to be sensitive to the vegetation variables being investigated. Therefore, the algorithm is calibrated to obtain reflectance values above the tree canopy. This depends on the geometric method of data collection and therefore requires slope-corrected reflectance to provide the best results. The biophysical processor calculates Level 2b for the Sentinel-2 biophysical products. From the reflectance data measured above the tree canopy, we can infer a set of biophysical variables, namely:

- Leaf Area Index (LAI)
- Fraction of Absorbed Photosynthetically Active Radiation (FAPAR,
- Fraction of Vegetation Cover (FVC/ Fcover)
- Chlorophyll content in the leaf (CCL /CAB)
- Canopy Water Content (CWC)

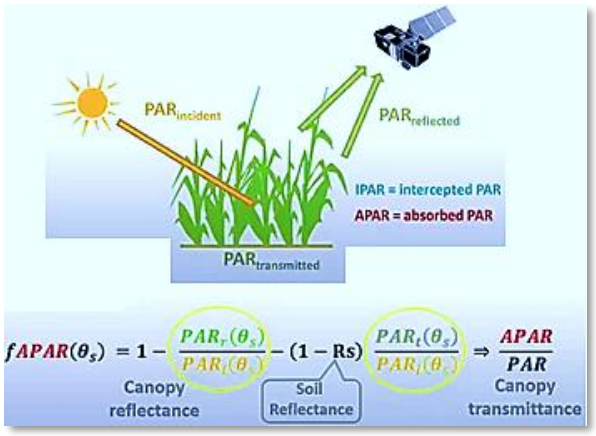


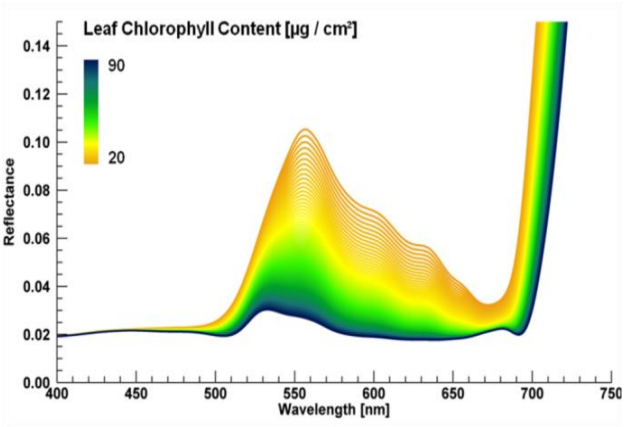


Figure 4. Graph of leaf area index and method of calculating FAPAR as a fraction of photosynthetically active radiation absorbed by plants

The S2 Toolbox biophysical variables retrieval algorithm relies on specific radiative transfer models associated with robust assumptions, particularly regarding tree canopy geometry (turbid medium model). All variables derived from these algorithms must be considered valid,

meaning that variables corresponding to the measured satellite signal reflected by a canopy must meet and be consistent with all assumptions made by the radiative transfer models. Depending on the variable, this may lead to discrepancies with ground values accessible from field measurements, which were made impossible due to the lockdown conditions imposed by the 2019-2021 COVID-19 pandemic. Furthermore, the algorithm is "generic," meaning it should be applicable to any vegetation type with the same reflectance. One of the strong assumptions built into any single-pixel retrieval algorithm such as this is that the target pixel belongs to a horizontal patch with sufficient homogeneity (at the pixel scale) to prevent unexpected loss or gain of radiation fluxes.

LAI and CAB are two biophysical indicators of crop health and are essential for yield prediction. The objective of this study is to determine the best method for estimating LAI and CAB for operational use in monitoring agricultural areas (Figure 3). Spectral indices for vegetation analysis are developed based on the principle that healthy vegetation strongly reflects in the near-infrared (NIR, Brown et al., 2019) spectrum while strongly absorbing the visible When characterizing vegetation function by biophysical indices, such as leaf area index (LAI), fraction of absorbed photosynthetically active radiation (FAPAR), and fractional vegetation cover (FVC), LAI is generally defined as half of the total green leaf area per unit ground surface area (Figure 5, A & B).

However, since remote sensing is a single-angle observation and is not sensitive to potential variation in leaf distribution within the canopy, which assumes a random distribution of leaves within the canopy volume, it is an informative index related to foliage clumping. While FAPAR measures the fraction of radiation absorbed by leaves in the 0.4-0.7 µm spectrum Figure 5, E & F), FVC is the ratio of the vertically projected area of vegetation to the total surface area (Figure 5, C & D).

*14-08-2015 S2A MSIL C1*

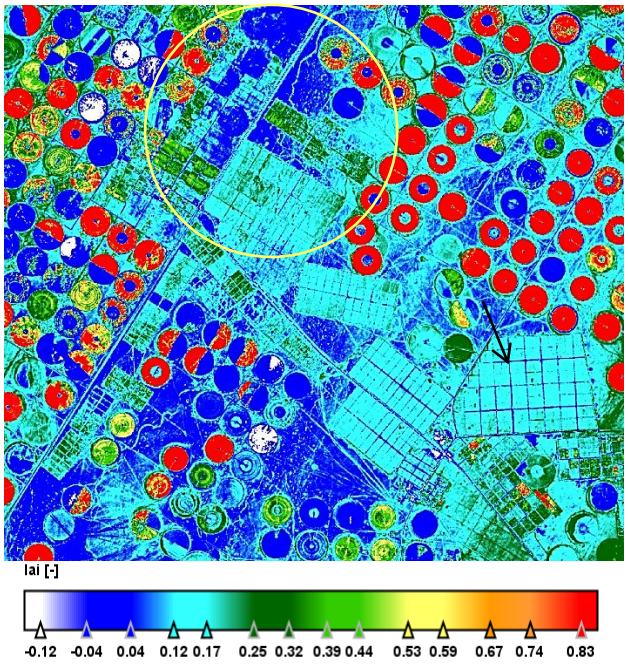


**A** *Leaf Area Index (LAI)*

***Younger or middle-aged plants have a different leaf area index (LAI), and elderly plants have a lighter milky tint.***

*14-08-2015 S2A MSIL C1*

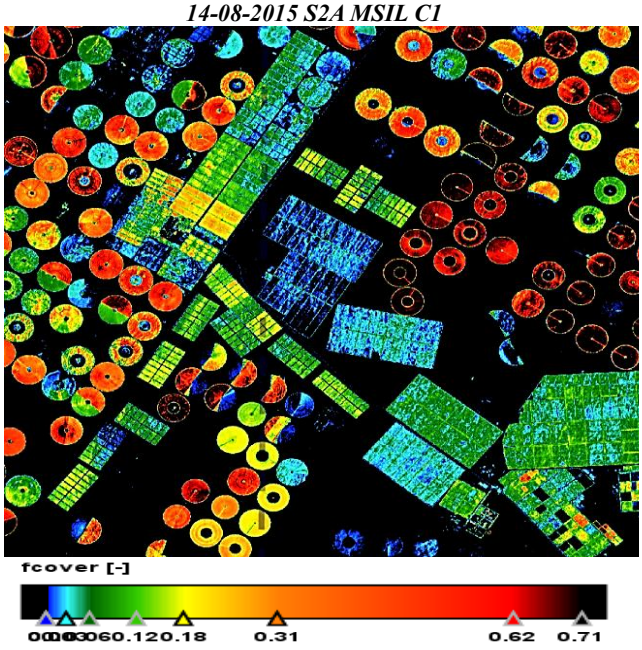


**C** *Fraction of Vegetation Cover (FVC/ Fcover)*

***The state of agriculture in 2015: crops and vegetables are grown in pivot irrigation circles, while olive fields are squares.***

*23-07-2021 S2A MSIL C1(6 Years Difference)*

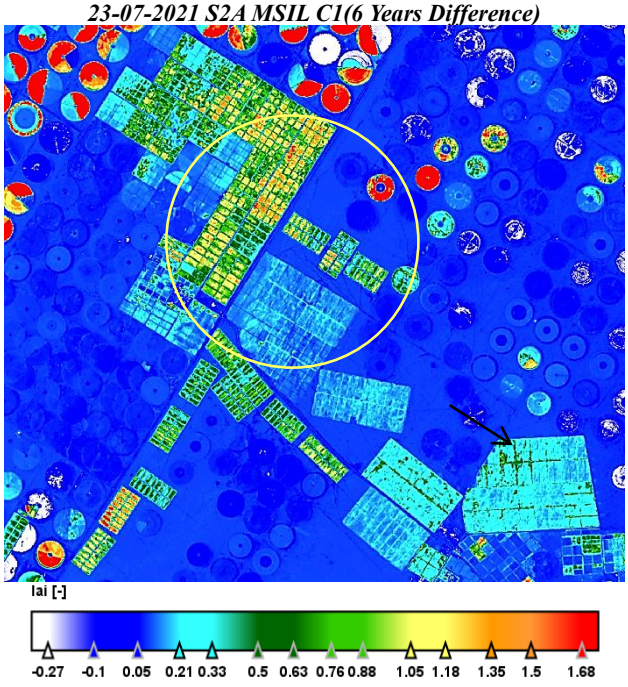


**B** *Leaf Area Index (LAI)*

*Growth stages / difference in leaf shape/area composition (maturity stage) and old farms appear in a light milky colour.*

*23-07-2021 S2A MSIL C1(6 Years Difference)*

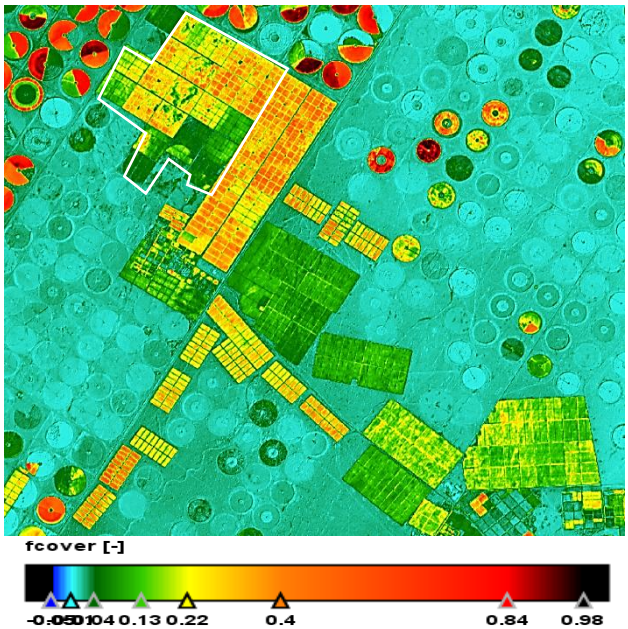


**D** *Fraction of Vegetation Cover (FVC/ Fcover)*

*14-08-2015 S2A MSIL C1*

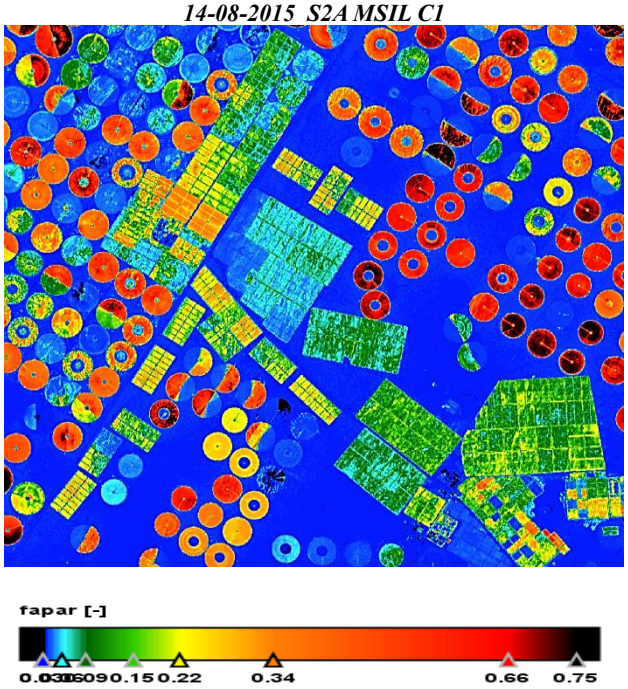


**E** *Fraction of Absorbed Photosynthetically Active Radiation (FAPAR)*

*In older plants (2015), light absorption is constant.*
*23-07-2021 S2A MSIL C1(6 years Difference)*

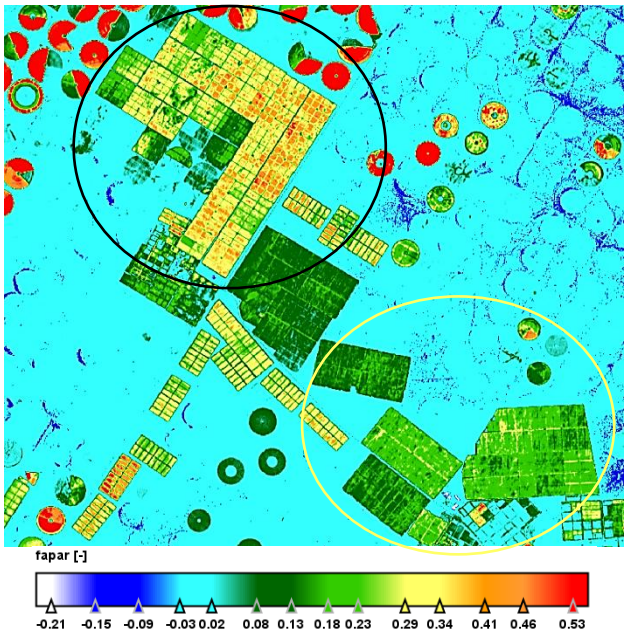


**F** *Fraction of Absorbed Photosynthetically Active Radiation (FAPAR)*

*Intense olive culture (ripening stage) exhibits high light absorption, whereas older cultivation (2021, yellow circle) exhibits a stable state.*

Figure 5. Time comparison (A-F, 6 years difference) of Sentinel 2 images for 2015 and 2021 to infer plant characteristics using Biophysical Processor.

Due to their high capabilities in describing the energy and momentum exchange between the surface and the atmosphere, LAI and FAPAR are recognized as essential climate variables (ECVs) by the Global Climate Observing System (GCOS) in terrestrial ecosystems for monitoring and modeling large-scale agroeco-systems. ECVs play a vital role in climate and hydrological cycles through plant transpiration, photosynthesis, and surface transpiration. Therefore, fine spatial resolution products of LAI, FAPAR, and FVC are essential for various applications, especially in heterogeneous landscapes for monitoring and modelling large-scale agroecosystems.

## 3. Inferring Chlorophyll Content in Plants

Remote sensing information from the early stages of the growth period can be used to quantitatively measure appropriate fertilizer demand, enabling optimal crop growth, which is particularly dependent on nitrogen supply. Since nitrogen content is directly related to chlorophyll content and, consequently, photosynthesis, its supply is most important for crop growth and productivity (Error: Reference source not found, B). If nitrogen supply is too low (Error: Reference source not found, A), chlorophyll becomes ineffective and declines, leading to reduced yield and economic loss. Conversely, if nitrogen supply is too high, it is washed out and seeps into water bodies, leading to eutrophication of aquatic ecosystems (Error: Reference source not found, A), as well as economic losses. Consequently, knowledge of canopy chlorophyll (Error: Reference source not found, B) concentration is of great importance for assessing nitrogen variability and stress.

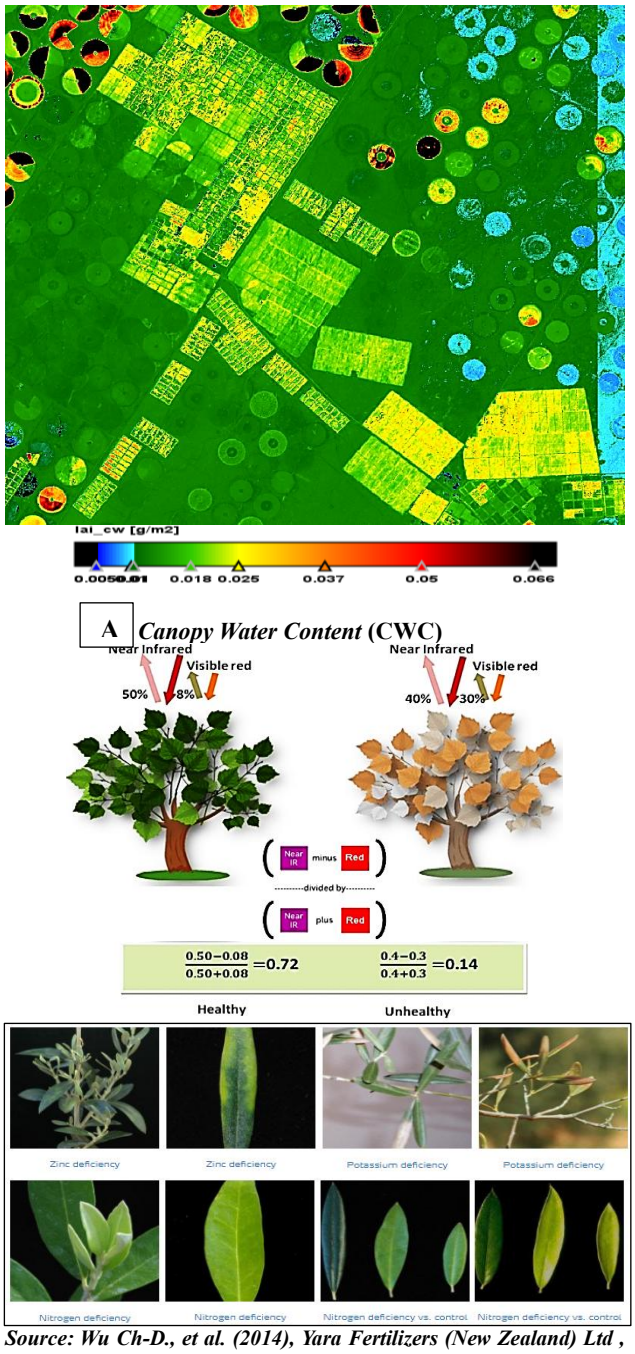


***Source: Wu Ch-D., et al. (2014), Yara Fertilizers (New Zealand) Ltd , 2021.***

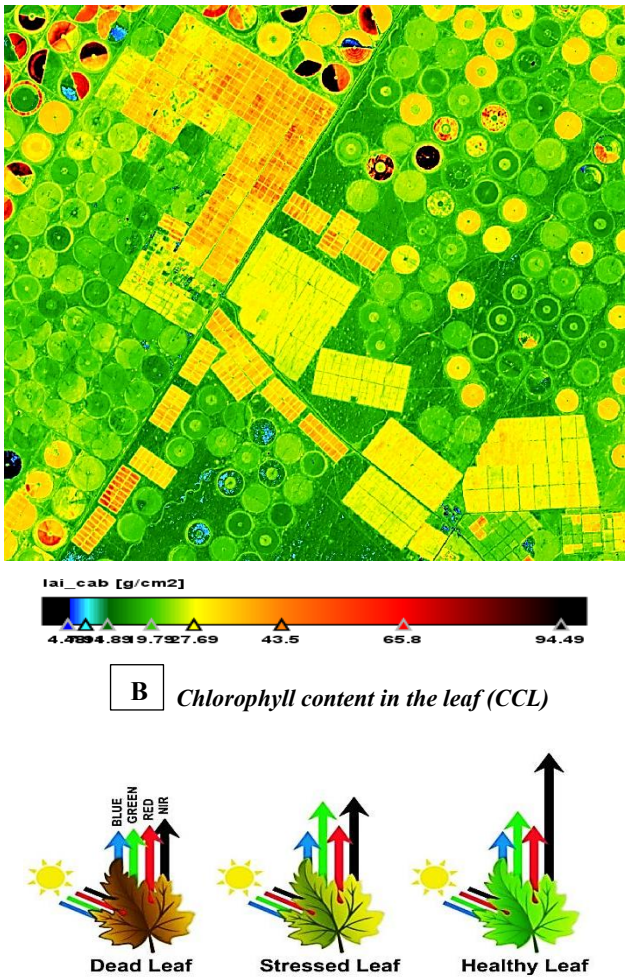


Figure 6. Deduction of chlorophyll and water content in plants (2021).

*Moisture Stress Index (MSI) 2015*

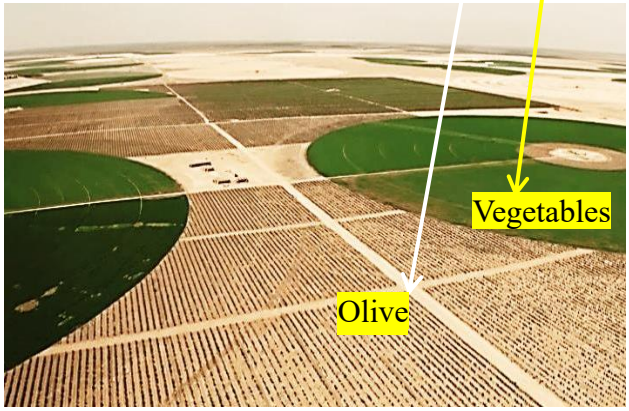


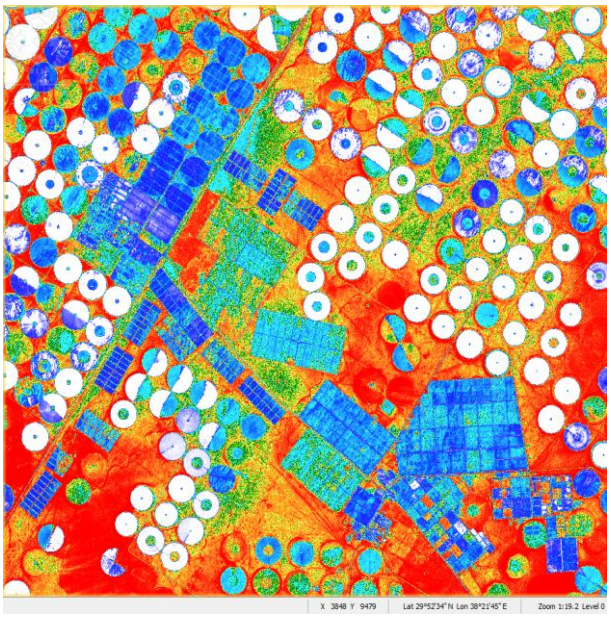

*NDTI water content (2015)*

Figure 7: Deduction of moisture content in plants (for the year 2015).

The Moisture Stress Index (MSI) is a reflectance measurement sensitive to increasing leaf water content (Figure 7). As leaf water content increases in vegetation canopies, the absorbance increases around 1599 nm. The absorbance at 819 nm is virtually unaffected by changing water content and is therefore used as a reference. Applications include canopy stress analysis, productivity prediction and modelling, fire hazard analysis, and ecosystem physiology studies. The MSI is inversely proportional to other water VIs; higher values indicate greater water stress and lower water content.

## 4. Variation of Soil Indices

The Redness Index (RI) algorithm was developed to quantify soil color variations (Pouget et al. 1990). The Color Index (CI) algorithm was also developed to distinguish soils in the field (Pouget et al. 1990). Low CI values have been shown to be associated with high carbonate or sulfate concentrations, and higher values are associated with crusty soils and sands in arid regions (Escadfal, 1989). In most cases, CI provides complementary information to BI and NDVI. Used in non-temporal analyses, it helps to better understand the evolution of soil surfaces (Figure 8).

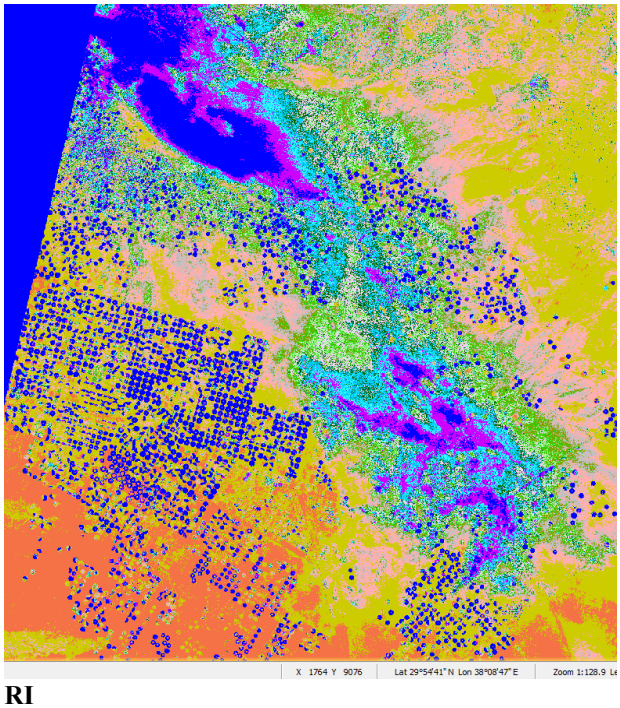

**RI**

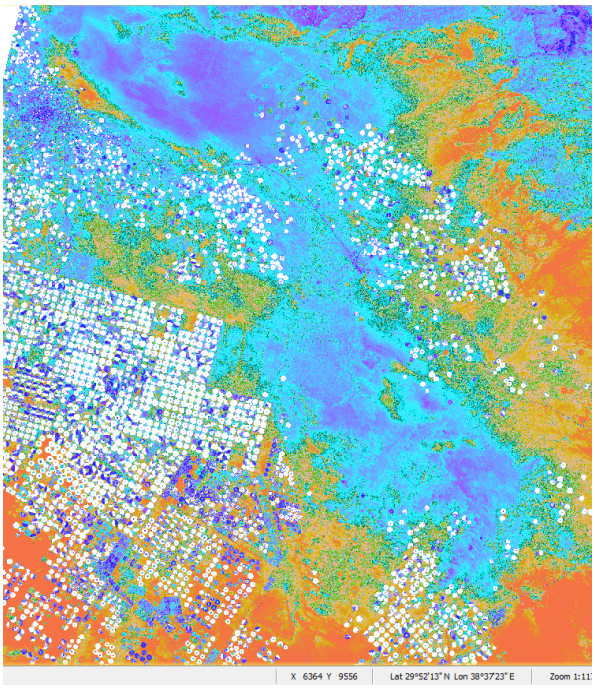

**CI**

Figure 8: Soil content inference RI & CI (2015).

## 5. SENTINEL-1 Radar Image Analysis Methods

The Interferometric Wideband (IW) mode allows for the integration of a large swath width (250 km) with moderate geometric resolution (5 m x 20 m). IW mode images three sub-slices using terrain observation with progressive scanning SAR (TOPSAR).

Using TOPSAR (Figure 9, Figure 11), in addition to beam steering in the range as in SCANSAR, the beam is also electronically steered back and forth in the azimuth direction for each burst, avoiding scaling and resulting in a high-quality image. Interferometry is ensured by sufficient overlap between the Doppler spectrum (in the azimuth domain) and the wavenumber spectrum (in the elevation domain). TOPSAR ensures consistent image quality throughout the swath.

IW mode is the default acquisition mode on Earth. The Gray Level Co-occurrence Matrix (GLCM) will extract 10 texture features from the radar image (contrast, dissimilarity, homogeneity, second angular moment, energy, maximum likelihood, entropy, mean, variance, correlation).

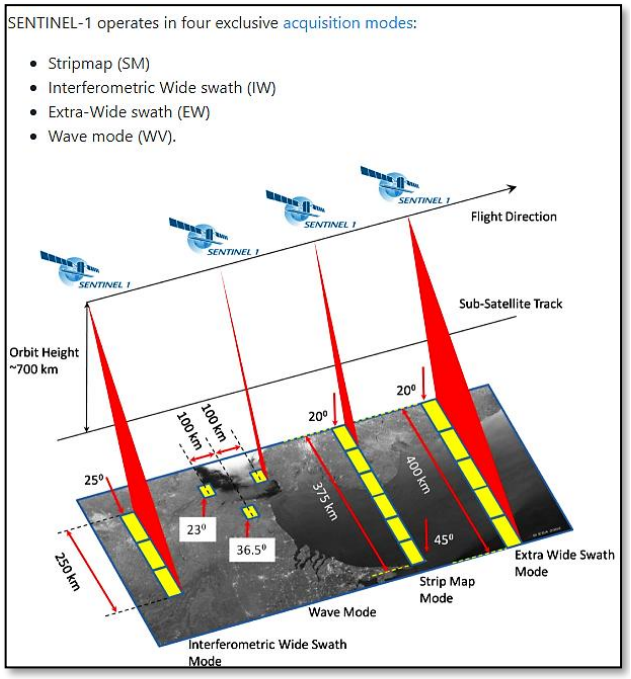


Figure 9: Wide patch overlap placement


Figure 10. Monthly follow-up and comparison of the SENTINEL-1 radar images to infer olive tree growth characteristics.

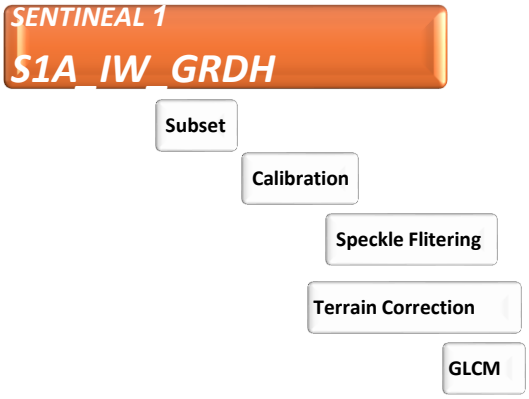


Figure 11: Methods for processing and analyzing SENTINEL-1 radar images to infer olive tree characteristics.

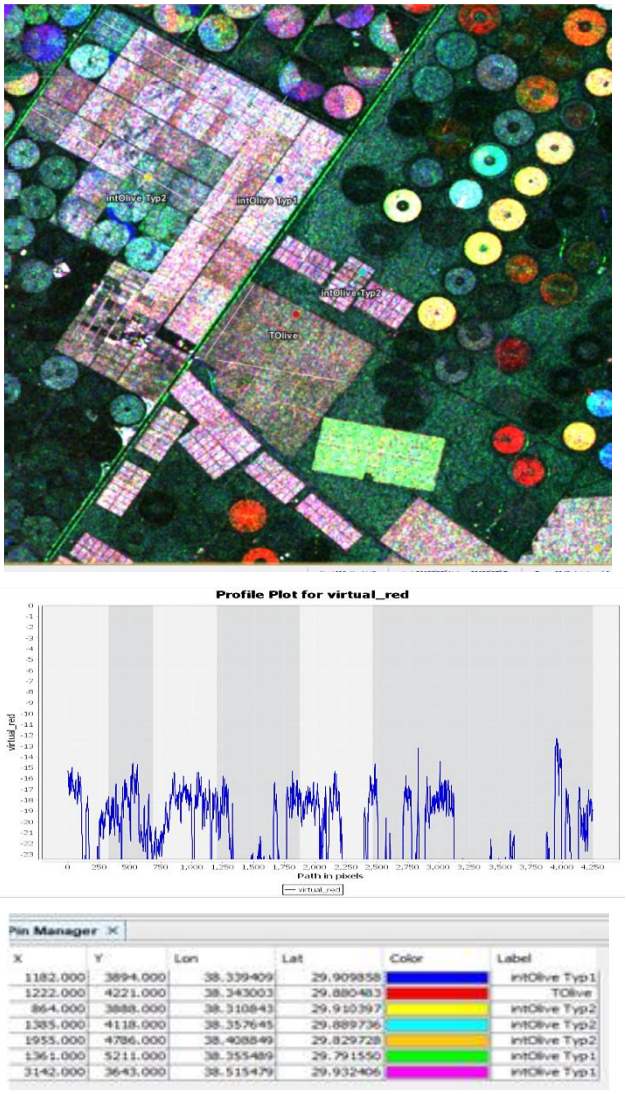


Figure 12: Monthly follow-up and comparison of the timescale of SENTINEL-1 radar images every two months to identify olive tree species.

## 6. Methods for analyzing World View 3 images at 31 cm ground resolution

Olive's trees show a lot of variation and are affected by factors such as shape, size (Alshammari et al., 2022), oil content, taste, chemical properties, and ripening time. To increase productivity and produce high-quality oil fruits, proper cultivation and ongoing care are crucial. When planting olive trees in straight rows from north to south, it ensures even sunlight exposure throughout the day. Planting them in an east-west direction can lead to shading issues, reducing yield and fruit quality. To produce larger and better yields, olives are typically propagated from cuttings rather than seeds.

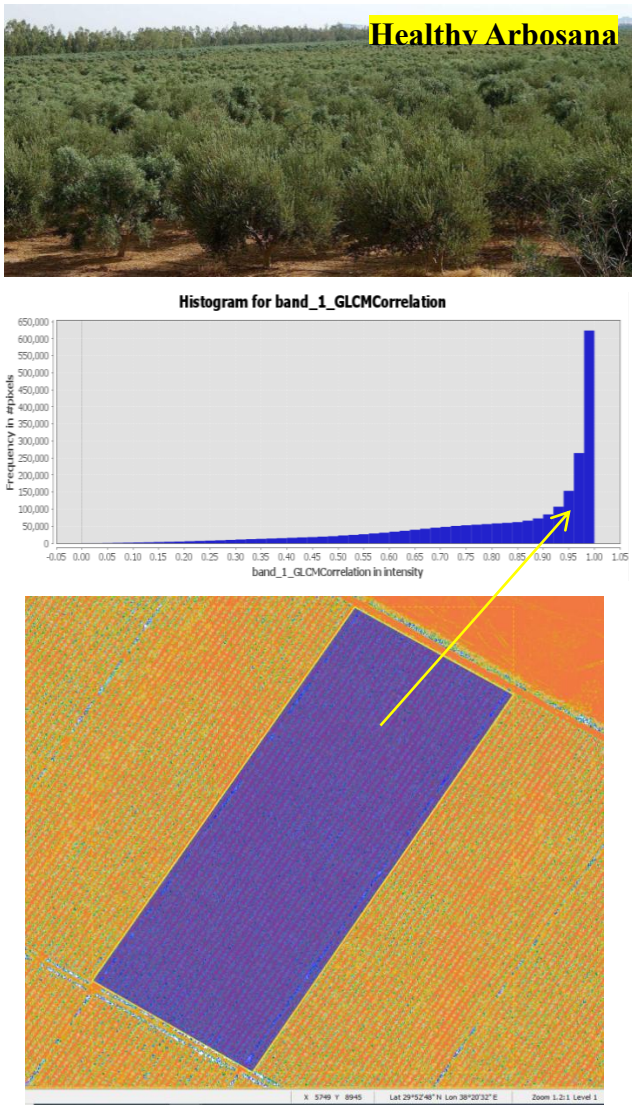


Figure 13: The correlation coefficient shows that most olive trees are of one type.

For orchards with large tree crowns or areas with varying vegetation, the results may be uncertain. This is also true for areas where neighbouring pixels differ significantly. Therefore, special algorithms may be needed to detect these situations and suggest alternative methods for retrieval (Díaz-Varela et al., 2015).

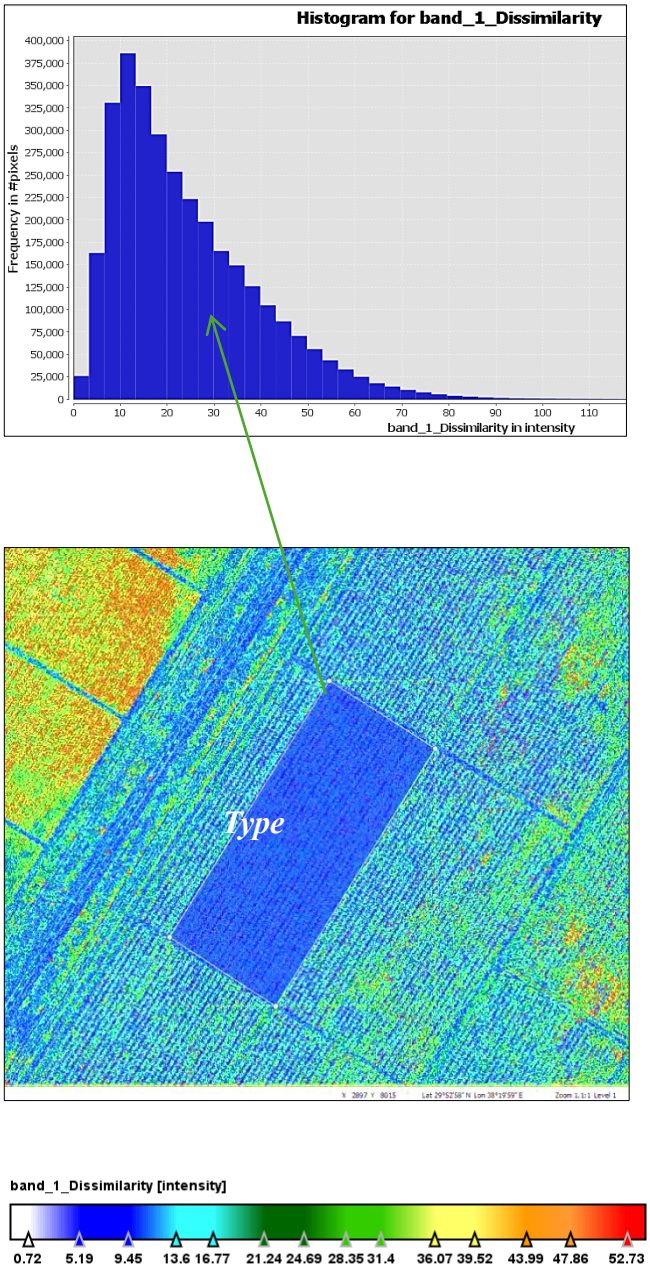


Figure 14: The coefficient of variation shows that olive trees are of different types.

Therefore, the Emirate of Al Jouf has a climate that is ideal for cultivating olive trees. The varieties grown there are referred to by different names, depending on how local farmers describe them. Some varieties, such as Arbequin/Arbequino, Arbosana, and Traditional, are known for their rapid growth and

productivity, producing within 3 years and coping with the stress of harvest.

Table 5. Main tree densities for olive groves. Source: De la Rosa et al., 2007

| Production system | Spacing Tree | Density (trees/ha) |
|---|---|---|
| Traditional Olive | 7 - 20 m | 30 - 200 trees |
| Intensive Olive | within the row: 3 - 4 m<br>Between rows: 6 - 8 m | 250 – 600 trees |
| High Intensive Olive | Within row: 0.9 - 1.5 m<br>Between rows: 3-4 m | 1.655 - 2.990 trees |

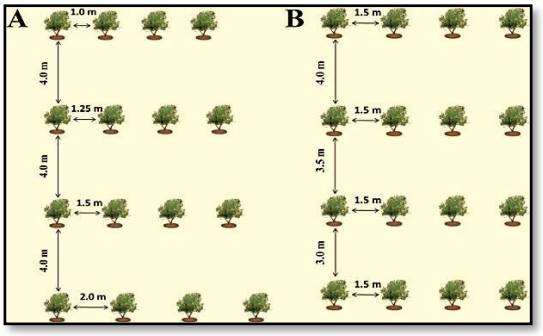


Figure 15: example of different planting distances for Arbequina trees producing olive oil. Source: Rodrigues et al., 2018.

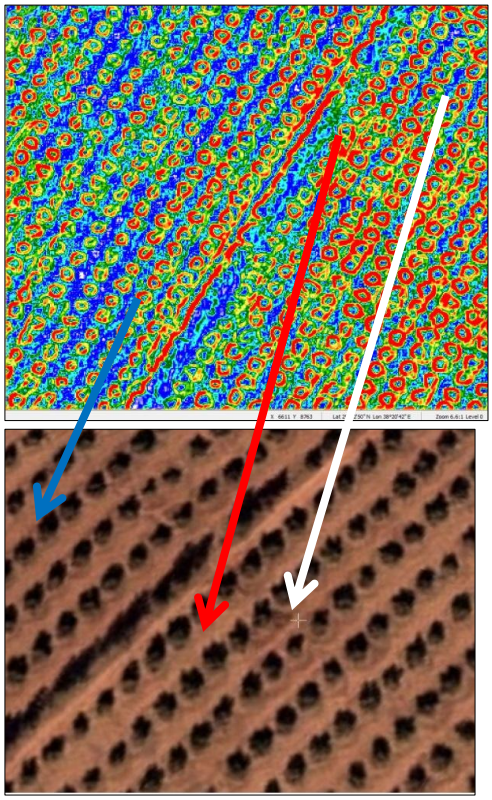

Figure 16: Identifying tree crowns for growth studies and monitoring plant health. The arrows showed different crown sizes.

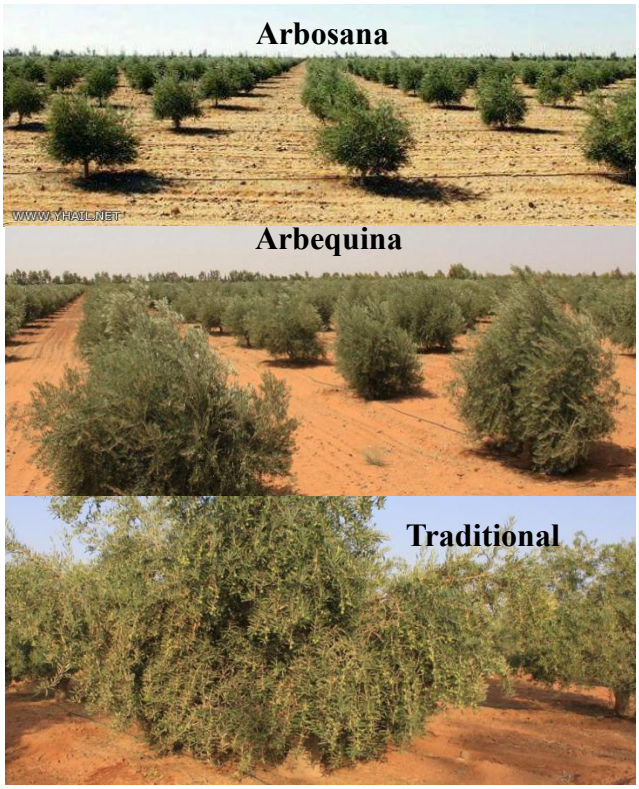


Figure 17: 3 different types of trees to be studied in terms of growth and fruit monitoring.

To ensure intensive olive cultivation, precision farming methods are employed, which involve:

- Automatically planning tree lines at fixed intervals of 1.5 m in length and 4 m in width (Table 1, Figure 10), as any deviation from this can cause the harvesting machine to break during harvest (Figure 15, Table 1).

- Effect of tree density: The main factor for olive tree productivity is the number of trees/ha in addition to other agro-climatic factors. However, the effect of density on olive oil quality and composition needs further studies.

For example, Arbequina olive oil-producing trees are planted at different distances. The first group is planted in a row (2.0 m, 1.5 m, 1.25 m, 1.0 m, 1.0 m, the distance between the rows is 4.0 m). The second group is planted at different distances between the rows (4.0 m; 3.5 m; and 3.0 m, with the space within the same row set at 1.5 m), resulting in a density of planted trees

from 1250 to 2500 trees/ha (Figure 15, Figure 17).

Tree density may affect quality parameters, composition, antioxidant activity and oxidative stability. Increasing plants in a row and between rows may slightly increase free acidity, decrease peroxide value and specific extinction coefficients, and fatty acid composition (Rodrigues et al., 2018).

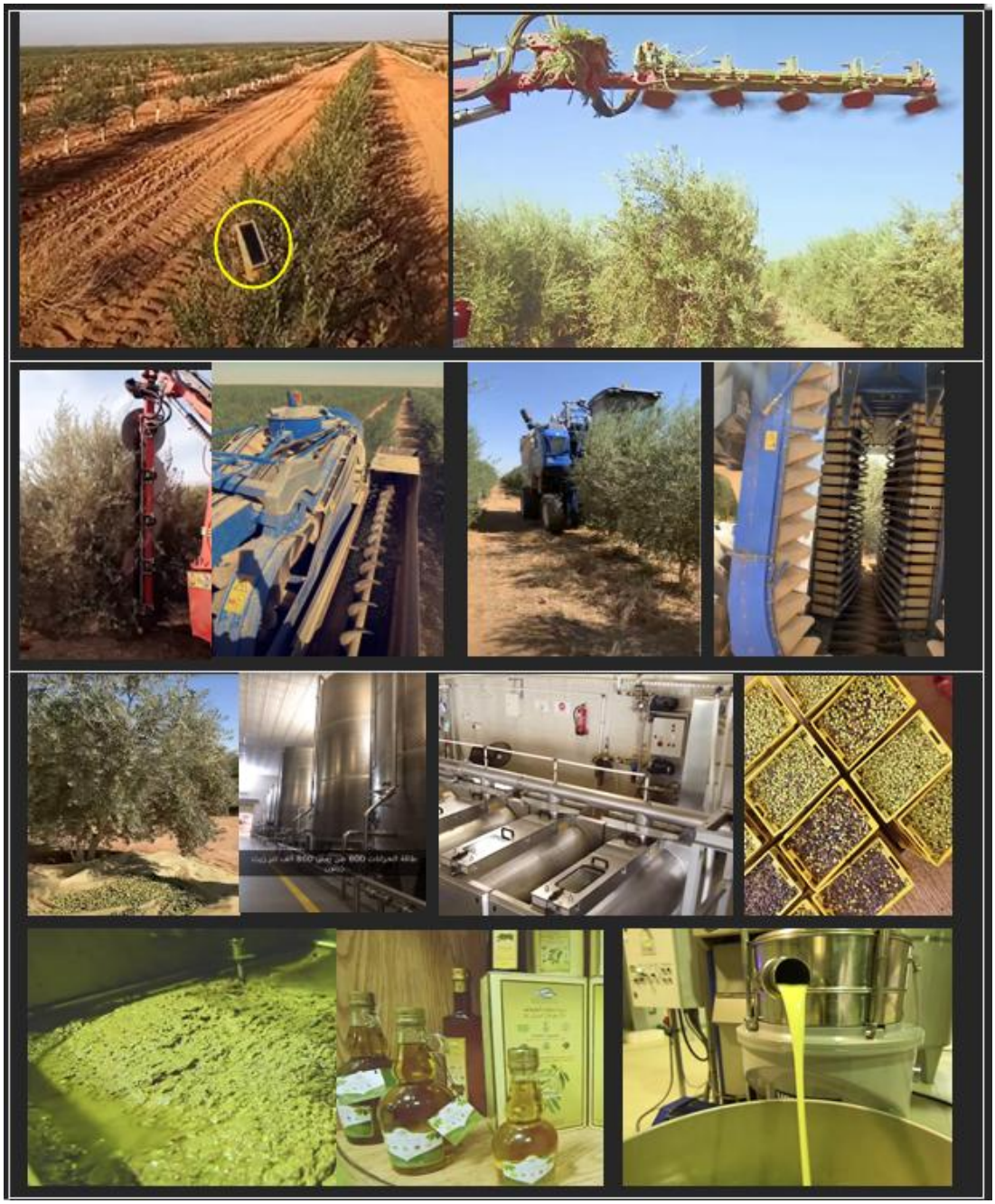

Figure 18: Stages of intensive olive tree care, manual and mechanised harvesting, and oil extraction (photos from existing projects in the Busa'ata region of Al Jouf area).

## 7. Discussion, Conclusion, and Future Work

The fused application of medium- and high-resolution satellite data—specifically Sentinel-1, Sentinel-2, and WorldView-3—demonstrates significant efficacy for assessing the health and productivity of olive trees under changing global climatic conditions. Sentinel-2 exhibited superior capability for delivering essential biophysical indicators, including Leaf Area Index (LAI), Leaf Chlorophyll Content (LCC), and Leaf Cover (LC), each of which underpins evaluations of canopy vigor and temporal growth trajectories. Complementary to this, Sentinel-1's radar measurements elucidated subsurface soil moisture gradients, thereby revealing zones of hydric stress whilst optical pathways remained opaque to those contrasts. WorldView-3, by virtue of its elevated spatial resolution, enabled delineation at the individual-tree scale, thereby allowing discrimination of planting density variances and canopy architectural heterogeneities within high-input olive orchards (Figure 16). Results substantiate that systematic temporal observation, executed at intervals between monthly and seasonal resolutions, is prerequisite for mapping growth trajectories, stress manifestations, and underlying yield prognostics. An additional synthetic outcome of the investigation is the enhanced interpretative scope derived from the deliberate synergistic application of radar and optical sensing; this multimodal strategy integrates vegetative responses and soil moisture status into a cohesive operational monitoring framework. This holds particular significance for the Tabarjal and Al-Bassita areas, where contemporary olive-production systems exhibit pronounced discrepancies with historic orchards in planting intensity, architectural supervision of the canopy, and consecutive yield phases.

The analysis therefore emphasizes, from a managerial standpoint, the actionable value of remote sensing within the broader paradigm of precision agriculture. Through its capacity to reveal stress anomalies at an embryonic stage, to refine irrigation timing, and to highlight poorly structured soil units that demand geographically exact adaptations, the technology furnishes decision-makers with timely and spatially explicit data. The relevance of this finding is amplified within the Kingdom of Saudi Arabia, where major enterprises such as Al-Jouf and Nadec oversee extents in excess of several thousand hectares and operate within pronounced labor restrictions. By facilitating coherent monitoring across broad areas with reduced recourse to financially burdensome and labor-intensive ground surveys, the approach contributes to the rational control of operational resources. Moreover, the underlying protocols exhibit explanatory and prescriptive applicability that transcends the confines of olive groves; the same methodologies may be harnessed to optimize forest stewardship, to guide the allocation of water, to inform spatial development strategies, and to refine food-security initiatives in contexts characterized by aridity or semiaridity. Looking ahead, several areas need more research and technology development. First, using drone-based hyperspectral and thermal imaging could improve satellite monitoring. It can help detect early-stage diseases, pests, and nutrient deficiencies in more detail. Second, adopting artificial intelligence and machine learning models would allow for predictive analytics in yield forecasting and automated disease detection. Third, combining radar data with in-situ sensors and hydrological models could improve soil moisture mapping. This would support water-use efficiency in regions facing more water scarcity. Additionally, creating a digital twin of olive orchards could offer dynamic simulations of orchard growth. This would let farmers test management strategies virtually before putting them into practice. Finally, expanding the temporal analysis with long-term archives like Landsat could show wider trends in how climate change affects olive productivity over decades.

In conclusion, this study shows that remote sensing technologies are changing how olive

cultivation is managed. They provide scalable, precise, and affordable monitoring solutions (

). By combining satellite, drone, and IoT-based data, and using improved analytical methods, future research can go beyond just monitoring. It can create decision-support systems that directly guide farm operations. This change from observation to prediction and recommendation will be essential for maintaining the sustainability, resilience, and productivity of olive farming in Saudi Arabia and other dry regions worldwide.

## 8. References


Aguilar, M. A., Bianconi, F., Aguilar, F. J., & Fernández, I. (2014). Object-based greenhouse classification from GeoEye-1 and WorldView-2 stereo imagery. Remote sensing, 6(5), 3554-3582.

Alshammari, H. H., Altaieb, M. O., Boukrara, A., & Gasmi, K. (2022). Expansion of the olive crop based on modeling climatic variables using geographic information system (GIS) in Aljouf region KSA. Computers and Electronics in Agriculture, 202, 107280.

Barazzetti, L., Roncoroni, F., Brumana, R., & Previtali, M. (2016). Georeferencing accuracy analysis of a single worldview-3 image collected over Milan. The International Archives of the Photogrammetry, Remote Sensing and Spatial Information Sciences, Volume XLIB1.

Brown, L. A., Ogutu, B. O., & Dash, J. (2019). Estimating Forest Leaf Area Index and Canopy Chlorophyll Content with Sentinel-2: An Evaluation of Two Hybrid Retrieval Algorithms. Remote Sensing, 11(15), 1752.https://doi.org/10.3390/rs11151752

De la Rosa, R., León, L., Guerrero, N., Rallo, L., & Barranco, D. (2007). Preliminary results of an olive cultivar trial at high density. Australian Journal of Agricultural Research, 58(5), 392-395.

Díaz-Varela, R. A., De la Rosa, R., León, L., & Zarco-Tejada, P. J. (2015). High-Resolution Airborne UAV Imagery to Assess Olive Tree Crown Parameters Using 3D Photo Reconstruction: Application in Breeding Trials. Remote Sensing, 7(4), 4213-4232. https://doi.org/10.3390/rs70404213.

Escadafal R. (1989): Caractérisation de la surface des sols arides par observations de terrains et par télédétection; application : exemple de la région de Tataouine (Tunisie). In: Escadafal. R, Pontanier R. and Belghith A. eds.: Propriétés spectrales des surfaces et télédétection de variations spatiales et temporelles de l'infiltrabilité de sols arides (Menzel Habib) Tunisie. Edition de l'ORSTOM, collection : études et thèses, Paris, France VI. 317p.

Goldbergs, G., Maier, S. W., Levick, S. R., & Edwards, A. (2019). Limitations of high resolution satellite stereo imagery for estimating canopy height in Australian tropical savannas. International Journal of Applied Earth Observation and Geoinformation, 75, 83-95.

Gucci, R., & Cantini, C. (2000). Pruning and training systems for modern olive growing. Csiro Publishing.

Jiménez-Brenes, F. M., López-Granados, F., de Castro, A. I., Torres-Sánchez, J., Serrano, N., & Peña, J. M. (2017). Quantifying pruning impacts on olive tree architecture and annual canopy growth by using UAVbased 3D modelling. Plant Methods, 13(1), 55.

Krause, S., Sanders, T. G., Mund, J. P., & Greve, K. (2019). UAV-based photogrammetric tree height measurement for intensive forest monitoring. Remote Sensing, 11(7), 758.

Maneta, M. P., & Silverman, N. L. (2013). A spatially distributed model to simulate water, energy, and vegetation dynamics using information from regional climate models. Earth Interactions, 17(11), 1-44.

Maxar Technologies (2019A.). Worldview-3 datasheet. Retrieved from https://www.digitalglobe.com/

company/about-us (accessed 03 December 2019).

Mohan, M., Silva, C. A., Klauberg, C., Jat, P., Catts, G., Cardil, A., & Dia, M. (2017). Individual tree detection from unmanned aerial vehicle (UAV) derived canopy height model in an open canopy mixed conifer forest. Forests, 8(9), 340.

Orlandi, F., Aguilera, F., Galan, C., Msallem, M., & Fornaciari, M. (2017). Olive yields forecasts and oil price trends in Mediterranean areas: a comprehensive analysis of the last two decades. Experimental Agriculture, 53(1), 71-83.

Rabeh, S., Sabouni, I., Salem, S., and Sharari, A. (2017). Physico-chemical andmicrobiological characterisation of olive mill wastewater in Sakaka, Aljouf region,KSA. International Journal for Environment and Global Climate Change, 5(2).

Rodrigues, N., Casal, S., Peres, A. M., Baptista, P., Bento, A., Martín, H., & Pereira, J. A. (2018). Effect of olive trees density on the quality and composition of olive oil from cv. Arbequina. Scientia Horticulturae, 238, 222-233.

Pouget, R. (1990). Histoire de la lutte contre le phylloxéra de la vigne en France.

Tomaštík, J., Mokroš, M., Saloň, Š., Chudý, F., & Tunák, D. (2017). Accuracy of photogrammetric UAV-based point clouds under conditions of partially-open forest canopy. Forests, 8(5), 151.

## 9. Arabic References:

(1) عبدالرحمن بن أحمد السديري (٢٠٠٥م) الجوف - وادي النفاخ ، الطبعة الثانية مزيدة ومحدّثة ، مراجعة د. خليل بن إبراهيم المعيقل ، مؤسسة عبدالرحمن السديري الخيرية ١٤٢٥هـ، ١٤٢٦هـ (٢٠٠٥م).

# Assessment of Land Degradation in Ghana's Densu River Basin using Residual Trend Analysis from 1991 to 2020

Kwame Obeng

*Kwame Nkrumah University of Science and Technology, Kumasi, Ghana; kobeng.coe@knust.edu.gh*

Land degradation is an activity that has a global effect on the environment and humanity. Sustainable Development Goal 15 of the 2030 Agenda focuses on the relationship between sustainable management of natural resources and social and economic development which further seeks good land management and its importance in assessing desertification, drought and land degradation. The need to ensure good land management necessitated this study. This study examined the effect of human activities and climatic variables (soil moisture and rainfall) on degradation using Residual Trend (RESTREND) Analysis and Ordinary Least Square (OLS) Regression model respectively in the Densu River Basin of Ghana from 1991 to 2020. From the OLS regression analysis, the impact of rainfall on degradation was located at the Northern to middle part covering about 35% of the study area with soil moisture having an effect throughout the basin. RESTREND based on rainfall and soil moisture both showed a negative trend predominantly at the Southern part of the study area indicating the presence of anthropogenic activities which was also confirmed from ground truthing. Both positive and negative trends are significant covering about 87% of the study area. The research will be useful to the various local government assemblies, environmental protection agencies and other stakeholders to monitor and preserve the natural resource base in the basin.

# Challenges and prospects for the sharing of geospatial information: A Case Study in Flood Risk Management

Siddhant Rohit Ullal [a]*, Angela Blanco-Vogt [b]

[a] *Hochschule für Technik Stuttgart, 1st Author - siddhantullal23@gmail.com*
[b] *Hochschule für Technik Stuttgart, 2nd Author – angela.blanco-vogt@hft-stuttgart.de*

**Abstract**: The effective sharing of geospatial data is critical for modern governance, urban planning, and disaster resilience, particularly in the era of smart cities, AI, and IoT. However, systemic barriers like fragmented regulations, institutional silos, and incompatible data standards continue to hinder seamless data exchange. While technological advancements like digital twins and real-time sensor networks offer transformative potential, their benefits remain constrained by a lack of interoperability. This study examines these challenges through a literature review, a case study of flood risk management (FRM) in Regensburg, Germany, as well as a prototype for analysing data flow interoperability. The study reveals how disjointed governance and outdated data practices impede effective decision-making. Despite decades of available technical solutions, flood response efforts remain hampered by proprietary systems, inconsistent data formats, and short-term fixes. The root cause is not a lack of technology, but rather a failure in governance. To address this, the paper presents an integrated FRM framework comprising five interlocking pillars and open standards.

***Keywords:*** Geospatial Information, Governance, Interoperability, OGC-Standards, Smart Cities.

## 1. Introduction

The frequency and intensity of flood events are rising globally due to climate change, urbanization, and land use pressures. In Europe, weather, and climate-related disasters, including floods, have caused economic losses exceeding 450 billion euros in the past 4 decades (EEA, 2024).

The catastrophic floods in Southern Germany in 2024, which led to damages exceeding €1.5 billion and claimed lives (Perlis, 2025), have underscored the urgent need to reframe flood management strategies.

Traditionally, flood protection in Germany relied on structural interventions such as dikes and levees, implemented post-disaster. However, this reactive paradigm is giving way to a more anticipatory and integrated approach of FRM, which focuses on hazard mapping, early warning systems, citizen participation, and multi-level coordination (Alshaikh et al., 2023; Surminksi et al., 2020). The Regensburg case underscores that the missing link is not technology but political will. This isn't a technical gap but a governance failure: without binding policies to enforce standardization, even the best tools remain underutilized.

Spatial technologies are central to this evolution. Tools such as Geographic Information Systems (GIS), Remote sensing, Building Information Modelling (BIM), Internet of Things (IoT) sensors, and Digital Twins (DTs) enable real-time monitoring, dynamic simulations, and data-driven decision-making across flood phases (Baycheva-Merger et al., 2024; Josipovic & Viergutz, 2023). However, integration of these technologies remains inconsistent due to

semantic interoperability issues, fragmented governance structures, and insufficient adoption of open standards (Aschieri et al., 2024; Hofmeister et al., 2024).

This study investigates how spatial planning technologies are currently applied in German FRM, drawing on a case study of the city of Regensburg. By evaluating both the technical potential and institutional constraints, including those revealed through prototype development, the paper identifies practical pathways toward a harmonized, smart-city-compatible FRM framework.

## 2. Methodology

This study adopts a three-mixed-methods research design to investigate the integration and effectiveness of spatial planning technologies in FRM within the German context.

(1) The first part of the study involves carrying out a literature review and analysing the state of the art in the areas of spatial technologies and governance in FRM. This review was based on peer-reviewed academic literature, grey literature, policy documents, and technical reports, and had a geographic focus on Germany and the wider European Union.

(2) The second part of the methodology involves analysing how a city has incorporated these technologies into its FRM. The selection of the case study was made based on several compelling reasons. The city of Regensburg has experienced several significant flooding events, notably in 2002, 2013, and 2021, and most recently in 2024, which serve to underscore its vulnerability and the necessity for enhanced resilience measures.

Furthermore, Regensburg's commitment to smart city initiatives, incorporating digital technologies for urban governance, is congruent with the study's emphasis on data-driven flood management (Stadt Regensburg, 2023).

(3) A prototype development exercise was aimed at understanding the data flow and interoperability of data. This prototype will not focus on the front-end and UI applications but serves purely as an exploratory model. The data for this section is extracted from open sources and is focused on data that are required in the case of flooding, such as DEM, satellite data, and Flood maps.

## 3. Implementation of the methodology

### 3.1 Literature review on Spatial Technologies and Governance in FRM

Flood-based disaster management is usually divided into phases: Preparation involving forecasting, planning, and public training; Response requiring real-time communication, logistics, and citizen care; Recovery focusing on restoring infrastructure and continued support; and mitigation, which emphasizes learning from past events, strengthening systems, and promoting cooperation to reduce future risks (Josipovic & Viergutz, 2023).

Specific technologies offer capabilities that target certain phases of the disaster and the needs of the various stakeholders involved in FRM. Analysing the performance, strengths, limitations, and stakeholder alignment of various technologies across the FRM cycle, Table 2 summarizes their use in different disaster phases.

| Technology formats and standards | Prevention (Risk Reduction) | Preparedness (Readiness & Early Warning) | Response (During Flood Emergency) | Recovery (Post-Flood Restoration) |
|---|---|---|---|---|
| BIM: IFC, COBIE, IFC-GIS, bSDD | Detailed buildings/infrastructure models; assess flood impacts; plan resilient design; simulations (Khanmohammadi et al., 2020) | Integrated IoT sensors; real-time monitoring; forecast inundation; alert authorities; virtual simulations; model scenarios; proactive risk assessment; identify vulnerabilities. (Khanmohammadi et al., 2020) | Detailed data; informed emergency response; 3D BIM/GIS models; safe evacuation routes; navigate structures; enhance rescue efficiency. (Khanmohammadi et al., 2020) | Digital repository; asset conditions/damage; collaborative planning; model-linked repair plans; automated permitting; accelerate recovery (Khanmohammadi et al., 2020) |
| GIS: OGC: WMS / WFS /WCS, CityGML, GML, KML, INSPIRE Directive | Integrate flood extents/depths/risk indicators; hazard maps; inform land-use planning/regulations; precision risk identification (LAWA, 2010; Surminksi et al., 2020) | MCA analysis; overlay hazard/population/infrastructure data; assess vulnerabilities; plan interventions; visualize cascade effects; contingency planning; communicate evacuation routes; interactive maps (Schneider et al., 2024) | Aggregate real-time data; common operational picture; multi-agency coordination; impact assessment; evacuation planning; public communication. (European Commision, 2021; Schneider et al., 2024) | Catalogue damage; guide aid/reconstruction allocation; track restoration; web-based dashboards; integrate lessons; improved risk models (Surminksi et al., 2020). |
| Digital Twin: CityGML, IFC, DTDL, Firmware NGSI | Simulate flood scenarios; test mitigation strategies; evaluate interventions; real-time; inform climate-resilient planning; risk-informed development; EU Floods Directive (EU Missions, 2025; Kaynak et al., 2025). | Real-time data inputs (rainfall/river levels/sensors); early-warning/decision-support; immersive VR/AR drills; rehearse responses; bolster readiness/planning (Kaynak et al., 2025). | Interactive crisis management; integrate live sensor data; update flood extents in real-time; 3D operational view; uncover cascade effects; predictive capabilities; targeted interventions (Kaynak et al., 2025). | Hindcasting events; analyze damage pathways; simulate improvements; assess future risk impact; stakeholder coordination; shared 3D environment; visualize/ discuss reconstruction (Kaynak et al., 2025). |
| Remote Sensing: Sentinel, CEOS, OGC, GeoTIFF, NTECDF, Coverage-JSON | High-resolution data (satellite imagery / aerial surveys/radar); DEMs (LiDAR/satellite stereoscopy); delineate flood zones; simulate scenarios (Munawar et al., 2022). | Meteorological sensing; real-time precipitation monitoring; hydrological models; early warning (EFAS); detect flood indicators; wide-area monitoring. (Munawar et al., 2022). | Overcome ground limitations; near-real-time flood mapping; low-altitude imagery/damage / inaccessible areas; integrated GIS; situational awareness; operational coordination. (DLR, 2024; Munawar et al., 2022). | Assess damage; aerial / satellite imagery; document impacts; quantify infrastructure/debris/river alterations (Munawar et al., 2022). |
| IoT: SensorThings API, MQTT, LoRaWAN IEEE | Dense real-time monitoring; environmental variables; proactive prevention; enhance flood modelling; continuous localised records; refine hazard maps/infrastructure design (iot for all, 2024). | Real-time early warning; sensors; cloud analysis; linked to sirens/drills (Munawar et al., 2022). | Real-time situational awareness; transmit water-level data; monitor inundation; protect infrastructure; alert shutdowns; public alert systems; broadcast updates; flash-flood scenarios (iot for all, 2024). | Damage assessment; water-quality sensors; contamination risks; public health; event data analysis; assess defence failures/interventions (Turner & Sun, 2024) |
| Hydrological Models: WATERML 2.0, HEC, MIKE | Simulate river flow / rainfall-runoff / inundation; identify high-risk zones; guide land-use planning; data-driven mitigation (LAWA, 2010; Wang, 2022) | Flood forecasting; basin-specific models (MIKE/HEC-RAS / WASFLOOD); integrate weather forecasts/gauge data; predict water levels/inundation (Surminksi et al., 2020). | Near real-time operation; update with rainfall/gauge data; refine forecasts; inform evacuation/emergency routing (Surminksi et al., 2020). | Model-based hindcasts; reconstruct dynamics; assess defenses; findings; inform upgrades/overflow areas (Bentivoglio et al., 2022). |

| | | | | |
|---|---|---|---|---|
| Web-based Platforms:<br>OGC web platform, INSPIRE, Restful API | Open-access interactive GIS portals; flood hazard/risk maps; support urban planning; awareness (Surminksi et al., 2020). | Collaborative portals; public warning; live water levels/forecasts; real-time alerts/resources; community preparedness (Almoradie et al., 2015; Surminksi et al., 2020). | Real-time information exchange; live crisis maps; dashboards; crowd-sourced updates (web / social media); digital command centre; link stakeholders (Surminksi et al., 2020). | Map damage assessments; track restoration; participatory planning; coordination/transparency / inclusive rebuilding (Almoradie et al., 2015). |

Table 1.Technology in the various phases of floods

### 3.2 Contextual Case: Regensburg

In early June 2024, the city of Regensburg in Bavaria experienced a flood. In accordance with EU and German law, Regensburg had maintained up-to-date flood hazard maps and an FRM plan by 2015, named the "Blue Plan". The city's "Blue Plan" identified all areas that could flood during a 100-year event and served as the foundation for planning protective measures (Bundesamt für Justiz, 2023; Hochwasserschutz-Regensburg, 2025; Surminksi et al., 2020).

One component of the early warning systems is the NINA app and cell broadcast to residents' phones when a disaster emergency is declared. The city administration, led by the mayor, activated the Führungsgruppe Katastrophenschutz (FüGK), the regional disaster management command unit (Nachrichten, 2024). The recommendations of flood laws have been considered, but there are still loopholes and instances of urban development in flood zones (Mehryar & Surminski, 2020).

Although Regensburg has introduced several smart city initiatives, the integration of these technologies into FRM remains limited. The city has shown interest in developing a DT. However, public documentation on its specific application to FRM is minimal (Richthofen et al., 2023). Other promising technologies include BIM and IoT. The successful use of aerial imagery by the Center for Satellite Based Crisis Information (DLR, 2025) during the 2024 flood offers a glimpse of what a more technologically connected FRM approach might achieve.

Institutions such as the German Aerospace Center (DLR) offer high-resolution satellite (Sentinel-1, TerraSAR-X) and aerial imagery (10 cm resolution), validated by experts, though it lacks a public API. Bavaria's Flood Notification Service (HND) provides authoritative gauge data, which is quality-assured but also not openly accessible via API. WasserBLIcK, a standardized national flood hazard/risk dataset by LAWA / BfG, is highly reliable and accessible through Open WMS / WFS services via the BfG portal. The Bavarian Environmental Atlas (GDI-BY) delivers state-level details, including hazard zones, flood depths, and historical data, with open OGC services and downloadable upon request. The national Germany Geoportal (Geoportal.DE) aggregates authoritative datasets with WMS/WFS services. Lastly, the Regensburg City Geoportal provides city-specific flood overlays, validated by local engineers, but does not offer an open API.

### 3.3 Prototype development

Flood-specific information—such as HQ100 flood zones, historical inundation extents, and potential water accumulation zones—is obtained from (Bundesland-Bavaria, 2024), improving hazard characterisation. For BIM integration, models developed in Revit, ArchiCAD, or through Autodesk Construction Cloud are utilized. The emphasis here is on data interoperability, specifically the conversion of. rvt and .ifc formats into GIS-compatible structures.

| Data | Data Sources | Fata Formats | API. |
|---|---|---|---|
| DGM 1 | (Bayerische Vermessungs-verwaltung, 2024) | GeoTIFF, XYZ | No |
| Orthophoto | | GeoTIFF | Yes |
| 3D buildings LOD2 | | CityGML | No |
| Remote Sensing data | (CDSE, 2024) | GeoTIFF | Yes |
| HQ100 flood zones | (Bundesland-Bavaria, 2024) | GeoTIFF | Yes |
| Water level gauge | (WSV.de, 2025) | .json | Yes |
| BIM data | Revit Sample Model | .ifc / .rvt | - |

Table 2. Data sources selected for the prototype.

Figure 1 illustrates how data flow is integrated, processed, and delivered to stakeholders.

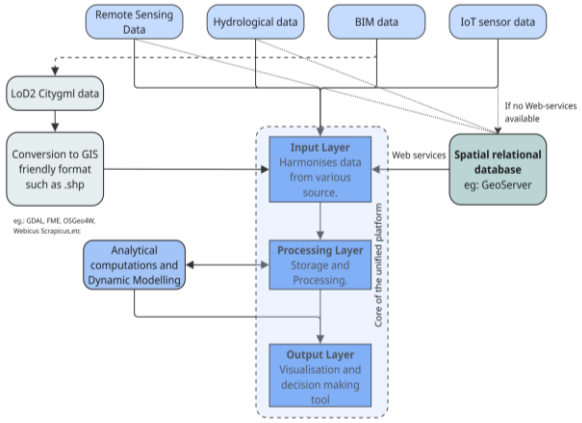


Figure 1. Data integration workflow

The prototype exercise also showed major limitations. A key dependency is on data availability and quality. Maintaining up-to-date, high-quality data is an ongoing challenge; it necessitates continuous investment in sensors, surveys, and data curation. This relates to another limitation: the necessity for sustained governance and funding. The platform will require maintenance and governance.

The integration of BIM and LOD2 CityGML models also presents barriers. For BIM, there is a requirement for manually georeferencing the models in GIS. When CityGML files are converted to IFC, they encounter the same georeferencing issue. Providing the LOD2 file as a service also poses challenges due to the complex geometries involved and the intricate data structure of the CityGML file.

Models and predictions face inherent uncertainty. Although the system offers advanced analytics, flood modelling lacks precision, leading to significant forecast uncertainties (e.g., rainfall prediction error, assumptions about model parameters). Users should interpret results cautiously and not depend solely on automated outputs for crucial decisions.

Finally, as with any smart city technology, there are bound to be security and privacy concerns. Having data in one single platform may also include some personal data that can make it a target for cyber threats.

The prototype illustrates how a unified platform can dismantle silos to provide real-time situational awareness. The current requirement is for an integrator to advocate for the adoption of open, standards-based APIs and incorporate data-sharing mandates into procurement procedures.

## 4. Integrated Spatial Framework for FRM from the perspective of a Smart City Manager

The approach of Chaturvedi et al., (2019), based on modern standards like OAuth, SAML, and OpenID, provides a critical foundation for secure data exchange. This is a necessary first step to overcome the persistent governance challenge in Germany's FRM landscape: the fragmentation of institutional roles and its resulting siloed, uncoordinated decision-making. To address this fragmentation, the figure 2 presents an integrated FRM framework built upon five interlocking pillars: Spatial Technologies, Policy Mandates, Governance, Data Management, and Citizen Engagement. Together, these pillars enable holistic, data-informed flood risk reduction, which in turn strengthens trust in public institutions. A smart city expert could orchestrate this framework, leveraging such security standards to finally break down information silos.

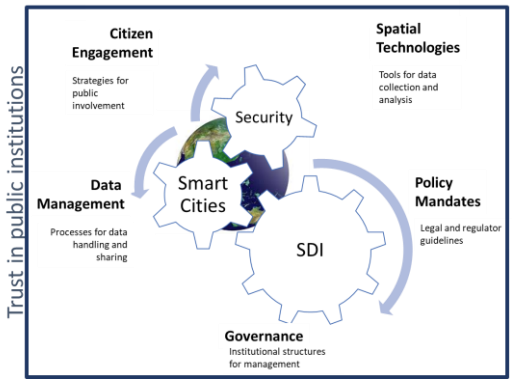


Figure 2. Proposed integrated FRM-Framework

## 5. Discussion

Despite the availability of advanced modelling tools and high-resolution spatial datasets, their full potential remains untapped due to inconsistent formats, governance gaps, weak semantic interoperability, lack of security standards and standardized ontologies. A growing challenge in the age of IoT and Digital Twins is balancing data utility with privacy protection. Without strong privacy-preserving measures and transparent governance frameworks, these systems risk exposing sensitive information, violating compliance standards, or eroding public trust.

Various stakeholders, including municipal planners, emergency responders, researchers, and the public, use different databases, each with unique interfaces and technical specifications. This fragmented data environment reduces efficiency and causes confusion, especially during emergencies that require rapid decision-making.

The Regensburg case highlights the need for policy reforms that prioritize data interoperability and stakeholder coordination. It also indicates that an integrating role is necessary to facilitate collaboration among stakeholders, which requires a strong regulatory framework that mandates data sharing and standardizes data formats and protocols. A major challenge in Regensburg's FRM landscape is the abundance of disparate data sources and the absence of a centralized system to manage them.

The prototype demonstrated how data from various sources with different formats can be brought together on a common platform, using open standards and APIs. At the same time, practical barriers became evident, for example, difficulties in aligning BIM models with GIS coordinates and the necessity to manually georeference 3D city models. The exercise exposed data format mismatches, metadata inconsistencies, and the importance of adhering to standards like web services, among others, for smooth data exchange. These lessons directly inform the framework's emphasis on standardized data governance and technical interoperability as cornerstones of successful smart FRM.

Sensor networks could provide real-time data on water levels, structural strain, and evacuation routes. Nonetheless, these technologies are still in early stages of deployment, and challenges such as interoperability between platforms and data formats continue to restrict their effectiveness.

The challenges and prospects of sharing geospatial information hinge on interoperability, integrating Spatial Data Infrastructures (SDIs), smart city technologies, and robust security frameworks. This integration is no longer optional, but it is a cornerstone of ethical, efficient, and intelligent governance.

Future work must further explore the role of spatial technologies in flood governance, with a focus on next-generation innovations to enhance FRM. For instance, AI-powered flood modelling improves predictive accuracy, while blockchain data platforms ensure secure information sharing, addressing data integration and cybersecurity challenges. Additionally, integrating cloud computing with IoT networks enhances scalability and reliability of flood monitoring systems, allowing real-time processing of extensive sensor data for early warning. Further studies in ways to integrate BIM and GIS can further ease the workflow while also reducing the loss of data. These innovations can resolve

technical gaps like interoperability and trust in data sharing.

## 6. References


Almoradie, A., Cortes, V. J., & Jonoski, A. (2015). Web-based stakeholder collaboration in flood risk management. Journal of Flood Risk Management, 8(1), 19–38. https://doi.org/10.1111/jfr3.12076

Alshaikh, R. Z., Abdulmunem, S. A., & Alkinani, A. S. (2023). A Review on Urban Planning and Its Role in Managing Flood Risks. Urban Planning and Construction, 1(1), 1–8. https://doi.org/10.55121/upc.v1i1.104

Aschieri, D. L. D., Sobrino, N., & Macii, E. (2024). Web-GIS Application for Hydrogeological Risk Prevention: The Case Study of Cervo Valley. Sustainability, 16(22), 9833. https://doi.org/10.3390/su16229833

Baycheva-Merger, T., Selter, A., Seijger, C., & Häublein, S. (2024). Digital Opportunity or a Threat? Adoption of Internet of Things (IoT) Monitoring Systems for Natural Resources in Germany. Environments, 11(3), 39. https://doi.org/10.3390/environments11030039

Bayerische Vermessungsverwaltung. (2024). Open Data - Geodata Bayern. Https://Geodaten.Bayern.de/Opengeodata/Index.Html.

Bentivoglio, R., Isufi, E., Jonkman, S. N., & Taormina, R. (2022). Deep learning methods for flood mapping: a review of existing applications and future research directions. Hydrology and Earth System Sciences, 26(16), 4345–4378. https://doi.org/10.5194/hess-26-4345-2022

Bundesamt für Justiz. (2023). WHG - Gesetz zur Ordnung des Wasserhaushalts 1) 2).

Bundesland-Bavaria, G. (2024). Geoportal Bayern - suche. Bayern.De. https://geoportal.bayern.de/geoportalbayern/suche/suche?0&q=hochwasser

CDSE, C. D. S. E. (2024). Copernicus Sentinel Data. Https://Dataspace.Copernicus.Eu/Data-Collections/Copernicus-Sentinel-Data.

Chaturvedi, K., Matheus, A., Nguyen, S. H., & Kolbe, T. H. (2019). Securing Spatial Data Infrastructures for Distributed Smart City applications and services. Future Generation Computer Systems, 101, 723–736. https://doi.org/10.1016/j.future.2019.07.002

DLR. (2024). Vorher-Nachher: Hochwasserlage Regensburg. Https://Www.Dlr.de/de/Aktuelles/Nachrichten/2024/Hochwasserkarten-Und-Lageinformationen-Fuer-Sueddeutschland/Vorher-Nachher-Hochwasserlage-Regensburg.

DLR. (2025). Center for Satellite Based Crisis Information. Https://Www.Dlr.de/En/Zki/about-Us/Zki.

EEA. (2024). Economic losses from weather- and climate-related extremes in Europe. https://www.eea.europa.eu/en/analysis/indicators/economic-losses-from-climate-related

EU Missions. (2025). Coupling High-Resolution Flood Modelling and 3D Digital Twins for Climate Change Adaptation. https://climate-adapt.eea.europa.eu/en/mission/solutions/mission-stories/coupling-high-resolution-flood-modelling-story34

European Commision. (2021). Forging a climate-resilient Europe - the new EU Strategy on Adaptation to Climate Change. Communication from the Commission to the European Parliament, the Council, the European Economic and Social Committee and The Committee of the Regions. https://eur-lex.europa.eu/legal-content/EN/TXT/?uri=COM:2021:82:FIN

Hochwasserschutz-Regensburg. (2025). Blauer Plan | Hochwasserschutz Regensburg.

Hofmeister, M., Brownbridge, G., Hillman, M., Mosbach, S., Akroyd, J., Lee, K. F., & Kraft, M. (2024). Cross-domain flood risk assessment for smart cities using dynamic knowledge graphs. Sustainable Cities and

Society, 101, 105113. https://doi.org/10.1016/j.scs.2023.105113

iot for all. (2024). Preventing Flood Damage with IoT Sensors. Https://Www.Iotforall.Com/Preventing-Flood-Damage-with-Iot-Sensors.

Josipovic, N., & Viergutz, K. (2023). Smart Solutions for Municipal Flood Management: Overview of Literature, Trends, and Applications in German Cities. Smart Cities, 6(2), 944–964. https://doi.org/10.3390/smartcities6020046

Kaynak, S., Kaynak, B., Mermer, O., & Demir, I. (2025). City-Scale Digital Twin Framework for Flood Impact Analysis: Integrating Urban Infrastructure and Real-time Data Analytics. EarthArXiv (California Digital Library). https://doi.org/10.31223/x53f0t

Khanmohammadi, S., Arashpour, M., & Bai, Y. (2020, October 14). Applications of Building Information Modeling (BIM) in Disaster Resilience: Present Status and Future Trends. https://doi.org/10.22260/ISARC2020/0191

LAWA. (2010). German Working Group on Water Issues of the Federal States and the Federal Government Recommendations for the Establishment of Flood Hazard Maps and Flood Risk Maps Adopted at the 139th LAWA General Meeting in Dresden on 25/26 March 2010 LAWA Permanent Committee on Flood Protection and Hydrology (LAWA-AH). https://www.lawa.de/documents/lawa_hwgk 15062010_text_germany_eng_1552299627. pdf

Mehryar, S., & Surminski, S. (2020). The role of national laws in managing flood risk and increasing future flood resilience.

Munawar, H. S., Hammad, A. W. A., & Waller, S. T. (2022). Remote Sensing Methods for Flood Prediction: A Review. Sensors, 22(3), 960. https://doi.org/10.3390/s22030960

Nachrichten, R. (2024). Gefahr durch Hochwasser steigt: Katastrophenfall in Regensbu... Regensburger Nachrichten - News, Meldungen Und Aktuelles Aus Der Region. https://www.regensburger-nachrichten.de/panorama/94854-gefahr-durch-hochwasser-steigt-katastrophenfall-in-regensburg-ausgerufen

Perlis. (2025). EUR 1,564M – Final perils industry loss estimates for the southern Germany floods of early June 2024.

Richthofen, von, Saad, A., Cyganski, J., Sanchez, M. A., Kroeske, M., Kniffki, S., Vogt, L., Skulic, E., & Berres, L. (2023). Wissenschaftliche Begleituntersuchung zu digitalen Zwillingen von Kommunen im Bundesgebiet. Zenodo. https://doi.org/10.5281/zenodo.10014903

Schneider, M., Priesmeier, P., Fekete, A., Lichte, D., & Fiedrich, F. (2024). Cascading Effects of Critical Infrastructures in a Flood Scenario: A Case Study in the City of Cologne. Proceedings of the International ISCRAM Conference, 21. https://doi.org/10.59297/ws32ka31

Stadt Regensburg. (2023). Smart-City-Strategie. In mein.regensburg.de. https://mein.regensburg.de/smartcitystrategie

Surminksi, S., Roezer, V., & Golnaraghi, M. (2020). Flood Risk Management in Germany: Building flood resilience in a changing climate. Flood Risk Management, The Geneva Association.

Turner, R., & Sun, C. (2024). Near Real-Time Responsive Flood Event Representation: An Open-Source Interactive Web Application Architecture. ISPRS Annals of the Photogrammetry, Remote Sensing and Spatial Information Sciences, X-4–2024, 365–372. https://doi.org/10.5194/isprs-annals-x-4-2024-365-2024

Wang, L. (2022). A review of the flood management: from flood control to flood resilience. Heliyon, 8(11). https://doi.org/10.1016/j.heliyon.2022.e11763

WSV.de. (2025). Pegel Online Webservice. Https://Www.Pegelonline.Wsv.de/Webservice/GuideRestapi.

# Technical Session: Data sharing and Collaborative Geoinformation Portals

# From Technocracy to Data Sovereignty, Open Data and Use of Open-Source Geospatial Technologies

Franz-Josef Behr

*Stuttgart University of Applied Sciences, Germany; franz-josef.behr@hft-stuttgart.de*

When Donald Trump was inaugurated on January 20, 2025, the heads of major US technology companies such as Amazon, Meta, Google, Tesla Motos and Apple stood just a few meters away from him in Capitol Rotunda (The Guardian 2025). They had previously donated millions to the election campaign and the inauguration. Even some of them, such as Meta CEO Mark Zuckerberg, had already adapted business concepts to Trump's policies in advance. Trump himself and the Department of Government Efficiency (DOGE), for which E. Musk is a senior advisor, are aggressively pushing ahead with the restructuring of the state. And many are concerned that even sensitive data of citizens is no longer secured on the basis of GDPR-compliant data transfers between the EU and the United States, but could be misused or access jeopardized. In the emerging technocracy, as in the case of DOGE, experts from different fields are deployed to advise political decision-makers, regardless of whether democratic principles and the rule of law are called into question in the process (Thiel 2009). Search engines, digital media, web browsers, mail servers, cloud solutions, navigation systems and map apps: a large proportion of our data is in the hands of large US companies. Here issues such as digital colonialism play a role (Ziai 2020). Resources from the "global South" are used to create data and information as input for AI applications) (Anwar & Graham 2022, Malik 2022a, Dachwitz & Hilbig 2025). Widespread applications can also be used, to influence different areas of the economy (Malik 2022a).

We have thus made ourselves dependent at various levels on algorithms that influence our opinions, on platforms that control our communication, on corporations that dominate political processes (https://digitalrechte.de/). It is therefore worth looking at possible alternatives to established and often easy-to-use US services at local and indigenous level. Basically, there are plenty of them: A website with the name “European Alternatives” (https://european-alternatives.eu/alternatives-to) was launched. It lists apps that were developed in Europe at and therefore also comply with European data standards. Other collections, such as the “Open Alternative” website (https://openalternative.co/alternatives), collect applications that were developed according to the open-source principle. As experts in the procurement and processing of geospatial data, we need to address the use, storage and processing of geodata in particular. In doing so, we must keep our data sovereignty in mind and focus on the use of own or open-source products: Using data, know-how and financial resources locally, regionally or nationally. free vector geodata and remote sensing data as well as the offerings of the OSGeo Foundation can make a significant contribution to digital sovereignty. In addition to introductory background information on the drivers of technocracy, aspects of data sovereignty, ideas about the principles of commons, freely available data sources and the extensive range of open-source solutions are presented.

***Keywords:*** Digital Colonialism, Digital Sovereignty, Technocracy, Open Data, Open Source, OSGeo Foundation

**References**

Anwar, M. A., & Graham, M. (2020). Digital labour at economic margins: African workers and the global information economy. Review of African Political Economy, 47(163), 95–105. https://doi.org/10.1080/03056244.2020.1728243

Coleman, Danielle (2019). Digital Colonialism: The 21st Century Scramble for Africa through the Extraction and Control of User Data and the Limitations of Data Protection Laws. Michigan Journal of Race and Law, 24(2), 417–439. https://doi.org/https://doi.org/10.36643/mjrl.24.2.digital

Dachwitz, Ingo. & Hilbig, Sven (2025). Digitaler Kolonialismus. Wie Tech-Konzerne und Großmächte die Welt unter sich aufteilen. https://doi.org/10.17104/9783406823039

Malik, Satyajeet. (2022a, April 29). Series on Digital Colonialism: How Meta aims to dominate India's agriculture sector. https://netzpolitik.org/2022/series-on-digital-colonialism-how-meta-aims-to-dominate-indias-agriculture-sector/

Malik, Satyajeet. (2022b, May 6). Series on Digital Colonialism: Global labor chains of the western AI. https://netzpolitik.org/2022/series-on-digital-colonialism-global-labor-chains-of-the-western-ai/#netzpolitik-pw

Neuerer, Dietmar. (2025, April 16). Datentransfer: Faeser pocht auf Einhaltung von US-Zusagen zu Spionageschutz. https://www.handelsblatt.com/politik/deutschland/datentransfer-faeser-pocht-auf-einhaltung-von-us-zusagen-zu-spionageschutz/100120631.html

The Guardian. (2025, January 20). Trump inauguration: Zuckerberg, Bezos and Musk seated in front of cabinet picks | Trump administration | The Guardian. https://www.theguardian.com/us-news/2025/jan/20/trump-inauguration-tech-executives

Thiel, Peter. (2009). The Education of a Libertarian | Cato Unbound. Retrieved May 24, 2025, from https://www.cato-unbound.org/2009/04/13/peter-thiel/education-libertarian/

Ziai, Aram (2020): Neocolonialism in the global political economy of the 21st century, in: *Momentum Quarterly* 9 (3), 128-140. https://www.momentum-quarterly.org/momentum/issue/view/308

# The role of geospatial information infrastructure for large scale topographic mapping acceleration in Indonesia

Winhard Ronald Tampubolon

*Geospatial Information Agency of Indonesia, Directorate for Geospatial Information Standard and Technology, Jl. Raya Jakarta-Bogor KM 46, 16911, Bogor, Indonesia, winhard.r@big.go.id, winhard@daad-alumni.de*

**Abstract**: Legislation in Act Nr. 4 / year 2011 about Geospatial Information (UUIG) mandates the fundamental availability of Geospatial Data and Information (GD/I) as a basis for accountable, measurable and objective decision-making process. However, the challenges of implementing GD/I, especially at the highest level of detail or on a large scale for the territory of the Republic of Indonesia, which covers a land area 5 times the size of the Federal Republic of Germany, certainly require an accelerative and innovative breakthrough strategy. The strategy for implementing GD/I through an innovative acceleration process has been chosen as the optimal solution based on considerations of production cost efficiency factors in the form of the application of standardized Geospatial Processing Center (GPC) and the development of Human Resources (HR) in the GD/I field as its main driving force. In accordance with UUIG, the role of Geospatial Information Infrastructure (IIG) which includes policy, institution, technology, standard and HR is a key factor towards the aforementioned acceleration process. The IIG components should be developed in an integrated (non-partial) manner and connected to each other, for example in the development of innovation in GD/I acquisition technology, it is necessary to develop standards that are always dynamic in keeping up with developments in science and technology. As a comparison, the Federal Republic of Germany has a large-scale basic mapping technical unit equipped with the latest equipment including GD/I human resources with technical competencies covering data acquisition processes, geospatial processing and presentation and updating of geospatial data (geodata) in each region of the 16 states. Considering that the conditions and readiness of IIG between regions in our country are still not standardized, the acceleration process of Basic GD/I is still carried out centrally in this case by the Geospatial Information Agency (BIG) as the National Mapping Agency in accordance with UUIG. As a consequence, the role of GD/I standards becomes very essential and fundamental as a reference for the provision and implementation of GD/I on a massive scale, even to the individual level, by referring to the Competency Qualification Standards for implementing GD/I. In addition, there is also a significant role of the Geospatial Reference System, especially when associated with the increasingly high resolution of geospatial data produced to achieve the highest level of accuracy. For this reason, a Geodetic Control Network standard is needed that can be referred to by stakeholders. In addition to the need for technology and methodology that are well standardized, of course, certified professional personnel are needed with knowledge qualifications, skills, and/or expertise and work attitudes that are relevant to the implementation of their duties and job requirements in what is called the Job Competency Standard (SKJ) in the government scope or the Indonesian National Work Competency Standard (SKKNI) in the industrial world. Meanwhile, the Indonesian National Standard (SNI) acts as a reference for the GD/I industrial sector in developing its business voluntarily so that its quality, objectivity, efficiency and effectiveness are certainly guaranteed. Especially in the GD/I industrial

sector which is market-driven, in addition to SKKNI and SNI, competency standards can also refer to international standards or special standards. For example, in supporting the acceleration of the production of Large-Scale GD/I Scale 1:5,000 and 1:1,000 and the realization of the Electronic-Based Government System (SPBE), a living and dynamic standard is needed related to the parallel implementation of GD/I activities, especially in the next 5 years. Since 2023, the Technical Committee 07-01 Geographic Information/Geomatics has increased its role to become a Participating Member (P-Member) in the ISO/Technical Committee (TC-211) Geographic Information by nominating experts who are active in various Working Groups (WG-1 and WG-6).

***Keywords:*** standard, geospatial, competency, Radar, SDI

## 1. Introduction

A form of legislation in Act Nr. 4 / year 2011 about Geospatial Information in Indonesia (UUIG, 2011) aims on the provision of Geospatial Data and Information (GD/I) as a basis for accountable, measurable and objective decision-making process. Based on aforementioned regulation, Geospatial Information Agency of Indonesia (BIG) is responsible to provide the GD/I access in order to enable the accountable governance as an integrated way with high availability. In order to integrate the GD/I into the business process, a kind of production system must be developed by following certain standard i.e. Open Geospatial Consortium (OGC) as introduced by Jacob et al. (2018). This standard will be used as a reference in the context of both geospatial infrastructure development and progression perspective.

However, the challenges of implementing GD/I, especially at the highest level of detail or on a large scale for the territory of the Republic of Indonesia, certainly require an accelerative and innovative breakthrough strategies. Indeed, it covers a land area 5 times the size of the Federal Republic of Germany. Therefore, the implementation strategy of GD/I production through an innovative acceleration program has been initiated to cover the whole Indonesian territory.

This acceleration requires massive production system that can be used by the responding stakeholders. Consequently, it opens possibility as the optimal solution based on considerations of production cost efficiency factors in the form of the application of standardized Geospatial Processing Center (GPC) and the development of Human Resources (HR) in the GD/I field as its main driving force. The term infrastructure has been selected to best describe how geospatial data shall be built and connected each other (Coleman, 1994). However, in addition to the aforementioned term, geospatial information infrastructure must extend the capability to increase productivity. This infrastructure inevitably will outperform current old-fashioned data center in conjunction with the new growing development of cloud computing system.

At the initial phase, the requirement of the GPC must be identified by doing literature study to generate Proof of Concept (PoC). To make GD/I more useful, the Cloud Computing System provides a lot of advantages such as effective GIS data processing, intelligent resource management, etc (Franchi, F. et al, 2024). One important example also comes from Disaster Management (DM) applications in a way of addressing related changes for geospatial big data analysis (Waleed, M., Sajjad, M., 2023). It can be inferred that the requirement for changes is mandatory to accommodate the geospatial data utilization more massively and collaboratively.

### 1.1 Geospatial standard

There are some major aspects to develop the up-to-date standard as a credible reference:

- Regulation

In order to ensure consistency and persistency, technical directive must be strengthened by legal formal actions. As identified by

Sjoukema et al. (2022) for Infrastructure for Spatial Information in the European Community (INSPIRE), the Spatial Data Infrastructure (SDI) shall be organized governmentally. Moreover, to take SDI into governance power, it is mandatory to provide some regulations as a framework umbrella.

- Technology

Current trend and state of the art of the technology infrastructure are aiming their ways on maximizing virtualization capabilities. Moreover, it can also enable the maximum number of users to perform massive D/IG production.

NoSQL database such as MongoDB has prominent capability to replicate with high availability through different nodes and infrastructure (Rathore et al., 2024). In this case, the virtualization scheme will maximize the deployment of different databases to support effective geospatial queries.

- Algorithm

Appropriate GPC workflow must follow the technological design in order to achieve best performance. As will be elaborated in , the algorithm can be adjusted with respect to the nature of each involved GD/I in the aforementioned acceleration program.

- Institution

To bring geospatial aspect into the governing process is a big leap especially for Indonesia as one of the developing countries with big potential. For instance, Governance and Institutions is one puzzle component of important strategic pathway in the United Nation-Integrated Geospatial Information Framework (UN-IGIF, 2023).

- Human Resources

As the developed GPC will operate and handle massive datasets this research also identifies the Human Resources (HR) competency standards requirements. That identification can be subsequently used by corresponding stakeholders involved in the national G/DI provision based on regulation as well as technological/industrial point of views (Tampubolon et al., 2022). The standards of G/DI empowerments are fundamental especially in certain situation where there are various technology and method available in the society as well as G/DI industries. For this purpose, the proper professional certification must be essentially well defined to prepare excellent GI human resources as the primary source for the provision of reliable GI data and information in favour of the LSTM and updating acceleration program.

### 1.2 Objectives and motivation

To ensure the compliance between standard and the latest available technologies, it is required that the future developed GPC must be used in the context of Large-Scale Topographic Mapping (LSTM) acceleration in Indonesia. By comparing the performance of open source and commercial platform from different processing scheme, the standard of GD/I processing can be customized with the optimized solution.

With respect to conventional geospatial data acquisition projects i.e. LSTM in a scale of 1:5000, the geospatial data processing can be improved to increase the resolution and accuracy of the output. It cannot be avoided that GCPs data as an important input must be used to increase the planimetric and elevation accuracy. Indeed, it shall be used in the GPC by a compliance to the LSTM requirements. Therefore, this research demonstrates an objective based on the high-end product to set up GPC with minimum redundancy measures amid budgetary limitation.

Another goal of this paper is to give recommendations for a proper usage of space borne data for an improved data processing chain in the special case of Indonesia. It includes the GCP requirements as well as the processing schemes based on certain assessment standards in the context of LSTM in Indonesia.

### 1.3 Research workflow

This research mainly concentrates on the establishment of GPC with respect to any involving components such as standard and user requirements (Error: Reference source not

found). To identify and validate the user requirements, it is necessary to perform independent quality assurance.
In principle, there are 3 important indicators to be used for the establishment of GPC namely accessibility, productivity, and quality. Finally, this research aims to process LiDAR, radar and photogrammetric data in appropriate geometric accuracy for LSTM purpose.

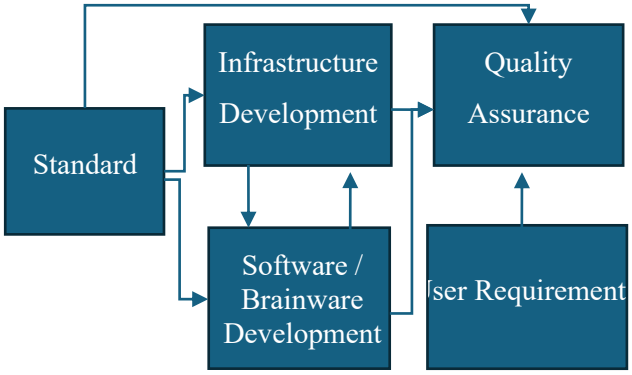


Figure 1. Research workflow.

### 1.4 Scope of works

Based on business process of GD/I, it is important to initially encounter what kind or type of geospatial data that must be processed by the GPC. Subsequently, the standard must be determined to keep the platform interoperable and measurable. By referring to the aforementioned standard, the GPC can be built with four important aspects namely infrastructure (hardware and software), storage (database), connectivity (access), and number of users (massiveness).

| Data nature and workflow | Aspects | | | |
|---|---|---|---|---|
| | Infrastructure | Storage | Access | Number of users |
| Radar | HPC (CPU) | 5 PB | VPN | 500 |
| LiDAR and Photogrammetry | HPC (CPU) | 5 PB | VPN | 500 |
| GIS processing | CPU Server | 1 PB | Web Service | 500 |
| GeoAI | HPC (GPU) | 2 PB | Web Service | 500 |
| G/DI publication | CPU Server | 1 PB | Web Service | Public |

Table 1. Scope of works

## 2. Algorithm and Workflow

### *2.1* Geospatial data sources

The continuous development of new space-born platforms (GNSS, VHRS, SAR), digital aerial mapping, and GIS triggers not only National Mapping Agencies (NMAs) but also private sectors to map and visualize massively the entire world. The potential data sources with respect to its sensors were also listed that have been used as a customized solution for Indonesian territories (Tampubolon, 2020) e.g. aerial photogrammetry, satellite imageries, geodetic control survey, others (LiDAR, radar, UAV, etc.). However, it is interesting that the UAV data is not mentioned as a potential data source in the aforementioned study. In addition, from the NMA's perspective the utilization of satellite imageries to produce official topographic maps is relatively infrequent, while private companies such as Google, Microsoft are giving more effort to the production of orthoimages from VHRS.

As explained in before the focus of this paper is about the geometrical quality of the output instead of specific technology pre-requisite as an input to the LSTM work chain. However, there was a guidance resp. standard of the geospatial data collection as regulated in the Regulation of Head of BIG No 2/2012 that mentioned about the acceptable methodologies:

(a) Survey and acquisition using sensor based on land, marine, air or space vessels;
(b) Census;
(c) Other methods following the trend of technology.

Based on the aforementioned regulation, available data acquisition technologies are listed in Table 2 to identify the potential data sources for LSTM.

| Data source | Processing | Coverage | Administrative aspect |
|---|---|---|---|
| Optical satellite-based | National orthorectification | Global | National license |
| Radar satellite-based | End product | | Exclusive license |
| Airborne InSAR | Complicated | Regional-based | Security clearance |
| Airborne LiDAR | | | |
| Aerial metric camera | | | |
| UAV/Drone | Customized | Small AOI-based | Survey permit |
| Terrestrial survey | | | |

Table 2. Geospatial data sources

### 2.2 Geospatial Artificial Intelligence (GeoAI)

In an initial step, Generative Artificial Intelligence (GenAI) will be implemented to handle non-geospatial data analysis. For example, geographical names (toponyms) consist of textual information derived by multi discipline contributions. For so long Relational Database Management Systems (RDBMS) such as geodatabase, PostgreSQL have been used as the geospatial data storage that can also perform some geospatial analysis within their platform. However, in various cases it has been shown that the bigger the data, the lower also the performance. Therefore, the implementation of NoSQL database in handling some technical and operational geospatial analysis is planned to be developed in the GPC (see Figure 2).

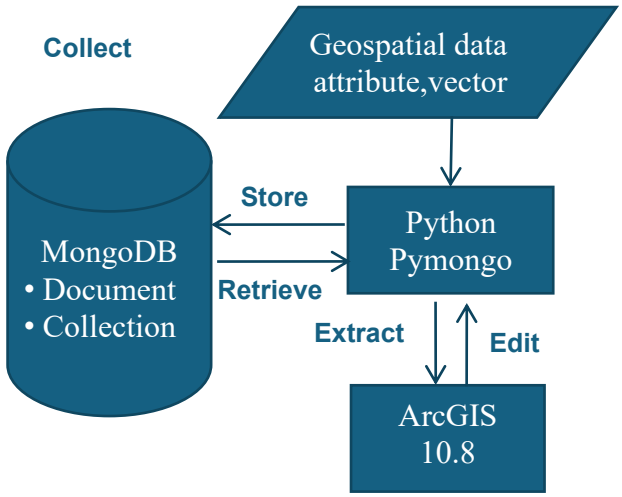


Figure 2. NoSQL platform design.

Even though the interaction between geospatial and AI has been established in many applications, there is no built-in method currently existed. The term of GeoAI somehow has been introduced to address incubation between both geospatial and AI as a set of high-end tools. The gap between AI and geospatial analysis, providing tools for processing, analyzing, and visualizing geospatial data using advanced machine learning techniques. Whether you're working with satellite imagery, LiDAR point clouds, or vector data, GeoAI offers intuitive interfaces to apply cutting-edge AI models.

This paper discusses about the role of geospatial signature for topographical object recognition from different vector datasets. Its characteristic can be used to identify common objects i.e. points which subsequently play a role in geometrically transforming OSM data into official Large Scale Topographical Map. Hence automation process concentrates on three steps approach namely geospatial signature identification, transformation and finally vector data ingestion. Despite its technical achievement, the implementation of this approach is currently ongoing using mongodb and python scripting environment in ArcGIS platform.

### 2.3 GI Human Resources

As a consequence, the role of GD/I standards becomes very essential and fundamental as a reference for the provision and implementation

of GD/I on a massive scale, even to the individual level, by referring to the Competency Qualification Standards for implementing GD/I. In addition, there is also a significant role of the Geospatial Reference System, especially when associated with the increasingly high resolution of geospatial data produced to achieve the highest level of accuracy.

## 3. Geospatial Processing Center (GPC)

The acceleration cycle of basic GD/I provision, especially by utilizing radar Interferometry technology, is expected to be raised to an international standard through the active role as mentioned above. No less important, competency standards are the main basic requirements in national GD/I implementation activities.

### 3.1 Cloud computing system

To establish the Cloud Computing System environment, the GD/I business process must be fixed initially (Sjoukema et al., 2022).

#### 3.1.1 *Infrastructure*

The GPC will hand over the multi-source geospatial data records (radar, LiDAR, photogrammetry) to the MongoDB server for processing. In this case, the role of config server is essential to combine dataset information and data fragmentation information for effective distribution. Each shard includes at least three members that store data, including a primary member and two secondary members (Cheng et al., 2020).

When the master database goes down, two slaves will run for election, one of which will become the master database. After the original master database recovers, it may join the current replication cluster as a slave. The horizontal expansion of the sharding mode can make more efficient use of unused computer resources, while using replication sets for sharding can reduce the time that the database cannot provide data support and achieve 100% availability. In this way, the framework can provide secure, efficient, and fast multi-source remote sensing data storage and retrieval capabilities for big EO data services.

#### 3.1.2 *Application sites*

Given the geospatial data processing requirement, there are several schemes to get the physical data either by providing extracted GIS-ready data (download) or enabling a direct access to the geodatabase (service), namely:

- Cloud Computing System

Founded in 2007 by OSM founder Steve Coast, Cloudmade has actively developed spatial-enabled applications and services. In a close relationship to the OSM project, Cloudmade provides the flat files OSM data in several formats such as shapefile, osm bz2, gpx during the offline process from the OSM database. Since there are some additional processes to prepare the extracted data in the country wise unit by using clipping operation, the update status will be approximately 1 week later from the actual live datasets.

- API

API in OSM has been built based on the RESTful request, which uses the form of http GET, PUT, POST and DELETE messages. Current version of OSM API was released on April 2009 by the version 0.6, where the new URL https://api.openstreetmap.org (within OAuth) has been launched.

The RESTful request enables the manipulation (access, edit and delete) function of the resources by using standard HTTP request. Therefore, the given URL can directly extract the requested resources to the local storage in the xml (*.osm) format.

Limitations in API are mostly related to the data extraction capability, which is basically classified as feature and bandwidth limitation. The API restricts querying boundary only to the extent of 0.5 x 0.5 degrees per-request.

- XAPI

The Extended API (XAPI) serves the user with more flexible capability, which has bigger querying boundary i.e. 10 x 10 degrees per request. The advantage using XAPI also relates with the bandwidth capacity, where there is no bandwidth limitation as limited in the API.

This service is supported by a lot of servers, which can be checked from the Platform Status[14] functionality. Therefore, the access can be switched from one to another depends on the service availability.

### 3.2 Big data and Volunteered Geographic Information

In the G/DI area, there are some related applications and technologies with big data utilization such as Volunteered Geographic Information (VGI), Disaster Management (DM), participatory mapping, etc.

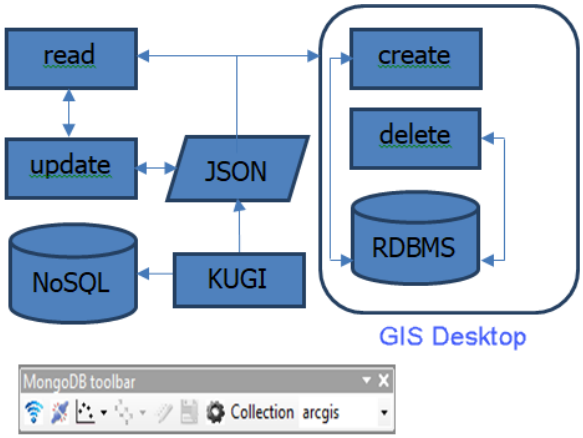


Figure *3*. Prototype of hybrid geospatial processing platform.

### 3.3 GeoAI and Mapupdating

#### 3.3.1 *Dynamic time series data*

Differential Interferometric Synthetic Aperture Radar (D-InSAR) has been implemented in a time series manner to detect earth surface deformation for DM purpose. Especially in the situation where accurate DEM reference and/or GCP are not available, this time series analysis will contribute to the Decision Support System (DSS).

$$\Phi = \Phi_{flat} + \Phi_{height} + \Phi_{differential} \quad (1)$$

From equation (1), the differential phase component can be subtracted from unwrapped phase ($\boldsymbol{\Phi}$) if the flat earth phase and height phase are known (Richards, 2007). Afterwards the deformation (d) in meter from multi temporal datasets can be calculated using equation (2), where $\boldsymbol{\lambda}$ = wavelength in m (X Band).

$$d = \frac{\lambda \Phi_{differential}}{4\pi} \quad (2)$$

#### 3.3.2 *Spatial Data Infrastructure*

In the framework of Geospatial Information National Network (JIGN), SDI may concentrate on a service establishment as a geospatial data warehouse which enables spatial data filtering process internally. Indeed, the LSTM involves a huge amount of geospatial raw data that need to be regularly synchronized from different sources. The SDI puts spatial data discovery, evaluation, and application as a Key Performance Indicator (KPI) for corresponding users and providers within all levels of government, the private sector, the non-profit sector, and by the general public users (communities).

The infrastructure developed based on the concept of reliability and availability, in such a similar way with a highway or telecommunications network, where facilitates the access to geographically related information using well defined set of standard practices, protocols, and specifications. The applications that run in such an infrastructure are not specified in detail in this document. But, like transportation networks, an SDI will enable the virtual network as the packages to support the geographic visualization and information.

Specifically, an SDI must be more than a single data set or database; an SDI hosts geographic data and attributes, sufficient documentation (metadata), a means to discover, visualize, and evaluate the data (catalogues and Web mapping), and some method to provide access to the geographic data. Beyond this are additional services or software to support applications of the data. To make an SDI functional, it must also include the organizational agreements needed to

[14] http://wiki.openstreetmap.org/wiki/Platform_Status (last accessed 31.08.2025)

coordinate and administer it on a local, regional, national, and or trans-national scale.

Although the core SDI concept includes within its scope either base data collection activities or myriad applications built upon it, the infrastructure provides the ideal environment to connect applications to spatial data. Therefore, it will influence both data collection and applications construction through minimal appropriate standards and policies.

In this case, the interoperability connection within commercial platform will take part in the spatial data access and in the spatial data extraction into an SDI. Technically there are 2 involved spatial databases in the development of mentioned SDI. As a representation of commercial software, the ESRI Geodatabase and Oracle Spatial have been used to establish the intermediate processing medium and to access the reference data. On the other side, PostgreSQL has been used to establish the prototype of open-source geodatabase as an alternative for further evaluation.

### 3.3.3 *GeoAI algorithm*

MongoDB has introduced an open-source NoSQL document storage database with a replication using data partitioning approach across multiple machines. This approach provides robust ad hoc query support as well as spatial indexing of simple points as inferred in equation 3 and 4.

$$G_{sign}(dX, dY) = \sum_{n=1}^{m}(dist * \sin \propto), \sum_{n=1}^{m}(dist * \cos \propto) \quad (3)$$

$$Dev_{sign}(dX, dY) = (\min_{m} \sqrt{dX^2 + dY^2}) \quad (4)$$

For so long, the term of NoSQL database has been introduced as a potential alternative solution in the GPC. Advantageously, it can extend the powerful capability of GIS data processing into a type of distributed infrastructure platform.

The evaluation of the performance will lead to the more robust approach of geospatial data processing in comparison with conventional RDBMS. There are some aspects to be further investigated such as query response, geoprocessing time and geospatial data extraction.

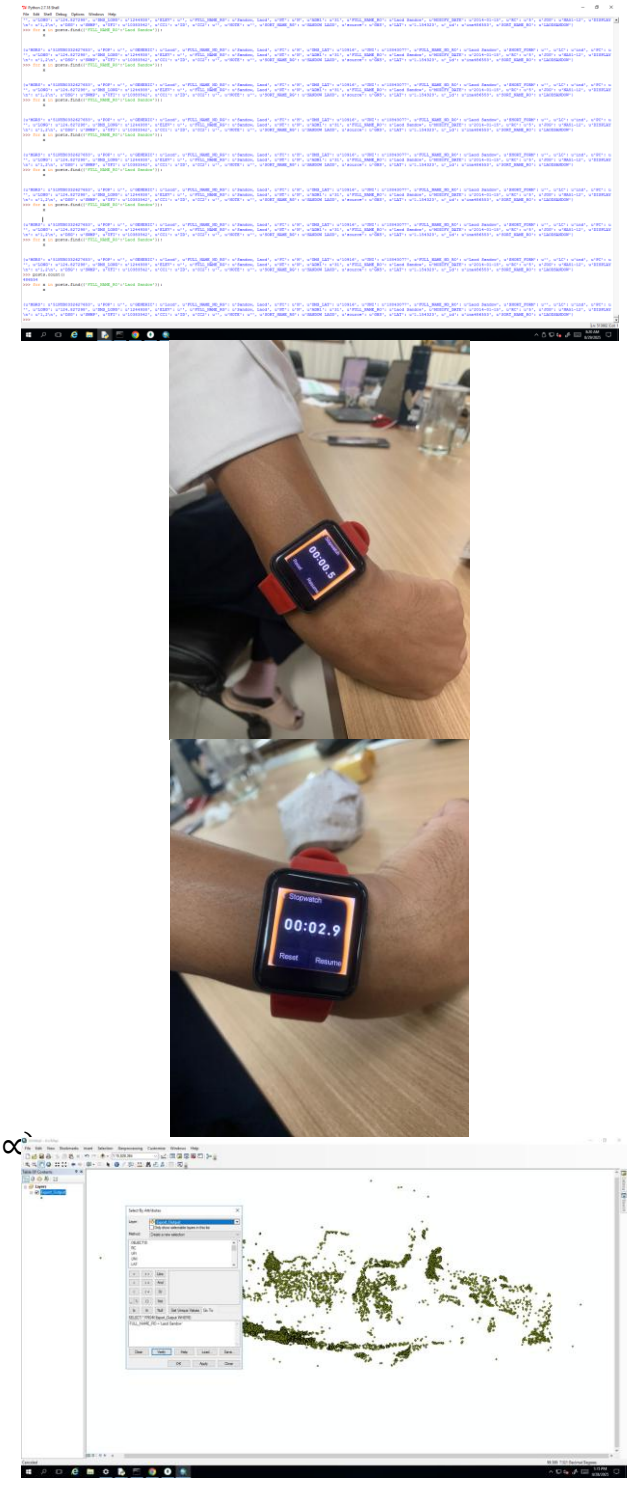


Figure 4. Performance comparison of NoSQL vs RDBMS.

As depicted in Figure 4 (upper part), for only attribute querying on toponym (geographical names) features based on MongoDB collection (embedded documents) takes only 0,5 second (middle left part). On the other hand, the same

attribute query from RDBMS (ArcGIS geodatabase) needs 2,9 seconds to get (Figure 4, middle right and lowest parts). This advantage can help the GeoAI implementation especially by incorporating the Geospatial Signature (point-based s. equation 3 and 4). The accuracy and performance of GeoAI will be subsequently improved especially in a High-Performance Computing (HPC) based on Graphic Processing Unit (GPU).

## 4. Conclusion and Future works

From this study, it has been shown that up-to-date geospatial processing framework data, in this case GPC, can play an important role not only in LSTM but also in DM analysis. Despite neglecting other important aspects such as budgetary factors in our investigations, it is likely that the GPC shall be built on a CCS environment as depicted in  and supported by the results of the detail investigations in section 3.1 and 3.2.

Basically, radar interferometry is a potential technology to be used as a support of the Tsunami Early Warning System (TEWS) not only by DEM Generation but also by D-InSAR technique. D-InSAR can be applied especially in the active volcano island to monitor the trend of deformation in advance.

The acceleration cycle of basic GD/I provisions, especially by utilizing Radar Interferometry technology, is expected to be raised to an international standard through the active role as mentioned above. No less important, competency standards are the main basic requirements in national GD/I implementation activities. Based on the analysis of national HR needs, it is possible to identify qualifications that require specific studies related to IG business and industry processes, both in terms of national/international qualifications and specifically in the industry as intended. This will accelerate and incubate the realization of excellent HR, as one of the determining factors for the implementation of GD/I whose quality can be accounted for, especially to support national development planning, monitoring and evaluating activities.

Finally, we have established the hybrid approach of NoSQL and RDBMS for handling geospatial data processing using both commercial and open-source platforms. Our investigations show that within the hybrid platform 2D Index partitions present effective and efficient CRUD operation compared to RDBMS. In the future, this hybrid geospatial processing management approach can be extended for cartographic and visualization purposes in the GPC development.

## 5. Acknowledgements

We would like to thank German Academic Exchange Service (DAAD) for supporting this research publication being presented in the Applied Geoinformatics for the Society and Environment (AGSE) Conference 2025.

## 6. References

Cheng, Yinyi, Kefa Zhou, Jinlin Wang, and Jining Yan. 2020. Big Earth Observation Data Integration in Remote Sensing Based on a Distributed Spatial Framework. In Remote Sensing 12, no. 6: 972. https://doi.org/10.3390/rs12060972

Choi, Yosoon. 2023. GeoAI: Integration of Artificial Intelligence, Machine Learning, and Deep Learning with GIS. In Applied Sciences 13, no. 6: 3895. https://doi.org/10.3390/app13063895.

Coleman, David J., McLaughlin, John D., 1994. Building A Global Spatial Data Infrastructure: Usage Paradigms and Market Influences, GEOMATICA Vol. 48, No.3, pp. 225 to 236.

Daniel, M., Yuhong, He., Moore, G.W.K., 2024. Trends and applications in wildfire burned area mapping: Remote sensing data, cloud geoprocessing platforms, and emerging algorithms, Geomatica, Volume 76, Issue 1, 100008, ISSN 1195-1036, https://doi.org/10.1016/j.geomat.2024.100008.

Franchi, F., Graziosi, F., Fina E. D., and Galassi, A., 2024. A Survey of Cloud-Enabled GIS Solutions Toward Edge Computing: Challenges and Perspectives, in IEEE Open Journal of the

Communications Society, vol. 5, pp. 312-331, doi: 10.1109/OJCOMS.2023.3344198.

Guo, Dongming, and Erling Onstein. 2020. State-of-the-Art Geospatial Information Processing in NoSQL Databases. In ISPRS International Journal of Geo-Information 9, no. 5: 331. https://doi.org/10.3390/ijgi9050331

Jacob H.J., Emad E., Rune H. J., Thomas S.T. 2018 Open geospatial infrastructure for data management and analytics in interdisciplinary research, Computers and Electronics in Agriculture, Volume 145, pp. 130-141, ISSN 0168-1699, https://doi.org/10.1016/j.compag.2017.12.026.

Rathore, Mukesh, and Sikha S. Bagui. 2024. MongoDB: Meeting the Dynamic Needs of Modern Applications. In Encyclopedia 4, no. 4: 1433-1453. https://doi.org/10.3390/encyclopedia4040093

Sjoukema, Jaap-Willem, Jalal Samia, Arnold K. Bregt, and Joep Crompvoets. 2022. The Governance of INSPIRE: Evaluating and Exploring Governance Scenarios for the European Spatial Data Infrastructure. In ISPRS International Journal of Geo-Information 11, no. 2: 141. https://doi.org/10.3390/ijgi11020141

Tampubolon, W. 2016. Hybrid Concept of NoSQL and Relational Database for GIS Operation, Association of Geographic Information Laboratories in Europe (AGILE) Conference, https://www.unibw.de/geoinformatik/mitarbeiter/archiviert/pdf-dateien-tampubolon/agile-2016_121_paper.pdf.

Tampubolon, W. 2020. Investigations for an improved Large Scale Topographic Mapping in Indonesia, Dissertation, Universität der Bundeswehr München.

Tampubolon, W., Reinhardt, W., and Behr, F.-J. 2022. Acceleration of Human Resource Development for the UAV data processing in Indonesia, AGILE GIScience Ser., 3, 62, https://doi.org/10.5194/agile-giss-3-62-2022.

UN-IGIF, 2023. A Strategic Guide to develop and strengthen National Geospatial Information Management, Second Edition. https://ggim.un.org/UN-IGIF/documents/Part_1_UN-IGIF_Overarching_Strategy_Second_Edition_27Feb2023.pdf.

Waleed, M., Sajjad, M., 2023. On the emergence of geospatial cloud-based platforms for disaster risk management: A global scientometric review of google earth engine applications, International Journal of Disaster Risk Reduction, Volume 97, 104056, ISSN 2212-4209, https://doi.org/10.1016/j.ijdrr.2023.104056.

# Multitemporal monitoring of cloud forest ecological restoration using remote sensing: evidence for local climate change adaptation

Monica Alejandra Acosta Vega

*Francisco José de Caldas District University, Hochschule Für Technik Stuttgart; Maav94@hotmail.com*

**Abstract**: This study evaluates the effectiveness of a restoration project in a tropical cloud forest ecosystem in the rural area of Prado, Facatativá, Cundinamarca, through a multitemporal analysis of satellite time series from 2009 to 2024. Eight key years were selected (2009, 2011, 2013, 2015, 2018, 2020, 2022, and 2024). Landsat and Sentinel images, processed on the Google Earth Engine platform, were used, and the study was complemented with statistical analyses in Python. For a reliable analysis, images were carefully selected from the dry season (December to March) to mitigate cloud cover. Cloud masks were also applied to avoid noise or outliers, and images were resampled to a 30-meter resolution to ensure data comparability between sensors. The results demonstrate a clear recovery of the ecosystem. The biomass indices LAI and NDVI showed a sustained increase, with the distribution of their values shifting to higher ranges. Similarly, the moisture indices LSWI and NDMI indicated an improved capacity for vegetation water retention. However, fluctuations were observed across the years due to natural effects from factors such as precipitation, temperature, and solar radiation. In the context of a changing climate, a comprehensive analysis of these factors requires further research to disentangle the influence of the restoration process from interannual climate variability. The Mann-Kendall trend analysis confirmed that the increase in NDVI values is statistically significant ($p = 0.0461$, $Tau = 0.6071$), validating the project's effectiveness. These findings demonstrate the success of the restoration process and highlight the potential of remote sensing for long-term monitoring of tropical ecosystems.

***Keywords:*** Ecological restoration, Cloud forest, Remote sensing, Multitemporal analysis, Vegetation indices, landsat/sentinel.

## 1. Introduction

Cloud forests are vital ecosystems that play a crucial role in providing ecosystem services, particularly hydrological regulation (Karger et al., 2021) Thanks to their ability to capture atmospheric water, they contribute to aquifer recharge and supply for local communities. However, they face severe threats from deforestation, land-use change, and climate change (Karger et al., 2021).

The Prado rural district in Facatativá (Cundinamarca) illustrates this issue. A 0.70 km² public property underwent severe degradation due to extensive cattle ranching, which caused vegetation loss and erosion. Given its importance as a recharge zone, an ecological restoration project was launched in 2010 as an environmental compensation initiative by the company BioD, following CAR's guidelines. The process included the planting of native species and community

participation in maintenance and monitoring during the following two years. Evaluating the success of such projects is essential to validate methodologies and guide future investments. However, traditional monitoring methods are often costly and limited. Remote sensing offers an effective alternative by enabling multitemporal and large-scale analyses (Chazdon & Guariguata, 2016). This study leverages Google Earth Engine and statistical analysis in Python with Landsat and Sentinel image series (2009–2024), applying biophysical indices (LAI, NDVI, LSWI, and NDMI) to assess biomass recovery and hydrological functionality. The results provide evidence of restoration effectiveness and propose a replicable methodology for future projects.

## 2. Study Area

The study area is located in Prado, in the municipality of Facatativá, Cundinamarca, Colombia (Image 1). The property, covering 0.70 km², is part of a cloud forest ecosystem. Historically, the land suffered severe degradation due to extensive cattle ranching, leading to significant vegetation loss and erosion processes. The need for restoration became evident because of the area's hydrological importance, functioning as a recharge zone and water source for local aqueducts, as well as its suitability for forest protection and production.

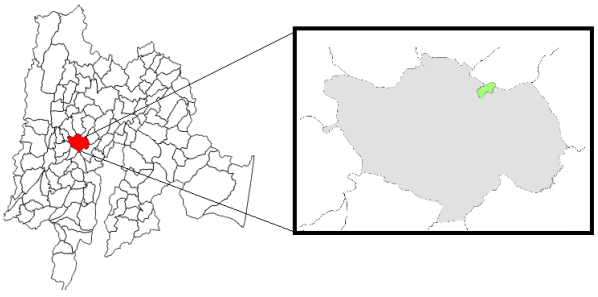

Figure 1. Location area of interest

## 3. Methodology

### 3.1 Satellite Data Sources

Images from the Landsat 7 LE07/C02/T1_L2, Landsat 8 LC08/C02/T1_L2, and Sentinel-2 (COPERNICUS/S2_SR_HARMONIZED) missions were used. The multitemporal analysis period covered the years 2009, 2011, 2013, 2015, 2018, 2020, 2022, and 2024, selecting images mainly from the dry season (December–March) in order to minimize cloud cover and ensure comparability across the years. The combination of different sensors responded, on the one hand, to the need to cover the entire study period starting in 2009, and on the other, to a methodological strategy to compensate for the loss of usable images due to persistent cloudiness in humid montane ecosystems. This practice is recommended in the literature, as the integration of optical sensors with different spectral and temporal characteristics improves the continuity of time series and reduces data gaps (see, e.g. Chu et al., 2019))

### 3.2 Image Processing in Google Earth Engine

Image processing was carried out on the Google Earth Engine (GEE) platform. For each year of analysis, three representative images from the dry season (December–March) were selected, with the aim of minimizing the effect of cloud cover. From these images, median composites were generated, which reduced intra-annual variability and mitigated the presence of residual clouds. Additionally, cloud masks specific to each sensor (functions *maskLandsatSR* and *maskS2clouds*) were applied, removing pixels contaminated by clouds and shadows.

The selection of only three images per year was due to the limited availability of cloud-free scenes in cloud forest ecosystems, which constitutes an important methodological restriction that must be considered when interpreting the results.

Since Sentinel-2 provides a spatial resolution of 10 m in its optical bands, while Landsat provides 30 m, it was necessary to apply bilinear resampling (*resample('bilinear')*) and reproject to 30 m in order to harmonize both data sources. This standardization of spatial resolution is essential to ensure comparability of the time series and to avoid biases in the calculation of spectral indices and trends, since

resolution differences can generate discrepancies in change detection or biomass estimation.(Adagbasa & Mukwada, 2022)

### 3.3 Calculation of Biophysical Indices

The following spectral índices were calculated:

#### 3.3.1 *Normalized Difference Vegetation Index (NDVI):*

NDVI is a spectral index based on the normalized difference between near-infrared (NIR) and red (RED) reflectance. It allows for estimating vegetation vigor and density, being highly sensitive to photosynthetic activity (Huang et al., 2021).

$$NDVI = \frac{NIR - RED}{NIR + RED} \quad (1)$$

Bands: SR_B4 and SR_B3 (Landsat 7), SR_B5 and SR_B4 (Landsat 8), B8 and B4 (Sentinel-2).

#### 3.3.2 *Normalized Difference Moisture Index (NDMI):*

NDMI is built from the normalized difference between NIR and SWIR1 bands. It is designed to detect changes in vegetation water content and evaluate drought stress conditions (Dutrieux et al., 2016)

$$NDMI = \frac{NIR - SWIR_1}{NIR + SWIR_1} \quad (2)$$

Bands: SR_B4 and SR_B5 (Landsat 7), SR_B5 and SR_B6 (Landsat 8), B8 and B11 (Sentinel-2).

#### 3.3.3 *Índice de Área Foliar (LAI):*

LAI represents the leaf area per unit of ground surface (m² of leaves/m² of soil). It can be estimated from NDVI using empirical logarithmic functions. In this study, it was estimated from NDVI following Turner et al. (1999):

$$LAI = -ln\left(\frac{0.69 - NDVI}{0.59}\right) \quad (3)$$

#### 3.3.4 *Land Surface Water Index (LSWI)*

LSWI uses the normalized difference between NIR and SWIR and is sensitive to water content in both vegetation and soil. It is useful for studies of seasonal dynamics, drought monitoring, and restoration assessments. (Chandrasekar et al., 2010)

$$LSWI = \frac{NIR - SWIR}{NIR + SWIR} \quad (4)$$

### 3.4 Statistical Analysis and Visualization

For each index, the annual mean and standard deviation were calculated using the functions ee.Reducer.mean() and ee.Reducer.stdDev() in Google Earth Engine. Subsequently, in order to identify trends over the study period, a per-pixel linear regression fit was applied using ee.Reducer.linearFit. This procedure allows for evaluating the direction and magnitude of vegetation changes, distinguishing increases, decreases, or lack of significant variation in NDVI values. (Gaitan et al., 2015)

The values extracted from Google Earth Engine were processed in Python using the libraries Pandas, Matplotlib, and SciPy. Boxplots were generated to represent the annual distribution of NDVI, allowing the evaluation of median, dispersion, and presence of outliers for each year. This approach is particularly useful in vegetation studies because it highlights both central trends and spatial heterogeneity in cover (Forkel et al., 2013; Hilker et al., 2009), Line graphs were used to illustrate temporal evolution, and spatial trend maps were also created. Additionally, the non-parametric Mann-Kendall test was applied to evaluate the statistical significance of the observed trend. This test is especially suitable for ecological time series analysis, as unlike parametric models such as simple linear regression, it does not require normality assumptions and has low sensitivity to outliers (Kh Aswad et al., 2020).

### 3.5 Data Control and Quality Strategies

Due to the high cloudiness characteristic of cloud forests, the availability of satellite images free from atmospheric contamination was limited. As a strategy, only images from

the dry season were selected, when cloud cover is less frequent. Even so, in several years it was only possible to integrate three scenes for the generation of the median composites.

This restriction constitutes one of the main limitations of the study and reflects the inherent challenges of remotely monitoring humid tropical ecosystems.

## 4. Results

### 4.1 Normalized Difference Vegetation Index (NDVI)

The NDVI showed an improvement in the index over the years, with predominantly yellow tones in 2009 and coverage with NDVI values close to 1 by 2024 (image 2)

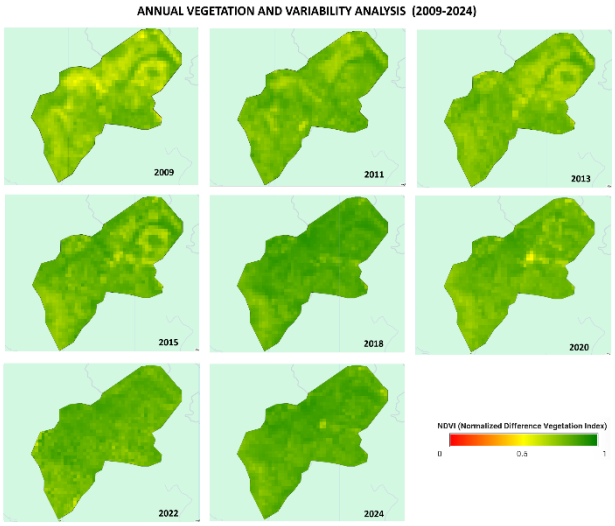


Figure 2. Annual Vegetation and Variability of NDVI (2009-2024)

To highlight the changes over time, a linear regression was performed to obtain the trend map (NDVI Slope), which shows a progressive increase in vegetation cover and vigor within the restoration area (Image 3). Most of the polygon exhibits positive increases in the index, suggesting a process of vegetation recovery in response to restoration actions.

However, specific sectors with decreases in NDVI were identified, possibly associated with anthropogenic pressures, edaphic limitations, or ecosystem dynamics (Image 3).

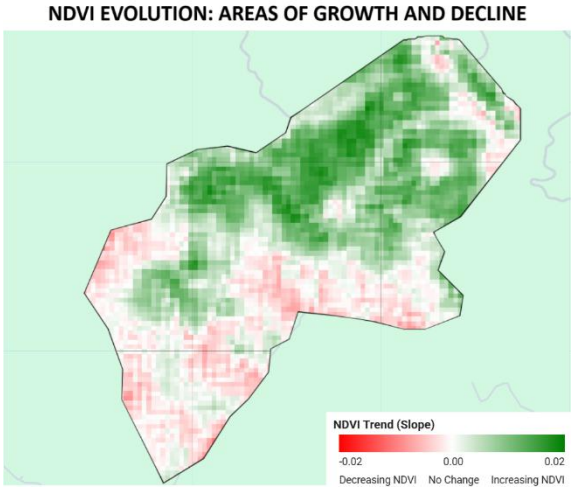


Figure 3. NDVI trend (slope)

The temporal analysis of the annual mean NDVI reveals interannual fluctuations with notable peaks and declines (Image 4). These variations can be mainly attributed to two factors: (i) the limited availability of cloud-free images during the dry season, which reduces the representativeness of some years and constitutes a frequent limitation in ecosystems with high cloudiness, and (ii) the natural dynamics of the cloud forest, where climatic variability and moisture pulses generate changes in vegetation productivity and, consequently, in the reflectance recorded by the sensors.

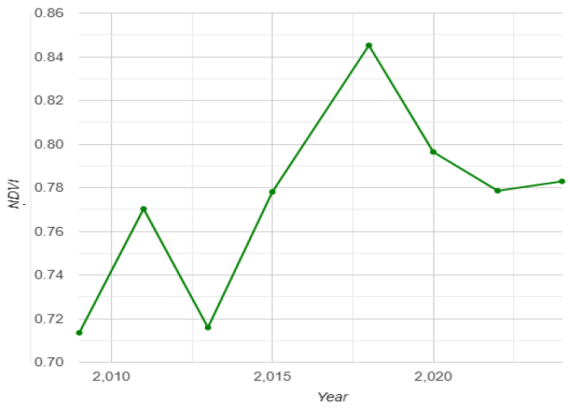


Figure 4. NDVI mean per year

Despite these oscillations, the linear trend analysis confirms a sustained increase in vegetation cover and vigor. The positive slope of 0.0037 per year (Image 5) indicates that, on average, the ecosystem has experienced a steady recovery between 2010 and 2024. This result is consistent with the ecological

restoration processes implemented in the area and validates that the actions undertaken have had a positive impact on the recovery of vegetation cover.

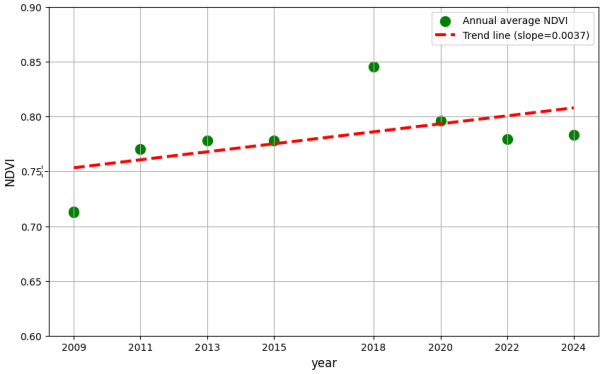


Figure 5: Restoration trend (Anual NDVI)

The analysis of NDVI distribution by year highlights the transition from a heterogeneous and degraded landscape (2009–2013, with dispersed and negative values reflecting bare soil and sparse vegetation) toward denser and more homogeneous coverage from 2015 onwards (values concentrated at NDVI > 0.7). In 2018, the highest uniformity was reached, while in 2022 a wider dispersion reappeared with both low and high values simultaneously, possibly linked to the high rainfall recorded that year. Overall, the boxplot illustrates how restoration promoted vegetation recovery,

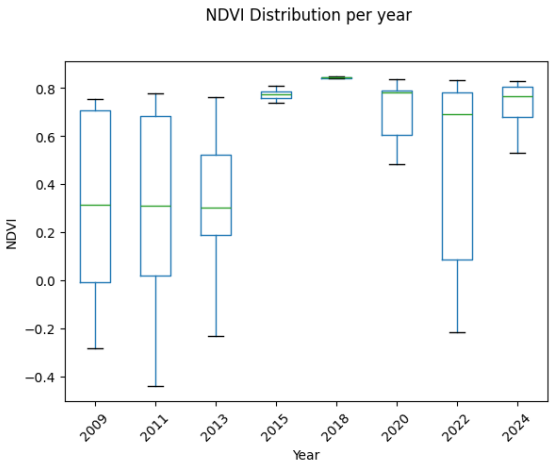


Figure 6: NDVI distribution per year

Taken together, the results demonstrate that although there are interannual variations in the spectral signal, restoration has promoted a sustained regeneration process, corroborated both by spatial analysis (slope map) and temporal statistics (annual mean series and trend analysis).

### 4.2 Leaf Area Index (LAI)

The temporal analysis of the Leaf Area Index (LAI) provided quantitative evidence of biomass recovery in the restoration area. The series of satellite images processed in Google Earth Engine revealed a significant change since the beginning of the project in 2010.

Image 7 shows a visible improvement in vegetation cover. In 2009, the area displayed low to medium biomass, as indicated by pale and light green tones. As the project progressed, especially between 2011 and 2018, biomass density increased progressively, reflected in a wider extent of dark green tones in the image. In recent years (2020–2024), the area has reached dense and homogeneous vegetation cover, indicative of a mature ecosystem undergoing consolidation.

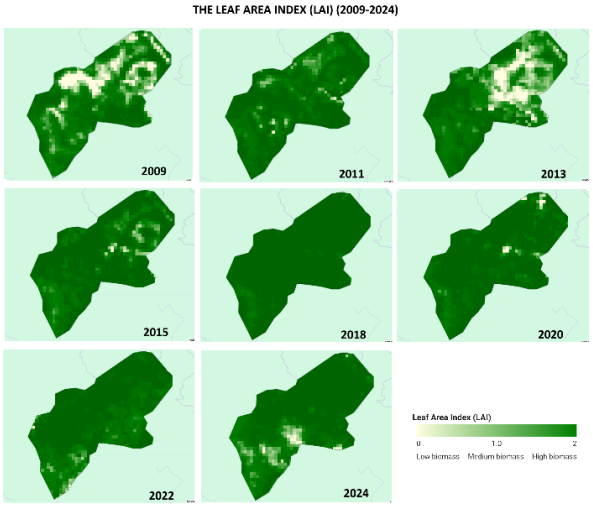


Figure 7: The graph of annual mean LAI

The graph of annual mean LAI confirms this trend. As shown in image 6, the mean LAI value exhibited a notable increase throughout the study period, with a peak in 2018. Interestingly, this year did not coincide with particularly high rainfall, since precipitation recorded in the AOI was relatively low (Image 7). This result suggests that the increase in leaf index was not directly driven by water availability, but rather reflects local processes

of vegetation recovery associated with the restoration project, or a temporal lag with respect to rainfall from previous years. Previous studies have documented that in tropical montane ecosystems, the response of vegetation indices may depend both on climatic factors and on internal ecosystem dynamics (Myneni et al., 1997)

### 4.3 Hydrological Recovery (LSWI)

The Land Surface Water Index (LSWI) was used to evaluate the recovery of the hydrological cycle and the retention of moisture in soil and vegetation, an ecosystem service that is critical for cloud forests. The results showed average values across all years, although an increase in moisture was observed between 2009 and 2024. In 2022, values were closer to 1, which is consistent with the fact that, according to IDEAM, late 2021 and early 2023 were marked by the La Niña phenomenon, characterized by intense and persistent rainfall throughout the country. (Fondo adaptación & Programa de las Naciones Unidas para el Desarrollo, 2023)

The multitemporal analysis of LSWI images (Image 8) demonstrates a shift from dry to humid conditions. In the initial years of the project (2009–2011), the area was characterized by low LSWI values, represented by light tones on the map, indicating an ecosystem with a limited capacity for moisture retention. As restoration progressed, subsequent years' images showed a gradual transition toward darker and more uniform colors, suggesting an increase in soil moisture and biomass. This change consolidated in 2022 and 2024, which exhibited the highest LSWI values, indicating a hydrologically recovered ecosystem with greater capacity to regulate the water cycle.

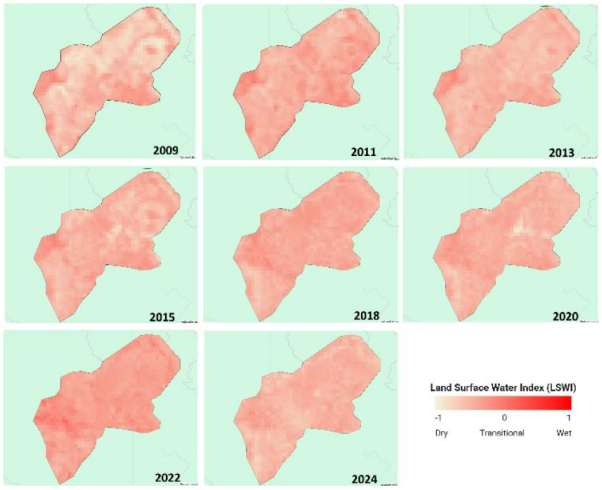


Figure 8: The land surface water Index (LSWI) (2009-2024)

### 4.4 Normalized Difference Moisture Index (NDMI)

The Normalized Difference Moisture Index (NDMI), a key indicator of vegetation water content, demonstrated the effectiveness of the restoration efforts in reestablishing the ecosystem's moisture conditions. The multitemporal NDMI maps (image 9) show a progression from a relatively dry landscape to a consistently moist environment.

In the initial years of the study (2009–2011), NDMI images displayed light tones and low values, indicating vegetation with limited water content. As the restoration process matured, the area experienced a progressive increase in vegetation water content. This is visually expressed through a shift toward darker and deeper blue tones in the images from more recent years.

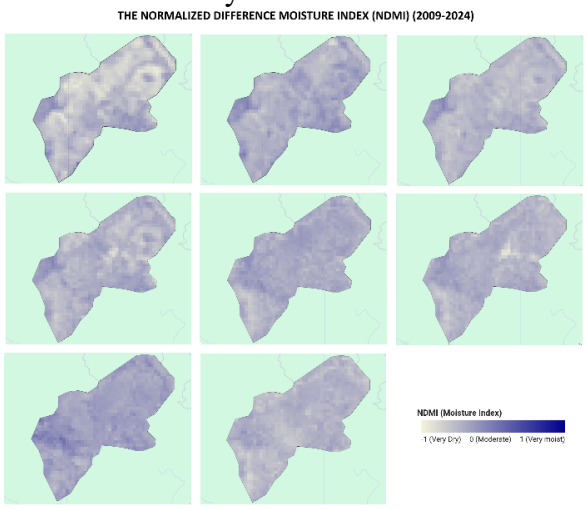


Figure 9: The Normalized difference moisture index (NDMI) (2009-2024)

This index is consistent with the results obtained from the LSWI. This indicates that recovery was not limited to specific areas but extended across the entire study zone, resulting in a more robust ecosystem that is resilient to degradation.

### 4.5 Statistical trends

The statistical analysis confirmed the patterns observed in the spectral indices. The Mann-Kendall test applied to the NDVI showed a statistically significant increasing trend ($\tau$ = 0.6071, p = 0.0461). The p-value below 0.05 indicates that the probability of this trend occurring by chance is very low (Kocsis & Anda, 2018). Therefore, the results of the analysis confirm that the changes observed in the NDVI over the study period are not due to random fluctuations, but to a real and sustained process of ecosystem recovery.

Complementarily, the linear regression analysis of the time series revealed a positive slope across most of the study area, corroborating the trend of increasing vegetation cover and biomass. These quantitative results reinforce the validity of the visual and spatial analysis carried out using vegetation indices.

## 5. Discussion

The analysis revealed the effectiveness of the ecological restoration process initiated in 2010. The spectral indices confirm a sustained structural and functional recovery of the vegetation, although with interannual fluctuations that must be interpreted with caution.

In the case of NDVI, the time series (2010–2024) showed peaks and declines associated both with the limited availability of cloud-free images in humid montane ecosystems-an effect widely documented (Chu et al., 2019; Regmi et al., 2020) and with local climatic dynamics, where moisture pulses, seasonality, and extreme events directly influence vegetation productivity. Despite these oscillations, the positive linear trend (0.0037 per year) and the slope map indicate a sustained increase in vegetation vigor, although small sectors with declining values persist, possibly linked to anthropogenic pressures or edaphic limitations.

The other indices complement this perspective: LAI showed an increase in foliar biomass, NDMI reflected higher water content in the vegetation, and LSWI suggested a recovery of surface moisture, pointing to the restoration of hydrological functions. Taken together, the results indicate a recovery process that is both structural and functional.

These findings are consistent with previous studies in tropical environments, where high interannual variability in vegetation indices contrasts with long-term positive trends that reflect the effectiveness of restoration (Chazdon Robin & Uriarte Maria, 2016; Rodrigues et al., 2009). However, cloudiness reduced the number of observations, and the exclusive use of optical sensors limited the detection of changes in vertical structure. It is therefore recommended that future studies integrate SAR sensors to complement monitoring.(Tesser et al., 2025).

In summary, despite limitations, the results confirm that ecological restoration has promoted vegetation recovery, with a sustained positive trend in spectral indices. This supports its effectiveness and provides a useful methodology for monitoring projects in high-cloud ecosystems.

## 6. Conclusions

The multitemporal analysis of satellite images demonstrated that the ecological restoration initiated in 2010 has led to a sustained recovery of vegetation up to 2024. The results obtained from spectral indices (NDVI, LAI, NDMI, and LSWI) show improvements in both the structure (foliar biomass, vegetation cover) and the functionality of the ecosystem (water content, vegetation vigor).

Although interannual fluctuations were recorded, mainly associated with high cloud cover and the climatic variability of cloud forests, the positive linear trend of NDVI (0.0037 per year) confirms a consistent process of ecological recovery. These variations also reflect the sensitivity of the ecosystem to

climatic variability and the effects of global change, reinforcing the importance of long time series to distinguish restoration signals from environmental fluctuations.

The observed recovery acquires additional value in the context of climate change, as forest restoration contributes to mitigation through carbon sequestration and improved hydrological resilience. Vegetation recovery not only increases biomass and cover but also strengthens the ecosystem's capacity to regulate the water cycle, buffer climatic extremes, and sustain biodiversity.

Methodological limitations derived from the low availability of cloud-free images highlight the need to integrate other sources of information in the future, such as radar sensors and data with higher spatial and temporal resolution, to enable more robust monitoring. Likewise, the combination of satellite data with carbon and climate models could strengthen the evaluation of the role of restored ecosystems in climate change mitigation and adaptation.

Overall, the study demonstrates the usefulness of satellite monitoring as a key tool for assessing the effectiveness of restoration projects in hard-to-access ecosystems, providing valuable information for decision-making in conservation and natural resource management, as well as for designing adaptation and mitigation strategies to address climate change.

## 7. References


Adagbasa, E. G., & Mukwada, G. (2022). Mapping vegetation species succession in a mountainous grassland ecosystem using Landsat, ASTER MI, and Sentinel-2 data. PLoS ONE, 17(1 January). https://doi.org/10.1371/journal.pone.0256672

Chandrasekar, K., Sesha Sai, M. V. R., Roy, P. S., & Dwevedi, R. S. (2010). Land Surface Water Index (LSWI) response to rainfall and NDVI using the MODIS Vegetation Index product. *International Journal of Remote Sensing*, *31*(15), 3987–4005. https://doi.org/10.1080/01431160802575653

Chazdon Robin, & Uriarte Maria. (2016). Natural regeneration in the context of large-scale forest and landscape restoration in the tropics. *Wiley* , 709–715.

Chu, D., Shen, H., Guan, X., Chen, J. M., Li, X., Li, J., & Zhang, L. (2019). Long time-series NDVI reconstruction in cloud-prone regions via spatio-temporal tensor completion.

Fondo adapatción, & Programa de las Naciones Unidas para el Desarrollo. (2023). Evaluación de daños, pérdidas e impactos asociados a la ocurrencia del fenómeno de la niña 2021 - 2023.

Dutrieux, L. P., Jakovac, C. C., Latifah, S. H., & Kooistra, L. (2016). Reconstructing land use history from Landsat time-series: Case study of a swidden agriculture system in Brazil. *International Journal of Applied Earth Observation and Geoinformation*, *47*, 112–124. https://doi.org/10.1016/j.jag.2015.11.018

Forkel, M., Carvalhais, N., Verbesselt, J., Mahecha, M. D., Neigh, C. S. R., & Reichstein, M. (2013). Trend Change detection in NDVI time series: Effects of inter-annual variability and methodology. *Remote Sensing*, *5*(5), 2113–2144. https://doi.org/10.3390/rs5052113

Gaitan, J., Donaldo, B., & Azcona, C. (2015). Tendencia del NDVI en el período 2000-2014 como indicador de la degradación de tierras en Argentina: ventajas y limitaciones. Volumen 32(AGRISCIENTIA).

Hilker, T., Coops, N. C., Coggins, S. B., Wulder, M. A., Brown, M., Black, T. A., Nesic, Z., & Lessard, D. (2009). Detection of foliage conditions and disturbance from multi-angular high spectral resolution remote sensing. *Remote Sensing of Environment*, *113*(2), 421–434. https://doi.org/https://doi.org/10.1016/j.rse.2008.10.003

Huang, S., Tang, L., Hupy, J. P., Wang, Y., & Shao, G. (2021). A commentary review on the use of normalized difference vegetation

index (NDVI) in the era of popular remote sensing. *Journal of Forestry Research*, *32*(1), 1–6. https://doi.org/10.1007/s11676-020-01155-1

Karger, D. N., Kessler, M., Lehnert, M., & Jetz, W. (2021). Limited protection and ongoing loss of tropical cloud forest biodiversity and ecosystems worldwide. *Nature Ecology & Evolution*, *5*(6), 854–862. https://doi.org/10.1038/s41559-021-01450-y

Kh Aswad, F., Yousif, A. A., Ibrahim, S. A., & Aswad, F. K. (2020). Trend Analysis Using Mann-Kendall and Sen's Slope Estimator Test for Annual and Monthly Rainfall for Sinjar District, Iraq. In *Journal of University of Duhok* (Vol. 32, Issue 2). https://www.researchgate.net/publication/343787766

Kocsis, T., & Anda, A. (2018). Parametric or non-parametric: Analysis of rainfall time series at a Hungarian meteorological station. *Idojaras*, *122*(2), 203–216. https://doi.org/10.28974/idojaras.2018.2.6

Myneni, R. B., Ramakrishna, R., Nemani, R., & Running, S. W. (1997). Estimation of global leaf area index and absorbed par using radiative transfer models. *IEEE Transactions on Geoscience and Remote Sensing*, *35*(6), 1380–1393. https://doi.org/10.1109/36.649788

Regmi, R., Ma, Y., Ma, W., Baniya, B., & Bashir, B. (2020). Interannual Variation of NDVI, Precipitation and Temperature during the Growing Season. *Applied Ecology and Environmental Sciences*, *8*(5), 218–228. https://doi.org/10.12691/aees-8-5-5

Rodrigues, R. R., Lima, R. A. F., Gandolfi, S., & Nave, A. G. (2009). On the restoration of high diversity forests: 30 years of experience in the Brazilian Atlantic Forest. *Biological Conservation*, *142*(6), 1242–1251. https://doi.org/https://doi.org/10.1016/j.biocon.2008.12.008

Tesser, D. S., McDonald, K. C., Podest, E., Lamb, B. T., Blüthgen, N., Tremlett, C. J., Newell, F. L., Villa-Galaviz, E., Schaefer, H. M., & Nieto, R. (2025). Monitoring Tropical Forest Disturbance and Recovery: A Multi-Temporal L-Band SAR Methodology from Annual to Decadal Scales. *Remote Sensing*, *17*(13). https://doi.org/10.3390/rs17132188

# GeoASG®: A SaaS Solution for Geo Data-Driven Sustainability Management

Diana Catalina Blanco Figueroa [a, *], Neira Yolima Figueroa Galvis [a]

[a] *Sistemas Sostenibles S.A.S - cblanco@sistemassostenibles.com.co,*

**Abstract**: GeoASG® is a SaaS (Software as a Service) platform designed to strengthen sustainability management through geospatial intelligence. In response to the fragmentation of ESG (Environmental, Social, and Governance) data across Latin America, GeoASG® consolidates key information to promote traceability, transparency, and accountability. This paper presents a theoretical-methodological framework that guides the integration of geospatial data into sustainability processes, enabling evidence-based decision-making. A pilot implementation is being conducted in a pharmaceutical company to validate its adaptability and scalability across sectors. Additionally, a survey of 85 organizations from diverse industries in Latin America identified main barriers and expectations, while co-creation processes with companies from technology, energy, healthcare, transportation, and environmental services informed the evolution of the platform's functionalities. Drawing on emerging literature on digital sustainability leadership and ESG frameworks such as SASB (Sustainability Accounting Standards Board), GRI (Global Reporting Initiative), and CSRD (Corporate Sustainability Reporting Directive), this work advocates for the democratization of geospatial technologies beyond expert domains. In this way, GeoASG® supports organizations with limited resources in strengthening ESG governance and reporting, contributing to a more inclusive and evidence-driven sustainability transition at both organizational and territorial scales.

***Keywords:*** Geospatial Intelligence, ESG Reporting, SaaS Platform, Sustainability Reporting, Latin America

## 1. Introduction

Sustainability management has evolved into a data-driven discipline that demands not only environmental stewardship but also robust social responsibility and sound governance practices (Eccles, Ioannou, & Serafeim, 2014). Across Environmental, Social, and Governance (ESG) frameworks, traceability, transparency, and accountability have become fundamental pillars for both regulatory compliance and stakeholder engagement (Kotsantonis, Pinney, & Serafeim, 2016). However, the effective implementation of ESG strategies continues to face significant challenges, especially in regions such as Latin America, where data fragmentation, inaccessibility, and siloed systems hinder the integration and operationalization of sustainability goals (Organisation for Economic Co-operation and Development - OECD, 2020; Economic Commission for Latin America and the Caribbean - ECLAC, 2021).

Geospatial intelligence, understood as the strategic use of spatially referenced data to support decision-making in environmental, social, and governance (ESG) management, plays a pivotal role in addressing these

challenges. It offers advanced capabilities for spatial analysis, real-time monitoring, and territorial management. Despite advances in geoinformatics, data science, and cloud technologies, many organizations still lack access to geospatial tools that are tailored, affordable, and scalable. Small and medium-sized enterprises (SMEs) often operate without the technical or financial capacity to implement complex ESG management systems, limiting their ability to measure impact, assess risk, and report performance effectively.

This paper introduces GeoASG®, a Software as a Service (SaaS) platform developed to democratize access to geospatial intelligence for sustainability management. By integrating environmental, social, and governance data into a flexible and interoperable platform, GeoASG® aims to support organizations in making more informed, evidence-based decisions. Grounded in interdisciplinary research and informed by real-world needs, this work proposes a conceptual and operational framework for the development of GeoASG®. It also presents findings from a preliminary stakeholder survey, in which 85 companies operating in Latin America participated, highlighting the perceived barriers, priorities, and expectations regarding geospatial ESG solutions. Additionally, it incorporates insights from companies that have interacted with the GeoASG® platform throughout its development stages—ideation, minimum viable project, and iterative refinements—helping to define the requirements and functionalities that enhance their processes, responses, results, and solutions to sustainability-related challenges.

Through this contribution, we seek to demonstrate how cloud-based geospatial platforms can bridge the gap between sustainability theory and practice, enabling more inclusive and impactful ESG strategies at both organizational and territorial scales.

## 2. Methodology

This study employed a mixed-methods approach to gather insights from professionals engaged in sustainability-related roles across diverse industry sectors. The primary instrument was an online survey composed of both closed and open-ended questions, designed to capture organizational characteristics, ESG management practices, challenges faced, and the perceived value of geospatial and SaaS-based solutions.

The survey was distributed to a targeted sample of professionals from sectors including transportation (railway and aviation), health, technology, and manufacturing. A total of 85 responses were collected over a two-week period in March 2025. Participants represented both large enterprises (with over 250 employees) and small businesses (with fewer than 50 employees), allowing for a comparative perspective on ESG readiness and digital tool adoption.

Survey questions focused on: The types of ESG frameworks and standards currently followed (e.g., ISO 14001, GRI, SASB); Operational and strategic challenges in sustainability reporting and management; Perceived importance of implementing a digital ESG platform; Key functionalities and geolocation tools considered essential for an ESG platform; Barriers to adoption such as cost, skills gaps, or data accessibility; Frequency of ESG reporting and metrics used; Willingness to invest in a SaaS-based ESG solution

In addition to the survey, the methodological approach incorporated continuous feedback from early users and strategic clients, who were involved throughout the design and development of GeoASG®. During its first year, during the pilot phase, the MVP is expected to benefit between 5 and 10 organizations, primarily from the public sector, NGOs, and small enterprises across Latin America. These organizations operate in key sustainability-related areas such as environmental management, territorial planning, sustainable agriculture, and climate monitoring. The involvement of these clients, many of whom work in regions facing critical challenges in accessing reliable geospatial data

and technology, was essential to ensure the solution's usability, relevance, and impact.

This included: Workshops and interviews were conducted to co-define priorities and expected functionalities. Three workshops were held during the initial phase of the project, involving representatives from public institutions, private organizations, and civil society actors engaged in sustainability management and geospatial data use. The methodology followed a participatory, user-centered approach, combining co-creation dynamics, semi-structured interviews, and practical need-mapping exercises. Each workshop was structured in three phases: (1) collaborative diagnosis to identify current challenges in the use of ESG and geospatial data; (2) solution exploration through group sessions to prototype key MVP functionalities; and (3) validation, where participants provided feedback on the proposed technologies and their real-world applicability. This methodology ensured that the design of the GeoASG® platform was closely aligned with users' concrete needs, enhancing its relevance, usability, and scalability.

Testing and evaluation during the minimum viable product (MVP) phase were carried out through a functional prototype designed to ensure scalability, interoperability, and effective geospatial visualization. Rather than focusing on specific technologies, the MVP emphasized delivering a user-friendly interface, secure data management, and reliable tools for ESG integration. Its initial version demonstrated the capacity to visualize ESG data linked to geographic variables, manage key indicators, and support territorial decision-making.

Iterative improvements based on real-time user interaction: These participatory design components ensured that the platform evolved in response to actual business needs, reinforcing its usability, adoption, and long-term value. This user-centered approach aligns with emerging best practices in sustainable computing frameworks and digital leadership programs such as ESC (Pazienza et al., 2024) and LEADS (Joblin et al., 2023), highlighting the value of co-creation, interdisciplinary literacy, and sustainability-oriented innovation. The combination of quantitative insights and qualitative co-creation forms the basis of the platform's robust and adaptable design.

## 3. Results

### 3.1 Respondent Profile and Context

The survey engaged 85 professionals from diverse sectors: transportation, manufacturing, technology, healthcare, and consulting, mainly located in Latin America. Participants held leadership, operational, and technical roles within organizations of varying sizes. Their responses reflect a wide range of experiences and institutional maturity in relation to sustainability reporting and ESG data management.

### 3.2 Barriers to Effective Sustainability Management

Participants identified regulatory compliance, data collection, and impact measurement as their most pressing challenges. The lack of interoperable systems and standardized indicators was implicit in responses describing difficulty accessing reliable data, integrating across departments, and maintaining up-to-date records. This fragmented approach results in incomplete diagnostics, limited traceability, and inconsistent reporting—factors that impede strategic sustainability planning.

Other limitations cited include Insufficient technical capacity or trained staff; Limited financial resources to invest in digital systems; Disconnection between operational activities and ESG objectives; These obstacles reflect the need for systems that go beyond regulatory checklists and instead facilitate dynamic, evidence based ESG strategies that can evolve over time.

### 3.3 Interest in Geo-Enabled SaaS Solutions

When evaluating the potential of a digital ESG platform, more than 70% of respondents considered such a tool to be important or very important. This indicates a clear recognition of the role of digital transformation in sustainability governance. Respondents

expressed particular interest in platforms that could:

Automate and streamline ESG data collection; to provide real-time alerts for environmental or social risks, the GeoASG® MVP focuses on the transmission of dynamic data relevant to sustainability management. This includes real-time climate data—such as temperature, precipitation, humidity, and wind speed—sourced from local sensors or external meteorological services. It also incorporates early warning alerts for critical events like wildfires, floods, landslides, or other natural hazards. Environmental quality data, including air emissions, water pollutants, and air quality indicators, can be integrated when connected IoT sensors are available. In certain projects, real-time data on land use and mobility—such as traffic patterns, agricultural machinery movement, or activities in protected areas—may also be included. Additionally, participatory platforms allow community members to report incidents such as deforestation or pollution. These real-time data streams enable organizations to make more informed decisions, respond quickly to critical situations, and reinforce the preventive dimension of sustainable management.

Support compliance tracking and generate standardized reports; Enable georeferenced visualizations of projects and impacts; Improve collaboration and communication among departments; These needs resonate strongly with the conceptual underpinnings of the GeoASG® platform, which aims to address these gaps by integrating geospatial technologies with ESG frameworks in an accessible, modular, and scalable interface.

### 3.4 Geospatial Intelligence: A Valued but Underused Resource

Nearly all respondents agreed that geolocation and mapping tools are either important or very important for sustainability decision-making. Their perceived utility includes Early identification of geographic risks and vulnerable zones; Improved visualization and communication of ESG strategies.

However, actual use of geospatial tools remains limited due to lack of internal capacity, software accessibility, and integration with other corporate systems. This disconnects between perceived value and actual usage highlights an opportunity for democratizing geospatial intelligence through user-friendly SaaS models like GeoASG®.

### 3.5 Willingness to Adopt a SaaS-Based ESG Platform

Responses to investment readiness were mixed. While some respondents indicated hesitation due to cost concerns, others showed a clear willingness to adopt a digital solution if it demonstrated practical benefits and ease of implementation. Flexibility in pricing, along with localized content and support, were identified as factors that could facilitate adoption—especially among SMEs and organizations with limited IT resources.

## 4. GeoASG® Conceptual and Operational Framework

The results of the survey validate the need for an integrated and accessible platform to support sustainability governance, particularly in the Latin American context. In response to these findings, GeoASG® is conceived as a comprehensive framework that empowers organizations to manage Environmental, Social, and Governance (ESG) data through geospatial intelligence in a practical and adaptable way.

### 4.1 Foundational Principles

The development of GeoASG® is guided by five key principles: integration of fragmented ESG data; incorporation of territorial perspectives through geospatial analysis; accessibility and democratization to ensure usability in different organizational contexts; compliance and accountability aligned with local and international standards; and openness to promote interoperability and collaborative data ecosystems.

### 4.2 Functional Dimensions

Rather than a rigid architecture, GeoASG® is organized around functional dimensions that address critical aspects of sustainability management. These include monitoring of

environmental indicators and impacts, assessment of social investment and community engagement, evaluation of governance practices, geospatial visualization of risks and opportunities, and automated reporting consistent with international frameworks. Together, these dimensions provide organizations with a holistic and adaptable approach to sustainability management, ensuring traceability, comparability, and integration across diverse contexts and sectors.

As illustrated in Figure 1, the GeoASG® framework integrates key principles and functional dimensions that collectively support ESG data management and sustainability reporting.


Figure 1. GeoASG® Framework (created by Sistemas Sostenibles SAS, 2025)

### 4.3 Alignment with Survey Insights

GeoASG® directly responds to the needs highlighted in the survey: it addresses data silos and collection gaps through integrated processes; it reduces skill and resource limitations by offering intuitive and accessible functionalities; it lowers adoption barriers through flexible deployment options; and it supports spatialized ESG risk management, which was consistently rated as highly relevant by respondents.

### 4.4 Toward Inclusive ESG Intelligence

GeoASG® promotes a shift from fragmented ESG efforts to a territorial and systemic model of sustainability intelligence. By combining geospatial perspectives with sustainability reporting, it fosters accountability, inclusiveness, and resilience. In this sense, GeoASG® is more than a digital tool: it represents a methodological framework designed to strengthen sustainability governance, especially in resource-constrained settings across Latin America.

## 5. Discussion

The insights from the survey and the implementation of GeoASG® at a pharmaceutical corporation reveal critical dimensions of how geospatial SaaS platforms can transform ESG management into practice. While the theoretical framework emphasizes interoperability, data integration, and the democratization of GIS tools, this case study demonstrates how these principles manifest in a real-world scenario—particularly in the pharmaceutical sector, where traceability, regulatory compliance, and risk mitigation are essential.

First, the fragmented and siloed data structures reported by survey participants reflect the broader regional challenge of ESG data governance. GeoASG® addresses this by offering centralized and real-time integration capabilities that enhance traceability across the entire value chain, ensuring greater visibility in both environmental and social performance.

Second, the perceived barriers to adoption—limited technical skills, high costs, and data complexity—are mitigated through the accessible, SaaS-based design of GeoASG®. Its user-centric interfaces, automated ESG reporting, and AI-powered predictive analytics were key to delivering value in the pilot project, and they align well with the needs expressed by survey respondents.

Third, the case illustrates the added value of geospatial intelligence in pharmaceutical supply chains. The platform's ability to identify underserved areas, monitor environmental impacts, and improve equitable

access to treatment validates the territorial approach promoted in this paper. These capabilities demonstrate how ESG strategies become not only compliant, but also strategic tools for innovation, resilience, and inclusiveness.

Lastly, this case also reveals the importance of co-creation and scalability. The pilot phase enabled iterative improvement and contextualization of GeoASG®, paving the way for large-scale deployment. This phased implementation strategy could be adapted for other sectors and regions, offering a roadmap to ESG digital transformation that is adaptable and cost-effective.

## 6. Adoption Framework and Strategic Approach

We analyze four essential attributes for the successful implementation and adoption of GeoASG®: geospatial intelligence of environmental, social and governance (ESG) components, ESG and sustainability consulting, training and education for sustainability, and technology management for ESG. For each of these pillars, we assess the relevance of their activities and identify the gap between the current and desired states within organizations. As illustrated in Figure 2, these four attributes articulate the value proposition of GeoASG® and guide its adoption strategy.


Figure 2: GeoASG® Value Proposition Venn Diagram (created by Sistemas Sostenibles SAS, 2025)

This comprehensive approach enables more strategic decision-making, prioritization of high-impact initiatives, and a more effective method for engaging organizations in the adoption process. It emphasizes progressive implementation, capacity building, and continuous improvement to ensure long-term value. As a SaaS platform, GeoASG® provides training, ongoing support, monitoring, and iterative development, reinforcing product innovation and sustainability throughout its lifecycle. This methodology ensures that organizations can not only comply with ESG reporting obligations but also embed sustainability into their operational DNA.

## 7. Value Proposition

The value proposition diagram for GeoASG® was derived from a series of co-creation workshops held with a leading pharmaceutical company in Latin America. During these collaborative sessions, we identified the company's key sustainability reporting needs, challenges in data integration, and opportunities for spatial analysis and digital transformation. These findings informed the core service pillars of GeoASG®, which are reflected in the diagram (Figure 3).

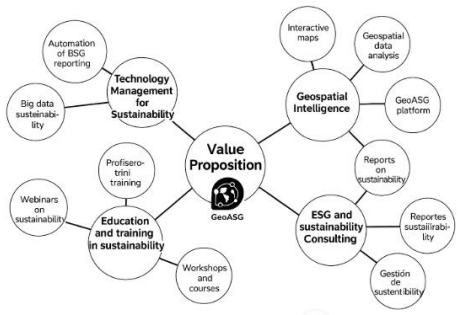


Figure 3: GeoASG® Value Proposition and Use Case with a Pharmaceutical Company

### 7.1 Specific Use Cases from the Pharmaceutical Company

The company required a comprehensive ESG solution to generate sustainability reports aligned with global frameworks (GRI, SASB, TCFD); integrate and automate data from internal systems; analyze environmental risks and operational footprints through spatial data; monitor social investments and supplier compliance; and enhance strategic decisions through dashboards combining geospatial and ESG information.

The pilot highlighted several categories of data integrated into GeoASG®, including corporate systems, environmental and social indicators, public geospatial datasets, and stakeholder-generated information. From these sources, the platform supported the calculation of key indicators such as greenhouse gas emissions per facility, water and waste metrics, workforce diversity statistics, supplier sustainability indexes, and compliance scorecards. In addition, spatial analyses such as risk maps, overlays of operation zones with biodiversity and vulnerability layers, and heatmaps of social investment enabled more localized and evidence-based decision-making.

The value proposition of GeoASG® is structured around four core pillars that support organizations in achieving their sustainability goals through a data-driven and technology-enabled approach. Rather than focusing on specific tools, GeoASG® emphasizes interoperability, scalability, and geospatial intelligence as guiding principles. The platform integrates Environmental, Social, and Governance (ESG) indicators derived from both quantitative and qualitative variables, structured in accordance with international frameworks such as GRI, SASB, and local sustainability standards. The process for indicator development includes defining metrics, identifying required variables (e.g., $CO_2$ emissions, employee turnover, recycled waste percentage, or corruption incident reports), collecting data from diverse sources, ensuring consistency and validation, and applying advanced analytical and geospatial methods.

Data is managed securely in the cloud to guarantee integrity and territorial contextualization, enabling organizations to analyze the spatial distribution of sustainability indicators and make informed, location-based decisions. Through this flexible foundation, GeoASG® offers a reliable and adaptable tool to enhance ESG reporting and support territorial sustainability strategies.

The four pillars that shape GeoASG® are: (1) Technological Solutions for Sustainability, incorporating advanced analytics, intelligent visualization, and automation of ESG reporting; (2) Geo-Intelligence and Artificial Intelligence, providing predictive models, interactive maps, and territorial analyses; (3) Training and Capacity Building, with programs to strengthen data literacy and ESG competencies; and (4) Sustainability and ESG Consulting, offering strategic advice on circular economy, risk management, and ESG strategy development. Together, these pillars position GeoASG® as a comprehensive partner in the sustainability journey, combining technological resources with expert guidance to support effective ESG integration and reporting.

## 8. Conclusions and Future Work

This paper presents the customer requirements for the future platform GeoASG®, a solution for ESG management grounded in geospatial intelligence, data integration, and accessibility. The framework is designed to support sustainability strategies across four key dimensions: environmental, social, governance, and territorial, ensuring alignment with international standards.

The findings confirm that many organizations in Latin America face significant challenges in ESG data governance, including fragmentation, low digital maturity, and limited interoperability. These conclusions are based on consultations carried out during the initial phases of the project and exploratory workshops, which involved key stakeholders from at least five countries: Colombia, Mexico, Chile, Argentina, and Peru. Across these diverse engagements, common needs were identified, such as fragmented ESG data systems, limited local technical capacity, and the absence of interoperable tools capable of integrating geospatial analysis into ESG strategies. At the same time, there is a strong and growing recognition of the value of digital platforms, especially those that integrate geospatial technologies and provide actionable, visual, and automated tools.

The GeoASG® framework represents a first step to address these needs, incorporating functional dimensions for monitoring, geospatial visualization, and automated reporting. The system is designed to support organizations of different sizes and technical capacities in building evidence-based sustainability strategies aligned with international standards. The pilot deployment with a pharmaceutical corporation provides a real-world validation of the platform's relevance and impact, showing how GeoASG® can improve ESG reporting, transparency, and decision-making.

### 8.1 Future Work

Scalability and Sectoral Expansion: The success of the pilot suggests that GeoASG® can be scaled to other industries such as energy, construction, or agribusiness. Sector-specific modules can enhance its adaptability.

AI Integration: Expanding predictive analytics to support scenario modeling, risk forecasting, and investment decision-making.

Policy and Academic Engagement: Collaboration with academic institutions and regulatory agencies can promote standardization and encourage broader adoption of spatially enabled ESG tools.

Inclusion of Stakeholders: Integrating community-generated data and participatory tools to ensure socially just and inclusive sustainability reporting.

Ultimately, GeoASG® aspires to be a catalyst for the territorialization of sustainability, enabling organizations to move beyond fragmented data toward cohesive, transparent, and impactful ESG action. GeoASG® emerges as a comprehensive SaaS solution that empowers organizations to transform their ESG and sustainability strategies through intelligent geodata, advanced analytics, and tailored support. By combining cutting-edge technologies like artificial intelligence, geospatial data processing, and automated ESG reporting, with targeted training and expert consulting, GeoASG® bridges the gap between data complexity and actionable insights. The platform's modular value proposition ensures that clients can adopt the tools and services that best suit their sustainability maturity and goals. As organizations increasingly face regulatory pressure, stakeholder scrutiny, and climate-related risks, GeoASG® offers not only a digital infrastructure but a trusted partner to guide decision-making and foster meaningful impact. The adoption strategy is built around transparency, technical support, and user empowerment, reinforcing the role of GeoASG® in enabling sustainable transformation across sectors.

## 9. References


Contini, G., Grandi, F., & Peruzzini, M. (2024). A Framework to Enhance Corporate Sustainability in Manufacturing Through Digital Technologies and System Thinking. In M. Peruzzini et al. (Eds.), Advances in Transdisciplinary Engineering, IOS Press. https://doi.org/10.3233/ATDE240898

Eccles, R. G., Ioannou, I., & Serafeim, G. (2014). The Impact of Corporate Sustainability on Organizational Processes and Performance. Management Science, 60(11), 2835–2857. https://doi.org/10.1287/mnsc.2014.1984

Economic Commission for Latin America and the Caribbean (ECLAC). (2021). The challenge of achieving the Sustainable Development Goals in Latin America and the Caribbean: An assessment based on the 2019 voluntary national reviews. United Nations. https://www.cepal.org/en

European Commission. (2021). Guidance on Corporate Sustainability Reporting. https://ec.europa.eu/info/publications/210621-sustainable-finance-platform-technical-annex_en

GRI (Global Reporting Initiative). (2021). Sustainability Reporting Standards. https://www.globalreporting.org

IFRS Foundation. (2023). SASB and Other ESG Frameworks. Retrieved from https://sasb.ifrs.org/about/sasb-and-other-esg-frameworks/.

ISO. (2015). ISO 14001:2015 — Environmental management systems — Requirements with guidance for use. International Organization for Standardization.

Joblin, M., Yew, D., & Yano, A. (2023). LEADS: An Education Framework for Leadership in Environmental and Digital Innovation toward Sustainability. White Paper. Retrieved from https://www.nature.com/articles/s41599-023-01919-0

Kotsantonis, S., Pinney, C., & Serafeim, G. (2016). ESG Integration in Investment Management: Myths and Realities. Journal of Applied Corporate Finance, 28(2), 10–16. https://doi.org/10.1111/jacf.12169

OECD. (2020). Data Governance for Growth and Well-being. https://www.oecd.org/publications/data-governance-for-growth-and-well-being

OECD. (2020). Latin American Economic Outlook 2020: Digital Transformation for Building Back Better. OECD Publishing. https://www.cepal.org/en/publications/46030-latin-american-economic-outlook-2020-digital-transformation-building-back-better

Pazienza, P., Distaso, A., & Valente, M. (2024). The ESC Framework: Environmental Sustainability and Computing. AI & Society. https://link.springer.com/article/10.1007/s11334-023-00548-9

Sostenibilidad y Tecnología Blog. (2024). "Inteligencia geoespacial para la gestión ESG en América Latina." https://sostenibilidadytecnologia.org/GeoASG

United Nations. (2015). Transforming Our World: The 2030 Agenda for Sustainable Development. https://sdgs.un.org/2030agenda

White, G. B., & Fernandez, A. (2023). Digital Sustainability Tools and ESG Frameworks: A Practical Guide for Latin America. Springer.

# Geospatial Approaches to Plant Invasion Risk under Climate Change: A Synthesis of Recent Advances (2020–2025)

*Sooraj Nediya Parambath *, Aleesha Fathima S L, Jaishanker R, Gopakumar V, Sajeev C Rajan and Vishnu M.*
*Kerala University of Digital Sciences, Innovation and Technology (Digital University Kerala); * sooraj.np@duk.ac.in*

**Abstract**: Climate change is altering ecological boundaries, creating conditions that enable invasive alien species to spread and thrive in areas that were previously unsuitable or unoccupied. Multi-pronged approaches are widely utilized to analyse the distribution, dynamics, and risk of biological invasions across spatial and temporal scales. This synthesis examines the application of remote sensing and geospatial techniques to assess and predict plant invasion risks under different climate change scenarios. Fifty peer-reviewed articles were selected from the Scopus and Web of Science databases, published between 2020 and 2025, based on the inclusion and exclusion criteria. The review focuses on the integration of satellite data, GIS-based approaches, and species distribution models (SDMs), especially those incorporating future climate projections such as Representative Concentration Pathways (RCPs) and Shared Socioeconomic Pathways (SSPs). Key trends identified include the growing use of high-resolution imagery, advancements in geospatial techniques, machine learning for distribution and risk modelling, and a focus on early detection and proactive management strategies. However, significant gaps remain in coverage across various geographical regions. The results emphasize the need for transboundary monitoring and predictive tools to improve invasive plant management in response to global environmental change.

***Keywords:*** Invasive Alien Species, Plant Invasion, Risk Assessment, Climate Change, SDM, RCPs, SSPs

# Workshops

# Assessing smartphone sensors for mobile data capturing and mapping

Paul Rawiel

*University of Applied Sciences, Stuttgart, Germany; paul.rawiel@hft-stuttgart.de*

Smartphones are widely distributed devices with many different sensors on board that can be used for a huge variety of applications that are related climate monitoring, efficient transport, mobile mapping and many more. To build so called apps on android smartphones for applications in the above-mentioned areas, it is essential to know about the different sensors that come with the device, how to access the data measured by these sensors, how to process that data and how to visualize the results.

The workshop offers a hands-on experience to make a first step into the programming of apps for android devices based on the programming language java and the development environment Android Studio.

Participants will learn how to program an app using the Android Studio and install it on an Android Smartphone. As an example, a compass will be programmed using the magnetic field sensor and the accelerometer of the smartphone.

Participants should bring an android smartphone and a cable to connect it to the computer.

***Keywords:*** Android Studio, Java Programming, Smartphone Sensors, App Programming

# Digital Data Acquisition with QField Cloud and QGIS

Hamidreza Ostadabbas

*Geoinformatics Department at die STEG Stadtentwicklung GmbH; Hamidreza.Ostadabbas@steg.de*

This workshop introduces participants to modern digital data acquisition workflows using QField Cloud and QGIS. The goal is to empower users to collect, manage, and synchronize spatial data and multimedia (images/videos) using mobile devices in real-world urban and environmental projects. Participants will learn how to design custom attribute forms, and collect spatial data, photos, and videos using mobile devices.

We'll explore real-time synchronization between field and office teams via QField Cloud. The session is ideal for urban planners, surveyors, and GIS users involved in fieldwork. No advanced coding required – just practical tools for smarter data acquisition. Includes a live demo and interactive field simulation.

By the end of the workshop, participants will be able to:
• Understand the workflow between QGIS (desktop) and QField/QField Cloud (mobile/cloud).
• Configure and publish attribute forms in QGIS for structured field data collection.
• Use mobile devices to capture images, videos, GPS locations, and other field observations.
• Synchronize data between field teams and office teams using QField Cloud.
• Apply the workflow to urban planning or GIS-related fieldwork.
Workshop Topics
• Introduction to QGIS and QField ecosystem
• Creating and configuring attribute forms in QGIS
• Setting up a project in QField Cloud
• Collecting spatial data, images, and videos using smartphones or tablets
• Offline/online synchronization with QField Cloud
• Best practices in mobile data acquisition (field tips, accuracy, etc.)
• Live demonstration & hands-on session
Requirements:
• Laptop with QGIS installed (latest version)
• Android/iOS smartphone or tablet (with QField app installed)
• QField Cloud account (free or organizational)

AGSE Publishing
ISBN 978-3-943321-23-4